UNIVERSITY OF MICHIGAN
JUL 19 1954
PHYSICS LIBRARY

THE JOURNAL OF CHEMICAL PHYSICS

VOLUME 22 NUMBER 7

JULY, 1954

published by the
AMERICAN INSTITUTE OF PHYSICS
Lancaster, Pa., and New York, N. Y.

Physics.

THE JOURNAL OF CHEMICAL PHYSICS

BOARD OF EDITORS

CLYDE A. HUTCHISON, JR., *Editor*

Associate Editors

Term ending December 31, 1954	Term ending December 31, 1955	Term ending December 31, 1956
THEODORE W. BERLIN	RICHARD M. BADGER	BRYCE L. CRAWFORD, JR.
S. F. DAILEY	DAVID M. DENNISON	H. S. GUTOWSKY
HARALD H. EYRING	JOHN G. KIRKWOOD	WILLIAM N. LIPSCOMB
HARRISON SKULL	G. B. KISTIAKOWSKY	ELLIOTT W. MONTROLL
CHARLES P. SMYTH	A. W. LAWSON	GEORGE SCATCHARD
FRANK H. WESTHEIMER	S. S. PENNER	J. W. STOUT
	ROBERT L. SCOTT	GREGORY H. WANNIER

THE JOURNAL OF CHEMICAL PHYSICS is published monthly by the American Institute of Physics. Its purpose is to bridge a gap between journals of physics and journals of chemistry. The artificial boundary between physics and chemistry has now been in actual fact completely obliterated, and a large and active group is engaged in research which is as much the one as the other. It is to this group that the Journal is rendering its principal service and wishes its greatest appeal, both as a prompt and effective medium for publication of research and as a convenient and carefully edited assemblage of pertinent information.

Information for Contributors

Send manuscripts to Clyde A. Hutchison, Jr., Editor, *The Journal of Chemical Physics*, Institute for Nuclear Studies, University of Chicago, Chicago 37, Illinois. Unless otherwise stated submission of a manuscript is a representation that it has been neither copyrighted, published, nor submitted for publication elsewhere. Textual material (abstract, body of the paper, tabular material, references, and figure captions) must be in English, typewritten (except mathematical expressions) double spaced with wide margins on a durable, white paper, preferably letter size. The original copy, not the carbon, should be submitted. For general style, spellings, abbreviations, and forms consult recent issues of this journal. The authors (or institutions) are requested to pay a publication charge of $15.00 per page which, if honored, entitles them to 100 free reprints. Instructions will be sent with galley proofs.

An abstract must accompany each article. It should be adequate as an index and as a summary.

All but the simplest mathematical expressions should be carefully printed in by hand. Be sure to distinguish between capital and small letters. Indicate clearly superscripts and subscripts by inverted carets and carets, respectively. Avoid complicated superscripts and subscripts. Avoid repetition of a complicated expression by representing it by a symbol. Identify in the margin Greek letters and unusual symbols. Use fractional exponents instead of root signs. Use the solidus (/) for fractions wherever its use will save vertical space.

References should appear as footnotes, numbered consecutively. Literature citations of technical journals should be in the form indicated in the Style Manual of the American Institute of Physics and Chemical Abstracts (Chem. Abstracts 45, I-CCLV (1951)).

Tables may be typewritten on sheets separate from the running text. Each table must have a caption which will make the data in the table intelligible without reference to the text. Avoid complicated column headings.

Wherever possible figures should be planned for the width of a column (3 in.). A convenient reduction ratio is about 2:1 or 3:1. Lettering should be large enough on the original that when reduced it shall not be less than about $\frac{1}{16}$ in. (~1.5 mm). Line drawings must be in *india ink* on white paper or tracing cloth. Coordinate paper is not desirable but if used must be blue lined and the coordinate lines which are to show must be inked over. Photographs should have maximum black and white contrast. Identify each original drawing or photograph on the back with the author's name and the figure number. Figures should be numbered consecutively. Captions should be typed on a separate sheet of paper.

A limited number of alterations in proof are unavoidable, but the cost of making extensive alterations after the article has been set in type will be charged to the author.

Proof and all correspondence concerning papers in the process of publication should be addressed to the Publication Manager, American Institute of Physics, 57 East 55 Street, New York 22, New York.

Subscription Price

	U. S. and Canada	Elsewhere
To members of the American Institute of Physics and Affiliated Societies	$12.00	$13.00
To all others	15.00	16.00

Back Number Prices

Yearly rate when complete year is available: $17.00.
Single copies: $1.50 each.

Subscriptions, renewals, and orders for single copies should be addressed to the American Institute of Physics, 57 East 55 Street, New York 22, New York.

Changes of address should be sent to the American Institute of Physics.

The Journal of Chemical Physics is published monthly at Prince and Lemon Streets, Lancaster, Pennsylvania.

Entered as second-class matter December 30, 1932, at the Post Office at Lancaster, Pa., under the Act of August 24, 1912. Acceptance for mailing at special rate of postage, provided for in paragraph (d-2), section 34.40, P. L. & R. of 1948, authorized February 8, 1933.

Physics.
Faloon

THE JOURNAL
OF
CHEMICAL PHYSICS

VOLUME 22, NUMBER 7 JULY, 1954

The Electrical Properties of Some Complex Compounds. Part 1

P. E. FIELDING
Department of Applied Chemistry, New South Wales University of Technology, Broadway, Sydney, Australia
(Received February 2, 1954)

Electrical measurements on dicobalt decamine-μ-peroxy complex (Vortmann's salt) are described. The current formulation contained Co^{III} and Co^{IV} in crystallographically equivalent positions and hence it was thought that the complex might be an intrinsic semiconductor. An apparent dielectric constant K of 10^6 was found to be due to chemical polarization caused by traced of acid on the material. It is concluded on the basis of conductivity measurements that the material is not an intrinsic semiconductor.

INTRODUCTION

THIS communication describes measurements made on dicobalt decammine-μ-peroxy sulfate acid sulfate first described by Maquenne[1] and later formulated by Werner[2] as containing Co^{III} and Co^{IV} in the cation:

$$[(NH_3)_5Co^{III}-O-O-Co^{IV}(NH_3)_5]^{5+}.$$

When this investigation was begun, Werner's formulation seemed to be well established and it was thought that the salts of the complex cation might, owing to the presence in it of Co^{III} and Co^{IV}, exhibit semiconducting properties.

EXPERIMENTAL

It was found that the sulfate of the complex cation was the most convenient salt to prepare. Samples used in the present work were made by several different methods including those described by Gleu and Rehm[3] and Maquenne.[1] When crystallized from 2N H_2SO_4 the salt could be represented by the formula

$$(NH_3)_{10}Co_2O_2\begin{matrix}2SO_4\\HSO_4\end{matrix}\cdot 3H_2O.$$

(From acid of higher concentration a different salt was obtained):

$$(NH_3)_{10}Co_2O_2\begin{matrix}SO_4\\3HSO_4\end{matrix}\cdot 3H_2O.$$

Considerable care had to be exercised in drying the salt and in removing the last traces of acid, retention of which had a most marked effect on both dielectric and conductivity measurements. Initial resistance *versus* temperature characteristics were measured in a cell similar to that used by Eley.[4] The electrodes were of stainless steel 1 cm diameter and 0.2 cm apart the material being tightly packed in by tapping the cell. The resistance of the material packed in this manner was too high to be measured by simple potentiometric equipment. A Megger applying 10^3 volts across the sample indicated that the resistance of the material contained in the cell was of the order 3×10^8 ohms. The results exhibited polarization effects which were thought to be caused by the high field applied across the measuring cell (i.e., 5×10^3 volts/cm). In order to avoid polarization measurements were carried out at low field strengths by means of a potentiometric circuit using a 10^8 ohm dropping resistor. The conductivity cell was immersed in a thermostat capable of reaching -20°C. An inversion point between 8° and 11° was observed. Below this temperature the temperature coefficient of resistance was negative and above positive. A further inversion point between 60°–70°C was observed, but if the temperature reached for a particular run exceeded 80°C, then the rest of the readings became unstable and the results obtained for the ascending temperature cycle were destroyed. This was thought to be caused by thermal decomposition. No polarization effects were observed and Ohm's law was found to be obeyed at 15°, 8°, and 1°C. This

[1] L. Maquenne, Compt. rend. **96**, 344 (1883).
[2] A. Werner, Ann. Physik. **375**, 1 (1910).
[3] K. Gleu and K. Rehm, Z. anorg. u allgem. Chem. **237**, 86 (1938).
[4] Eley, Nature **162**, 819 (1948).

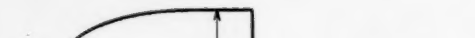

FIG. 1. Voltage wave form across sample. (A plus sign should be inserted between R_s and R_p in the equation, top right.)

method was thought to suffer from a number of disadvantages including large intergranular contact resistance due to the low packing density, and also to the difficulty of subjecting the cell to a wide range of temperatures. It was considered desirable to reach temperatures below $-20°$C, as the upper limit of 80°C imposed a restricted temperature range. Hereafter, solid samples were pressed from the powder. The samples used were disks 2.54-cm diameter, about 3–4 mm thick, pressed in a die under a pressure of 2×10^4 lb/sq in. when the density attained was 98 percent that of the solid. Gold or platinum electrodes were used and held in place by a jig. The initial dielectric measurements indicated a dielectric constant K as high as 10^6. This high value of K was eventually traced back to polarization capacitance at the electrode-sample interfaces, an effect which could be removed by washing the salt well in absolute alcohol, to remove the last trace of acid and drying in an air oven at 55°C.

In order to examine the cause of the apparent high dielectric constant, a circuit was used that applied a constant current square wave pulse to the sample. The wave form across the tablet as shown in Fig. 1 was observed on a cathode-ray oscillograph.

An analysis of the wave form depicted in Fig. 1 shows that the equivalent circuit of the test sample is as in Fig. 2. The wave form of E_s is identical with the current pulse, that is a square wave. A constant current pulse flowing into a parallel RC combination gives rise to E_p, having a time constant $t_{\frac{1}{2}}=R_pC_p$. In the test, arrangements were made to reproduce Fig. 1 by a suitable combination of resistors and condensers.

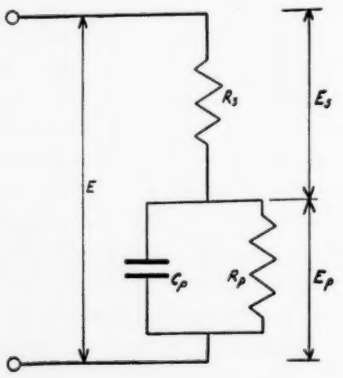

FIG. 2. Equivalent circuit of sample.

Two platinum probes were embedded in the tablet in order to determine whether the effect was located at the interface or distributed throughout the bulk of the substance.

Alternating current measurements were also carried out on samples pressed from carefully dried material. Silver electrodes were evaporated onto the faces. Measurements of the equivalent parallel capacitance and resistance between 50 cy/sec-60 kc/sec were carried out on a substitution bridge with an accuracy of ±1 percent. Similar measurements were also carried out between 70 kc/sec-90 Mc/sec on Q meters, the accuracy being ±10 percent.

Direct current measurements were made on disks 0.63 cm diameter and approximately 0.2 cm between electrodes. The edges of the samples were raised to form a guard ring (see Fig. 3). Silver paste was used for the electrodes and guards. As the resistance of the tablets was of the order 2×10^7 ohms, a Wheatstone bridge was employed for measuring the resistance-temperature characteristics, a Baldwin-Farmer electrometer being the null indicator. The high resistance standards were a set of Welwyn pyromatic resistors. The bridge was capable of measuring 10^6–10^{10} ohms with an

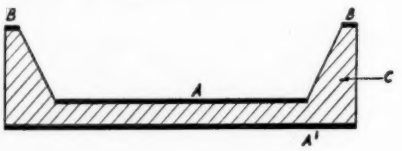

FIG. 3. Shape of sample for dc measurements. A, A^1 Electrodes, B guard ring, C substance.

accuracy of ±1 percent. The whole sample was embedded in Markon II plastic which had no effect on the electrical properties. The temperature range covered was $-125°$ to $+70°$C. A cryostat, after the design of Putley,[5] was used to maintain the sample at a given temperature $\pm0.5°$C, the temperature being measured with a copper constantan thermocouple.

The resistivity of a single crystal was also measured by using electrodes of evaporated silver. A few measurements were made parallel to the axis of the monoclinic crystals but they were not continued owing to the difficulty of growing suitable crystals.

RESULTS

During a series of ac bridge measurements, capacities corresponding to a dielectric constant of 10^6 were observed. This apparent high dielectric constant was examined by means of the pulse method.

When a constant current pulse was applied between the electrodes, the resultant voltage wave form between the two probes was identical with the input current wave form: between either probe and electrode the wave form was as in Fig. 1. This showed that R_s

[5] Putley (private communication).

represented the resistance of the material and R_p and C_p the polarization resistance and capacity. For samples containing acid, R_s and R_p were comparable, whilst C_p had values up to 40 mf. With acid-free samples, only R_s remained observable.

The dielectric constant was found from ac measurements, to be equal to 10 over the frequency range 50 cy/sec-90 Mc/sec. The resistive component of the impedance decreased with increasing frequency, no minimum being reached at 90 Mc/sec. Hence, dc measurements do not give the resistivity, but relative values only.

Several samples were examined and the variation in resistance over the temperature range of 195C° was less than 20 percent, the temperature coefficient of resistance being negative. These changes of resistance with temperature are far too small to be considered significant.

The resistivity of the single crystal was 3×10^7 ohms cm measured at 20°C.

These results are discussed in a separate communication by Fielding and Mellor.

ACKNOWLEDGMENTS

Thanks are expressed to Dr. F. Gutmann for his continual interest and help in the work, and to Mr. E. G. Hopkins for his help in determining the cause of the polarization.

THE JOURNAL OF CHEMICAL PHYSICS VOLUME 22, NUMBER 7 JULY, 1954

The Electrical Properties of Some Complex Compounds. Part 2

P. E. FIELDING, *Department of Applied Chemistry, New South Wales University of Technology, Sydney, Australia*

AND

D. P. MELLOR, *Department of Chemistry, Sydney University, Sydney, Australia*

The possibility of several complex compounds being intrinsic semiconductors is discussed in the light of experimental work presented in this paper and in Part 1. It is concluded that complexes containing metal atoms in different oxidation states in crystallographically equivalent positions are capable of acting as intrinsic semiconductors. Additional support is given to the alternative structure of Vortmann's salt proposed by Brimn.

ONE of the most thoroughly investigated semiconducting compounds is magnetite[1] Fe_3O_4, a substance whose electrical properties are largely influenced by the fact that it contains iron atoms in different oxidation states but in crystallographically equivalent positions. No previous investigation appears to have been made so far of the electrical conductivity of the small class of compounds which like magnetite contain metal atoms in different oxidation states. Compounds of this class such as $Pd(NH_3)_2Cl_3$, $Pt(NH_3)_2Br_3$, $CsAuCl_3$, $(NH_3)_2SbBr_6$, and $Fe_4^{III}(Fe^{II}(CN)_6)_3$ are characterized by their marked absorption of light. The first four are black or nearly so. It has been suggested that this absorption arises from the transition of an electron between the metals in different oxidation states. If this is the case then these compounds may be expected to be intrinsic semiconductors. The electrical conductivity of the first compound chosen for investigation, Vortmann's salt (described in Part 1), is so small and exhibits such a small variation with temperature, the temperature coefficient of resistance at any temperature up to that of thermal decomposition being of the order of 1 percent C°, that it is clearly not an intrinsic semiconductor. Analytical data[2] and magnetic susceptibility[3] measurements on Vortmann's salt support the constitution proposed by Werner.[4] An alternative constitution consistent with the known physical and chemical properties, but not involving different oxidation states for cobalt has been suggested by Brimn.[5]

In this formulation the odd electron is considered to be present in a three electron bond linking the bridging oxygen atoms.

$$(NH_3)_5Co^{III}-O\dddot{=}O-Co^{III}(NH_3)_5)^{5+}.$$

If the cobalt atoms in Vortmann's salt were indeed present as Co^{III} and Co^{IV}, it would be unique in the sense of being the only finite complex where bridged metal atoms differ in their oxidation number. The fact that Vortmann's salt is not an intrinsic semiconductor lends some support to the alternative proposal of Brimn.[5] This support would even be stronger if it could be shown that complex compounds of known

[1] E. J. W. Verwey, *Semiconducting Materials* (Butterworths Scientific Publications, London, 1951), p. 151.

[2] K. Gleu and K. Rehm, Z. anorg. u. allgem. Chem. **237**, 86 (1938).

[3] L. Malatesta, Gazz. chim. ital. **72**, 287 (1938); J. P. Mathieu, Compt. rend. **218**, 907 (1944).

[4] A. Werner, Ann Physik **375**, 1 (1910).

[5] J. Klinberg, *Unfamiliar Oxidation States and Their Stabilization* (University of Kansas Press, Lawrence, 1950), p. 100.

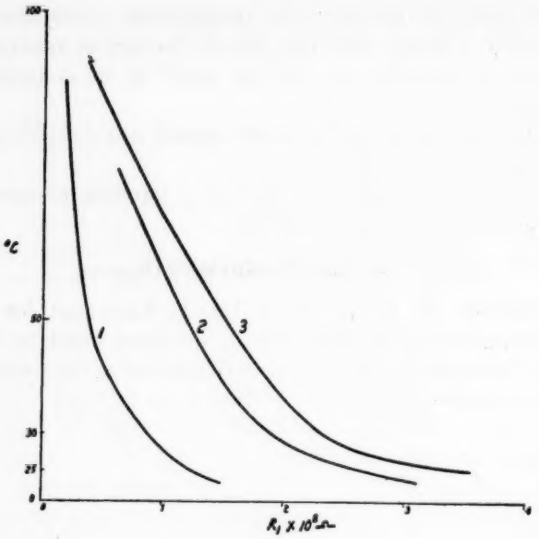

FIG. 1.

crystal structures, in which there is no doubt about the difference in oxidation states of the metal atoms, are indeed intrinsic semiconductors. Attention was therefore directed to $Pd(NH_3)_2Cl_3$. The results of the x-ray analysis[6] of this compound reveal the presence of finite square $[Pd^{II}(NH_3)_2Cl_2]$ and octahedral $[Pd^{IV}(NH_3)_2Cl_4]$ complexes arranged alternately in columns throughout the crystal in such a manner that the Pd^{II} and Pd^{IV} are separated by chlorine atoms.

EXPERIMENTAL

The first samples of the foregoing compound were prepared from dichloro-diammine palladium according to the method of Cohen and Davidson.[7] Tablets were compressed under a pressure of approximately 5×10^3 lb/sq in. and the electrical conductivity measured between nickel electrodes. In the temperature range 20° to 90°C the resistance decreased from 7×10^7 ohms to 8×10^6 ohms. There was however, some evidence of chemical attack on the electrodes. Platinum electrodes were therefore used for succeeding experiments. One sample was cycled continuously between 20° and 90°C. A negative temperature coefficient was found for each branch of the cycle but the results were not reproducible (see Fig. 1). As the number of cycles was increased, the resistance increased.

The substance was evidently undergoing thermal decomposition. The two samples obeyed Ohm's law over the range of applied potential differences.

Owing to the high value of its resistivity and the smallness of its negative temperature coefficient it is not possible to classify $Pd(NH_3)_2Cl_3$ as an intrinsic semiconductor.

The next substance to be investigated was $(NH_4)_2SbBr_6$ in which the antimony is believed to be present in the finite complexes ($Sb^{IV}Br_6$) and ($Sb^{VI}Br_6$). Electrical measurements on this salt were vitiated by the fact that free bromine was invariably present, presumably from thermal decomposition. The negative temperature coefficient of resistance observed in $(NH_4)_2SbBr_6$ was much larger than that observed with the two previous compounds but in view of the effect of small amounts of bromine on the results further work on it was abandoned. It is to be noted that in neither of the palladium nor the antimony compounds were there any unpaired electrons associated with the metal atoms.

Preliminary measurements on alkali-free Prussian blue indicate that this compound is indeed an intrinsic semiconductor and has a negative temperature coefficient of resistance of 7 percent per C°. This work will be fully described in Part III. It is thus evident that a metal complex containing metal atoms in different oxidation states in crystallographically equivalent positions acts as an intrinsic semiconductor. Since Vortmann's salt does not exhibit this type of conduction, there is serious doubt whether it contains Co^{III} and Co^{IV} as previously assumed. Preliminary results of a crystal analysis of Vortmann's salt by N. C. Stephenson[8] lend additional support to this view in so far as they appear to indicate that the two $Co(NH_3)_5$ groups in the complex ion are identical in shape and size.

ACKNOWLEDGMENTS

Thanks are expressed to Mr. N. C. Stephenson for permission to use unpublished data.

[6] C. S. Adams, M. S. thesis, Sydney University, 1952.
[7] A. J. Cohen and N. Davidson, J. Am. Chem. Soc. **73**, 1955 (1951).
[8] N. C. Stephenson, private communication.

Theory of Thermal Diffusion in Liquids and the Use of Pressure to Investigate the Theory*

W. M. RUTHERFORD AND H. G. DRICKAMER
Department of Chemistry and Chemical Engineering, University of Illinois, Urbana, Illinois
(Received January 29, 1954; revised manuscript received April 2, 1954)

A theory of thermal diffusion in liquids is presented which involves: (1) a molecular interpretation due to Denbigh of the results of the thermodynamics of irreversible processes in terms of regular solution theory; (2) a correction for differences in shape and size of the molecules.

Thermal diffusion measurements have been made to 10 000 atmospheres pressure on a series of binary mixtures in a single stage system. The results indicate that the theory is satisfactory.

WHILE there has been considerable interest in thermal diffusion in liquids, there have been relatively few quantitative measurements. In view of the present status of the kinetic theory of liquids, a precise treatment of the theory, based on molecular dynamics, is scarcely to be expected. Nevertheless, it is the purpose of this work to combine some accurate measurements with a reasonably satisfying quantitative molecular picture of the phenomenon.

Measurements have been made in a single stage apparatus for a series of binary systems of organic compounds, one of which was always CS_2, over a pressure range to 10 000 atmospheres. Carbon disulfide was chosen as the reference component because it was a nonpolar molecule of simple symmetry, there are satisfactory PVT data available, and the relaxation times were reasonable. The pressure range afforded large changes in the relative physical properties of the components and permitted a severe test of the theory.

THEORY

We shall use the flux equation for a binary system in the form

$$\mathbf{J}_1=-\frac{n^2m_1m_2}{\rho}\left[\mathbf{grad}X_1-\alpha X_1X_2\frac{1}{T}\mathbf{grad}T\right], \quad (1)$$

where

n = number density;
ρ = density g/cc;
D = diffusion coefficient;
X = mole fraction;
T = absolute temperature;
α = thermal diffusion ratio $=ST$,

where

S = Soret coefficient.

The steady-state separation then gives

$$\ln\left(\frac{X_1}{X_2}\right)_H\left(\frac{X_2}{X_1}\right)_C=\alpha\ln\frac{T_H}{T_C}. \quad (2)$$

A. Thermodynamics of Irreversible Processes

The thermodynamics of irreversible processes gives the following relationship for the steady-state concentration gradient resulting from a temperature gradient.[1,2]

$$\frac{1}{X_1}\mathrm{grad}X_1=-\frac{(Q_1-h_1)}{X_1\dfrac{\partial\mu_1}{\partial X_1}}\frac{1}{T}\mathbf{grad}T$$

$$=\frac{-Q_1^*}{X_1\dfrac{\partial\mu_1}{\partial X_1}}\frac{1}{T}\mathbf{grad}T, \quad (3)$$

$$\frac{1}{X_2}\mathbf{grad}X_2=\frac{-Q_2^*}{X_2\dfrac{\partial\mu_2}{\partial X_2}}\frac{1}{T}\mathbf{grad}T, \quad (4)$$

where the Q^* are "heats of transport," quantities not defined in classical thermodynamics. Applying the Gibbs-Duhem equation one obtains

$$X_1Q_1^*+X_2Q_2^*=0. \quad (5)$$

Denbigh[3] has presented a molecular description of the heats of transport based on the theory of regular solutions. The net result [Eq. (11)] of Denbigh's theory is essentially the same as that of Prigogine's kinetic theory discussed later in the paper, but we prefer to use Denbigh's viewpoint for this work. The molecules are assumed to be of approximately the same size and shape distributed randomly with a coordination number Z, and pair interaction energies W_{11}, W_{22}, and W_{12}. The heat of mixing is

$$\frac{NZ}{2}(2W_{12}-W_{11}-W_{22}).$$

* This work was supported in part by the U. S. Atomic Energy Commission.

[1] S. R. deGroot, *The Thermodynamics of Irreversible Processes* (Interscience Publishers, Inc., New York, 1952).
[2] K. G. Denbigh, *The Thermodynamics of the Steady State* (John Wiley and Sons, Inc., New York, 1951).
[3] K. G. Denbigh, Trans. Faraday Soc. **48**, 1 (1952).

Denbigh defines the energy to remove a molecule of type 1 from a region against the cohesive forces as

$$W_{H1}=-\frac{NZf}{2}(X_1W_{11}+X_2W_{12}), \tag{6}$$

where f is the fraction of nearest neighbor "bonds" bonds broken in a jump. It will be assumed to be one in this paper, except where specifically indicated otherwise. The relative probabilities of the hole left being filled by a molecule of type one or two is in the ratio X_1/X_2. The probable energy supplied when the hole is filled is

$$W_L=X_1W_{H1}+X_2W_{H2}. \tag{7}$$

Denbigh defines

$$Q_1^*=W_{H1}-W_L \tag{8}$$

with a similar equation for Q_2^*. The chemical potential is

$$\mu=\mu_0+RT\ln X_1+(1-X_1)^2\frac{NZ}{2}(2W_{12}-W_{11}-W_{22}). \tag{9}$$

Then,

$$\alpha=\frac{Q_2^*-Q_1^*}{X_1\dfrac{\partial\mu_1}{\partial X_1}} \tag{10}$$

assuming

$$W_{12}=[W_{11}W_{22}]^{\frac{1}{2}}$$

and defining

$$H_1=-NZW_{11};\quad H_2=-NZW_{22},$$

$$\alpha_D=\frac{(X_1H_1^{\frac{1}{2}}+X_2H_2^{\frac{1}{2}})(H_2^{\frac{1}{2}}-H_1^{\frac{1}{2}})}{2[RT-X_1X_2(H_1^{\frac{1}{2}}-H_2^{\frac{1}{2}})^2]}. \tag{11}$$

(A physical interpretation of the H_i's will be discussed later.) This will be referred to as α_D as it was obtained essentially in this form by Denbigh and applies to regular solutions.

In case the molecules are of considerably different size and shape, we can make several modifications. The chemical potential can be written[4]

$$\mu_1=\mu_{1\text{ reg. sol.}}+RT\ln\frac{\varphi_1}{X_1}+\varphi_2RT\left(1-\frac{V_1}{V_2}\right), \tag{12}$$

where

$$\varphi_i=(X_iV_i)/X_1V_1+X_2V_2).$$

(The V_i's are molal volumes.) Then

$$X_1\frac{\partial\mu_1}{\partial X_1}=RT\left[1+X_1X_2\left(\frac{V_2-V_1}{\bar{V}}\right)^2\right]-X_1X_2(H_1^{\frac{1}{2}}-H_2^{\frac{1}{2}})^2. \tag{13}$$

The expressions for the Q_s^* can be modified in three essentially equivalent ways.

(1) The W_{Hi} and W_L will be defined as by Denbigh. W_L will still represent the most probable energy supplied when a hole is filled from a mixture of composition X_1, X_2. However, if the molecules are of different size and shape it may be that, on the average, more or less than one molecule will move in to a hole left by one of the molecules. Let us define ψ_1 as the number of molecules moving in to a hole left by a molecule of type one, with a similar definition for ψ_2. Then

$$Q_1^*=W_{H1}-\psi_1W_L, \tag{14}$$

$$Q_2^*=W_{H2}-\psi_2W_L. \tag{15}$$

The Gibbs Duhem equation then gives

$$X_1\psi_1+X_2\psi_2=1. \tag{16}$$

Thus, on the average, when one molecule moves out of our region, one moves in. Further, when $X_1\rightarrow1\psi_1\rightarrow1$, as $X_2\rightarrow1\psi_2\rightarrow1$ as is physically necessary. The equation for α becomes

$$\alpha=\frac{(X_1H_1^{\frac{1}{2}}+X_2H_2^{\frac{1}{2}})(H_2^{\frac{1}{2}}-H_1^{\frac{1}{2}})+(\psi_1-\psi_2)(X_1H_1^{\frac{1}{2}}+X_2H_2^{\frac{1}{2}})^2}{2\left[RT\left(1+X_1X_2\left(\dfrac{V_1-V_2}{\bar{V}}\right)^2\right)-X_1X_2(H_1^{\frac{1}{2}}-H_2^{\frac{1}{2}})^2\right]}, \tag{17}$$

$$\alpha=\alpha_D\dagger+\frac{(\psi_1-\psi_2)(X_1H_1^{\frac{1}{2}}+X_2H_2^{\frac{1}{2}})^2}{2\left[RT\left(1+X_1X_2\left(\dfrac{\Delta V}{\bar{V}}\right)^2\right)-X_1X_2(H_1^{\frac{1}{2}}-H_2^{\frac{1}{2}})^2\right]}. \tag{17b}$$

(2) Another possible modification of the W_H's and W_L when molecules are of different size or shape, is to consider that the f's and Z's are different for the two types of molecules.

$$W_{H1}=\frac{-Nf_1Z_1}{2}(X_1W_{11}+X_2W_{12}), \tag{18}$$

$$W_{H2}=\frac{-Nf_2Z_2}{2}(X_2W_{22}+X_1W_{12}). \tag{19}$$

All values of f_iZ_i satisfy the Gibbs Duhem equation.

[4] J. H. Hildebrand and R. L. Scott, *Solubility of Non-Electrolytes* (Reinhold Publishing Corporation, New York, 1950), third edition.

† Except for the volume term in the denominator.

Then,

$$Q_2^*-Q_1^*=-(X_1W_{11}^{\frac{1}{3}}+X_2W_{22}^{\frac{1}{3}}) \times N(f_1Z_1W_{11}^{\frac{1}{3}}-f_2Z_2W_{22}^{\frac{1}{3}}). \quad (20)$$

This equation cannot simply be expressed in terms of molal quantities so we shall consider two special cases

$$\text{(2a)} \quad f_1=f_2, \quad Z_1\neq Z_2.$$

For this case the equation for α becomes

$$\alpha=\alpha_D+(H_1H_2)^{\frac{1}{3}}[X_2(\delta-1)-X_1(1/\delta-1)], \quad (21)$$

where

$$\delta=(Z_1/Z_2)^{\frac{1}{3}},$$

$$(\psi_1-\psi_2)(X_1H_1^{\frac{1}{3}}+X_2H_2^{\frac{1}{3}})^2 = (H_1H_2)^{\frac{1}{3}}[X_2(\delta-1)+X_1(1/\delta-1)]. \quad (22)$$

Let

$$\sigma=(\psi_1-\psi_2)\frac{(X_1H_1^{\frac{1}{3}}+X_2H_2^{\frac{1}{3}})^2}{(H_1H_2)^{\frac{1}{3}}},$$

$$\delta=\frac{\sigma+(X_2-X_1)\pm[\sigma^2+2(X_2-X_1)\sigma+1]^{\frac{1}{2}}}{2X_2}, \quad (23)$$

where only the positive root has physical significance.

The results can then be discussed in terms of the ratio Z_1/Z_2 although the individual coordination numbers cannot be calculated. This viewpoint seems physically less likely than the one taken in Sec. 1.

(2b) We can also consider the case

$$Z_1=Z_2; \quad f_1\neq f_2.$$

An analysis of the case yields

$$f_1-f_2=\frac{H_2^{\frac{1}{3}}}{X_1H_1^{\frac{1}{3}}+X_2H_2^{\frac{1}{3}}}(\psi_2-\psi_1). \quad (24)$$

Only the difference in f's is calculable. Most of our discussion of results will be in terms of ψ_1 and ψ_2. These results can easily be modified for interpretation in terms of Z_1/Z_2 or f_1-f_2.

(3) Failure of geometric mean. It is worthwhile to consider the possibility that the geometric mean would not express interaction between unlike molecules. This would be true in associated solution, or where hydrogen bonding is involved.

Let

$$H_{12}=(H_1H_2)^{\frac{1}{3}}+\Delta. \quad (25)$$

The equation for α becomes

$$\alpha=\alpha_D+\frac{(X_2-X_1)\Delta+(\psi_1-\psi_2)\{(X_1H_1^{\frac{1}{3}}+X_2H_2^{\frac{1}{3}})^2+2X_1X_2\Delta\}}{2\left[RT\left(1+X_1X_2\left(\frac{\Delta V}{\bar{V}}\right)^2\right)-X_1X_2(H_1^{\frac{1}{3}}-H_2^{\frac{1}{3}})^2-2X_1X_2\Delta\right]}. \quad (26)$$

One can see that if Δ is significant α may vary widely with composition. This is true for water-alcohol mixtures.

B. Kinetic Theories

Rather similar kinetic theories of thermal diffusion have been developed by Wirtz and Hiby[5,6] and by Prigogine.[7–9] Both considered molecular motion to be a stepwise activated process. Wirtz and Hiby considered as sort of "place exchange" mechanism and arrived at an expression

$$\alpha=\frac{(q_{H2}-q_{L2})-(q_{H1}-q_{L1})}{RT}, \quad (27)$$

where q_H's are activation energies (or free energies) for breaking cohesive bonds and the q_L's are activation energies (or free energies) for hole formation.

Prigogine considered the q_L the same for the two molecules. (His result can also be obtained by assuming instantaneous equilibrium redistribution of the holes.) He obtained

$$\alpha=q_{H2}-q_{H1}/RT. \quad (28)$$

Now the diffusion coefficient can be written

$$D=D_0\exp-(q_{H1}+q_{H2}+q_L/RT). \quad (29)$$

So if D_0 is independent of T, the q's are free energies.

It is tempting to interpret differences between Eq. (11) and experiment in terms of entropy terms which would appear in (27) or (28). This is not possible, however. It is necessary to consider the dependence of the q on temperature and composition. Let us take Eq. (28). [A similar analysis could be given for (27).] Let

$$q_{H1}(T+\tfrac{1}{2}\Delta T)=q_{H1}(T)+\frac{\Delta T}{2}\frac{\partial q_{H1}}{\partial T} \quad (30)$$

with similar expressions for $q_{H2}(T+\frac{1}{2}\Delta T)$, $q_{H1}(T-\frac{1}{2}\Delta T)$, $q_{H2}(T-\frac{1}{2}\Delta T)$ etc. Following through Prigogine's analysis one obtains

$$\alpha=\frac{\left(q_{H2}-T\frac{\partial q_{H2}}{\partial T}\right)-\left(q_{H1}-T\frac{\partial q_{H1}}{\partial T}\right)}{RT}, \quad (31)$$

[5] K. Wirtz, Physik. Z. **44**, 221 (1943); Naturwiss. **31**, 349 (1943); Naturforsch. **3a**, 672 (1948).
[6] K. Wirtz and J. W. Hiby, Physik. Z. **44**, 369 (1943).
[7] Prigogine, de Broukere, and Amand, Physica **16**, 577 (1950); **16**, 851 (1950).
[8] Prigogine, de Broukere, and Buess, Physica **18**, 915 (1952).
[9] I. Prigogine and R. Buess, Physica **15**, 465 (1949).

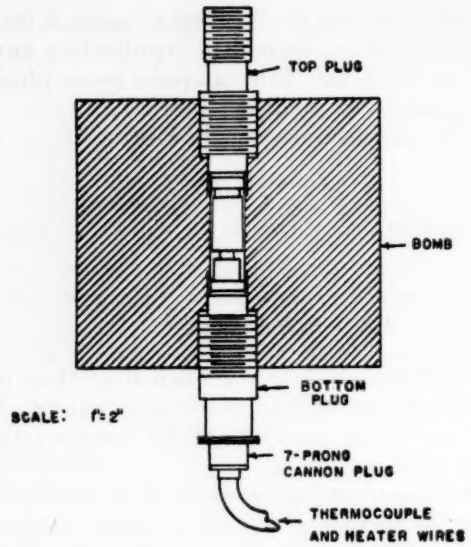

FIG. 1. High-pressure bomb and thermal diffusion cell.

or if the q's are free energies

$$\alpha=\frac{H_2^*-H_1^*}{RT}, \tag{32}$$

which disallows consideration of entropy terms in discussing differences between (28) and (11).

If one further considers the q's to depend on composition as well as temperature,

$$q_{H_1}(T+\tfrac{1}{2}\Delta T)=q_{H_1}(T)+\frac{\Delta T}{2}\frac{\partial q_{H_1}}{\partial T}+\frac{\Delta T}{2}\frac{\partial q_{H_1}}{\partial X_1}\frac{\partial X_1}{\partial T}, \tag{33}$$

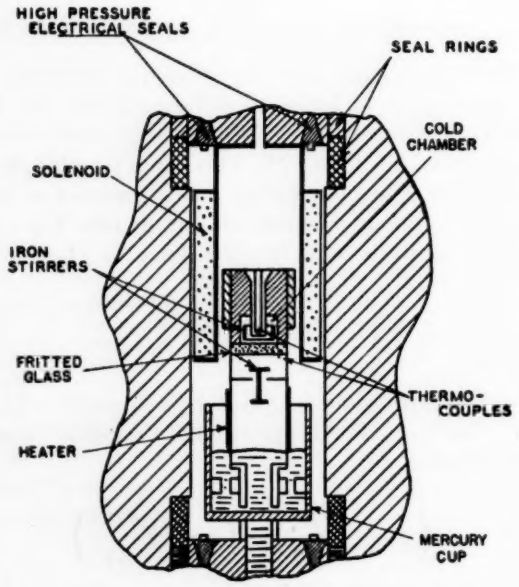

FIG. 2. Detail of thermal diffusion cell.

TABLE I. Measured and calculated coefficients for the system CS_2—ethyl iodine (50 percent CS_2 and 40°C).

P (atmos)	α	α_D	ψ_1	ψ_{CS_2}
300	−0.55	−0.58	1.005	0.995
1000	−0.51	−0.55	1.005	0.995
1700	−0.61	−0.58		
1800	−0.67	−0.59	0.995	1.005
3000	−0.82	−0.58	0.975	1.025
4000	−0.69	−0.43	0.980	1.020
5000	−0.74	−0.50	0.985	1.015
7000	−0.70	−0.60	0.995	1.005
10 000	−0.70	−0.52	0.990	1.010

A positive value of α denotes that CS_2 goes to the cold wall.

TABLE II. Measured and calculated coefficients for the system carbon disulfide-normal butyl chloride (50 percent CS_2 and 40°C).

P (atmos)	α	α_D	ψ_1	ψ_{CS_2}
100	0.30	...	...	...
300	0.25	−0.53	1.100	0.900
1040	0.04	−0.88	1.115	0.885
3000	−0.23	−1.30	1.110	0.890
5000	−0.39	−1.40	1.090	0.910
7000	−0.29	−1.34	1.075	0.925
8000	−0.29	−1.32	1.070	0.930
9000	−0.29	−1.32	1.070	0.930
10 000	−0.29	−1.49	1.080	0.920

A positive value of α denotes that CS_2 goes to the cold wall.

TABLE III. Measured and calculated coefficients for the system carbon disulfide-normal butyl bromide (50 percent CS_2 and 40°C).

P (atmos)	α	α_D	ψ_1	ψ_{CS_2}
300	−0.23	−0.75	1.080	0.920
1000	−0.38	−1.02	1.080	0.920
1800	−0.51	−1.15	1.075	0.925
3000	−0.77	−1.45	1.070	0.930
4000	−0.78	−1.56	1.080	0.920
5000	−0.68	−1.58	1.080	0.920
7000	−0.64	−1.45	1.060	0.940
10 000	−0.53	−1.66	1.080	0.920
Measured and calculated coefficients for the system carbon disulfide-normal butyl bromide (20 percent CS_2 and 40°C)				
7000	−0.64	−1.72	1.025	0.900
Measured and calculated coefficients for the system carbon disulfide-normal butyl bromide (80 percent CS_2 and 40°C)				
7000	−0.87	−1.52	1.075	0.980

A positive value of α denotes that CS_2 goes to the cold wall.

TABLE IV. Measured and calculated coefficients for the system carbon disulfide-normal butyl iodide (50 percent CS_2 and 40°C).

P (atmos)	α	α_D	ψ_1	ψ_{CS_2}
300	−0.65	−1.04	1.070	0.930
1000	−0.54	−1.16	1.075	0.925
1800	−0.63	−1.28	1.090	0.910
3000	−0.55	−1.42	1.090	0.910
4000	−1.09	−1.52	1.050	0.950
5100	−1.14	−1.58	1.045	0.955
7000	−0.92	−1.64	1.060	0.940
8500	−0.48	−1.81	1.100	0.900
10 000	−0.82	−1.99	1.075	0.925

TABLE V. Measured and calculated coefficients for the system carbon disulfide-benzene (50 percent CS_2 and 40°C).[a]

P (atmos)	α	α_D	ψ_1	ψ_{CS_2}
100	0.16	−0.49	1.125	0.875
1000	0.10	−0.86	1.110	0.890
1500	−0.04	−1.03	1.100	0.900

[a] A positive value of α denotes that CS_2 goes to the cold wall.

TABLE VI. Measured and calculated coefficients for the system carbon disulfide-chlorobenzene (50 percent CS_2 and 40°C).

P (atmos)	α	α_D	ψ_1	ψ_{CS_2}
100	−0.86	−1.20	1.065	0.935
500	−0.47	−1.26	1.110	0.890
950	−0.27	−1.27	1.125	0.875
1700	−0.13	−1.44	1.150	0.850
3000	−0.45	−1.72	1.135	0.865
5000	−0.62	−1.97	1.135	0.865
7000	−0.51			

etc., one obtains

$$\alpha=\frac{H_2^*-H_1^*}{RT-X_1\dfrac{\partial F_1^*}{\partial X_1}}, \tag{34}$$

which compares in form to Eq. (11) in so far as one may identify differences of activation quantities with differences in the heats of transport and thermodynamic properties.

TABLE VII. Measured and calculated coefficients for the system carbon disulfide-bromobenzene (50 percent CS_2 and 40°C).[a]

P (atmos)	α	α_D	ψ_1	ψ_{CS_2}
100	−0.33	...	...	...
500	−0.43	−1.26	1.110	0.890
1000	...	−1.34	1.110	0.890
1700	−0.36	−1.45	1.130	0.870
3000	−0.60	−1.65	1.115	0.885
4000	−0.76	−1.76	1.105	0.895

[a] A positive value of α denotes that CS_2 goes to the cold wall.

TABLE VIII. Measured and calculated coefficients for the system carbon disulfide-carbon tetrachloride (20 percent CS_2 and 40°C).[a]

P (atmos)	α	α_D	ψ_1	ψ_{CS_2}
100	−0.97	−0.59	0.975	1.085
500	−0.86	−0.70	0.985	1.045
1000	−1.03	−1.00	1.000	1.000
1500		−1.27	1.010	0.965
1800	−1.07			

Measured and calculated coefficients for the system carbon disulfide-carbon tetrachloride (80 percent CS_2 and 40°C)

100	−0.95	−0.51	0.825	1.045
300	−1.12	−0.56	0.855	1.035
1000	−1.11	−0.87	0.945	1.015
1500	−1.18	−1.09	0.975	1.005

[a] A positive value of α denotes that CS_2 goes to the cold wall.

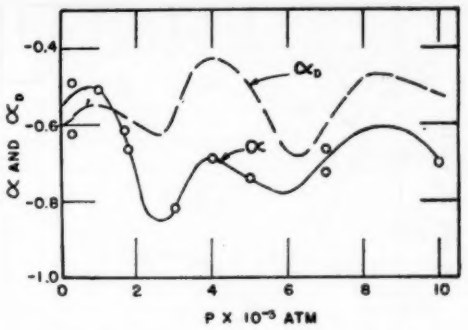

FIG. 3. α and α_D *vs* pressure $CS_2-C_2H_5I$.

C. A Physical Measure of the Quantities H_1 and H_2

A comparison of the equations derived in Sec. (A) above with experiment depends on the identification of the $H_i=-NZW_{ii}$ with macroscopic properties of the pure components. There is no rigorous way to do this. We propose the following measure of H_i

$$H_i=p_i^*(\partial H/\partial p)_i, \tag{35}$$

where

$$p_i^*=[T(\partial p/\partial T)_v]_i, \tag{36}$$

$$\left(\frac{\partial H}{\partial p}\right)_i=\left[V-T\left(\frac{\partial V}{\partial T}\right)_p\right]_i. \tag{37}$$

We present the following arguments for our choice.

(1) H_i as defined goes to zero for an ideal gas. The form of motion we are talking about should not govern transport in an ideal gas.

(2) For a simple molecular model

$$T\left(\frac{\partial p}{\partial T}\right)_v=kT\frac{\partial \ln v_f}{\partial V}, \tag{38}$$

where

$$v_f=\int\int\int_{\text{cell}}\exp\left(\frac{-E(r)}{kT}\right)r^2dr\,\sin\theta d\theta d\varphi.$$

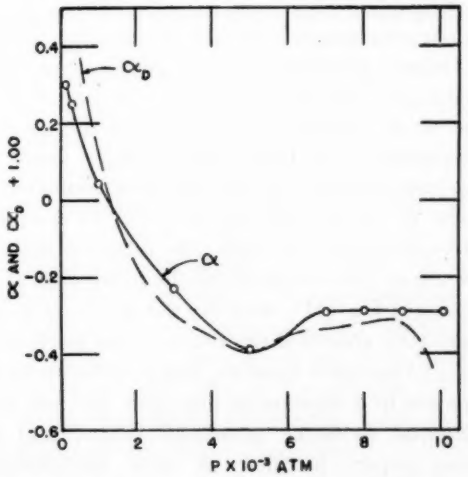

FIG. 4. α and α_D *vs* pressure $CS_2-n\text{-}C_4H_9Cl$.

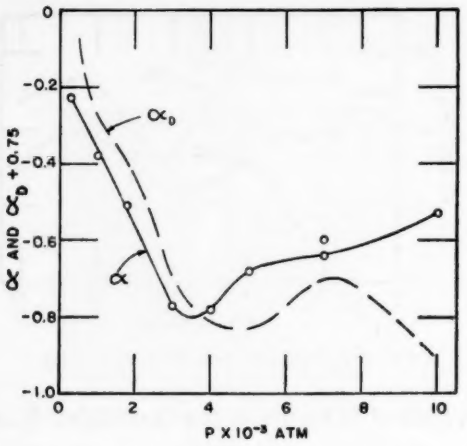

FIG. 5. α and α_D *vs* pressure $CS_2-n\text{-}C_4H_9Br$.

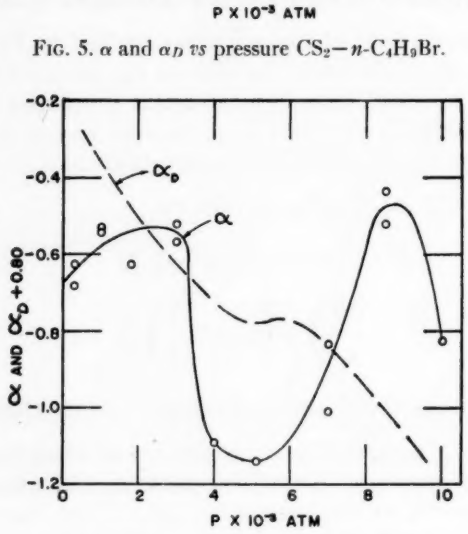

FIG. 6. α and α_D *vs* pressure $CS_2-n\text{-}C_4H_9I$.

$E(r)$ is the potential energy in the cell above the potential at the equilibrium position. This is obviously a quantity sensitive to the form of molecular interaction. Further, Hildebrand, Scott, and others[4] have found $T(\partial p/\partial T)_v$, or an equivalent quantity, a sensitive measure of the solubility of molecules of like size and shape. Prigogine[7,8] first used the cohesive energy density as a qualitative measure of thermal diffusion separation.

(3) Other quantities having similar properties are unsatisfactory. For instance $V^*(\partial E/\partial V)$ where V^* is the volume or an equivalent quantity has the wrong pressure dependence, and becomes negative below 10 000 atmospheres, eliminating the use of the geometric mean. However H_i as defined by (35) fits as well at high pressures as at low. Of course, the ultimate justification for the use of (35) is empirical. In particular, it will be convincing if Eq. (11), with the use of (35) fits the data for essentially spherical molecules of the same size; i.e., if $\psi_1 \cong \psi_2 \cong 1$ for these systems, and if deviations for other systems are in a reasonable direction. We feel that the experimental evidence presented below, and in the following paper, justifies, at least tentatively, our assumption.

EQUIPMENT AND PROCEDURE

The equipment consisted of an apparatus for generating, transmitting and measuring the pressure, a high-pressure bomb, and a thermal diffusion cell which fitted in the bomb.

The intensifier used for pressure generation, was identical with the one described in an earlier paper.[10] The pressure could be measured either directly with a manganin gauge, or with a Bourdon gauge on the low pressure end, which was calibrated against the manganin gauge. For pressures below 2000 atmospheres, a hand pump was used directly, and pressures were measured on a Bourdon gauge calibrated agalnst a dead weight gauge.

The high-pressure bomb (Fig. 1) was 8 inches o.d. with a $\frac{7}{8}$-in. diameter inner hole, with $2\frac{1}{2}$ inches of usable length. The bottom closure was a plug with fine electrical seals. The bomb was immersed in a bath maintained at about 17°C.

The thermal diffusion cell (Fig. 2) was a two chamber device. The chambers were separated by a piece of fine porosity fritted glass one millimeter thick. Pressure was transmitted to the cell through a mercury seal. The cell consisted of a thin-walled stainless steel tube about one

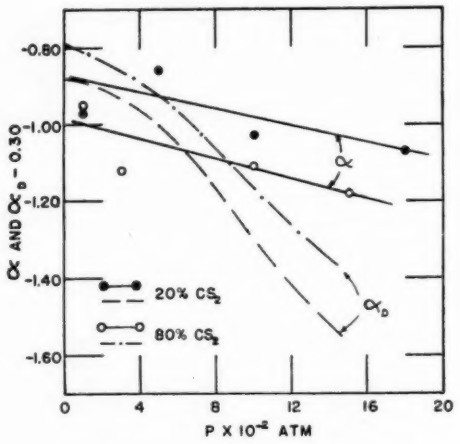

FIG. 7. α and α_D *vs* pressure CS_2-CCl_4.

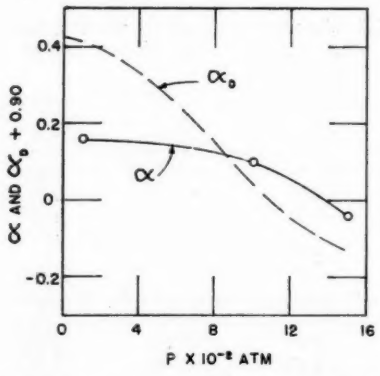

FIG. 8. α and α_D *vs* pressure $CS_2-C_6H_6$.

[10] R. C. Koeller and H. G. Drickamer, J. Chem. Phys. **21**, 267 (1953).

centimeter inside diameter mounted in a cup of mercury. A brass cap, containing the cold chamber, screwed into the top of this tube. The remainder of the cell constituted the hot chamber. The cold side volume was 0.15 cc, the hot side volume was 1.1 cc. The purpose of the large hot side was to minimize remixing effects since a portion of the cold chamber contents passed into the hot chamber upon decompression.

A heater of No. 30 Chromel wire was wound around the lower part of the cell and supplied heat to the lower chamber. It was possible to maintain a 10°C temperature difference across the fritted glass with an average temperature of 40°C.

The cold chamber thermocouple was inserted in a thermowell drilled in a No. 2–56 screw which fitted through the center of the cap. The hot side couple was sealed through two No. 70 holes in the edge of the cap and the junction rested on the lower side of the fritted glass. The cell was mounted on the bottom plug of the bomb, which provided five electrical connections, four for the two thermocouples and one for the heater. The second heater connection was made through ground.

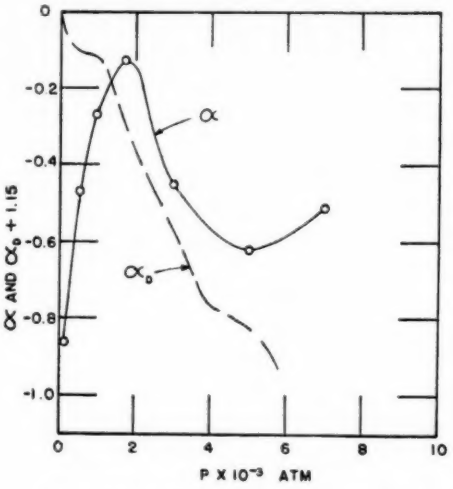

FIG. 9. α and α_D *vs* pressure $CS_2-C_6H_5Cl$.

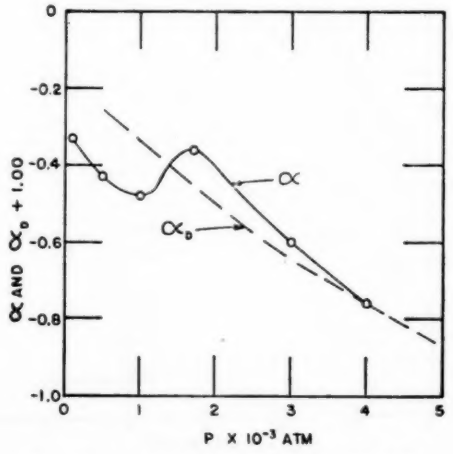

FIG. 10. α and α_D *vs* pressure $CS_2-C_6H_5Br$.

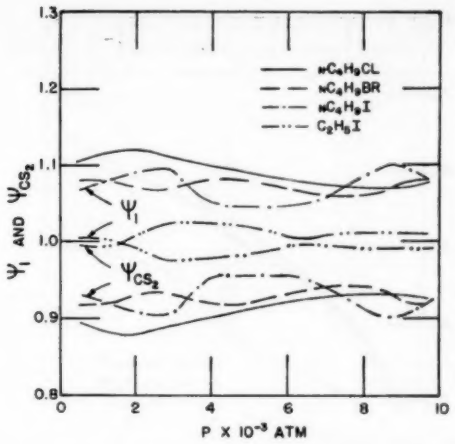

FIG. 11. Steric factors ψ_1 and ψ_{CS_2} *vs* pressure for CS_2-alkyl halide systems.

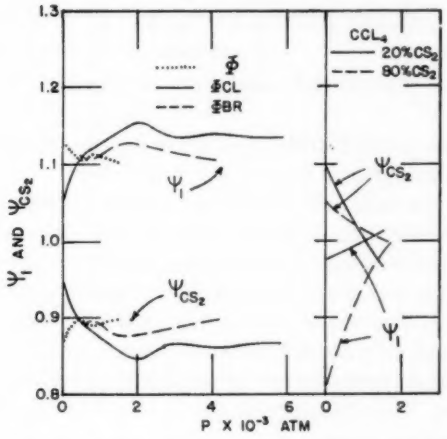

FIG. 12. Steric factors ψ_1 and ψ_{CS_2} *vs* pressure for CS_2-CCl_4, C_6H_6, C_6H_5Cl, C_6H_5Br.

An iron stirrer was placed in each cell. A solenoid was mounted on the top plug in such a manner that, when the apparatus was assembled, the stirrers were in the field of the solenoid. Once each second the solenoid was activated by a dc pulse which lifted the stirrers. The pulse lasted 0.2 second with 0.8 second off-time for the stirrers to fall to their initial positions.

After loading and filling, the cell was allowed to stand several hours at a low pressure to eliminate concentration gradients due to evaporation during loading.

The runs lasted from 3 to 20 hours. Considerable effort was made to insure steady state, and the runs were generally at least four relaxation times. Hot and cold temperatures were recorded throughout the run on a four point 0–5 millivolt recording potentiometer. At the end of the run the bottom plug was removed, and the contents of each chamber analyzed in a Bausch and Lomb precision refractometer. The cell was immersed in water during sampling to eliminate evaporation. The cold side sample was taken by removing the thermowell. Access to the bottom chamber was attained by cutting

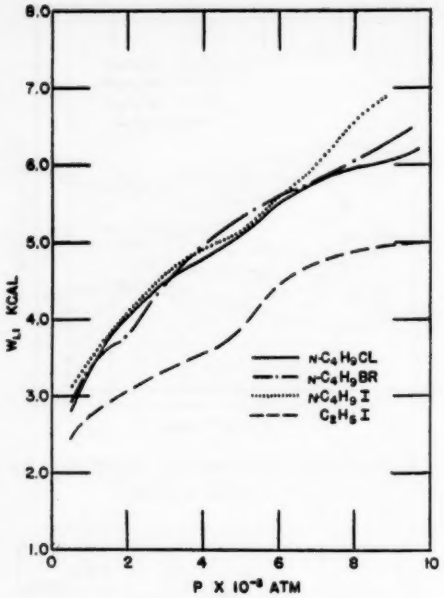

FIG. 13. Hole energies W_{L_1} *vs* pressure.

the thermocouple wires and inserting the hypodermic needle through one hole into the chamber.

Since the cold side thermocouple was in contact with the pressure transmitting fluid, it was necessary to correct the reading to the temperature above the fritted glass. This was done by a special calibration. After this correction was made, the values of α obtained in this cell agreed very closely with the values obtained on an atmospheric pressure cell of considerably different construction. The atmospheric pressure cell is described in the following paper.

The chemicals used were the best grade available and were used directly or with a single redistillation. The carbon disulfide and benzene were Baker and Company reagent grade. The butyl chloride and ethyl iodide were obtained from the Mathieson Company. Eastman Kodak was the source of carbon tetrachloride, chlorobenzene, bromobenzene, butyl bromide, and butyl iodide.

DISCUSSION OF RESULTS

The results are shown in Tables I–VIII and Figs. 3–13. The values of H for the various components were calculated from the PVT of Bridgman.[11] Where possible these were fitted to atmospheric pressure data or low pressure data from various sources. The fit between high pressure and atmospheric data was particularly poor for C_6H_5Cl, and, to a lesser extent CCl_4. In Fig. 14 H_i is plotted *versus* pressure for the various compounds.

A positive value of α denotes that CS_2 goes to the cold wall.

We shall consider first the system $CS_2-C_2H_5I$ (Fig. 3) since these are molecules of approximately the same size and shape. We can see that Eq. (11) for α_D fits the results very closely. As can be seen from Fig. 11, the values of ψ_1 and ψ_2 [from Eq. (17)] vary only slightly from one. This system offers a very satisfactory corroboration of the theory. The data for CCl_4-CS_2 seem to indicate a similar result, although not in such a conclusive manner.

The butyl halide systems all show a deviation from Eq. (11) of about the same magnitude and in the direction which one would expect. The shapes of the curves of α and α_D agree very well for butyl chloride and butyl bromide. There is no obvious explanation for the differing pressure effects on α and α_D for butyl iodide. The average deviation has the correct magnitude.

The values of ψ_1 and ψ_2 (Fig. 11) for the butyl halides are somewhat larger than for ethyl iodide, as might be expected. The values vary only slightly from halide to halide and are essentially independent of pressure. There is a slight tendency for the ψ_1 for butyl chloride to be larger than for butyl bromide, which again is slightly larger than the value for butyl iodide. Apparently the iodide is a little more spherically symmetrical, while the chloride acts more like a straight chain compound.

Figure 12 shows the values of ψ_1 and ψ_2 for the systems $CS_2-C_6H_6$, $CS_2-C_6H_5Cl$, and $CS_2-C_6H_5Br$ as well as CS_2-CCl_4. It is interesting to note that the effective size and shape of "hole" is about the same for all the substituted benzenes.

An attempt was made to study the effect of concentration in the systems CCl_4-CS_2 and $C_4H_9Br-CS_2$. It is difficult to interpret much from the CS_2-CCl_4 data

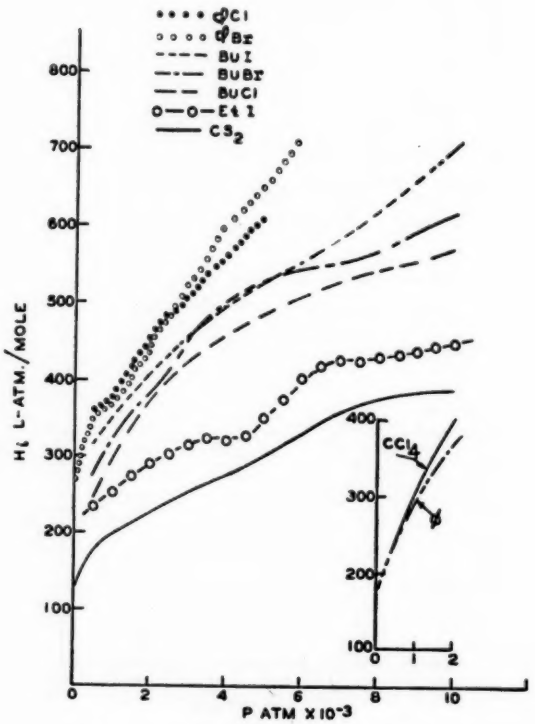

FIG. 14. Cohesive energies *vs* pressure.

[11] P. W. Bridgman, Proc. Am. Acad. 49, No. 1, 4 (1913); 66, No. 5, 185 (1931); 68, No. 1, 4 (1933).

as the H_i for CCl_4 is extrapolated from a higher temperature and there are some discrepancies in it. Further the separations at low CS_2 concentration involved very small differences in refractive index.

For $CS_2-C_4H_9Br$ we note that both ψ_1 and ψ_2 tend to decrease with increasing C_4H_9Br concentration. That is, the number of molecules to fill a hole decreases as the probability of a butyl bromide molecule filling the hole increases. This is physically necessary and it is important to notice it occurs. If the energy released on filling a hole ($\psi_1 W_L$ and $\psi_2 W_L$) is calculated for both molecules as a function of concentration, we find that this quantity increases for both molecules with increasing C_4H_9Br concentration even though the ψ's decrease.

In Fig. 13 are plotted the energies released when a hole is filled ($\psi_1 W_L$) for the alkyl halide systems. We see that the butyl halides all give virtually the same value for this quantity, and that it increases with increasing pressure. This behavior is quite reasonable. As would be expected, C_2H_5I has a considerably smaller value for this "hole energy" than do the butyl halides. The value of $\psi_2 W_L$ (i.e., the energy released when a hole left by a CS_2 molecule is filled) turns out to depend only slightly on the system involved and to increase with pressure, as can be seen from Table IX.

TABLE IX. Hole energies $W_L=\psi(X_1H_1^{\frac{1}{3}}+X_2H_2^{\frac{1}{3}})^2$ for CS_2 (50 percent) in binary mixture with alkyl halides.[a]

P (atmos)	NC_4H_9Cl	NC_4H_9Br	NC_4H_9I	C_2H_5I
950	2.62	2.82	2.98	2.70
1950	3.12	3.35	3.40	3.12
2900	3.56	3.86	3.76	3.51
3900	3.90	4.21	4.32	3.68
4900	4.22	4.49	4.65	3.97
5800	4.63	4.87	5.03	4.49
6800	4.89	5.08	5.30	4.76
7750	5.15	5.29	5.49	4.94
8700	5.24	5.43	5.61	5.03
9700	5.35	5.50	5.95	5.12

[a] Kcal/mole.

On the whole, the results indicate that the theory is quite satisfactory, and, in particular, that the form chosen for the H_i is reasonable.

W. M. Rutherford would like to acknowledge financial assistance from the Standard Oil Company of Ohio and from the U. S. Atomic Energy Commission.

Thermal Diffusion in Binary Liquid Mixtures of Molecules of Simple Symmetry*

R. L. Saxton, E. L. Dougherty, and H. G. Drickamer
Department of Chemical and Chemical Engineers, University of Illinois Urbana, Illinois

(Received January 29, 1954)

A single-stage two-cell apparatus for measuring thermal diffusion in liquid mixtures has been developed. Thermal-diffusion measurements are presented for a series of binary mixtures of molecules of simple symmetry over a range of temperature from 5°–55°C. The theory presented in a previous paper applies quite satisfactorily. The results indicate that the proposed measure of the cohesive energy

$$H_i=\left(T\frac{\partial p}{\partial T}\right)_i\left(V-T\frac{\partial V}{\partial T}\right)_i,$$

gives reasonably quantitative results.

IN the preceding paper[1] a theory of thermal diffusion in liquids was presented. Theory was based on:

(1) The equation for the thermal diffusion ratio derived from the thermodynamics of irreversible processes,

$$\alpha=\frac{Q_2^*-Q_1^*}{X_1(\partial\mu_1/\partial X_1)}. \tag{1}$$

(2) A molecular interpretation of the heats of transport Q^* for regular solutions due to Denbigh[2] which gives

$$\alpha_D=\frac{(X_1H_1^{\frac{1}{3}}+X_2H_2^{\frac{1}{3}})(H_2^{\frac{1}{3}}-H_1^{\frac{1}{3}})}{2[RT-X_1X_2(H_1^{\frac{1}{3}}-H_2^{\frac{1}{3}})^2]}. \tag{2}$$

(3) A modification of the theory to take care of the effect of differences of molecular shape and size giving

$$\alpha=\frac{(X_1H_1^{\frac{1}{3}}+X_2H_2^{\frac{1}{3}})(H_2^{\frac{1}{3}}-H_1^{\frac{1}{3}})+(\psi_1-\psi_2)(X_1H_1^{\frac{1}{3}}+X_2H_2^{\frac{1}{3}})^2}{2[RT(1+X_1X_2(\Delta V/\bar{V})^2)-X_1X_2(H_1^{\frac{1}{3}}-H_2^{\frac{1}{3}})^2}, \tag{3}$$

where ψ_1 is the probable number of molecules of the solution needed to fill a hole left by a type one molecule, with a similar interpretation of ψ_2.

(4) A definition of the H_i in terms of molal properties,

$$H_i=\left(T\frac{\partial p}{\partial T}\right)_i\left[V-T\frac{\partial V}{\partial T}\right]_i. \tag{4}$$

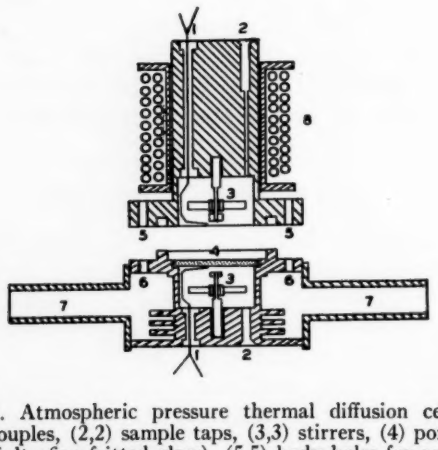

FIG. 1. Atmospheric pressure thermal diffusion cell. (1,1) Thermocouples, (2,2) sample taps, (3,3) stirrers, (4) porous diaphragm (ultrafine fritted glass), (5,5) body holes for connecting screws, (6,6) tapped holes for connecting screws, (7,7) coolant tubes, (8) slip-on electrical heater.

For solutions of molecules of nearly the same size and shape Eq. (2) should apply, i.e., ψ_1 and ψ_2 should be very close to one.

To test these hypotheses runs have been made on a series of binary solutions with molecules of approximately the same size and shape. The mixtures included:

CCl_4 91 percent–CBr_4 9 percent,
$C_2H_2Cl_4$ 92 percent–CBr_4 8 percent,
$C_2H_2Cl_4$ 50 percent–CCl_4 50 percent,
$C_2H_2Cl_4$ 50 percent–$C_2H_2Br_4$ 50 percent,
CCl_4 50 percent–$C_2H_2Br_4$ 50 percent,
$C_2H_4Cl_2$ 50 percent–$C_2H_4Br_2$ 50 percent.
(all compositions are in mole percent).

The chemicals used were Eastman best grade or Matheson best grade.

EXPERIMENTAL PROCEDURE

There have been very few reliable measurements of the thermal-diffusion ratio. The use of a thermal-diffusion column is tempting because large separations are possible, but the complex hydrodynamics make a quantitative calculation of α impossible.

The simplest form of convection free unit is a column of liquid heated at the top. Unfortunately, this system tends to be unstable, particularly if the density gradient due to the concentration gradient is in the opposite direction to that caused by the temperature gradient.

* This work was supported in part by the U. S. Atomic Energy Commission.

[1] W. M. Rutherford and H. G. Drickamer, J. Chem. Phys. (to be published).

[2] K. Denbigh, Trans. Faraday Soc. 48, 1 (1952).

The method can be used for special systems. Particularly elegant versions have been developed by Tanner[3] and by Thomaes.[3a]

For general use a two-cell system separated by a membrane of ultrafine porosity fritted glass has been developed. The problems in the two-cell system are to insure sufficient stirring to guarantee uniform composition in the cells without stirring into the membrane, and to measure the effective average temperature difference across the membrane. The apparatus shown in Fig. 1 appears to have met these requirements. It consists of two cells each with a stirrer activated by a single external magnet. The temperature difference across the fritted glass is measured by thermocouple sealed in each cell. Samples were removed at the sample taps and analyzed in a Bausch and Lomb Precision type refractometer.

TABLE I. Values of α and of the steric factors ψ_1 and ψ_2.

System[a]	Temp	α	α_D[b]	ψ_1	ψ_2
CBr_4[a] 9%–CCl_4[b] 91%	10°	1.76	1.65	1.01	0.998
	25°	1.58	1.50	1.04	0.995
	40°	1.50	1.30	1.035	0.995
	55°	1.42	1.22	1.04	0.995
CBr_4[a] 8%–$C_2H_2Cl_4$[b] 92%	10°	1.2	0.7	0.97	1.005
	25°	1.16	0.63	0.965	1.007
	40°	1.12	0.58	0.96	1.008
	55°	1.08	0.50	0.955	1.01
$C_2H_4Br_2$[a] 50%–$C_2H_4Cl_2$[b] 50%	10°	0.94	0.73	0.975	1.025
	25°	0.90	0.70	0.980	1.020
	40°	0.83	0.67	0.975	1.025
	55°	0.81	0.65	0.97	1.03
$C_2H_2Br_4$[a] 50%–CCl_4[b] 50%	10°	1.8	1.86	1.02	0.98
	25°	1.56	1.75	1.02	0.98
	40°	1.36	1.65	1.04	0.96
	50°	1.23	1.55	1.05	0.95
$C_2H_2Br_4$[a] 50%–$C_2H_2Cl_4$[b] 50%	10°	1.12	1.52	1.045	0.955
	25°	1.00	1.44	1.05	0.95
	35°	0.92	1.38	1.055	0.945
$C_2H_2Cl_4$[a] 50%–CCl_4[b] 50%	25°	0.24	0.92	1.08	0.92

[a] No. 1 compound concentrated at cold wall.
[b] α_D calculated from Eq. (2).

The following tests have been applied to the equipment to insure satisfactory operation.

(1) The apparatus has been operated at ΔT's from 5° to 30°C, at the same average temperature, and the same value for α resulted.

(2) For two systems stable under a temperature gradient the value of α obtained in this equipment checked within 10–15 percent the value obtained in an open column of liquid. The differences were probably in measurement of ΔT.

(3) Essentially the same value of α resulted when the cell was operated horizontally, with the cold side up, or with the cold side down. (This last is the normal mode of operation.)

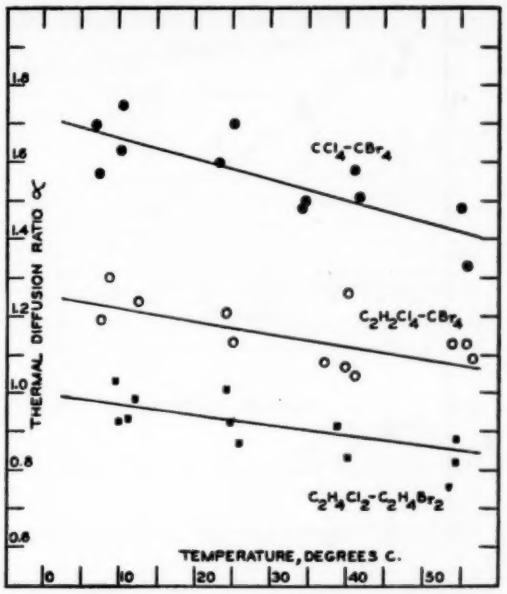

FIG. 2. α *vs* temperature for CCl_4–CBr_4, $C_2H_2Cl_4$–CBr_4, $C_2H_4Cl_2$–$C_2H_4Br_2$.

(4) Some ten to fifteen cells of varying size and shape have been constructed, and these have been taken apart and reassembled numerous times. In general, the check from cell to cell is within 10–20 percent. When the cells are first calibrated with a standard mixture, the results corrected for the calibration show less than half the above spread. The deviations are probably due to small variations in thermocouple location.

(5) The separation obtained was found to be independent of stirrer speed above some minimum value, if ultrafine fritted glass (porosity 5–10 microns) was used. For coarser fritted glass it was found that the higher stirring speeds resulted in convection into or through the membrane.

The standard mixture used was a 50-mole percent mixture of *n*-C_3H_7I and *n*-C_7H_{16}. This system was chosen because of ample separation in refractive index units and the stability against convection in an open column. For this mixture at 27°C $\alpha = 2.0$.

The relaxation time varied from an hour or so to a day or more, depending on cell volume, and diffusion coefficients in the mixture. All points reported were repeated three or four times, and on two or more different cells.

Most of the data were obtained using a ΔT across the frit of about 10°C.

The experimental results are shown in Table I and Figs. 2 and 3. The spread in points is due to the relatively small difference in refractive index between the samples.

The evaluation of the H_i depends on knowledge of the factors $T(\partial p/\partial T)$, V, and $T(\partial V/\partial T)$. Values of

[3] C. Tanner, Trans. Faraday Soc. **23**, 75 (1927).
[3a] G. Thomaes, Physica **17**, 885 (1951).

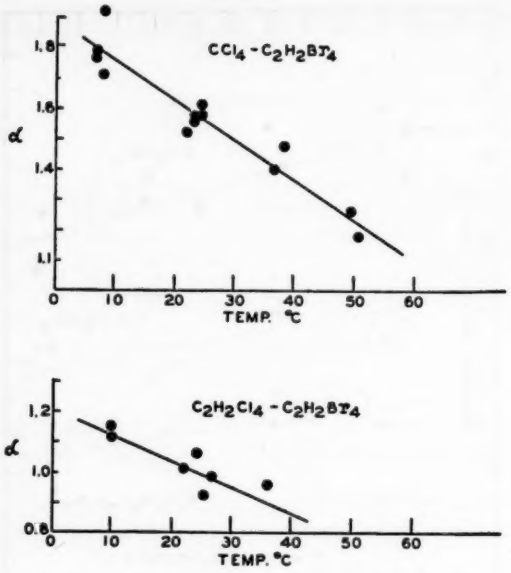

FIG. 3. α *vs* temperature for CCl_4–$C_2H_2Br_4$ and $C_2H_2Cl_4$–$C_2H_2Br_4$.

V and $\partial V/\partial T$ were available for all compounds except CBr_4 which is solid at room temperature. For CBr_4 the values of these variables were estimated by comparing values for CCl_4, $C_2H_2Cl_4$, and $C_2H_2Br_4$ in the liquid and solid states. Direct measurements of $T(\partial p/\partial T)$ were available[4] for CCl_4, $C_2H_4Cl_2$, and $C_2H_4Br_2$. Approximate values can be obtained from vapor pressure data.[5]

$$T\frac{\partial p}{\partial T}\cong\frac{(\Delta E)_v}{V_{\text{liq}}}, \tag{5}$$

where ΔE_v is the energy of vaporization. It was assumed that the relative values obtained in this manner were correct, and the values were corrected to those obtained directly for CCl_4. For $C_2H_2Br_4$ surface tension measurements were used and corrected in the same manner. For CBr_4 the thermal pressure was estimated from solubility measurements as described by Hildebrand.[5] Since these solubility data have not previously been published, they are included in Table II. The cohesive energies are shown in Fig. 4.

From Table I, it can be seen that the values of ψ_1 and ψ_2 do not differ radically from one. In all cases, the correct sign of α is predicted and the magnitude is fairly close for all systems except CCl_4–$C_2H_2Cl_4$.

TABLE II. Solubility of CBr_4 in *n*-octane and methylcyclohexane.

Temp.	Mole Fr CBr_4	Sol. parameter[b]
	CBr_4–*n*-Octane	
0°[a]	0.1932	11.58
25°	0.461	10.85
39.9°	0.7233	10.51
	CBr_4–Methylcyclohexane	
0°[a]	0.1468	11.21
25°	0.3418	10.69
39.9°	0.571	10.43

[a] The 0° solutions were probably not saturated.
[b] $(\text{Cal./cc})^{\frac{1}{2}}$.

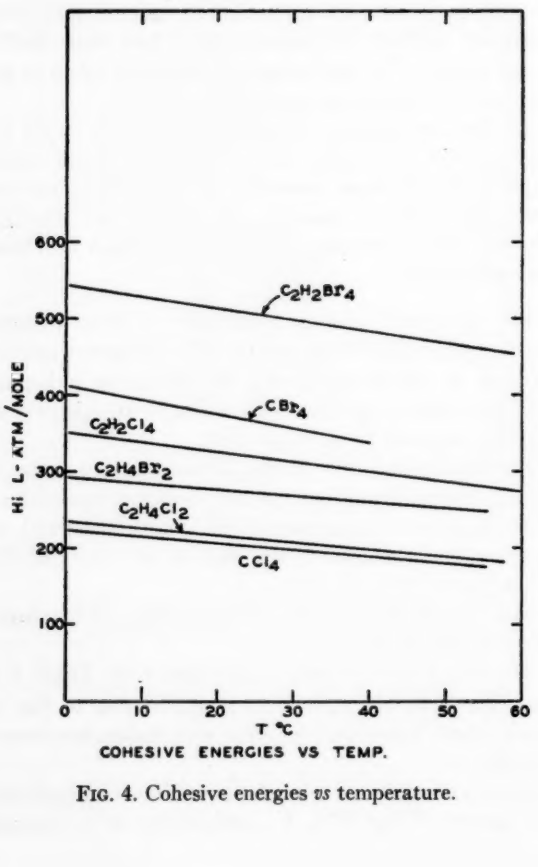

FIG. 4. Cohesive energies *vs* temperature.

Since the cohesive energies for CBr_4, $C_2H_2Br_4$, and $C_2H_2Cl_4$ were obtained in a somewhat indirect manner, it is quite possible that they are not consistent with the values for the other compounds. The agreement in general would be much closer if $C_2H_2Cl_4$ had a lower thermal pressure by about 15 percent and $C_2H_2Br_4$ had a lower thermal pressure by about 20 percent. If this adjustment is made, the calculated α would agree with experiment almost within experimental error except for CCl_4–$C_2H_2Cl_4$. We have no explanation for the deviation found for that system. In general, the theory predicts roughly the correct temperature dependence for α as the values of ψ vary only slightly with temperature.

It is planned to present a more comprehensive test of the theory in future papers.

R. L. Saxton would like to acknowledge a fellowship from E. I. du Pont Company. E. L. Dougherty would like to acknowledge a fellowship from the Pan American Refining Corporation.

[4] Westwater, Franz, and Hildebrand, Phys. Rev. **31**, 135 (1928).
[5] J. H. Hildebrand and R. L. Scott, *Solubility of Nonelectrolytes* (Reinhold Publishing Corporation, New York, 1950).

Infrared Study of the Effect of Solvent upon ν(NH) in Pyrrole

MARIE-LOUISE JOSIEN AND NELSON FUSON
Université de Bordeaux, France and Fisk University, Nashville, Tennessee

(Received January 28, 1954)

New data are presented on the NH group stretching frequency of pyrrole in dilute and concentrated solutions in fourteen different solvents and in several solvent mixtures. It is shown that in nonpolar solvents ν(NH) of pyrrole obeys the Kirkwood-Bauer relationship, $\delta\nu/\nu = C(D-1)/(2D+1)$, where C is a constant, and D is the solvent dielectric constant. Furthermore, it is shown that C is only slightly affected as ν(HCl) of hydrochloric acid, ν(OD) of methanol-*d*, or ν(OH) of methanol, ethanol, propanol, or phenol is substituted for the ν(NH) of pyrrole. The deviations from the Kirkwood-Bauer relationship produced by polar solvents and aromatic hydrocarbon solvents are analyzed in terms of hydrogen bonding and the formation of molecular complexes. The effect of solvent upon band intensity is also briefly examined. A classification of types of OH and NH solution frequencies is suggested.

I. INTRODUCTION

WE recently reported an investigation of the NH stretching vibration and N—H···N hydrogen bonding of pyrrole and other aromatic compounds.[1,2] Shortly after we submitted this work for publication, Jones and Badger's[3] report on the influence of solvent dielectric constant upon the infrared spectrum of methanol was published. This prompted us to make a similar study of the effect of solvent upon the NH vibration in pyrrole and to draw a comparison with methanol,[3] methanol-*d*,[4] ethanol,[5] propanol,[6] phenol,[7] and hydrochloric acid[8] results. We believe that this paper also contains the answer to the questions on our previous paper[1] raised by Tuomikoski[9] and referred to by Linnell.[10]

II. EQUIPMENT

This work has been done on the Fisk University single beam infrared spectrometer which has been described elsewhere.[1,11] A lithium fluoride prism was used for all this work. Sharp band positions in the 3000 cm^{-1} region could be determined to within ± 1 or ± 2 cm^{-1}. Cells used ranged in thickness from 0.01 mm to 10 mm. For the thinner cells aluminum foil spacers were used; for the thicker cells lead spacers proved most satisfactory. In each case rock salt cell windows were sealed to the spacers with Glyptol cement or with Bonding Agent R-313.

III. EXPERIMENTAL RESULTS

Table I contains the pyrrole ν(NH) data in fairly concentrated solutions (2, 4, and 8 molar) and in dilute solution (0.013 molar). Solvents used in this study included *n*-hexane, cyclohexane, carbon tetrachloride,[12] chloroform, carbon disulfide, 1,2-dichloroethane, benzene, toluene, *m*-xylene, mesitylene, nitrobenzene, acetone, acetophenone, and pyridine. Generally these were commercial solvents of the highest purity available. Several were specially purified for us.

Acetone, acetophenone, and pyridine are solvents which absorb very strongly in the spectral region where ν(NH) of pyrrole is expected. Satisfactory spectra of the NH band for concentrated pyrrole solutions in these solvents could be obtained in 0.01-mm and 0.02-mm cells. To obtain ν(NH) for dilute solutions of pyrrole requires cells about 1.0 mm in thickness. For this cell thickness these solvents were opaque. As a means of avoiding this difficulty dilute pyrrole spectra for these solvents were obtained in a solvent mixture of, for example, one part acetone to ten parts CCl_4. The results of these mixed solvent spectra are also included in the 0.013 molar column of Table I.

The solvent effects upon the pyrrole NH bands of a 1:1 mixture of toluene and CCl_4 and of 1:1 and 10:1 mixtures of CCl_4 with nitrobenzene and with dichloroethane were also studied. The results are given in Table I.

The spectrum of pyrrole in the vapor state was measured, the room temperature pyrrole vapor being studied both at 2-mm Hg pressure in a 150-mm cell and at 7-mm Hg pressure in a 100-mm cell. The N—H

[1] Fuson, Josien, Powell, and Utterback, J. Chem. Phys. **20**, 145 (1952).
[2] M. L. Josien and N. Fuson, Compt. rend. **232**, 833 (1951).
[3] L. H. Jones and R. M. Badger, J. Am. Chem. Soc. **73**, 3132 (1951).
[4] S. Searles and M. Tamres, J. Am. Chem. Soc. **73**, 3704 (1951); M. Tamres, J. Am. Chem. Soc. **74**, 3375 (1952); and Searles, Tamres, and Barrow, J. Am. Chem. Soc. **75**, 71 (1953).
[5] P. Tuomikoski, Suomen Kemistelehti **B23**, 44 (1950); the English abstract of this paper, Chem. Abstracts **45**, 38 (1951), unfortunately omits any reference to Tuomikoski's application of the Kirkwood-Bauer relationship to his ethanol results.
[6] A. Stuart, J. Chem. Phys. **21**, 1115 (1953).
[7] W. Luttke and R. Mecke, Z. Electrochem. **53**, 241 (1949); R. Mecke, Discussions Faraday Soc. **9**, 161 (1950).
[8] W. West and R. T. Edwards, J. Chem. Phys. **5**, 14 (1937); W. West, J. Chem. Phys. **7**, 795 (1939).
[9] P. Tuomikoski, J. Chem. Phys. **20**, 1054 (1952).
[10] R. H. Linnell, J. Chem. Phys. **21**, 179 (1953).
[11] Josien, Fuson, and Cary, J. Am. Chem. Soc. **73**, 4445 (1951).
[12] B. M. Zeshulinskij, Zhur. Fiz. Khim. **24**, 1442 (1950). This reference, which is devoted to the 2nd harmonic of the pyrrole (NH) frequency in various solvents, does quote values of the fundamental ν(NH) for pyrrole in CCl_4 solution (3500 cm^{-1}) and for pure liquid pyrrole (3410 cm^{-1}). The frequency shifts he speaks of are those between the CCl_4 solution frequency and the frequency in other solutions rather than the $(\nu_v - \nu_s)$ used by us.

TABLE I. N—H stretching frequencies of pyrrole in different solvents and mixtures of solvents.

Solvent name	Solvent structure	N—H frequencies (cm^{-1}). 0.013 molar	2.0 molar	4.0 molar	8.0 molar
n-hexane	C_6H_{14}	3500	3498, 3406		
Cyclohexane	C_6H_{12}	3498	3498, 3402		
Carbon tetrachloride	CCl_4	3497[a]	3493, 3409		
Chloroform	$CHCl_3$	3486[a]	3484, 3411		
Carbon disulfide	CS_2	3481[a]	3476, 3401		
1,2-dichloroethane	$C_2H_4Cl_2$	3465	3463, 3403		
10% dichloroethane—90% CCl_4		3496			
50% dichloroethane—50% CCl_4		3476			
Benzene	C_6H_6	3458[a]	3453, 3400		
Toluene	$C_6H_5CH_3$	3448	3445, 3408[b]	3440, 3403	
50% toluene—50% CCl_4		3491, 3455			
m-xylene	$C_6H_4(CH_3)_2$	3445	3443		
Mesitylene	$C_6H_3(CH_3)_3$	3439	3430		
Nitrobenzene	$C_6H_5NO_2$	3449	3448	3442[c]	3435[c]
10% nitrobenzene—90% CCl_4		3490, 3450			
50% nitrobenzene—50% CCl_4		3450[c]			
Acetone	CH_3COCH_3		3395		
10% acetone—90% CCl_4		3492, 3390[c]			
Acetophenone	$C_6H_5COCH_3$		3389		
10% acetophenone—90% CCl_4		3492, 3405[c]			
Pyridine	C_5H_5N		3219		
10% pyridine—90% CCl_4		3493, 3250[c]			
Pyrrole (pure liquid)	C_4H_4NH				3395[d]

[a] Frequency taken from Table IV of reference 1.
[b] Shoulder.
[c] Broad band.
[d] Pure pyrrole is 14.4 molar; band is broad; frequency taken from Table I of reference 1.

valence vibration band for pyrrole vapor was found at 3530 ± 3 cm^{-1}.[13]

The differences between the pyrrole vapor NH frequency and the different pyrrole NH frequencies in dilute solution range from 30 cm^{-1} to 280 cm^{-1}. Thus, the corresponding relative frequency shifts, in going from vapor to solution, range from less than 1 percent to almost 8 percent.

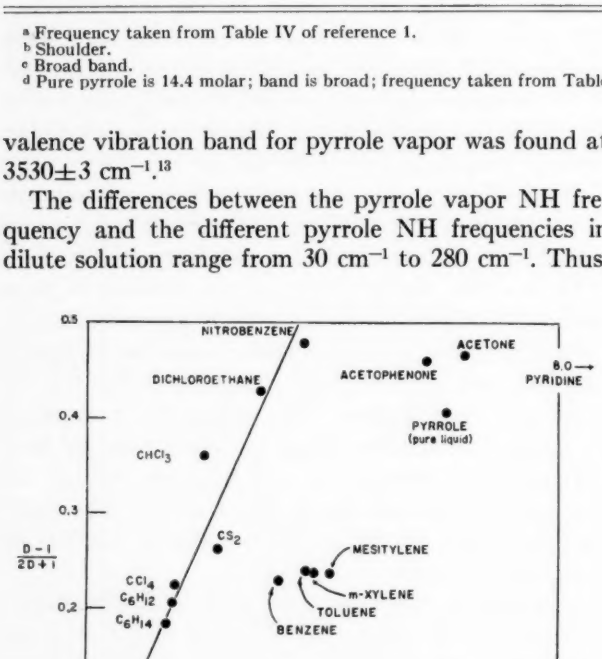

FIG. 1. Relative frequency shift of ν(NH) of pyrrole in dilute solution and of pure liquid pyrrole as a function of the dielectric constant of the solvent.

[13] This vapor NH frequency differs slightly from the preliminary measurement of this frequency, 3535 cm^{-1}, which this laboratory previously reported (N. Fuson, and M. L. Josien, J. Chem. Phys. **20**, 1043 (1952)). Tuomikoski (see reference 9) also uses the value of 3530 cm^{-1} in constructing the middle curve of his Fig. 1.

IV. DISCUSSION OF DILUTE SOLUTIONS

It is well known that the position of a particular absorption band in the vibration spectrum of a compound in solution is found at lower frequencies than the same band for the compound in the vapor state, but very little experimental study has been made of the magnitude of this effect in particular solvents.[1,3,4,6–9] Kirkwood,[14] and a year later Bauer and Magat[15] derived the following expression for the vibrational frequency shift of an oscillating dipole when the shift results from instantaneously induced polarization of the surrounding medium by the vibrating dipole

$$(\nu_v-\nu_s)/\nu_v=C(D-1)/(2D+1),$$

where ν_v and ν_s are the frequencies of the particular infrared absorption band measured in the vapor and solution states, respectively, C is a constant which depends upon the dimensions of the solute molecule and on the details of the dipole model,[8] and D is the dielectric constant of the solvent.

Figure 1 is a graph of $(\nu_v-\nu_s)/\nu_v$ *versus* $(D-1)/(2D+1)$ for pyrrole. The data upon which this figure is based are tabulated in Table II. The 0.013 molar solutions were dilute enough[1] so that no trace remained of

[14] J. G. Kirkwood's analysis is first referred to in the literature in reference 8.
[15] E. Bauer and M. Magat, J. phys. radium **9**, 319 (1938).

the absorption band resulting from pyrrole-pyrrole interaction. The dielectric constants taken from the literature are for the solvents at approximately the temperature of the samples while the spectra were being obtained. The vapor frequency point is, of course, at the origin since the relative shift is zero, and since $(D-1)/(2D+1)$ for vapors (dielectric constant approximately unity) is also zero.

Jones and Badger's frequency data[3] for the shift of the third harmonic of the hydroxyl stretching frequency of methanol in different solvents has been changed to relative frequency shifts, recorded in Table II, and

TABLE II. Relative frequency shifts of NH, OH, OD, and HCl stretching vibrations of the solute as a function of dielectric constant of the solvent.

Solvent Name	Structure	D[a]	$\frac{D-1}{2D+1}\times 10^3$	$(\nu_v-\nu_s)/\nu_v\times 10^2$ ν(NH) Pyrrole[b]	3ν(OH) Phenol[c]	3ν(OH) Methanol[d]	ν(OH) Ethanol[e]	ν(OH) Propanol[f]	2ν(HCl) Hydrochloric acid[g]	ν(OD) Methanol-d[h]
n-hexane	C_6H_{14}	1.88	183	0.85		0.84	1.16			
Cyclohexane	C_6H_{12}	2.04	205	0.91	1.07	0.94				
Cyclohexene	C_6H_{10}	2.22	224		1.07 4.80					
Carbon tetrachloride	CCl_4	2.23	225	0.94	1.17	1.03	1.27	0.98	1.73	1.14
Benzene	C_6H_6	2.27	229	2.04	1.17 2.65	2.02	1.47			2.02
Tetrachloroethylene	C_2Cl_4	2.29	231		1.21			1.09		
Mesitylene (1,3,5-trimethylbenzene)	$C_6H_3(CH_3)_3$	2.34	236	2.58		1.27 3.20				2.40
m-xylene (1,3-dimethylbenzene)	$C_6H_4(CH_3)_2$	2.36	237	2.41		1.20 2.77				2.20
Toluene (methylbenzene)	$C_6H_5CH_3$	2.37	239	2.32	1.17 2.99	1.42 2.14				2.10
Pseudocumene (1,2,4-trimethylbenzene)	$C_6H_3(CH_3)_3$	2.41	242			1.04 2.85				
α-Methyl naphthalene	$C_{10}H_7CH_3$	2.6	258			2.30				2.17
Carbon disulfide	CS_2	2.64	261	1.39	1.60		1.68	1.44	0.42	
Trichloroethylene	C_2HCl_3	3.43	309		1.40					
Phosphorus trichloride	PCl_3(20°C)	3.43	309						1.98	
Pentachloroethane	C_2HCl_5	3.55	315		1.60	1.27		1.44		
Phosphorus trichloride	PCl_3(−65°C)	4.20	340						2.36	
Diethyl ether	$(C_2H_5)_2O$	4.33	345		7.20					4.67
Anisol	$C_6H_5OCH_3$	4.37	346		3.08					
Chloroform	$CHCl_3$	4.85	360	1.25	1.50	1.38		1.55		
Chlorobenzene	C_6H_5Cl	5.69	379		1.93					
1,2-dichlorobenzene	$C_6H_4Cl_2$	7.47	405							1.62
1,1,2,2-Tetrachloroethane	$C_2H_2Cl_4$	7.61	407			1.48				1.91
Dichloromethane	CH_2Cl_2	8.3	414					1.66		
1,2-Dichloroethane	$C_2H_4Cl_2$	10.0	428	1.84						
Pyridine	C_5H_5N	12.5	443	8.0						
Phosphorus oxychloride	$POCl_3$(20°C)	12.7	443						2.64	
Acetophenone	$C_6H_5COCH_3$	18.0	459	3.6	5.56					
Benzaldehyde	C_6H_5CHO	18.0	459		5.09					
Acetone	$(CH_3)_2CO$	21.5	466	4.0	8.20		3.46			4.04
Sulfur dioxide	SO_2	22.4	467						2.74	
Nitrobenzene	$C_6H_5NO_2$	33.7	478	2.30	3.18					
Nitromethane	CH_3NO_2	39.4	480		2.80					
Pyrrole (pure liquid)	C_4H_4NH	7.48	406	3.82						
$[(\nu_v-\nu_s)/\nu_v]/[(D-1)/(2D+1)]$[i]				0.044	0.46	0.052	0.060[j]	0.044	0.07	

[a] The values of the dielectric constants for these solvents at about 20–30°C were taken from the International Critical Tables (reference 3), or from references 7 and 11, with the following exceptions: pyrrole from R. Freymann, Compt. rend **202**, 952 (1936); pyridine and 1,2-dichlorobenzene from *Handbook of Chemistry and Physics* (Chemical Rubber Publishing Company, Cleveland, Ohio, 1952), 34th Edition, page 2163; and 1,2-dichloroethane from Walden, Ulich, and Werner, Z. physik. Chem. **116**, 261 (1925).

[b] Pyrrole relative frequency shifts calculated from solution frequencies given in Table I, using ν(NH) of pyrrole vapor = 3530 cm^{-1} (see discussion in text).

[c] Phenol relative frequency shifts calculated from solution frequencies given in reference 7, using 3ν(OH) of phenol vapor = 10 452 cm^{-1}, this being both the position of the Q branch and the center of the complex absorption band given in reference 16.

[d] Methanol relative frequency shifts calculated from $(\nu_v-\nu_s)$ data in reference 3, using 3ν(OH) of methanol vapor = 10 537 cm^{-1} as given in reference 3. Note that this is the center of the "smoothed out" PQR absorption band structure (rather than the frequency of the Q branch, 10 531 cm^{-1}) given in reference 16.

[e] Ethanol relative frequency shifts calculated from solution wavelengths given in reference 5, using 3ν(OH) of ethanol vapor = 10 536 cm^{-1}. This vapor frequency was obtained by measuring the center of the "smoothed out" absorption pattern given in reference 16. This frequency differs by 21 cm^{-1} from that of the Q branch, 10 515 cm^{-1}, given in reference 16. This Q-branch frequency was used by Tuomikoski in reference 5. The use of 10 515 cm^{-1} in the present case would change the K-B line inverse slope from 0.060 to 0.065.

[f] Propanol relative frequency shifts calculated from solution frequencies given in reference 6, using ν(OH) of propanol vapor = 3680 cm^{-1}, given by the same reference. If the vapor frequency of 3687 cm^{-1}, given by E. K. Plyler, J. Research Natl. Bur. Standards **48**, 281 (1952), is used, it changes the K-B line inverse slope from 0.044 to 0.052.

[g] Hydrochloric acid relative frequency shifts taken directly from reference 8, which used 2ν(HCl) for hydrochloric acid vapor = 5668 cm^{-1}.

[h] Methanol-d relative frequency shifts calculated from solution frequencies given in reference 4, using ν(OD) of methanol-d vapor = 2720 cm^{-1}, given in reference 17.

[i] This ratio is equal to the proportionality constant C of the Kirkwood-Bauer relationship and is the inverse of the K-B line slope as drawn in the figures in this paper.

[j] P. Tuomikoski (reference 5) has drawn attention to the similarity between this slope and that for HCl.

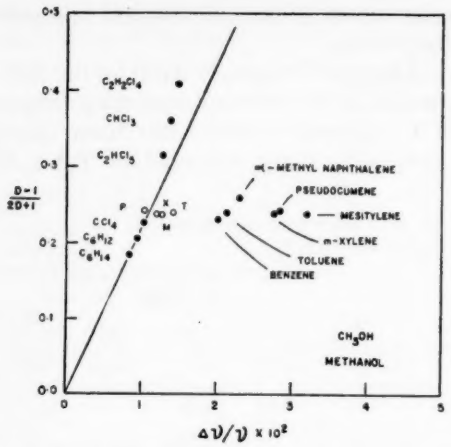

FIG. 2. Relative frequency shift of ν(OH) of methanol in dilute solution as a function of the dielectric constant of the solvent. The open circles labeled *P*, *X*, *M*, and *T* mark the high-frequency components of the methanol ν(OH) doublet band in pseudocumene, *m*-xylene, mesitylene, and toluene solvents, respectively.

plotted in Fig. 2 for comparison purposes. Luttke and Mecke's[7] phenol data on the third harmonic of ν(OH) has been processed in like manner, tabulated in Table II and plotted in Fig. 3. Table II also presents the relative frequency shifts calculated from Stuart's[6] propanol data on the OH fundamental, Tuomikoski's[5] ethanol data on the third harmonic of ν(OH), West and Edward's[8] hydrochloric acid data for the second harmonic of ν(HCl), and Searles, Tamres, and Barrow's[4] methanol-*d* data on the OD fundamental. Vapor frequencies reported by Badger and Bauer[16] were used in conjunction with the third harmonic solution data for methanol, phenol, and ethanol. The fundamental OD vapor frequency for the methanol-*d* was taken from Barker and Bosschieter.[17]

Nonpolar Solvents

The most striking similarity in the three compounds illustrated in Figs. 1 through 3 is that for each the line drawn from the origin (the vapor frequency point) through most of the nonpolar solvent points is approximately a straight line. The nonpolar solvent line on these graphs will henceforth be called the Kirkwood-Bauer or K-B line.

The K-B lines for methanol and phenol also pass through the points, shown as open circles in Figs. 2 and 3, corresponding to the higher-frequency member of the doublet bands observed for these compounds dissolved in aromatic solvents. The interpretation of the doublet nature of these bands will be discussed in a later section of this paper.

CS_2 is the one nonpolar solvent[18] whose point does not fall on the K-B line. This is true in all five cases (see Table II) for which CS_2 was used as a solvent. This CS_2 point lies about the same distance to the right of the K-B line for pyrrole, ethanol, propanol, and phenol. For hydrochloric acid, however, this CS_2 point falls to the left side of the line.

The results for pyrrole, phenol and pentanol given in Table II materially extend the experimental basis for the Kirkwood-Bauer relationship between relative frequency shift and dielectric constant of nonpolar solvents. It is now clear that this relationship holds to a first approximation for dipoles composed of HCl, OH, OD, and NH.

Additional evidence for the validity of the Kirkwood-Bauer relationship may be obtained from the study of the NH frequency of pyrrole in dilute solution when the solvent is a mixture of nonpolar liquids of very different dielectric constant. A qualitative example of this, given in Table I and Fig. 4C, is for 1,2-dichloroethane: CCl_4 mixtures.[19] For a 1:1 mixture of dichloroethane and CCl_4 (curve *b*), the band is single and sharp and is shifted to 3476 cm^{-1}, a frequency about midway between that for pyrrole in the two solvents separately (curves *a* and *c*). This is what is to be expected if it is assumed that the frequency for nonpolar solvents is a function only of $(D-1)/(2D+1)$, the 1:1 mixture giving a dielectric constant which is the average of that for dichloroethane and CCl_4. In a 1:10 dichloroethane: CCl_4 solvent mixture (curve *a*), the single NH band shifted slightly, if at all, from the NH-band position for pure CCl_4 solvent. This is consistent with the very small change of solvent dielectric constant from that of pure CCl_4, and with the hypothesis that there is no complex formed between dichloroethane and pyrrole.

Polar Solvents

In addition to the nonpolar points which fall close to the K-B lines, in each case illustrated in Figs. 1 through 3 there are many polar solvent points as well as aromatic points. Factors responsible for the scattering of these points will now be considered.

Pyridine

The solvent causing the largest pyrrole NH shift is pyridine. In contrast to the results previously mentioned for pyrrole in dichloroethane: CCl_4 solvent mixtures, as can be seen from Table I, the 10 percent

[16] R. M. Badger and S. H. Bauer, J. Chem. Phys. **4**, 711 (1936).
[17] E. F. Barker and G. Bosschieter, J. Chem. Phys. **6**, 563 (1938).
[18] There is still some discussion about the possibility of the CS_2 molecule not being entirely symmetrical in the liquid state. See, for example, G. Herzberg, *Infrared and Raman Spectra* (D. Van Nostrand Company, Inc., New York, New York, 1945), p. 276.
[19] Discussion has arisen concerning the polarity or nonpolarity of 1,2-dichloroethane. It seems to us possible, as a first approximation, to consider that in this case 1,2-dichloroethane may be included along with the nonpolar solvents. (See discussion given by G. Herzberg, reference 18, pp. 346–351.) *Note added in proof.*—In contradiction to the preceding footnote statement, the work of J. K. Brown and N. Sheppard, Trans. Faraday Soc. **48**, 128 (1952), shows conclusively that both the *cis*- and *trans*-forms of 1,2-dichloroethane exist in the liquid at room temperature, and thus that liquid dichloroethane is not a simple nonpolar solvent. We give a revised interpretation of the experimental data on pyrrole in CCl_4-dichloroethane mixtures in a Letter to the Editor of the J. Chem. Phys. (to be published shortly).

pyridine in CCl_4 solvent gave two pyrrole ν(NH) bands, the higher-frequency band being at approximately the same position as that for pure CCl_4. The second and much broader band, at 3250 cm^{-1}, is assigned to the ν(NH) in a complex resulting from N—H···pyridine hydrogen bonding. This shift for pyrrole in pyridine (8.0 percent) is so large compared to that for pyrrole-pyrrole interaction in pure liquid pyrrole (3.8 percent), that a very stable complex is probably formed. Linnell, who has pointed out this large shift, states that a 1:1 complex is compatible with his results obtained in comparing intensities of the bands assigned to pyrrole, to pyridine, and to the pyrrole-pyridine complex, respectively.[10]

Oxygenated Solvents

With the exception of nitro compounds, e.g., $C_6H_5NO_2$, all oxygenated solvent points fall far to the low-frequency side of the K-B line. The relative frequency distance from the K-B line for these compounds ranges from 3 percent to 8 percent. We interpret this shift as resulting from hydrogen bonding between the OH and OD (or the NH) of phenol and of ordinary and heavy methanols (or of pyrrole) and the oxygen atom in the solvent. In the case of pyrrole an added proof is presented by a mixed solvent study using acetone: CCl_4 and acetophenone: CCl_4, the results (see Table I) being very similar to that just described for pyridine.

Gordy, who has found relations between frequency shifts of this kind and the basicity of the solvent,[20] has used frequencies measured in benzene solution as the reference point from which to measure the shift. More recently others[4,12] have chosen CCl_4 solution frequencies as a reference. Throughout the work in this paper we have chosen the vapor frequency as the reference point. If solvents of widely different dielectric constants are used, this variety of choice of reference points might cause the question to be raised as to which of the following two types of reference points should be used: a fixed point such as that for the vapor, the benzene solution, or the CCl_4 solution; or the point on the K-B line having the same ordinate as the solvent point under consideration. The N—H band found when pyrrole-pyrrole bonding of the N—H···N type is present remains fixed in position within the limit of error and is not influenced by the dielectric constant of the solvent,[1] the same being true for the NH band position in both N—H···pyridine bonding and in N—H···O bonding. We are convinced, therefore, that the reference should be one of the fixed points, rather than the K-B line. Since shifts measured from the vapor point will always be toward lower frequencies, this vapor point has advantages over the use of an inert, nonpolar solvent frequency point.

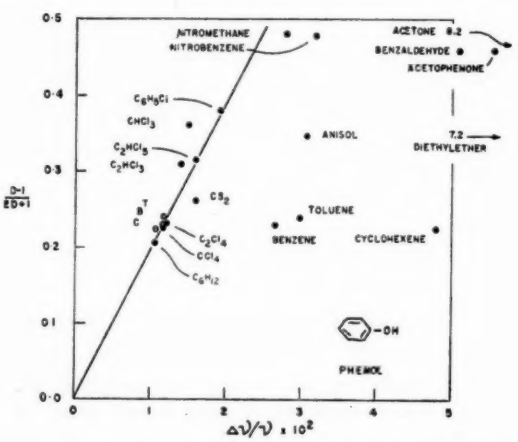

FIG. 3. Relative frequency shift of ν(OH) of phenol in dilute solution as a function of the dielectric constant of the solvent. The open circles labeled *T*, *B*, and *C* mark the high-frequency components of the phenol ν(OH) doublet band in toluene, benzene, and cyclohexene solvents, respectively.

[20] W. Gordy, J. Chem. Phys. **9**, 215 (1941), and previous papers by Gordy in the same journal.

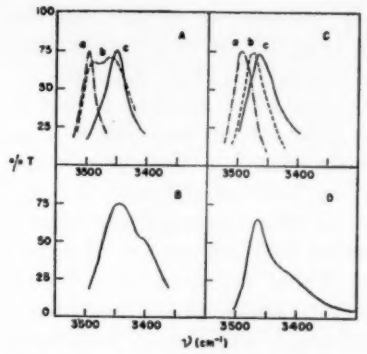

FIG. 4. Effect of solvent and of solvent concentration upon the NH frequency of pyrrole. A. 0.013-molar pyrrole in: a. CCl_4; b. 50 percent toluene–50 percent CCl_4 mixture; c. toluene. B. 2.0-molar pyrrole in toluene. C. 0.013-molar pyrrole in: a. 10 percent dichloroethane–90 percent CCl_4 mixture; b. 50 percent dichloroethane–50 percent CCl_4 mixture; c. dichloroethane. D. 2.0 molar-pyrrole in dichloroethane.

Nitrobenzene

The point for the solvent nitrobenzene in Fig. 1 appears as an exception to the general rule for oxygenated compounds. It falls almost exactly on the K-B line thus indicating that it behaves at first sight like a nonpolar solvent, in spite of the NO_2 group being present. One possible explanation is that the nitrobenzene molecules are in the form of dimers,[21] the active dipoles being buried in the center of the double molecule in such a way as to make it essentially nonpolar. In order to test this hypothesis a study of pyrrole ν(NH) was made in mixed solvents (see Table I). The 1:10 nitrobenzene: CCl_4 solvent mixture shows two bands, at 3490 cm^{-1} and 3450 cm^{-1}, in a manner similar to that for acetone: CCl_4 mixture, thus disproving the nonpolar hypothesis. Anticipating at this point a discussion coming later in this paper, it can be pointed out that the appearance of pyrrole's NH band in this 1:10 nitro-

[21] A. Rousset and R. Lochet, J. phys. radium **13**, 289 (1952). This paper contains a bibliography of the different approaches used in proving the dimerization of nitrobenzene.

benzene: CCl_4 mixture is similar to that for 1:1 toluene: CCl_4 (Fig. 4A, curve b) rather than to that for 1:1 dichloroethane: CCl_4 (Fig. 4C, curve b). The alternative explanation which remains is that nitrobenzene behaves as a polar solvent and that it is just a coincidence that the band shift is the same as would have been obtained on the basis of the nonpolar hypothesis. A further check on this conclusion can be obtained from the concentrated solution spectra of pyrrole in nitrobenzene (see Table I). Even in 4.0 and 8.0-molar concentrations the center of the broad band is at 3442 cm^{-1} and 3435 cm^{-1}, respectively, indicating that most of the pyrrole molecules are bound with the nitrobenzene.

Chlorinated Solvents

Jones and Badger[3] pointed out that for methanol the chlorinated solvent ν(OH) points fall on another straight line branching off the K-B line upwards and to the left. They suggest that this is a result of hydrogen bonding of the solvent hydrogen with the hydroxyl oxygen atom. The position relative to the K-B line of the chlorinated solvent ν(OH) point for propanol are very similar to those for methanol, but the other solvents, particularly phenol (Fig. 3), do not show chlorinated solvent points to fall into such a regular sequence. More experimental work is being done in order to be able to contribute further to an understanding of this phenomenon.

Aromatic Solvents and Cyclohexene

The graph points for pyrrole in the aromatic solvents also lie far to the low-frequency side of the K-B line, indicating that there is interaction between the NH group and neighboring aromatic solvent molecules. Added proof for this conclusion is given by a mixed solvent study using toluene and CCl_4 (see Table I). Just as in the case of pyridine and the oxygenated solvents, in a 1:1 toluene: CCl_4 mixture, as seen in Fig. 4, curve b, two bands are found in the ν(NH) region. The higher-frequency band at 3492 cm^{-1} is assigned, on the basis of curve a, to ν(NH) for pyrrole molecules in a CCl_4 environment. On the basis of curve b the lower-frequency band at 3445 cm^{-1} is assigned to ν(NH) for pyrrole hydrogen bonded to toluene.

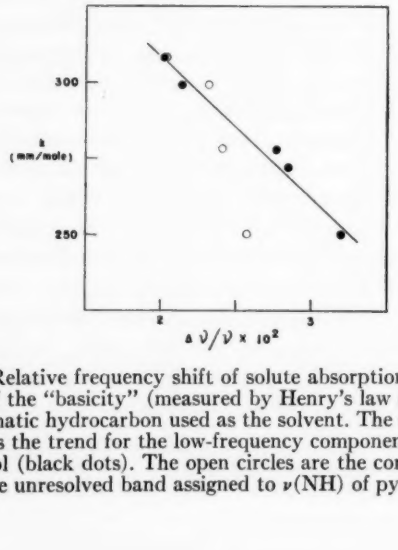

FIG. 5. Relative frequency shift of solute absorption band as a function of the "basicity" (measured by Henry's law constant k) of the aromatic hydrocarbon used as the solvent. The sloping line summarizes the trend for the low-frequency component of ν(OH) of methanol (black dots). The open circles are the corresponding data for the unresolved band assigned to ν(NH) of pyrrole.

Luttke and Mecke[7] in their study of the third harmonic of the phenol hydroxyl frequency in dilute solution found that when benzene and toluene were the solvents the OH absorption band was broadened (as compared with the corresponding band in CCl_4 solution) and was split into two components. This doublet structure was briefly mentioned in the nonpolar solvent discussion above. Jones and Badger[3] also observed this broadening of the third harmonic of the methanol hydroxyl stretching frequency in benzene and in toluene solutions as well as in other methyl substituted benzene solutions. They, too, were able to resolve the third harmonic OH band in these solvents into two components, benzene being the only exception. We have observed the same broadening of the *first* harmonic of the unassociated pyrrole NH stretching vibration band in benzene, toluene, *m*-xylene, and mesitylene solutions as compared to the NH band width in CCl_4. We have not, however, resolved into two components any of these unassociated first harmonic (i.e., fundamental) pyrrole NH bands dissolved in an aromatic solvent.

Luttke and Mecke explains this splitting by what they term "association isomerism." They suggest that the ". . . molecules of the solvent may be situated in two different positions relative to the OH bond and that they can remain in both positions for some time. Benzene, for instance, can have its molecular plane parallel (CH groups) or vertical (π electrons) to the OH group. . . ."[7] Jones and Badger,[3] on the other hand, attribute the two maxima in the OH band to the presence of solute molecules which interact strongly with the solvent,[22] and of other molecules free from solvent association. They state that the former is responsible for the low-frequency component of the OH band, the latter for the high-frequency component which falls, within experimental error, on the K-B line.[3] A study of Figs. 1, 2, and 3 convinces us that Jones and Badger's proposal is the more correct explanation of the experimental findings for both methanol and phenol, for we believe that it is more than coincidental that all seven of the high-frequency component points for methanol and phenol fall so close to the K-B line.

Another point of interest is that the shift of the lower-frequency component of the third harmonic methanol OH-band doublet is an increasing function of the "basicity" of the aromatic hydrocarbon used as the solvent.[23] Table III gives the data on which the graph in Fig. 5 is based. Data is also given for pyrrole ν(NH), for, though the fundamental band for this compound in

[22] The structure of the complexes of methylated benzenes with methanol has been recently discussed by R. S. Mulliken, J. Phys. Chem. **56**, 801 (1952).

[23] M. L. Josien, Compt. rend. **237**, 175 (1953).

aromatic solvents is not resolved, it gives a qualitative indication of the same dependence on "basicity."

Cyclohexene, when used as a solvent for phenol, produces a doublet OH band of the same appearance as that for the aromatic solvents. The explanation is the same.[23]

Conclusions on Dilute Solution Spectra

A few sentences are in order at this point to summarize the above findings in dilute solution. In nonpolar solvents the hydroxyl band vapor-to-solution relative frequency shift is almost the same in methanol, methanol-*d*, ethanol, propanol, and phenol, regardless of the nonpolar solvent used. In addition this relative frequency shift for the hydroxyl stretching modes of the alcohols and phenol is about the same as for the shift for the NH stretching mode of pyrrole in nonpolar solvents, i.e., all these molecules containing OH, OD, or NH groups behave in the same way in their interaction with nonpolar solvents in which they are dissolved, as is shown by the similarity in slope of the K-B line (see Table II).

In oxygenated solvents, pyridine, and aromatic solvents, however, the band position shifts vary considerably as one changes the solute, e.g., from methanol to phenol and to pyrrole, as should be expected since the strength of bonding in the complexes is dependent on the properties of each solute molecule involved.

V. DISCUSSION OF CONCENTRATED SOLUTIONS

In contrast to the single NH band found in the dilute solution spectra of pyrrole, two bands are found in most of the 2.0-molar solutions, as can be seen in Table I. Since this is not always the case, however, some discussion of this part of the table is also necessary.

Assignment of NH Bands

The two pyrrole NH bands for the nonpolar solvents and chloroform (top of Table I; see also Fig. 4D) can be assigned with confidence. The lower-frequency band is assigned to the NH frequency of pyrrole-pyrrole bonded molecules.[1,24,25] The higher-frequency band is assigned to the NH frequency of pyrrole which is affected only by the dielectric constant of the solvent. Its frequency is a few reciprocal centimeters lower than the single band in the corresponding dilute solution spectra, the difference being caused by the proximity of the partially overlapping associated band.

TABLE III. Comparison of the relative frequency shifts of methanol and pyrrole in different solvents with the corresponding solvent's Henry's law constant (a measure of "basicity").

Solvent	Henry's law constant,[a] k (mm)	Methanol $\Delta\nu/\nu$(OH) $\times 10^2$	Pyrrole $\Delta\nu/\nu$(NH) $\times 10^2$
Benzene	308	2.02	2.04
Toluene	299	2.14	2.32
m-xylene	278	2.77	2.41
Pseudocumene	272	2.85	...
Mesitylene	250	3.20	2.58

[a] Henry's law constant $k = p/N$, when p = pressure of HCl in Hg, and N = mole fraction of HCl. These k's are taken from H. C. Brown and J. D. Brady, J. Am. Chem. Soc. **74**, 3570 (1952).

In sharpest contrast to this nonpolar solvent case, the single broad band for pyrrole dissolved in pyridine, in acetophenone, and in acetone (bottom of Table I) can be assigned to the NH frequency of pyrrole-solvent bonded molecules. The pyrrole-pyrrole bonded NH frequency appears to be very weak or absent, the pyrrole-solvent interaction being dominant. In these three cases the pyrrole-solvent bonded NH frequency is shifted to even lower frequencies than that produced by pyrrole-pyrrole bonding. In the case of the pyrrole-in-pyridine solution the solvent associated NH band is far enough from the pyrrole-pyrrole interaction NH band so that it is possible to resolve them when the concentration is properly chosen. In a 7.0-molar pyrrole solution (1:1 pyrrole:pyridine), for example, the pyrrole-pyrrole interaction ν(NH) at *ca* 3400 cm^{-1} begins to appear as a weak shoulder on the pyrrole-pyridine interaction ν(NH) at *ca* 3200 cm^{-1}.[26]

Intermediate between these two extremes are the aromatic solvents and nitrobenzene (middle of Table I). In the case of 2.0-molar solutions of pyrrole in benzene and toluene (see Fig. 4B) a broad band is observed with a distinct shoulder present on the low-frequency side. For *m*-xylene and mesitylene a broad band is present, but no shoulder can be found. The indication is that two bands are present in each case but are not always resolved. The higher frequency and more intense component is the pyrrole-solvent bonded NH band,[27] the lower frequency and less intense component being the pyrrole-pyrrole bonded NH band. Several different concentrations of pyrrole in nitrobenzene were obtained in which the spectra looked much like that for pyrrole in mesitylene. We attribute the gradual shift in frequency as the concentration of pyrrole in nitrobenzene is increased from 0.013 to 8.0 molar to a change in the relative intensity of the two associated NH bands,

[24] P. Tuomikoski (see reference 9) states that "one may attribute the gradual frequency shifts of pyrrole with concentration to the polarizability of the liquid in bulk. . . ." As we observe a weakening of one fixed (higher) frequency band and the strengthening of another fixed (lower) frequency band rather than a gradual shift of pyrrole NH frequency when the concentration of pyrrole is increased, there is no alternative in explaining our results than to assume a pyrrole-pyrrole interaction through hydrogen bonding.

[25] P. Mirone, Atti accad. nazl. Lincei, Rend. Classe sci. fis. mat. e nat. **11**, 365 (1951); P. Mirone and M. Vampiri, *ibid.* **12**, 405 (1952). These authors have also studied ν(NH) of pyrrole. Their conclusions do not contradict ours. Their results are qualitatively similar to ours although their NH frequencies for pure liquid pyrrole and for a dilute solution of pyrrole in CCl_4 are 10–20 cm^{-1} higher than ours.

[26] See Fig. 8 of Buswell, Downing, and Rodebush, J. Am. Chem. Soc. **61**, 3252 (1939).

[27] Actually, as has been previously stated, in the case of the aromatic solvents this so-called "pyrrole-solvent" bonded NH band is thought to be an unresolved doublet the higher-frequency member being affected only by the dielectric constant of the solvent, the lower-frequency member being the pyrrole-solvent bonded band.

pyrrole-solvent and pyrrole-pyrrole, which are simultaneously present in the spectrum, but which are too close to be resolved.

Constancy of the Position of the Pyrrole-Pyrrole Bonded NH Band

The constancy of the low-frequency band component position in 2.0-molar solution (Table I), which has already been pointed out,[28] shows that when a pyrrole molecule is associated with another pyrrole molecule the NH group is shielded from the solvent in such a way that the NH···N associated NH frequency is almost totally unaffected by the dielectric constant of the particular solvent in which the pyrrole is dissolved. In certain cases (at the bottom of Table I), however, the solvent interacts so strongly with pyrrole that little or no pyrrole-pyrrole association is present.

Relative Intensities

It was pointed out in a preceding paper[1] that the pyrrole-pyrrole associated band at a given solution concentration is stronger, relative to the "unassociated band," in nonpolar solvents than in polar.[29] A preliminary study of pyrrole NH band intensities in a number of solvents (Table IV) show that the ratio of the intensity of the pyrrole-pyrrole bonded band to that of the solvent-bonded or the solvent-dielectric constant influenced band decreases as the dielectric constant increases. This is as would be expected since the smaller the dielectric constant the freer the pyrrole molecules will be to associate together. There are three solvent exceptions, CS_2, and benzene and toluene. The reason for the behavior of the former is not yet explained;[30] in the case of the latter two, complexes are formed[22] which presumably will affect the intensity ratios.

TABLE IV. Comparison of intensities of pyrrole NH bands in 2.0-molar solutions.

Solvent	D	I_1[a]	I_2[b]	I_2/I_1
Hexane	1.88	28[c]	70	2.50
Cyclohexane	2.04	46	70	1.52
CCl_4	2.23	38	43	1.13
Benzene	2.26	64	40[d]	0.62
Toluene	2.37	80	30[d]	0.37
CS_2	2.64	50	69	1.38
$CHCl_3$	4.85	53	34	0.64
$(CH_2Cl)_2$	10.0	65	10[d]	0.15

[a] Intensity, measured in percent absorption, of solvent-bonded or solvent-dielectric constant influenced ν(NH) of pyrrole.
[b] Intensity, measured in percent absorption, of pyrrole-pyrrole bonded ν(NH).
[c] Shoulder on the lower-frequency pyrrole-pyrrole bonded band.
[d] Shoulder on the higher-frequency pyrrole-solvent bonded band.

[28] See Table III and Fig. 6 in reference 1.
[29] This has recently been pointed out to hold also for propanol (see reference 6).
[30] CS_2 also seems to have an anomalous effect in the case of alcohols (see reference 6).

VI. CLASSIFICATION OF TYPES OF OH AND NH SOLUTION FREQUENCIES

(No *intra*molecular bonding was present in the molecules studied in this paper. In the classification that follows, therefore, *intra*molecular interactions are not included, *inter*molecular effects being considered exclusively.)

It has been pointed out,[1,31] in discussing the spectra of a compound in varying concentration in a given solvent, that such expressions as "wavelength shift" and "band shift" have been used ambiguously. They have been employed correctly to designate changes in location of a particular band with changing conditions. They have also been incorrectly used to designate the difference in location of bands, characteristic of monomer, dimer, and polymer states of aggregation, whose frequencies remain essentially constant but which may all be present simultaneously, their relative intensities varying greatly with changing conditions. As a result of this further work on the OH and NH group frequencies in various solvents and in various concentrations we have become increasingly aware of the confusion introduced by the adjectives "free" or "unassociated" and "bonded" or "associated" which are frequently used without any qualifying adverb in describing assignments of bands in solution spectra to OH, OD, or NH groups.

These terms are, of course, unambiguous when applied to spectra of hydroxyl and NH compounds in the vapor state. At sufficiently high temperatures and low pressures each molecule in a vapor is essentially in isolation, i.e., it is free or unassociated; at sufficiently low temperatures and high pressures it is possible for interaction between molecules to take place, i.e., for bonded or associated molecules to be present in addition to, or to the exclusion of, free molecules. In studies of compounds in solution, however, the inevitable presence of the solvent makes it difficult to speak any longer of "free" molecules.

The closest approach to the "free" state in solution is for a compound to be in dilute solution in a solvent in which the interaction of the solute with the solvent is a function of dielectric constant alone, that is, solvents which cause the OH or NH band "point" to fall on the K-B line. Examples of this spectral band type include: the NH band of pyrrole in a nonpolar solvent; and the higher-frequency component of the OH-band doublet for methanol in aromatic solvents.

Much less "free" are molecules of compounds in dilute solution in solvents in which bonding between the solute and solvent molecules is observed. Spectral band type examples include: the NH frequency for pyrrole in acetone, in which N—H···O bonding takes place; the lower frequency component of the OH-band doublet for methanol in aromatic solvents, in which N—H···Ar

[31] F. A. Smith and E. C. Creitz, J. Research Natl. Bur. Standards **46**, 145 (1951).

bonding is suggested; and the NH frequency for pyrrole in pyridine, in which R—NH···N—R′ bonding may be assumed.

NH and OH frequencies which are particularly difficult to categorize are those for a solute in chlorinated solvents in which the relative frequency shifts are less than the shifts attributed to the effect of the dielectric constant alone.

Also not "free" are many of the molecules in NH and OH compounds dissolved in concentrated solution. If two bands[32] appear in this case, one band can usually be described in one of the same ways as has just been done for dilute solution spectra bands. The other band is, then, the NH or OH band associated with the bonding together of two or more solute molecules, e.g., the NH frequency of a pyrrole molecule which is NH···N bonded to another pyrrole molecule.

[32] Each of these two bands may show substructure under certain conditions. The substructure in this particular case of concentrated solutions has not been present (and has, therefore, not been referred to) in this paper. It is, however, well knownf or carboxylic acids, e.g., M. L. Josien and N. Fuson, Compt. rend. **235**, 1025 (1952) and for alcohols, e.g., Fig. 6 and associated discussion in reference 31.

VII. ACKNOWLEDGMENTS

We should like to acknowledge the technical assistance on this problem of Miss Essie M. Shelton, of Fisk University.

This research has been supported jointly by research grant No. C-1520 from the National Cancer Institute, of the National Institutes of Health, U. S. Public Health Service, and by a Frederick Gardner Cottrell Grant from the Research Corporation.

THE JOURNAL OF CHEMICAL PHYSICS VOLUME 22, NUMBER 7 JULY, 1954

Evaluation of Some Electron Repulsion Integrals Needed in Molecular Quantum Mechanics. A Method of Calculation of Two Electron Multi-Center Repulsion Integrals without the Use of the Neumann Expansion*

ROLAND S. BARKER AND HENRY EYRING
Department of Chemistry, University of Utah, Salt Lake City, Utah

(Received April 6, 1953)

Consideration has been given to two of the electronic repulsion integrals arising in the quantum-mechanical energy calculation of the triatomic hydrogen molecular complex when no restrictions are placed on the effective nuclear charges of the composite atomic orbitals. The formulation of the integrals is first developed on a general basis and then restricted to the H_3 molecule. The possibility of extension of the mathematical processes to similar electron interaction integrals in more complex molecules is pointed out. The integration formulas are given as rapidly converging series.

I. INTRODUCTION

QUANTUM-mechanical calculations, for more than the simplest molecular structures, usually necessitate simplifying approximations which greatly restrict the significance of the agreement that can be obtained between calculated and experimental results. Approximations are usually introduced in the form of restrictions on the trial eigenfunction to be used with a variation type treatment. Such restrictions are made so that the integrals of the matrix elements in the secular determinant may be evaluated. Of these integrals, by far the most troublesome are those arising from the terms entering with the electron repulsion potentials of the Hamiltonian operator. The present surge of activity over molecular integrals has been in large part concentrated on extending the types of composite atomic orbitals used, and in removing restrictions on the effective nuclear charge parameters of such orbitals.[1] The three- and four-center electron repulsion integrals have received some attention recently from Coulson and Barnett[2] as well as from Lundquist and Lowdin.[3] Both supply alternative methods to those suggested by A. S. Coolidge.[4] Most of the methods currently undergoing development and refinement expand the reciprocal of the interelectronic distance, $1/r_{12}$, in associated Legendre functions of either spherical or confocal elliptical coordinates. In most cases this eventually leads to nonterminating series. According to a recent personal communication of C. A. Coulson, they have developed further and tabulated some of the functions needed in the Barnett-Coulson method.

An alternative method of integrating over the coordinates of first one electron and then the other has been applied to several special type electron repulsion

* This work was assisted in part by a grant from the National Science Foundation.

[1] See, for example, R. O. Brennan and J. F. Mulligan, J. Chem. Phys. **20**, 1635 (1952); C. C. J. Roothaan, J. Chem. Phys. **19**, 1445 (1951).

[2] M. P. Barnett and C. A. Coulson, Trans. Roy. Soc. (London) **A243**, 221 (1951).

[3] S. O. Lundquist and P. O. Lowdin, Arkiv Fysik (Stockholm) **3**, 147 (1951). This article has a bibliography on three and four centered integrals.

[4] A. S. Coolidge, Phys. Rev. **42**, 189 (1932).

integrals by Hirschfelder, Eyring and Rosen.[5] This method gave non-series expressions for two of the four integrals they considered, the others necessitated numerical integration. Extension of this method with the removal of the restriction of equal effective charges for the atomic orbitals and with added consideration of higher type orbitals is the subject of the present paper. The method is applicable to several integrals even for the case of unequal effective charges of the eigenfunction's composite atomic orbitals provided one introduces a Maclaurin expansion of the elliptical coordinate expression of one of the electronic distances.

II. THREE-CENTER ELECTRONIC REPULSION INTEGRAL FOR LINEAR MOLECULES WITH THE ORBITALS OF ONE OF THE ELECTRONS CENTERED ON THE SAME EXTERIOR NUCLEUS

The general formula for these three-center two electron integrals may be written,

$$L_{aa,\,bc}=\int \chi_a\chi_a'(1/r)\chi_b\chi_c d\tau \equiv (\chi_a\chi_a'|\,1/r\,|\chi_b\chi_c), \quad (2.1)$$

where the functions χ_a, χ_a', χ_b, χ_c represent the general AO's (atomic orbitals) on the nuclei "a," "b," and "c," and where "r" is the distance between electron one and electron two. The integration is, of course, over the position coordinates of both electrons.

For illustrative purposes we may specialize the above general integral to that currently occurring in calculations of the triatomic hydrogen activated complex $D-H-H$. Thus the orbitals are taken to be the $1s$ hydrogenic atomic orbitals:

$$\chi_a(1)=(\zeta_0^3/\pi)^{\frac{1}{2}}e^{-\zeta_0 r_{a1}}; \quad \chi_b(2)=(\zeta_m^3/\pi)^{\frac{1}{2}}e^{-\zeta^m r_{b2}}$$
$$\chi_a'(1)=(\zeta_0^3/\pi)^{\frac{1}{2}}e^{-\zeta_0 r_{a1}}; \quad \chi_c(2)=(\zeta_0^3/\pi)^{\frac{1}{2}}e^{-\zeta_0 r_{c2}},$$

where ζ_0=effective orbital charge associated with AO's of outer nuclei "a" and "c," ζ_m=effective orbital charge associated with AO of middle nucleus "b," r_{a1}=distance of nucleus "a" from electron 1, r_{b2}=distance of nucleus "b" from electron 2, and r_{c2}=distance of nucleus "c" from electron 2. The integral then becomes

$$L_{aa,\,bc}=(\zeta_0^9\zeta_m^3)^{\frac{1}{2}}/(\pi)^2\int\int \times(1/r_{12})e^{-2\zeta_0 r_{a1}-\zeta_m r_{b2}-\zeta_0 r_{c2}}d\tau_1 d\tau_2, \quad (2.2)$$

in which r_{12}=distance between electron 1 and 2, $d\tau_1$=volume element of electron 1, and $d\tau_2$=volume element of electron 2. Integration over the coordinates of electron 1, in this illustrative case, may then be performed directly by use of the well known two-center integration formula,[6,7]

$$G_{2,\,aa}=(\zeta_a^3/\pi)\int\int\int\frac{e^{-2\zeta_a r_{a1}}}{r_{12}}d\tau_1 = \zeta_a\int\int\int\frac{e^{-2\rho_{a1}}}{\rho_{12}}d\tau_1'$$
$$=(1/r_{a2})\{1-e^{-2\zeta_a r_{a2}}(1+\zeta_a r_{a2})\}, \quad (2.2')$$

where r_{a2}, the distance between electron 2 and nucleus "a," is the only parameter dependent on the position of electron 2 occurring in the integrated expression. Our illustrative integral, on substitution of (2.2′) in (2.2) becomes

$$L_{aa,\,bc}=(\zeta_0^3\zeta_m^3)^{\frac{1}{2}}/(\pi)\int 1/r_{a2} \times\{1-e^{-2\zeta_0 r_{a2}}(1+\zeta_0 r_{a2})\}e^{-\zeta_m r_{b2}-\zeta_0 r_{c2}}d\tau_2$$
$$=K_{a,\,bc}(R,\zeta_m,\zeta_0)-K_{a,\,abc}(R,\zeta_m,\zeta_0) -I_{abc}(R,\zeta_m,\zeta_0), \quad (2.3)$$

where

$$K_{a,\,bc}=(\zeta_0^3\zeta_m^3)^{\frac{1}{2}}/(\pi)\int(1/r_{a2})e^{-\zeta_m r_{b2}-\zeta_0 r_{c2}}d\tau_2, \quad (2.4)$$

$$K_{a,\,abc}=(\zeta_0^3\zeta_m^3)^{\frac{1}{2}}/(\pi)\int(1/r_{a2})e^{-2\zeta_0 r_{a2}-\zeta_m r_{b2}-\zeta_0 r_{c2}}d\tau_2, \quad (2.5)$$

$$I_{abc}=(\zeta_0^5\zeta_m^3)^{\frac{1}{2}}/(\pi)\int e^{-2\zeta_0 r_{a2}-\zeta_m r_{b2}-\zeta_0 r_{c2}}d\tau_2. \quad (2.6)$$

The three secondary integrals in the above case are three-center integrals in their own right, though now the integration is over the three coordinates of a single electron instead of the 6 coordinates of the two electrons in (2.2). The first of these three-variable three-center integrals, $K_{a,\,bc}$, is a special case of the three-center nuclear attraction integral treated by us in a previous paper[8] and may be evaluated by the general method described there. However, this integral (2.4) and the other two secondary integrals (2.5) and (2.6) may be evaluated by a special method now to be explained.

III. SPECIALIZED MACLAURIN'S EXPANSION OF THE ELLIPTICAL COORDINATE EXPRESSION OF THE CENTRAL ATOMIC ORBITAL EXPONENTIAL

Use of confocal elliptical coordinates for functions originally simply expressed in terms of distances from

[5] Hirschfelder, Eyring, and Rosen, J. Chem. Phys. **4**, 121 (1936).

[6] Eyring, Walter, and Kimball, *Quantum Chemistry* (John Wiley and Sons, Inc., New York, 1947), p. 197.

[7] Integration formulas which may be adapted for integration over the coordinates of the first electron for more complex AO's have recently been tabulated by Roothaan (reference 1, equations 31). The integrals include all the orbital possibilities arising from the principle quantum numbers 1 and 2 using Slater-type AO's with arbitrary values for the effective nuclear charges.

[8] R. S. Barker and H. Eyring, J. Chem. Phys. **21**, 912–917 (1953).

two points, consolidates such expressions into a single coordinate system and at the same time leaves the distance expressions from the two points and the volume element simple. For this reason the elliptical coordinate system[9] has been widely used in two-center problems of quantum mechanics, potential theory, and so forth. It is natural therefore to simplify our secondary three-center integrals (at least for expressions about two of the centers) by introduction of elliptical coordinates. The choice of centers "a" and "c" as the foci of the elliptical coordinates is best in this instance as will become clear later. For the triatomic hydrogen activated complex molecule here being described the three centers "a," "b," and "c" lie on a line with both the external centers "a" and "c" the same distance, R, from the middle center "b." The elliptical coordinates are defined by

$$\mu=\frac{r_a+r_c}{2R}; \quad \nu=\frac{r_a-r_c}{2R};$$

ϕ = azimuthal angle of the electron.

Conversely,

$$r_a=R(\mu+\nu); \quad r_c=R(\mu-\nu); \quad r_b=R(\mu^2+\nu^2-1)^{\frac{1}{2}}.$$

In these coordinates the volume element $d\tau=R^3(\mu^2-\nu^2)\times d\mu d\nu d\phi$, and the limits of integration for ϕ are 0 to 2π, for ν from -1 to 1, and for μ from 1 to ∞. After substitution of the above expressions into (2.4), (2.5), and (2.6) integration over ϕ gives,

$$K_{a,bc}=2R^2(\zeta_0^2\zeta_m^2)^{\frac{1}{2}}\int_1^\infty\int_{-1}^1 \times\exp[-\zeta_m R(\mu^2+\nu^2-1)^{\frac{1}{2}}] \times\exp[-\zeta_0 R(\mu-\nu)](\mu-\nu)d\nu d\mu, \quad (3.1)$$

$$K_{a,abc}=2R^2(\zeta_0^3\zeta_m^3)^{\frac{1}{2}}\int_1^\infty\int_{-1}^1 \times\exp[-\zeta_m R(\mu^2+\nu^2-1)^{\frac{1}{2}}] \times\exp[(-3\zeta_0 R\mu-\zeta_0 R\nu)](\mu-\nu)d\nu d\mu, \quad (3.2)$$

$$I_{abc}=2R^3(\zeta_0^5\zeta_m^3)^{\frac{1}{2}}\int_1^\infty\int_{-1}^1 \times\exp[-\zeta_m R(\mu^2+\nu^2-1)^{\frac{1}{2}}] \times\exp[-3\zeta_0 R\mu-\zeta_0 R\nu](\mu^2-\nu^2)d\nu d\mu. \quad (3.3)$$

[9] This statement should not be interpreted as implying that elliptical coordinates are always the choice for such problems. There are frequently reasons for the use of other coordinate systems, bipolar coordinates being often preferable. See for example R. J. Buehler and J. O. Hirschfelder, Phys. Rev. **83**, 623 (1951). C. A. Coulson and his co-workers have also made frequent use of bipolar coordinates in their work on similar problems from quantum mechanics.

These simplified integrals may all be integrated by series methods. Considering the limits of the variables and the existence of certain auxilary integration functions, we chose to expand $\exp[-\zeta_m R(\mu^2+\nu^2-1)^{\frac{1}{2}}]$. For purposes of expansion let $\nu^2-1=x$, and expand the function as a Maclaurin's series about the point $x=0$. Thus.

$$f(x)=\exp[-\zeta_m R(\mu^2+x)^{\frac{1}{2}}] =f(0)+f'(0)\frac{x}{1!}+f''(0)\frac{x^2}{2!}+\cdots. \quad (3.4)$$

Considerable mathematical development enables one to write (3.4) as,

$$\exp[-\zeta_m R(\mu^2+x)^{\frac{1}{2}}]=\exp(-\zeta_m R\mu) \times\left[1-\frac{\zeta_m R}{2\mu}x+\sum_{m=2}^{\infty}\left\{\frac{(2m-3)!}{(m-2)!2^{2m-2}}\left(\frac{1}{\zeta_m R\mu}\right)^{m-1} +\sum_{n=2}^{m}\frac{(2m-n-1)!}{(n-1)!(m-n)!2^{m-n}}\left(\frac{1}{\zeta_m R\mu}\right)^{m-n}\right\} \times\left(\frac{-\zeta_m R}{2}\right)^m\frac{x^m}{m!}\right]. \quad (3.5)$$

Expression (3.5) may be varified by mathematical induction. In examining the convergence of the above series it should be noted that $\mu\geq 1$, and $x\leq|1|$ as $\nu^2\leq 1$. A mathematical proof of the convergence of series (3.5) has been obtained by Don A. Baker (Department of Mathematics University of Utah) for the designated ranges of the variables. The numerical example of Sec. IV indicates the rapidity of convergence and the labor required to carry through numerical calculations.

On expressing the foregoing series in terms of the original variable ν and introducing this modification of (3.5) into the expressions for the secondary integrals (3.1), (3.2), and (3.3) the integration problems are all seen to reduce to consideration of terms of the form,

$$\int_1^\infty\int_{-1}^1\mu^{-n}\nu^m e^{-\alpha\mu}e^{-\beta\nu}d\nu d\mu =\int_1^\infty(e^{-\alpha\mu}/\mu^n)d\mu\int_{-1}^1\nu^m e^{-\beta\nu}d\nu.$$

Recurrence relations[10] and tabulated values, $\beta=0.0$ (0.25) 5.50 and $\beta=6.0$ (0.50) 7.0, of the auxiliary function,

$$B_m(\beta)=\int_{-1}^1\nu^m e^{-\beta\nu}d\nu,$$

[10] The recurrence formula,

$$B_m(\beta)=1/\beta\{(-)^m e^{\beta}-e^{-\beta}+mB_{m-1}(\beta)\},$$

follows from definition and an elementary integration formula.

have been given by Kotani, Amemiya, and Simose.[11] A tabulation of the function

$$E_n(\alpha)=\int_1^\infty (e^{-\alpha\mu}/\mu^n)d\mu$$

by G. Placzek is available from the National Research Council of Canada, Division of Atomic Energy, $MT/1$. This tabulation gives values of $E_n(\alpha)$ to six places for $n=0$ (1) 20; $\alpha=0.00$ (0.01) 2.00 and $\alpha=2.0$ (0.1) 10. Recurrence formulas are given in reference 11 as well as in a recent article by V. Kourganoff.[12]

IV. NUMERICAL CALCULATIONS

A numerical example using the proposed expansion, showing rapidity of the series convergence and indicating the labor required to carry through numerical calculations is given below. Since the proposed method does not depend upon the effective nuclear charges of the orbitals the particular integral with equal effective nuclear charge orbitals, $K_{a,\,bc}(R)$, may be evaluated by the proposed general method and the result obtained compared with that obtained from the equal-effective-charge-orbital formula used by Hirschfelder.[13] This special case formula is,

$$\begin{aligned}K_{a,\,bc}(R)&=(\zeta^3/\pi)\int(1/r_{a1})\exp(\zeta r_{b1}-\zeta r_{c1})d\tau_1\\&=(1/\pi)\int(\zeta/\rho_{a1})\exp(-\rho_{b1}-\rho_{c1})d\tau_1'\\&=\zeta\Big\{(-12U/\rho)+(9/\rho)I(\rho)-e^{-3\rho}\Big(2+\frac{9}{\rho}\Big)\Big\}\end{aligned}\quad(4.1)$$

where

$$U=I(\rho)[\ln 2+Ei(-2\rho)]-F(\rho)Ei(-4\rho),$$

$$I(\rho)=e^{-\rho}[1+\rho+(\rho^2/3)];\quad \rho_a=\zeta r_a,$$

$$F(\rho)=e^{+\rho}[1-\rho+(\rho^2/3)];\quad \rho_b=\zeta r_b;\quad \rho=\zeta R,$$

$$Ei(-a)=-\int_a^\infty (e^{-x}/x)dx.$$

For $\zeta=\zeta_m=\zeta_0=1$ and $R=2$ (4.1) gives the value 0.196678. The general formulation gives after integration over ϕ,

$$\begin{aligned}K_{a,\,bc}(R)&=K_{c,\,ab}(R)\\&=2R^2\int_1^\infty\int_{-1}^1\exp[-R(\mu^2+\nu^2-1)^{\frac{1}{2}}]\\&\quad\times\exp[-R(\mu+\nu)]\cdot(\mu+\nu)d\nu d\mu.\end{aligned}\quad(4.2)$$

[11] Kotani, Amemiya, and Simose, Proc. Phys.-Math. Soc. Japan **20**, Extra No. 1 (1938); **22**, Extra No. 1 (1940).
[12] V. Kourganoff, Ann. d'Astrophys. **10**, 282 (1947).
[13] J. O. Hirschfelder, dissertation, Princeton University (1935).

TABLE I. Values of $B_m(2)$ from Kotani.

m	$B_m(2)$
0	3.626 8604 078
1	−1.948 4654 872
2	1.678 0949 206
3	−1.245 0533 101
4	1.136 7537 877
5	−0.920 3112 2173
6	0.865 9267 4265
7	−0.731 4520 9181
8	0.701 0520 4061

Introduction of (3.5) in (4.2) then leads to the series formulation,

$$\begin{aligned}K_{c,\,ab}(R)&=8\int_1^\infty\int_{-1}^1 e^{-4\mu}e^{-2\nu}\\&\quad\times\Big[1-\frac{R}{2\mu}(\nu^2-1)+\Big\{\frac{R^2}{4\mu^2}+\frac{R}{4\mu^3}\Big\}(\nu^2-1)^2+\cdots\Big]\\&\quad\times(\mu+\nu)d\mu d\nu.\end{aligned}\quad(4.3)$$

Values of the auxilary functions $B_m(2)$ and $E_m(4)$ are given in Tables I and II. The value

$$\int_1^\infty e^{-4\mu}\mu d\mu=0.005\ 7236\ 3715$$

has also been tabulated.[11] Thus, the first term of the series gives the value,

$$\begin{aligned}T_1&=8\ (0.005\,7236\,3715)\ (3.626\,8604)\\&\quad-8\ (0.004\,57891)\ (1.948\,4654)\\&=0.094\,6848.\end{aligned}$$

Other terms are given in Table III. The sum of these first 5 terms gives $K_{a,\,bc}=0.185\,3503$, which compares favorably with a similar number of terms of C. A. Coulson's method[14] employing Bessel functions of half-integral orders.

V. THREE-CENTER ELECTRONIC REPULSION INTEGRAL FOR LINEAR MOLECULES WITH THE ORBITALS OF ONE OF THE ELECTRONS CENTERED ON THE MIDDLE NUCLEUS

The general formula for these three-center two electron integrals may be written

$$L_{bb,\,ac}=\int\chi_b\chi_b'(1/r)\chi_a\chi_c d\tau\equiv(\chi_b\chi_b'|\,1/r\,|\chi_a\chi_c),\quad(5.1)$$

where the symbols are similar to those given in Sec. II. For the triatomic hydrogen molecule the integral is

[14] C. A. Coulson, Proc. Cambridge Phil. Soc. **33**, 104 (1937).

reduced in the manner outlined before to,

$$L_{bb,ac}=(\zeta_0^3\zeta_m^3)/(\pi)^2\int\int \times(1/r_{12})e^{-2\zeta_m r_{b2}-\zeta_0 r_{a2}-\zeta_0 r_{c2}}d\tau_1 d\tau_2. \quad (5.2)$$

Integration over the coordinates of electron 1 is performed, as already described, to give

$$L_{bb,ac}=(\zeta_0^3/\pi)\int (1/r_{b2}) \times\{1-e^{-2\zeta_m r_{b2}}(1+\zeta_m r_{b2})\}e^{-\zeta_0 r_{a2}-\zeta_0 r_{c2}}d\tau_2,$$
$$=K_{b,ac}(R,\zeta_0)-K_{b,bac}(R,\zeta_0,\zeta_m) -I_{bac}(R,\zeta_0,\zeta_m). \quad (5.3)$$

where

$$K_{b,ac}(R,\zeta_0)=(\zeta_0^3/\pi)\int (1/r_{b2})e^{-\zeta_0 r_{a2}-\zeta_0 r_{c2}}d\tau_2, \quad (5.4)$$

$$K_{b,abc}(R,\zeta_0,\zeta_m)=(\zeta_0^3/\pi)\int \times(1/r_{b2})e^{-2\zeta_m r_{b2}-\zeta_0 r_{a2}-\zeta_0 r_{c2}}d\tau_2, \quad (5.5)$$

$$I_{bac}(R,\zeta_0,\zeta_m)=(\zeta_0^3/\pi)\int e^{-2\zeta_m r_{b2}-\zeta_0 r_{a2}-\zeta_0 r_{c2}}d\tau_2. \quad (5.6)$$

The secondary integral (5.4) has the integration formula,[5]

$$K_{b,ac}(R,\zeta_0)=(3U/4\zeta_0 R)-(\zeta_0 R+2)e^{-2\zeta_0 R},$$

where

$$U=I_{ac}(2\zeta_0 R)[\ln 4\zeta_0 R+C] -F_{ac}(2\zeta_0 R)Ei(-4\zeta_0 R),$$

$$I_{ac}(2\zeta_0 R)=e^{-2\zeta_0 R}[1+2\zeta_0 R+(2\zeta_0 R)^2/3],$$

$$F_{ac}(2\zeta_0 R)=e^{+2\zeta_0 R}[1-2\zeta_0 R+(2\zeta_0 R)^2/3],$$

C = Euler's constant = 0.577215665.

TABLE II. Values of $E_m(4)$ from Placzek.

m	$E_m(4)$
0	0.004 57891
1	0.003 77935
2	0.003 19823
3	0.002 76136
4	0.002 42340
5	0.002 15551
6	0.001 93872
7	0.001 76013
8	0.001 61073

TABLE III.

Term	Value
1	0.094 6848
2	0.050 1092
3	0.023 3381
4	0.011 2849
5	0.005 9332

The secondary integral (5.6) may be handled with the method described in Sec. IV. Thus, (5.5) is the only one of the three secondary integrals requiring further consideration. The method previously outlined may be modified by making the choice of "b" and "c" or "a" and "b" foci of the elliptical coordinate system. Then,

$$r_b=(R/2)(\mu+\nu);\quad r_c=(R/2)(\mu-\nu);$$
$$r_a=(\mu^2+\nu^2-6\mu\nu+8)^{\frac{1}{2}}$$
$$d\tau=(R^3/8)(\mu^2-\nu^2)d\phi d\nu d\mu.$$

On substitution of these expressions into (4.2) and integrating over φ, one has

$$K_{b,abc}=\zeta_0^3/\pi\int_1^\infty\int_{-1}^1 e^{-(R/2)(2\zeta_m+\zeta_0)\mu}e^{-(R/2)\zeta_0\nu} \times\exp[-(\zeta_0 R/2)(\mu^2+\nu^2-6\mu\nu+8)^{\frac{1}{2}}] \times(\mu-\nu)d\nu d\mu. \quad (5.7)$$

This time one expands

$$\exp[-(\zeta_0 R/2)(\mu^2+\nu^2-6\mu\nu+8)^{\frac{1}{2}}]$$

by a Maclaurin expansion about $\nu=-1$. This gives,

$$e^{-(\zeta_0 R)(\mu+3)}\left[1-\left\{\frac{1+6\mu}{\mu+3}\right\}\nu+\{\ \}\nu^2+\cdots\right]. \quad (5.8)$$

Substituting (5.8) in (5.7) and after letting $z=\mu+3$, evaluation proceeds as previously described. Further outline is unnecessary as the steps then parallel those previously considered in Sec. III.

ACKNOWLEDGMENTS

We should like to thank the following people for taking part in discussions of certain phases of this problem, Professors C. J. Thorne, E. Stewart, R. Lumry, and R. P. Smith.

Use of Nuclear Attraction Integral Approximations in Molecular Quantum Mechanics*

ROLAND S. BARKER AND HENRY EYRING
Department of Chemistry University of Utah

(Received November 9, 1953)

Most molecular quantum-mechanical studies of today make use of eigenfunctions composed of atomic orbitals. Such eigenfunctions give rise to difficult multicenter integrals which are usually evaluated by approximate methods. A study of the accuracy of such methods and of their derived results has long been desirable. Certain approximations for three-center nuclear attraction integrals are here examined.

Complete sample calculations are made with the approximate integral values for the triatomic activated complex molecule, H_3. The use of the Mulliken approximate evaluation of integrals in the Heitler-London treatment for H_3 gives a binding energy 7.6 kcal/mole less than does the use of exact integrals. On modifying the Heitler-London treatment by inclusion of screening constants for the outer and central atomic orbitals the Mulliken type approximate integrals gave for a trial calculation a binding energy 5.3 kcal/mole better than the best previous determination. This trial calculation (using the parametric values $R=1.8$, $Z_0=1$, $Z_m=1.08$) while the best of several tried is not likely the best that can be found. However, the binding energy of 72.7 kcal/mole calculated is 26 kcal/mole better than the Heitler-London value (53.4 kcal/mole) and 5 kcal/mole better than the Wang-like covalent-bond-plus-ionic-terms determination using a single screening parameter.

The cited trial calculation indicates that similar determinations now in progress using exact integral evaluations will give a substantial increase in the calculated binding energy of H_3. This would be, for this simplest polyatomic molecule, the first major advance since 1936. That the approximate calculation is essentially correct is substantiated by the increase in binding energy obtained with the proper screening constant variation for the diatomic molecule. In the H_2 case Wang obtained an improvement from 72.4 kcal/mole to 86.7 kcal/mole over the best covalent-plus-ionic term calculations.

1. INTRODUCTION

THE use of approximations for the multicentered electron repulsion integrals arising in molecular quantum mechanics was the subject of an earlier paper.[1] Indeed these electron repulsion integrals have been one of the major difficulties in making first principle molecular calculations with eigenfunctions constructed of free-atom atomic orbitals. However the electron repulsion integrals have not been the only difficulty. J. F. Mulligan[2] in his recent very commendable treatment of the CO_2 molecule also found it necessary to approximate the one-electron three-center nuclear attraction integrals. The exact evaluation of such integrals has been considered by Hirschfelder, Eyring, and Rosen[3] for special cases and by Coolidge,[4] Coulson,[5] and Barker and Eyring[6] for the generalized case. The general "exact" method integral treatments are, however, series calculations which become very unwieldy if considerable accuracy is required. For example Coulson[7] states that his method is "entirely satisfactory if one is prepared to give sufficient time to the evaluation" and "that a single integral can be calculated from start to finish in a couple of days."

Examination of approximations, their accuracy and the time requirements is thus worth while. Especially is this true for the above-mentioned general case integrals for which the relatively simple formula of Hirschfelder, Eyring, and Rosen cannot be used.

2. TYPES OF APPROXIMATIONS

The approximations before considered have been of two types, approximations based on physical reasoning and those based on mathematical deductions. The method used by J. F. Mulligan is of the first type. His method consists of the evaluation of "the interaction between the attractive nucleus and of a point charge corresponding to the overlapping charge cloud of the exchanged electron located where the overlapping charge cloud takes on its maximum value along the internuclear axis." Further detail of this method and of similar considerations used by R. S. Mulliken may be found in Mulligan's paper[2] on CO_2.

Methods of the second type, that is methods based primarily on mathematical considerations, will be given in considerable detail in the following sections of this paper. Two such methods may be cited as typical. The first is a completely general approximate method designated as the extended Rudenberg-Mulliken approximation (R-M approximation). The second is the restricted mixed orbital paramount charge method (P.C. approximation) first noted by Barker and Eyring[6] in their paper on exact evaluation of the general three-center nuclear attraction integral.

The R-M approximation is closely related to Mulliken's general approximation[1] for electron repulsion integrals (1.1), the general form of which is,

$$L_{AB,CD}=\int \chi_A(1)\chi_B(1)(1/r_{12})\chi_C(2)\chi_D(2)d\tau$$
$$\approx \tfrac{1}{4}I_{AB}I_{CD}\{L_{AA,CC}+L_{AA,DD}+L_{BB,CC}+L_{BB,DD}\}, \quad (1.1)$$

* Sponsored by the Office of Ordnance Research, U. S. Army.
[1] Barker, Eyring, Thorne, and Baker, J. Chem. Phys. **22**, 699 (1954).
[2] J. F. Mulligan, J. Chem. Phys. **19**, 347 (1951).
[3] Hirschfelder, Eyring, and Rosen, J. Chem. Phys. **4**, 121 (1936).
[4] A. Coolidge, Phys. Rev. **42**, 189 (1932).
[5] C. A. Coulson, Proc. Cambridge Phil. Soc. **31**, 244 (1935).
[6] R. S. Barker and H. Eyring, J. Chem. Phys. **21**, 912 (1953).
[7] C. A. Coulson, Proc. Cambridge Phil. Soc. **33**, 104 (1937).

where $\chi_A(1)$, $\chi_B(1)$, $\chi_C(2)$, $\chi_D(2)$ are atomic orbitals of electrons 1 and 2 centered on nuclei at "A," "B," "C," and "D," r_{12} is the distance between the electrons, $d\tau$ the volume elements of the electrons, $I_{AB}=\int\chi_A\chi_B d\tau_1$ (overlap integral), and $L_{AA,CC}=\int\chi_A\chi_A(1/r_{12})\chi_C\chi_C d\tau$ (a Coulombic integral).

Rudenberg's justification[8] of Mulliken's intuitively obtained expression (1.1) proceeeds by an expansion, leading after neglect of lesser terms, to the expression

$$\chi_A(1)\chi_B(1)\approx\tfrac{1}{2}I_{AB}\{\chi_A(1)\chi_A(1)+\chi_B(1)\chi_B(1)\}. \quad (1.2)$$

This and the similar expression for $\chi_C(2)\chi_D(2)$ gives Mulliken's formula (1.1). If the same type expression (1.2) is substituted into the definitive equation of the three-center nuclear attractive integral, the approximation referred to as the extended Rudenberg-Mulliken formula (1.3) is obtained.

$$K_{A,BC}=\int\frac{1}{r_A}\chi_B(1)\chi_C(1)d\tau_1$$
$$\approx\tfrac{1}{2}I_{BC}\{G_{A,B^2}+G_{A,C^2}\}, \quad (1.3)$$

where the G_{A,B^2} is a two-center single electron Coulombic attraction integral:

$$G_{A,B^2}=\int\frac{1}{r_A}\chi_B(1)\chi_B(1)d\tau_1.$$

The advantage of this nuclear attraction R-M approximation is that it reduces completely general three-center nuclear attraction integrals to two-center overlap and single electron Coulombic attraction integrals for which simple closed-form expressions are known.[9] Values of the required one-electron overlap and Coulombic integrals for 1s type orbital integrals have been tabulated.[10] The few exact numerical values of the three-center 1s orbital integrals readily available have been compared with values calculated using the R-M approximation in Tables I, II, and III. The exact values of the unsymmetrical configurational integrals are to be found in Taylor's recent article[11] on H_4. The symmetrical values may be calculated from the formula of Hirschfelder, Eyring, and Rosen.

TABLE I. Three-center unsymmetrical configurational integrals.

Integral	Exact values (Taylor)		Approximate values
$K_{a,bd}$	3.840 ev	0.1418a.u.	0.16533a.u.
$K_{a,cd}$	5.839	0.2157	0.22210
$K_{b,ad}$	2.655	0.09807	0.07993

[8] K. Rudenberg, J. Chem. Phys. **19**, 1459 (1951).

[9] C. C. J. Roothaan, J. Chem. Phys. **19**, 1445 (1951). This article gives explicit formulas for all the required two-center Coulombic and overlap integrals for Slater-type AO's arising from the principal quantum numbers 1 and 2.

[10] Thorne, Barker, and Eyring, Studies in Applied Mathematics No. 10 (University of Utah), "Tables of quantum mechanical integrals 1. Some two parameter integrals." The required integrals are tabulated for the ranges $R=1.0$ (0.1) 1.5, 1.50 (0.05) 2.00, 2.0 (0.1) 5.0, $Z=0.70$ (0.05) 1.00, 1.00 (0.02) 1.50.

[11] R. Taylor, Proc. Phys. Soc. (London) **A64**, 249 (1951).

TABLE II. $K_{a,bc}\approx\frac{1}{2}I_{ab}\{G_{a,b^2}+G_{a,c^2}\}$.

R	Exact value	Value using R-M approx.
1.00	0.501a.u.	0.516a.u.
1.50	0.313	0.331
2.00	0.197	0.212
2.50	0.124	0.135
3.00	0.0791	0.0866
4.00	0.0323	0.0354
6.00	0.00536	0.00589

TABLE III. $K_{b,ac}\approx\frac{1}{2}I_{ac}\{G_{b,a^2}+G_{b,c^2}\}=I_{ac}\cdot G_{a,b^2}$.

R	Exact value	Value using R-M approx.
1.00	0.465a.u.	0.428a.u.
1.50	0.242	0.203
2.00	0.117	0.0894
2.50	0.0539	0.0377
3.00	0.0240	0.0155
4.00	0.00443	0.00254
6.00	0.000128	0.000062

The integral notation employed in Table I is for the collinear system of four protons "a," "b," "c," and "d" spaced at equal intervals ($R=1.4a_0$), the equilibrium internuclear separation in H_2. The numerical calculations of all the tables are given in a.u. (atomic units), that is in units of the first Bohr radius $a_0=0.5292$A, and energies in units of e^2/a_0. The notation used in the other tables is for the collinear system of three protons "a," "b," and "c" spaced at equal intervals R.

The R-M approximation may be particularized for the single electron two-center exchange attraction integrals. Thus

$$J_{A,AB}=\int\frac{1}{r_{A1}}\chi_A(1)\chi_B(1)d\tau_1$$
$$\approx\tfrac{1}{2}I_{AB}\{G_{A,A^2}+G_{A,B^2}\}. \quad (1.4)$$

In many cases, however, the closed form expressions for the two-center exchange attraction integral $J_{A,AB}$ is simpler than the Coulombic attraction integral G_{A,B^2}. Thus for 1s AO's of the form, $A(1)=(Z^3/\pi)^{\frac{1}{2}}e^{-Zr_{A1}}$, the closed form equal orbital charge expressions are

$$J_{A,AB}=\int\frac{1}{r_{A1}}e^{-Z_Ar_{A1}}e^{-Z_Br_{B1}}d\tau_1$$
$$=Z(2R+1)e^{-ZR}, \quad (Z=Z_A=Z_B), \quad (1.5)$$

$$G_{A,B^2}=\int\frac{1}{r_{A1}}e^{-2Z_Br_{B1}}d\tau_1$$
$$=\frac{1}{R}[1-e^{-2Z_BR}(Z_BR+1)], \quad (1.6)$$

$$G_{A,A^2}=\int\frac{1}{r_{A1}}e^{-2Z_Ar_{A1}}d\tau_1$$
$$=Z_A. \quad (1.7)$$

TABLE IV. Equal orbital charge exchange attraction integral ($J_{a,ab} \approx \frac{1}{2} I_{ab}\{G_{a,a}^2 + G_{a,b}^2\} = \frac{1}{2} I_{ab}\{1 + G_{a,b}^2\}$).

R	Exact value	Value using R-M approximation
1.00	0.736a.u.	0.742a.u.
1.50	0.558	0.574
2.00	0.406	0.432
2.50	0.287	0.319
3.00	0.199	0.232
4.00	0.0916	0.118
5.00	0.0404	0.0579
6.00	0.0174	0.0275
8.00	0.00302	0.00572

Such two-center nuclear attraction integrals should, therefore, not usually be expanded by the R-M approximation. The unavailability of adequate exact values of mixed orbital charge three-center nuclear attraction integrals, however, makes examination of this two-center approximate formula (1.4) attractive for comparative purposes. Examination of integrals involving only $1s$ type orbitals simplifies the illustrative calculations. Equal orbital charge integrals are compared in Table IV. If one considers the mixed orbital charge case of (1.5), that is the case for $Z_A \neq Z_B$, the closed form expressions to be found in the appendix enable one to obtain the comparative mixed orbital approximate and "actual" values of Tables V and VI.

Mixed orbital charge integrals may be approximated more accurately if the corresponding "exact" equal orbital integrals are available by use of so-called distance normalization. Thus for example the exact equal orbital charge integral for a specified distance R, $J_{a,ab}(R,Z)$, may be evaluated exactly from formula (1.5). The approximate equal orbital charge integral designated as $J^{(\prime)}{}_{a,ab}(R,Z)$ may be obtained from (1.4) with $Z=Z_a=Z_b$. The approximate calculation will usually not agree exactly with the exact value but may be made to agree by multiplying by a so-called normalization factor, $\{(J_{a,ab})/(J^{(\prime)}{}_{a,ab})\}$. Such a procedure when the "exact" $J_{a,ab}$ integral is known is, of course, superfluous. However if one obtains the approximate mixed orbital charge integral to be designated as $J^{(\prime\prime)}{}_{a,ab}(R,Z_a,Z_b)$ and multiplies by the normalization factor obtained from the corresponding equal orbital, charge integrals the procedure is meaningful. Thus the obtained distance normalized approximate integral, $J^{(-)}{}_{a,ab}(R,Z_a,Z_b)$, is considerably nearer the exact integral value than the unnormalized $J^{(\prime\prime)}{}_{a,ab}(R,Z_a,Z_b)$:

$$J^{(-)}{}_{a,ab}(R,Z_a,Z_b) = \left\{\frac{J_{a,ab}(R,Z)}{J^{(\prime)}{}_{a,ab}(R,Z)}\right\} J^{(\prime\prime)}{}_{a,ab}(R,Z_a,Z_b). \quad (1.8)$$

Comparative values of mixed orbital charge integrals are given in Tables V and VI. The equal orbital charge approximate integrals used in the distance normalization were, for convenience, taken with $Z=1$. A similar distance normalization procedure may be employed for the three-center attraction integrals and for the multicenter electron repulsion integrals, obtained by the R-M and by the M approximations.

Another approximate formula for mixed orbital nuclear attraction integrals is available when exact values of the corresponding equal orbital charge integrals are available. This "Paramount Charge" approximation is obtained by taking all charges involved equal to the particular charge which most influences the integral's value. The approximation may be illustrated by the following formulas for the $1s$ orbital integrals $K_{a,bc}$ and $J_{b,ab}$.

$$K_{a,bc} = \int \frac{1}{r_{a1}} e^{-Z_b r_{b1}} e^{-Z_c r_{c1}} d\tau_1, \quad (Z_c \neq Z_b)$$

$$\approx Z_a \int \frac{1}{\rho_{a1}} e^{-\rho_{b1}} e^{-\rho_{c1}} d\tau_1',$$

where $\rho = Zr$, and $Z = Z_a = Z_c$.

$$J_{b,ab} = \int \frac{1}{r_{b1}} e^{-Z_a r_{a1}} e^{-Z_b r_{b1}} d\tau_1$$

$$\approx Z_b \int \frac{1}{\rho_{b1}} e^{-\rho_{b1}} e^{-\rho_{a1}} d\tau_1', \quad (1.9)$$

where $\rho = Z_b r$. Values for the P.C. approximation of the two-center attractive integrals are also included in Tables V and VI.

3. USE OF MIXED ORBITAL CHARGE APPROXIMATIONS IN COMPLETE MOLECULAR ENERGY CALCULATIONS

The use of approximate integrals to minimize configurational distance parameters in a trial eigenfunction for later use in exact integral calculations has been previously described.[1] Such use makes possible a

TABLE V. Mixed orbital charge exchange attraction integral $J_{a,ab}$ ($J_{a,ab}[R,Z_a,Z_b] \approx \frac{1}{2} I_{ab}\{Z_a + G_{a,b}^2\}$).

Integral	Exact value	R-M approx.	P. C. approx.	D. norm. R-M approx.
$J_{a,ab}(1.75,1,1.1)$	0.464a.u.	0.483a.u.	0.478a.u.	0.459a.u.
$J_{a,ab}(2.00,1,1.1)$	.0.389	0.413	0.406	0.389
$J_{a,ab}(2,1.1,1.20)$	0.371	0.402	0.390	0.378

TABLE VI. Mixed orbital charge exchange attraction integral $J_{b,ab}$ ($J_{b,ab}[R,Z_a,Z_b] \approx \frac{1}{2} I_{ab}\{Z_b + G_{b,a}^2\}$).

Integral	Exact value	R-M approx.	P. C. approx.	D. norm. R-M approx.
$J_{b,ab}(1.75,1,1.1)$	0.482a.u.	0.511a.u.	0.469a.u.	0.485a.u.
$J_{b,ab}(2.00,1,1.1)$	0.407	0.439	0.390	0.413
$J_{b,ab}(2,1.1,1.2)$	0.389	0.426	0.370	0.400

meaningful exact integral calculation with the proper parametric configurational distances thus saving many difficult exact integral minimizing calculations. Extension of the approximate calculations to selection of proper orbital charge parameters is natural. Further, trial of orbital charge parameter variations, possible with approximate integrals, discloses the feasibility of obtaining a major improvement in the molecular binding-energy calculations of polyatomic molecules by the parametric orbital charge procedure.

In the energy calculations for the normal diatomic H_2 molecule Wang[12] obtained a marked improvement over earlier calculations by inclusion of an orbital charge parameter in his trial eigenfunction. The Wang function differs from the Sugiura or Heitler-London wave function only in the inclusion of this orbital charge parameter in the constituent atomic orbitals. Thus the specific atomic orbitals of Wang are of the form $a(1)=(Z^3/\pi)e^{-Zr_{a1}}$. When $Z=1$ these electron orbitals are identical to those used earlier. With the diatomic H_2 molecule the effective nuclear charge of both the constituent orbitals associated with the two nuclei are known to be equal from symmetry considerations. The "best" parametric value of Z can then be obtained at once from the differential minimization procedure of elementary calculus. The required integrals are, except for a scale factor, the same as those used before. For polyatomic molecules the beautiful simplicity of the Wang method is considerably modified. If all the constituent electronic orbitals of the molecular wave function have the same orbital charge parameter, Z, complicating modification[13,14] allows the retention of the minimizing differentiational procedure for obtaining the "best" Z value. The required integrals are also again, except for a constant scale factor, the same as for the corresponding Heitler-London type treatment. Hirschfelder obtained, by such a modification of the Wang procedure, a "best" parametric value ($Z=1.059$ at $R=1.889a_0$) for the simultaneous variation of the constituent $1s$ atomic orbitals of the Heitler-London-like treatment of the H_3 molecule. He also obtained a "best" single orbital charge parametric value ($Z=1.0865$ at $R=1.84077a_0$) for the covalent structural plus ionic terms treatment of H_3 by further modification of the Wang procedure retaining the differentiational and the like integral features. If the constituent electron orbitals for H_3 or any polyatomic molecule contain two or more different screening constants (different orbital charges) the methods for obtaining "best" parametric values become much more complex. Many of the integrals arising are no longer, even by a scale factor, the same as those occurring in the corresponding treatments with no orbital charge parameters. Further, there is no longer any possibility of using the original Wang-like differentiational procedure to obtain the proper Z values. This latter consideration makes necessary a number of complete trial and error calculations to obtain the "proper" parametric values. Even for the simplest polyatomic molecule use of exact integral values in such repeated trial and error evaluations seems out of the question. As stated previously, one exact value of one of the simpler needed three-center mixed orbital integrals would require several days to evaluate by known methods. Thus if a mixed orbital covalent structural treatment for H_3 is to be completed, even in this age of electronic computing machines, some rapid method of obtaining the "proper" parametric values of the configurational and orbital charge parameters is a necessity. Once, however, such parametric values are obtained single exact evaluations of the several type multicenter integrals by known methods places the mixed orbital charge calculation for H_3 within the realm of reason.

Five multicenter mixed orbital charge integrals occur in either the covalent or the covalent-plus-ionic-terms treatments of H_3. These multicenter integrals have to be evaluated by series methods in all known exact integral procedures. One of these, the nuclear attraction integral $K_{a,bc}$ is obtainable from the R-M approximation (1.3). The four others, all electron repulsion integrals, are amenable to the M approximation (1.1). Thus the needed integrals may be obtained, either exactly or by good approximation, in a reasonable time. One may also approximate by (1.1) the two-center mixed orbital charge exchange integral $L_{ab,ab}$ for which exact values require series methods of intermediate practicality. Using a combination of exact and approximate integral evaluations, the trial and error selection of parametric values of the configurational and orbital charge constants may easily be accomplished. The parametric values so secured should be near the "best" values to use in a complete exact integral calculation. The details of such a mixed orbital energy calculation for H_3 are given in the next section.

4. APPROXIMATE H_3 ENERGY CALCULATIONS USING A MIXED ORBITAL CHARGE WAVE FUNCTION

The importance of the first-principle energy calculation of H_3 to chemical reaction rate theory has often been recognized.[3] The simple Heitler-London covalent structure treatment for this molecule has been considered in detail.[3,14] The corresponding treatment with mixed orbital charge parameters differs somewhat in setup and so is here briefly outlined. The variation principle is used. That is $E\leq\int\psi^*H\psi d\tau/\int\psi^*\psi d\tau$. The Hamiltonian operator H in atomic units (energy units of e^2/a_0, distance units of a_0) is of course the same as in the Heitler-London treatment. That is

$$H=-\tfrac{1}{2}(\nabla_1^2+\nabla_2^2+\nabla_3^2)+1/R_{ab}+1/R_{ac}+1/R_{bc}-1/r_{a1}-1/r_{a2}-1/r_{a3}-1/r_{b1}-1/r_{b2}-1/r_{b3}-1/r_{c1}-1/r_{c2}-1/r_{c3}+1/r_{12}+1/r_{13}+1/r_{23}. \quad (4.1)$$

[12] S. C. Wang, Phys. Rev. **31**, 579 (1928).
[13] C. A. Coulson, Proc. Cambridge Phil. Soc. **31**, 244 (1935).
[14] J. O. Hirschfelder, Doctoral thesis, Princeton University (1935).

TABLE VII. Variable orbital charge treatments of H_2 and H_3.

Treatment	H_2 R	Z	Binding energy (kcal/mole)
Heitler-London	1.66 (best)	1	72.4 (Sugiura)
Orbital charge variation	$1.45a_0$	1.166 (best)	86.5 (Wang)
Experimental	$1.40a_0$		109.3

Treatment	H_3 R	Z_0	Z_m	Binding energy	
Heitler-London	$1.7a_0$	1	1	39.9	(Coolidge-James)
	2.0 (best)	1	1	53.4	(H., E., and R.)
Orbital charge variation	$1.889a_0$	1.059	1.059	56.45	(H., E., and R.)
	1.8	1.0	1.08	~72.7	(Barker-Eyring)
Experimentally derived	...	...	...	103	kcal/mole

The covalent structural molecular wave function for H_3 in terms of constituent atomic orbitals is likewise written

$$\psi_{\text{eov}}=2\begin{pmatrix} a & b & c \\ \alpha & \beta & \alpha \end{pmatrix}-\begin{pmatrix} a & b & c \\ \beta & \alpha & \alpha \end{pmatrix}-\begin{pmatrix} a & b & c \\ \alpha & \alpha & \beta \end{pmatrix}. \quad (4.2)$$

The notation $\begin{pmatrix} a & b & c \\ \alpha & \beta & \alpha \end{pmatrix}$ represents the usual Slater determinant

$$\begin{pmatrix} a & b & c \\ \alpha & \beta & \alpha \end{pmatrix}=\frac{1}{(3!)^{\frac{1}{2}}}\begin{vmatrix} a(1)\alpha(1) & b(1)\beta(1) & c(1)\alpha(1) \\ a(2)\alpha(2) & b(2)\beta(2) & c(2)\alpha(2) \\ a(3)\alpha(3) & b(3)\beta(3) & c(3)\alpha(3) \end{vmatrix}. \quad (4.3)$$

The use of the orthonormal properties of the spin functions α and β reduces the variational energy expression to orbital integrals in the customary manner. The orbital integral notation $\int a(1)b(2)c(3)Ha(1)c(2)b(3)d\tau = (abc|H|acb)=a^2bccb$ has been used, where H represents the complete Hamiltonian operator given before and where the simple orbital type designations are $a(1)=(Z_0^3/\pi)^{\frac{1}{2}}e^{-Z_0r_{a1}}$, $b(2)=(Z_m^3/\pi)^{\frac{1}{2}}e^{-Z_mr_{b2}}$, etc. However, this reduction and collection of equal terms must be carried through with caution, as certain orbital integrals using mixed charge AO's are no longer equivalent. Thus $abbcac \neq abcbac$. The reduced orbital expression is

$$E_{\text{eov}}\leq\frac{6\{a^2b^2c^2+a^2bccb-acb^2ac-abbcac\}}{6\{1+I_{ab}^2(R,Z_0,Z_m)-I_{ac}^2(R,Z_0)-I_{ab}^2\cdot I_{ac}\}}. \quad (4.4)$$

The greatest departure of the equal and unequal or mixed orbital charge treatments, however, is to be found in the orbital to elemental integral conversion. The final elemental integral expressions obtained from the mixed orbital charge integrals are:

$$\begin{aligned}
1.\quad a^2b^2c^2&=\int a(1)b(2)c(3)Ha(1)b(2)c(3)d\tau \\
&=\frac{5}{2R}+\tfrac{1}{2}(2Z_0^2+Z_m^2)-(2Z_0+Z_m) \\
&\quad -2[G_{b,aa}+G_{a,bb}+G_{a,cc}] \\
&\quad +2K_{aa,bb}+K_{aa,cc}. \\
2.\quad a^2bccb&=\int a(1)b(2)c(3)Ha(1)c(2)b(3)d\tau \\
&=\left[\frac{5}{2R}-\tfrac{1}{2}Z_m^2-Z_0\right]I_{bc}^2 \\
&\quad +[Z_0J_{c,bc}+Z_mJ_{b,bc}]I_{bc} \\
&\quad -[G_{b,aa}+G_{c,aa}]I_{bc} \\
&\quad -2[K_{a,bc}+J_{c,bc}+J_{b,bc}]I_{bc} \\
&\quad +2I_{bc}\cdot L_{aa,bc}+L_{ab,ab}. \\
3.\quad b^2acac&=\int b(1)a(2)a(3)Hb(1)c(2)c(3)d\tau \\
&=\left[\frac{5}{2R}-Z_0^2+\tfrac{1}{2}Z_m^2-Z_m\right]I_{ac}^2 \\
&\quad +2[Z_0J_{a,ac}]I_{ac}-2G_{a,bb}I_{ac}^2 \\
&\quad -[2J_{a,ac}+K_{b,ac}]2I_{ac} \\
&\quad +L_{bb,ac}\cdot 2I_{ac}+L_{ac,ac}. \\
4.\quad abacbc&=\int a(1)a(2)b(3)Hb(1)c(2)c(3)d\tau \\
&=\left[\frac{5}{2R}-Z_0^2-\tfrac{1}{2}Z_m^2\right]I_{ab}^2\cdot I_{ac} \\
&\quad +[Z_mJ_{b,ab}+Z_0J_{c,bc}]I_{ac}I_{ab} \\
&\quad -[K_{a,bc}+J_{a,ab}+J_{b,ab}]2I_{ab}I_{ac} \\
&\quad -[K_{b,ac}+2J_{a,ac}-Z_0J_{a,ac}]I_{ab}^2 \\
&\quad +L_{ab,ac}2I_{ab}+L_{ab,bc}I_{ac}.
\end{aligned} \quad (4.5)$$

Results of the indicated calculations for H_3 lead to the values given in Table VII. Similar exact integral computations for the diatomic molecule H_2 are included for comparative purposes.

It may be noticed from Table VII that variation of orbital charge for the diatomic hydrogen molecule by Wang led to a binding energy of 86.5 kcal/mole which is a substantial improvement over the corresponding Sugiura treatment which contained no orbital charge parameter. Of course, by symmetry, orbital charges of the orbitals associated with both nuclei are the same. Thus but a single orbital charge parameter, Z, is needed. In fact it may be noted that the Wang treatment is an

improvement over both the covalent structural treatment (Sugiura) and the covalent-structure-plus-ionic-terms treatment (Weinbaum) which give binding energies for H_2 of 72.4 kcal/mole and 74.2 kcal/mole, respectively.

For the triatomic H_3 molecule a Wang-like variation of a single orbital charge parameter leads to a binding energy of only 56.45 kcal/mole which is but slight improvement over the covalent structural value (53.4 kcal/mole) and no improvement over the covalent-structure-plus-ionic-terms treatment value of 60.71 kcal/mole. However as Hirschfelder, Eyring, and Rosen[3] once stated: "It is not surprising that the variation of the screening constant on the three atoms simultaneously gives little improvement in the energy since one would expect that the central and outer atoms really ought to have different screening constants." Thus the need for a mixed orbital charge treatment was early recognized. That such a treatment would involve the evaluation of difficult mixed orbital charge integrals was also known and is undoubtedly the reason it has not been attempted until now.

When mixed orbital parameters are used (Z_0 for the orbitals on the outer and Z_m for the orbital on the middle nucleus) the distance normalized approximate evaluations of this paper give a value of 72.4 kcal/mole, which similar to the H_2 Wang calculation is larger than either the covalent structural or covalent-structure-plus-ionic-terms values. It should be noted that current constants ($e^2/a_0=27.206$ ev$=627.23$ kcal/mole) have been used for all energy comparisons. When current I.B.M. calculations are completed and the "best" values of the parameters Z_0, Z_m, and R obtained, it is hoped a complete exact value calculation will be forthcoming.

APPENDIX

There are 18 elemental integrals to be considered in the mixed orbital covalent structural treatment. These basic integrals may be written:

$$G_{a,b^2}(R,Z_m)=\int\frac{1}{r_{a1}}[b(1)]^2d\tau_1$$
$$=\frac{1}{R}[1-e^{-2Z_mR}(Z_mR+1)]. \quad (1)$$

$$G_{b,a^2}(R,Z_0)=\int\frac{1}{r_{b1}}[a(1)]^2d\tau_1$$
$$=\frac{1}{R}[1-e^{-2Z_0R}(Z_0R+1)]. \quad (2)$$

$$G_{a,c^2}(R,Z_0)=\int\frac{1}{r_{a1}}[c(1)]^2d\tau_1$$
$$=\frac{1}{2R}[1-e^{-4Z_0R}(RZ_0+1)]. \quad (3)$$

$$J_{a,ac}(R,Z_0)=\int\frac{1}{r_{a1}}a(1)c(1)d\tau_1$$
$$=Z_0[e^{-2Z_0R}(2Z_0R+1)]. \quad (4)$$

$$I_{ac}(2R,Z_0)=\int a(1)c(1)d\tau_1$$
$$=e^{-2Z_0R}\left(1+2Z_0R+\frac{(2Z_0R)^2}{3}\right). \quad (5)$$

$$K_{aa,cc}(2R,Z_0)=\int\frac{1}{r_{12}}[a(1)]^2[c(2)]^2d\tau_1d\tau_2$$
$$-\frac{1}{2R}\left[1-e^{-4Z_0R}\left\{\frac{(2Z_0R)^3}{6}+\frac{3(2Z_0R)^2}{4}+\frac{11(2Z_0R)}{8}+1\right\}\right]. \quad (6)$$

$$K_{b,ac}(R,Z_0)=\int\frac{1}{r_{b1}}a(1)c(1)d\tau_1$$
$$=\frac{3U}{4R}-Z_0(Z_0R+2)e^{-2Z_0R}, \quad (7)$$

where

$$U=I_{ac}(2R,Z_0)[C+\ln 4Z_0R]-F_{ac}(2Z_0,R)Ei(-4Z_0R)$$
$$C=0.577\ 21\ 567\cdots.$$

$$F_{ac}(2R,Z_0)=e^{2Z_0R}\left(1-2Z_0R+\frac{(2Z_0R)^2}{3}\right). \quad (7b)$$

$$L_{ac,ac}(2R,Z_0)=\int\frac{1}{r_{12}}a(1)c(1)a(2)c(2)d\tau_1d\tau_2$$
$$=\frac{Z_0}{R}\Big[e^{-4Z_0R}\Big\{\frac{25}{8}-\frac{23}{2}Z_0R-12(Z_0R)^2-\tfrac{4}{3}(2Z_0R)^3\Big\}+\frac{3}{Z_0R}\{I_{ac}^2(2R,Z_0)\times(C+\ln 2Z_0R)+F_{ac}^2(2R,Z_0)\cdot Ei(-8Z_0R)-2I_{ac}(2R,Z_0)\cdot F_{ac}(2R,Z_0)\cdot Ei(-4Z_0R)\}\Big]. \quad (8)$$

$$I_{ab}(R,Z_m,Z_0)=\int a(1)b(1)d\tau_1$$
$$=\frac{8(Z_m^3Z_0^3)^{\frac{1}{2}}}{RX^3}\{Z_m(RX-4Z_0)e^{-Z_0R}+Z_0(RX+4Z_m)e^{-Z_mR}\},^{15} \quad (9)$$

[15] This integral, as well as Eqs. (10) and (11), has been adapted from C. A. Coulson, Proc. Cambridge Phil. Soc. 38, 210 (1942).

where $X=(Z_m^2-Z_0^2)$.

$$J_{a,\,ab}(R,Z_m,Z_0)=\int\frac{1}{r_{a1}}a(1)b(1)d\tau_1$$

$$=\frac{4(Z_0^3Z_m^3)^{\frac{1}{2}}}{RX^2}[2Z_me^{-Z_0R}-(2Z_m+RX)e^{-Z_mR}]. \quad (10)$$

$$J_{b,\,ab}(R,Z_m,Z_0)=\int\frac{1}{r_{b1}}a(1)b(1)d\tau_1$$

$$=\frac{4(Z_0^3Z_m^3)^{\frac{1}{2}}}{RX^2}[2Z_0e^{-Z_mR}-(2Z_0-RX)e^{-Z_0R}]. \quad (11)$$

$$K_{aa,\,bb}(R,Z_m,Z_0)=\int\frac{1}{r_{12}}[a(1)]^2[b(2)]^2d\tau_1d\tau_2$$

$$=\frac{Z}{\rho}[1-(1-K)^2\{\tfrac{1}{4}(2+K)+\tfrac{1}{4}\rho_m\}e^{-2\rho_m}-(1+K)^2\{\tfrac{1}{4}(2-K)+\tfrac{1}{4}\rho_0\}e^{-2\rho_0}],^{16} \quad (12)$$

where

$$K=Z_m^2+Z_0^2/Z_m^2-Z_0^2;\quad Z=\tfrac{1}{2}(Z_m+Z_0);$$

$$\rho=\tfrac{1}{2}(Z_m+Z_0)R;\quad \rho_m=Z_mR;\quad \rho_0=Z_0R.$$

$$L_{ab,\,ab}(R,Z_m,Z_0)=\int\frac{1}{r_{12}}a(1)b(1)a(2)b(2)d\tau_1d\tau_2$$

$$\approx\tfrac{1}{2}I_{ab}^2\{L_{aa,\,aa}+L_{aa,\,bb}\}.^{17}$$

(M approx) (13)

$$K_{a,\,bc}(R,Z_m,Z_0)=\int\frac{1}{r_{a1}}b(1)c(1)d\tau_1$$

$$\approx\tfrac{1}{2}I_{ab}\{G_{a,\,b}^2+G_{a,\,c}^2\}.$$

(R-M approx) (14)

$$L_{aa,\,bc}(R,Z_m,Z_0)=\int\frac{1}{r_{12}}[a(1)]^2b(2)c(2)d\tau_1d\tau_2$$

$$\approx\tfrac{1}{2}I_{ab}\{L_{aa,\,bb}+L_{aa,\,cc}\}.$$

(M approx) (15)

$$L_{bb,\,ac}(R,Z_m,Z_0)=\int\frac{1}{r_{12}}[b(1)]^2a(2)c(2)d\tau_1d\tau_2$$

$$\approx I_{ab}\cdot L_{aa,\,bb}.$$ (M approx) (16)

$$L_{ab,\,ac}(R,Z_m,Z_0)=\int\frac{1}{r_{12}}a(1)b(1)a(2)c(2)d\tau_1d\tau_2$$

$$\approx\tfrac{1}{4}I_{ab}I_{ac}\{L_{aa,\,aa}+L_{aa,\,cc}+2L_{aa,\,bb}\}.$$ (M approx) (17)

$$L_{ab,\,bc}(R,Z_m,Z_0)=\int\frac{1}{r_{12}}a(1)b(1)b(2)c(2)d\tau_1d\tau_2$$

$$\approx\tfrac{1}{4}I_{ab}^2\{L_{aa,\,aa}+L_{aa,\,cc}+2L_{aa,\,bb}\}.^{18}$$ (M approx) (18)

ACKNOWLEDGMENT

We would like to thank Professor C. J. Thorne (Mathematics Department, University of Utah) for taking part in discussions of certain phases of this problem.

[16] This integral is taken from C. C. J. Roothaan, J. Chem. Phys. **19**, 1453 (1951).

[17] One may obtain "actual" values of this mixed orbital two-center exchange integral by the somewhat lengthy but relatively simple methods used by Rosen, Coolidge-James, Hirschfelder-Linnett, and Kotani.

[18] $L_{aa,\,aa}=\frac{5}{8}Z_0$. Details of this evaluation may be found in Eyring, Walter, and Kimball, *Quantum Chemistry* (John Wiley and Sons, Inc., New York, 1947, p. 103).

Rotational Energy Transfer in Diatomic Molecules

ROBERT BROUT
Department of Chemistry, University of Rochester, Rochester, New York
(Received February 3, 1954)

We have calculated the rotational energy transition probability upon collision using approximate results from a previous distorted wave calculation. For heavy homonuclear diatomic molecules, i.e. molecules with molecular weight >20, the mean transition probability is approximated by $\frac{1}{2}(d_0/r_0)^2$, where d_0 is the internuclear distance and r_0 the kinetic collision diameter. This expression is in agreement with relaxation times as calculated from shock wave data.

I.

IN a previous study[1] on rotational energy transfer in H_2 it was found that for a potential of the type

$$V=V_0e^{-\alpha r}(1+\lambda P_2(\cos\theta)) \tag{1}$$

the cross section for a transition where $\Delta j=2$, $\Delta m=0$ could be approximated by:

$$\sigma_{jj-2}=c\lambda^2\pi\frac{\alpha^2k_ik_f^3}{[\alpha^4+2\alpha^2(k_i^2+kf^2)+(k_i^2-kf^2)^2]^2}|M_{jj-2}|^2, \tag{2}$$

where

$$c=800,$$

$$k_i=(2\mu kT/\hbar^2)^{\frac{1}{2}},$$

$$k_f=(2\mu(kT+s\epsilon)/\hbar^2)^{\frac{1}{2}},$$

$$M_{jj-2}=\frac{(2j+1)^{\frac{1}{2}}(2j-3)^{\frac{1}{2}}}{2}\int_{-1}^{+1}P_1P_2P_j\,dx,$$

P_j= Legendre polynomial of order j,

where c has been fitted to give the accurate value of the transition probability in H_2 as calculated by a lengthy distorted wave procedure. It was found in the above study that this representation of the cross section gave a ratio σ_{31}/σ_{20} quite close to the ratio calculated by the accurate method. The reason why this should be so was, as indicated in I, because of the rapid approach of the distorted waves of all orders to their asymptotic values. Formula (2) is merely the scattering of the first distorted wave multiplied by a constant made to fit the scattering by all distorted waves.

It is the purpose of this article to extend these calculations to heavy diatomic molecules.

II.

It is first necessary to evaluate the matrix elements M_{jj-2}. We will assume that transitions for which $\Delta m\neq 0$ occur but negligibly, and all transitions for which $\Delta m=0$ are equally likely. This assumption is borne out by specific calculations in I.

[1] R. Brout, J. Chem. Phys. (to be published), hereafter referred to as I.

Then

$$|M_{jj-2}|^2=\frac{(2j-3)}{(2j+1)}\frac{(2j-3)(2j+1)}{4}\left|\int P_jP_2P_{j-2}dx\right|^2 \tag{3}$$

where the factor $(2j-3)/(2j+1)$ has been introduced to account for the fact that transitions cannot occur for $|m|\geqslant 2j$.

Performing the integration in (3)

$$|M_{jj-2}|^2=9/4j^2(j-1)^2/(4j^2-1)^2.$$

As most heavy diatomic molecules have significant j values for $j>5$, we may approximate

$$|M_{jj-2}|^2\approx 1/7. \tag{4}$$

We will now evaluate, by judicious approximation, the value of (2) averaged over all j, noting $|M_{jj-2}|^2$, as given by (4) is independent of j.

Let us denote $k_{\rm rot}^2=2\mu kT/\hbar^2$, where for heavy molecules $T_{\rm rot}<3°$K.

Then, noting that $k_f^2\approx k_i^2+4jk_{\rm rot}^2$, we may write (2)

$$\sigma_{jj-2}=\pi/7c\lambda^2\frac{\alpha^2k_i(k_i^2+4jk_{\rm rot}^2)^{\frac{1}{2}}}{[\alpha^4+2\alpha^2(2k_0^2+4jk_{\rm rot}^2)+16j^2k_{\rm rot}^2]^2}. \tag{5}$$

Now, for a diatomic molecule, of molecular weight 30

$$k_i^2=(2\mu kT/\hbar^2)\approx 180\text{A}^{-2} \quad \text{for} \quad T=300°\text{K}$$
$$4jk_{\rm rot}^2=45\text{A}^{-2} \quad \text{for} \quad j=6;$$

hence, to within 12 percent we may neglect $4jk_{\rm rot}^2$ with respect to $2k_i^2$. This approximation is of the order of the error made in the original approximation (2). We will expect in our final answer a deviation of some 25 percent from the true answer; hence our calculation will give a reasonably reliable estimate of transition probabilities, i.e., to within the approximate order of experimental error in sound dispersion or shock wave estimates of small relaxation times of the order of 10^{-8} second.

Proceeding with the above approximation

$$\sigma_{jj-2}=\pi/7c\lambda^2\frac{\alpha^2k_i^4}{[\alpha^4+4\alpha^2k_i^2+16j^2k_{\rm rot}^4]^2}. \tag{6}$$

We now average over j with the approximate distribution $P(j)=2j\exp(-j^2)(T_{\text{rot}}/T)$, where we approximate $j^2=j(j+1)$ for mathematical convenience.

The expression $\int\sigma_{jj-2}P(j)dj/\int P(j)dj$ is readily evaluated after one partial integration with the use of the asymptotic expression for the logarithmic integral.[2]

If we define $A=((\alpha^4+4\alpha^2k_i^2)/16k_{\text{rot}}^4)(T_{\text{rot}}/T)$, the final value of our cross section averaged over j is given by:

$$\bar{\sigma}=\pi/7c\lambda^2/256\alpha^2k_i^4(T_{\text{rot}}/T)^2[1/A+0.557+\log A]. \quad (7)$$

For $\alpha=4\text{A}^{-1}$ and normal values of T, T_{rot}, and μ, $A=0.5\times10^{-2}$. We may therefore neglect the last two terms in (7) in comparison with the first.

Using our definition of A, we may then express σ in the following form

$$\sigma=(\pi/7)(c\lambda^2/10)(T/T_{\text{rot}})(1/\alpha^2+4k_i^2). \quad (8)$$

Equation (8) is in a form convenient for calculation; however, it may be approximated further by noting that for $\alpha=4\text{A}^{-1}$, for molecules of molecular weight 30

$$\alpha^2/4k_i^2=1/7.$$

If we neglect α^2 in comparison with $4k_i^2$, we partially compensate for the approximation that went into (6), and (8) becomes

$$\bar{\sigma}_{\text{rot}}=(\pi/7)(c\lambda^2/64)(T/T_{\text{rot}})(1/k_i^2).$$

Abbreviating $c\lambda^2/7\times64=B$, the mean rotational deactivation transition probability for symmetric diatomic molecules is found

$$\bar{P}_{\text{deact}}=(\bar{\sigma}_{\text{rot}}|\sigma_{\text{kin}})=B/2(d_0/r_0)^2 \quad (9)$$

where $d_0=$internuclear distance and $r_0=$kinetic collision diameter. To derive (9), we use the definitions

$$kT_{\text{rot}}=\hbar^2/2I.$$

$I=\frac{1}{2}\mu d_0^2$; $\mu=$reduced mass of molecule$=$mass of one of the atoms, and approximate $k_i^2=2\mu kT/\hbar^2$.

In (9) we have the parameter $B=c\lambda^2/7\times64$ where $c=800$. λ^2 may be estimated by considering the potential $\Sigma e^{-\alpha(r_{ij})}$ summed up over four atoms, two on each of two molecules. One then averages over all the rotational configurations of one of the molecules, keeping the other fixed. The result is expanded in spherical harmonics, only those of order 2 being retained. In this manner for $\alpha=4\text{A}^{-1}$, $d_0=1\text{A}$, we find $\lambda=0.7$ (for H_2, $\lambda=0.45$ because of its small d_0).

Hence we may put $B=1$, thus giving a transition probability

$$\bar{P}_{\text{deact}}=\tfrac{1}{2}(d_0/r_0)^2.$$

For

O_2 $d_0=1.2$ $r_0=3.6$:

$\bar{P}_{\text{deact}}=0.057$ or 17 collisions to deactivate

N_2 $d_0=1.1$ $r_0=3.8$:

$\bar{P}_{\text{deact}}=0.043$ or 23 collisions to deactivate.

These are indeed the approximate rotational relaxation times found in shock wave experiments as conducted by Hornig and his co-workers.[3] In their work, they come to the conclusion that one needs more than one relaxation time to fit their data, in which case one must use the unaveraged formula (6).

From our final expression (10), we may deduce the following: the rotational energy deactivation probability does not sensibly vary from molecule to molecule when the molecular weight is greater than 20 and $T\gg T_{\text{rot}}$.

One may well ask why formula (10) is so simple. The answer is not hard to find. Firstly, the temperature does not appear because of the following compensation. The higher the temperature, the more the mean spreading of the rotational levels, hence the lower the transition probability. But this is compensated by the increase of the transition probability with kinetic energy as expressed by the numerator of (2). The mass does not appear for the same reason. As is well known, inelastic transition probabilities decrease with increase of mass;[4] however, an increase of mass brings the rotational levels closer together, thereby increasing the transition probability. The parameter of the potential, does not appear because the collision time is short with respect to the rotational frequency; hence we would not expect a measure of the "softness" of the potential to affect the transition probability. The only remaining molecular parameters are d_0 and r_0 for a rigid molecule, as assumed here. Hence, by dimensional considerations alone, we are led to $P=f(d_0/r_0)$. The form of f is given by (10).

III. ACKNOWLEDGMENT

The author is indebted to the Shell Fellowship Committee for financial aid tendered him as a post-doctoral fellow under a grant to the Department of Chemistry of the University of Rochester.

[2] E. Jahnke and F. Emde, *Tables of Functions* (Dover Publications, New York, 1945), p. 2.

[3] E. F. Greene and D. F. Hornig, J. Chem. Phys. **21**, 617 (1953).

[4] C. Zener, Phys. Rev. **37**, 556 (1931).

Infrared and Raman Spectra of 1,1-Dimethylhydrazine and Trimethylhydrazine*†

E. R. SHULL,‡ J. L. WOOD,§ J. G. ASTON, AND D. H. RANK
Department of Chemistry, the Pennsylvania State University, State College, Pennsylvania

(Received February 1, 1954)

Infrared spectra of 1,1-dimethylhydrazine between 700 and 1600 cm^{-1} for the gas phase and between 700 and 3500 cm^{-1} for the liquid phase and of trimethylhydrazine between 700 and 3500 cm^{-1} for the gas and liquid phases are reported along with the Raman spectra of the two compounds. Frequency assignments are given for both compounds.

I. INTRODUCTION

THE fundamental frequencies of 1,1-dimethylhydrazine and trimethylhydrazine were needed for calculations of the entropy of their vapors followed by comparison with the calorimetric values to yield values of the barriers hindering internal rotation about the N—N bond in the two compounds. Such a comparison has already been made for hydrazine,[1] methylhydrazine,[2] and 1,2-dimethylhydrazine.[3]

II. EXPERIMENTAL

(a) Materials

In both cases part of the calorimetric samples were used. The 1,1-dimethylhydrazine had 0.01 mole percent impurity,[4] and the trimethylhydrazine had 2.1 mole percent impurity.[5] The high percentage impurity in the latter case was due to the difficulty of preparation and a very closely boiling impurity which was difficult to

TABLE I. Infrared and Raman spectra 1,1-dimethylhydrazine.

Infrared (Gas)			Infrared (Liquid)			Raman (Liquid)			
ν	I[a]	Structure	ν	I[a]	Structure	$\Delta\nu$	I[a]	Pol.[b]	Breadth
						282	w	p	Diffuse and broad
						418	m	p	Narrow
						445	m	p	Narrow with diffuse wing at longer λ
803	vs	*PQR*	793	s	Broad	809	vs	p	Narrow
904	s	*PQR*	848	?					
961	m	*Q*	944	s	Broad	957	w	pp?	Diffuse
1016	vw		1009	s	Broad	1027	m	p	Narrow
1046	vs	*PQR*							
1090	m	*Q*	1069	s	Broad	1061	w	pp	Diffuse but not too broad
1139	s	*Q*?	1140	s	?	1150	s	p	Narrow
1153	Branch on 1139								
1214	m	*PQR*	1201	s	?	1212	m	dp?	Narrow
			1243	m	?	1248	m	pp	Diffuse but narrow
1301	m	*PQR*	1321	s	?	1325	vvw	dp?	Diffuse
						1405	m	dp	Narrow
1457	m	*PQR*	too strong to measure			1423	s	dp	Broad
1593	m	?	—			1599	w	pp	Diffuse
			2764	m		2774	?		Covered by Hg line
			2811	m		2817	?	p?	Narrow blends into Hg line
			2844			2849	m–s	p	Narrow
						2881	w	p	Narrow
			2944	m		2950	s	p	Narrow
			2975	w		2988	m	dp	Diffuse
			3126	vw		3141	m	p	Narrow
			3298	w		3330	vw	dp?	Diffuse

[a] vvw, vw, w, m, s, vs denote, respectively: extremely weak, very weak, weak, medium, strong, and very strong.
[b] dp, pp, p denote, respectively: depolarized, partly polarized, and polarized.

* Contribution from the College of Chemistry and Physics of the Pennsylvania State University.
† This research was carried out under Contract N6 ONR-269, Task Orders III, V, and X of U. S. Office of Naval Research.
‡ Present address: Tonawanda Laboratory, Linde Air Products Company Division of Union Carbide and Carbon Corporation, Tonawanda, New York.
§ Present address: Department of Chemistry and Biology, Sir John Cass College Aldegate, England.
[1] Scott, Oliver, Gross, Hubbard, and Huffman, J. Am. Chem. Soc. **71**, 2293 (1949).
[2] Aston, Fink, Janz, and Russell, J. Am. Chem. Soc. **73**, 1939 (1951).
[3] Aston, Janz, and Russell, J. Am. Chem. Soc. **73**, 1943 (1951).
[4] Aston, Wood, and Zolki, J. Am. Chem. Soc. **75**, 6202 (1953).
[5] J. G. Aston and T. P. Zolki (to be published).

TABLE II. Infrared and Raman spectra of trimethylhydrazine.

Infrared (Gas)			Infrared (Liquid)			Raman (Liquid)			
ν	I[a]	Structure	ν	I[a]	Structure	$\Delta\nu$	I[a]	Pol.[b]	Breadth
						307	w	dp	Diffuse
						414	m	dp	Narrow
						436	m	p	Narrow
						498	s	p	Narrow
712	vw		688	vw					
783	vs		739	vs	Broad	747	s	pp	Narrow
888	vs		883	vs	Broad	884	m	p	Diffuse
1007	vs	Broad	958	m	Sharp	965	m	dp	Narrow
1044	w		1005	m	Sharp	1013	m	dp?	Narrow
			1077	m	Sharp	1083	m	pp	Narrow
1134	s		1119	m	Sharp	1126	ms	p	Narrow
1168	m		1165	w					
1180?	m		1189	m	Sharp				
1270	m		1212	m	Sharp	1215	w	dp	Diffuse
						1398	m	dp	Narrow
1477	s		1485	s	Broad	1448	s	dp	Broad and diffuse
			2458						
			2485						
			2535						
			2571						
			2593						
			2685						
2858	s		2858	vs		2843	m?	dp?	
2970	s		2970	vs		2987	vs	dp	Broad
3082	m					3032	s	dp?	Narrow
3092	m	Sharp	3194	m					
3405	m		3405	vw		*ca* 3400	m	p	Narrow

[a] See notes at foot of Table I.

remove by fractional melting with the quantity of sample at our disposal.

(b) Raman Spectra

The Raman spectra were obtained with a three-prism spectrograph.[6] Excitation was the mercury blue line 4358A, produced by a pair of low-pressure mercury arcs[7] using a filter consisting of saturated aqueous sodium nitrite solution in two cylindrical condensers. Eastman 102a–0 spectroscopic plates backed with opaque red were used. The Raman shifts were determined from measurements on comparison spectra made using an iron-chromium (stainless steel) arc with a 20-in. $f/8$ camera (giving a linear dispersion of 19A/mm at 4600A) for the 1,1-dimethylhydrazine and with a 10-in. $f/3.5$ camera[8] (dispersion 32A/mm at 4600A) for the trimethylhydrazine. Qualitative depolarization determinations were obtained photographically by the method of polarized incident light[9] using a 5-in. $f/2$ camera.[8] Exposure times up to 40 hr were used.

TABLE III. Assignments for 1,1-dimethylhydrazine—trimethylhydrazine.

1,1-Dimethylhydrazine		Trimethylhydrazine	
Assignment	Frequency	Assignment	Frequency
Skeletal bend	418	Skeletal bend	307
Skeletal bend	445(2)	Skeletal bend	414
Skeletal stretch	803	Skeletal bend	436
Skeletal stretch	904	Skeletal bend	498
Skeletal stretch	961	Skeletal stretch	712
Rocking	961	Skeletal stretch	783
Rocking	1046(2)	Skeletal stretch	888
Rocking	1090(2)	Skeletal stretch	1007
Rocking	1139	CH_3 rock	1044(2)
CH_3 bend	1301(4)	CH_3 rock	1134(2)
CH_3 bend	1405	CH_3 rock	1168(2)
CH_3 bend	1457	NH bend	1180
NH_2 bend	1593	NH bend	1270
CH_3 stretch	2950(3)	CH_3 bend	1398(3)
CH_3 stretch	2988(3)	CH_3 bend	1477(6)
NH_2 stretch	3741	CH_3 stretch	2858(4)
NH_2 stretch	3330	CH_3 stretch	2970(2)
		CH_3 stretch	3082
		CH_3 stretch	3092(2)
		NH stretch	3405

(c) Infrared Spectra

The infrared spectra of the liquid and gas phases of the two compounds were obtained with a Perkin-Elmer Model 120 infrared spectrometer which had been modified to the Walsh double-pas optical arrangement[10] and equipped with prisms of lithium fluoride, sodium chloride, and potassium bromide. The gas phase spectra were obtained with a 10-cm cell at two pressures, a lower pressure to obtain detail in the strong bands and

[6] Rank, Scott, and Fenske, Ind. Eng. Chem., Anal. Ed. **14**, 816 (1942).

[7] D. H. Rank and J. S. McCartney, J. Opt. Soc. Am. **38**, 279 (1948); Rank, Sheppard, and Szasz, J. Chem. Phys. **16**, 698 (1948).

[8] D. H. Rank, J. Opt. Soc. Am. **40**, 462 (1950).

[9] A. E. Douglas and D. H. Rank, J. Opt. Soc. Am. **38**, 281 (1948); Rank, Saksena, and Shull, Disc. Faraday Soc. No. 9, 187 (1950).

[10] A. Walsh, J. Opt. Soc. Am. **42**, 96 (1952).

a higher one to detect weaker bands. The data on the two compounds are recorded in Tables I and II.

III. DISCUSSION

In considering the spectrum of 1,1-dimethylhydrazine comparison was made with the assignment for trimethylamine[11] when assigning frequencies to the skeletal modes. This is justified by the fact that the present molecule has an approximate geometrical symmetry of C_{3v} and the N—N force constant is not greatly different to that of C—C as can be seen by comparing the spectrum of methyl hydrazine[12] with that of dimethylamine. Regard was paid to this approximate symmetry in making use of the polarizations as a guide in the assignments. In assigning the NH stretching and bending frequencies comparison was made with the spectrum of methylhydrazine.[12]

In assigning frequencies to the skeletal modes of trimethylhydrazine comparison was made with *iso*-pentane,[13] and when treating the NH, stretching and bending comparison was made with sym. dimethylhydrazine.[12]

[11] Aston, Sagenkahn, Szasz, Moessen, and Zuhr, J. Am. Chem. Soc. **66**, 1171 (1944).
[12] Axford, Janz, and Russell, J. Chem. Phys. **19**, 704 (1951).
[13] Schumann, Aston, and Sagenkahn, J. Am. Chem. Soc. **64**, 1039 (1942).

TABLE IV. Combination frequencies for 1,1-dimethylhydrazine

Infrared (gas)	Raman (liquid)	Combination
1214	1212	418+803
	2774	418+803+1593
	2817	1405+1423
	2849	2×1457
	2881	1593+1301

The assignment is given in Table III while Table IV gives the explanation of frequencies unassigned for 1,1-dimethylhydrazine as combinations of assigned frequencies. In the case of trimethylhydrazine there are six unassigned combination bands between 2458 and 2685 cm^{-1} in the liquid infrared which do not appear in the liquid Raman spectrum. No attempt is made to assign these bands.

The frequency of 282 cm^{-1} in the Raman spectrum of 1,1 demethylhydrazine is probably due to internal rotation.[4]

THE JOURNAL OF CHEMICAL PHYSICS VOLUME 22, NUMBER 7 JULY, 1954

Infrared Spectra of Thionyl Chloride and Sulfuryl Chloride

DOWELL E. MARTZ AND ROBERT T. LAGEMANN
Department of Physics and Astronomy, Vanderbilt University, Nashville, Tennessee
(Received February 1, 1954)

The infrared spectra of thionyl chloride and sulfuryl chloride have been investigated from 400 cm^{-1} to to 5000 cm^{-1} with a prism spectrometer. Three of the fundamentals of $SOCl_2$ have been found and four for SO_2Cl_2. They and the various additional bands have been assigned to their appropriate symmetry species assuming $SOCl_2$ has C_s symmetry and SO_2Cl_2 has C_{2v} symmetry.

THE Raman spectra of thionyl chloride ($SOCl_2$) and sulfuryl chloride (SO_2Cl_2) have been extensively studied.[1–7] There is good agreement on the numerical values of the fundamental frequencies and at the same time some disagreement on the depolarization factors of the lines. For both molecules assignments of the observed frequencies to the corresponding normal modes have been made, most recently by Vogel-Hogler who gives a good summary of the various data. The infrared data are meager however. Schreiber[8] has studied both molecules over a narrow spectral range in CCl_4 solution. Also using a prism instrument, Vencov and Stefanescu[9] have made measurements on $SOCl_2$ out to 9μ. It has now been possible to examine the infrared vibrational spectrum of each molecule from 2 to 25μ and to give an analysis which includes the Raman and infrared data.

[1] H. Nisi, J. Phys. Japan **5**, 119 (1929).
[2] F. Matossi and H. Aderhold, Z. Physik **68**, 683 (1931).
[3] S. Venkateswaran, Nature **127**, 406 (1931).
[4] J. Cabannes and A. Rousset, Ann. phys. **19**, 229 (1933).
[5] K. Venkateswarlu, Proc. Indian Acad. Sci. **10A**, 156 (1939).
[6] R. Vogel-Hogler, Acta Phys. Austriaca **1**, 323 (1948).
[7] C. A. McDowell, Trans. Faraday Soc. **49**, 371 (1953).
[8] K. C. Schreiber, Anal. Chem. **21**, 1168 (1949).

EXPERIMENTAL

The samples of $SOCl_2$ and SO_2Cl_2 were obtained from the Hooker Electrochemical Company and were distilled immediately prior to study. Nevertheless, in the spectrum of $SOCl_2$ there was evidence of SO_2 and SO_2Cl_2 and in that of SO_2Cl_2 some SO_2. The infrared spectra of the gases were observed between 2 and 25μ in 10-cm cells with a Perkin-Elmer, Model 21, double-beam spectrometer equipped with NaCl and KBr prisms. Most of the runs were made with the gas at

[9] S. Vencov and D. Stefanescu, Bull. Soc. roumaine phys. **39**, 13 (1938).

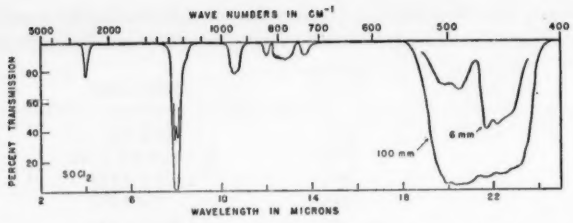

FIG. 1. Infrared spectrum of thionyl chloride.

room temperature. Other runs using liquid samples 0.26 mm thick and using a heated cell for gases did not reveal additional bands. The observed spectra are shown in Figs. 1 and 2. The positions of the absorption maxima are given in Tables I and II, which also list the Raman data obtained by Vogel-Hogler. The infrared spectrum of $SOCl_2$ reported by Vencov and Stefanescu[9] for the range 2–9μ does not agree with that described here, except that we both find the S—O stretching frequency. Although our results were obtained using a maximum pressure (100 mm) greater than theirs (38 mm) we do not find the many bands they report in the combination region and which they interpret as due to high-order combinations, although the lower order combinations are not found.

INTERPRETATION

$SOCl_2$

If the $SOCl_2$ molecule is a pyramid of one plane of symmetry and belongs to the C_s point group, it will have six normal vibrations active in both the Raman and the infrared: four of type A' and two of type A''. Four of the Raman lines (those associated with A' vibrations) should be polarized, and two (those associated with A'' vibrations) should be depolarized to the limit. On the other hand, if the $SOCl_2$ molecule is planar and of C_{2v} symmetry, the six normal modes will also be active in both the Raman and infrared. But, three lines, of symmetry species A_1, will be polarized in the Raman, and three others, two of species B_1 and one of B_2, will be depolarized in the Raman. For the C_s model all combination frequencies are active in both the Raman and infrared, and for the C_{2v} model all combinations are active except those few in the infrared arising from A_2 symmetry. Thus it is seen that the infrared will not furnish much evidence to determine the symmetry, whereas the Raman polarization measurements should furnish a crucial test. Unfortunately the various polarization data do not provide unanimous evidence for either model. Although Venkateswarlu[5] reports three polarized and three depolarized Raman lines, the other investigators report four polarized and two depolarized lines, supporting C_s symmetry. Furthermore, the electron diffraction data[10,11] support C_s symmetry, as does the theory of directed valence, and there is some evidence from the infrared spectrum in its favor, as will be pointed out. Accordingly we will interpret the vibrational spectrum on the basis of C_s symmetry.

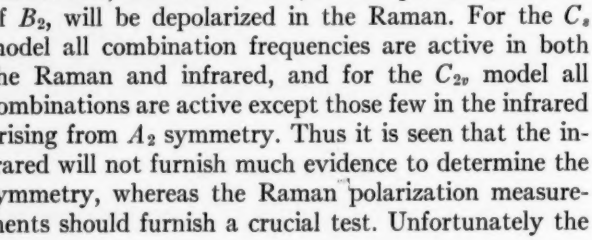

FIG. 2. Infrared spectrum of sulfuryl chloride.

The assignments of Table I take into consideration the Raman data and the three fundamentals found in the infrared region studied. Since SO_2 has its S—O symmetric stretching frequency at 1150.5 cm^{-1}, the infrared band at 1251 cm^{-1} in $SOCl_2$, which is polarized in the Raman, can be similarly assigned. (In SO_2Cl_2 the band at 1205 cm^{-1} has been assigned to the S—O stretch.) The S—Cl in-phase stretch has been assigned as 492 cm^{-1}, in view of the fact that this line is polarized in the Raman and very strong in the infrared, and because this vibration in S_2Cl_2 is found[12] at 448 cm^{-1}. The

TABLE I. Observed frequencies and band assignments for $SOCl_2$.

Raman, cm^{-1} Vogel-Hogler	Infrared, cm^{-1} Schreiber, liquid	Infrared, cm^{-1} Present work, gas	Assignment and approximate character	Type
194			ν_4(SCl$_2$ bending)	A'
284			ν_6(Torsion)	A''
344			ν_3(OSCl$_2$ deformation)	A'
443		455 vs	ν_5(S—Cl asymmetric stretch)	A''
490		492 vs	ν_2(S—Cl symmetric stretch)	A'
		735 w	$\nu_5+\nu_6$	A'
		778 w	$\nu_2+\nu_6$	A''
		800 w	$\nu_3+\nu_5$	A''
		833 w	$\nu_2+\nu_3$	A'
		950 m	$\nu_2+\nu_5$	A''
	1140 w		SO_2(?)	
	1200 knee			
1229	1238 s	1251 vs	ν_1(S—O symmetric stretch)	A'
	1350 m	1360 w	SO_2	
		2506 m	$2\nu_1$	A'

S—Cl asymmetrical stretch (A'') should be slightly lower in frequency and to it is assigned 455 cm^{-1}. The lowest frequencies, as is usual, probably correspond to bending motions and 194 is assigned to the SCl_2 bend (A'). The torsion vibration (A'') and the deformation (A') are assigned as 284 and 344, respectively, since the latter is polarized in the Raman and the former definitely not.

There is some evidence from the infrared, although not unequivocal, that $SOCl_2$ is not of C_{2v} symmetry. If one makes a plausible assignment of the fundamentals on the assumption of C_{2v} symmetry, one finds a forbidden band in the infrared. Thus, one might assign 492 cm^{-1} to the S—Cl in-phase stretch (A_1), 1251 to the S—O stretch (A_1), 194 to the S—Cl_2 bend (A_1), 443 to the S—Cl asymmetric stretch (B_1), 284 to the B_1 deformation, and 344 to the B_2 out-of-plane vibration,

[10] K. J. Palmer, J. Am. Chem. Soc. **60**, 2360 (1938).
[11] D. P. Stevenson and R. A. Cooley, J. Am. Chem. Soc. **62**, 2477 (1940).
[12] J. C. Morris, J. Chem. Phys. **11**, 230 (1943).

in analogy with assignments for F_2CO and Cl_2CO, which are planar. Now in the region of 800 cm^{-1} one finds three bands, 778, 800, and 833 cm^{-1}, which are readily explained on the basis of C_s symmetry (see Table I). But C_{2v} symmetry permits only two binary combinations in this region: namely, $(344, B_2)+(490, A_1)=(834, B_1)$, and $(284, B_1)+(490, A_1)=(744, B_1)$, whereas $(344, B_2)+(443, B_1)=(787, A_2)$ which is not allowed.

SO_2Cl_2

For this molecule considerable Raman data are available, all pointing to a symmetry of the C_{2v} point group. There are nine normal vibrations: four of type A_1; one type A_2; two type B_1; and two type B_2. The molecule has two planes of symmetry, one containing the two chlorine atoms and the sulfur, the other the two oxygen atoms and the sulfur. All fundamentals, overtones, and combinations are allowed in the Raman spectrum, while all fundamentals (except A_2), all overtones (except A_2^n, n odd), and all combinations (except $A_1 \times A_2$ and $B_1 \times B_2 = A_2$) are permitted in the infrared. The polarized lines in the Raman correspond to the A_1 vibrations, the depolarized lines to the others.

Four of the fundamentals were found in the infrared. The interpretation of the vibrational spectrum is given in Table II. The band at 1205 cm^{-1} is assigned to the SO_2 symmetrical stretch, since it is polarized in the Raman and the similar vibration in SO_2 occurs at 1150.5 cm^{-1}. The SO_2 asymmetric stretch is found at 1434 (1336 in SO_2 and 1229 in $SOCl_2$) and is depolarized in the Raman. The SO_2 bend should be found at about half the stretching frequencies and corresponds to the infrared band at 586 (524.5 in SO_2) which is depolarized in the Raman at 563. The S−Cl symmetric stretch, after consideration of the stretching frequencies in S_2Cl_2 and $SOCl_2$, may be assigned as 403–408, the doublet being caused by the chlorine isotopes. The S−Cl asymmetric stretch corresponds to the frequency 388, which is depolarized. (In both $SOCl_2$ and SO_2Cl_2 the symmetric stretch is believed by us to occur at a higher frequency than the asymmetric stretch.) The SCl_2 bending mode would be expected at a lower frequency and is assigned as 209. The torsion and rocking modes, A_2, B_1, and B_2, are probably found at 280, 363, and 577, respectively. From a consideration of the corresponding vibrations in SO_2F_2[13] we assign 577 to the B_2 mode and 586 to the A_1 (SO_2 bend) mode.

Of the nine fundamental vibrations previously determined by Raman investigations five lay in the infrared region covered by this work. Only four were observed. Failure to observe the other in the vicinity of 408 cm^{-1} is attributed to the unsatisfactory conditions existing when the KBr prism is used at its extreme spectral range. The torsion frequency, forbidden in the infrared, is expected to occur at a much lower frequency than our apparatus would detect.

[13] W. D. Perkins and M. K. Wilson, J. Chem. Phys. **20**, 1791 (1952).

TABLE II. Observed frequencies and band assignments for SO_2Cl_2.

Raman, cm^{-1} Vogel-Hogler	Infrared, cm^{-1} Schreiber, liquid	Infrared, cm^{-1} Present work, gas	Assignment and approximate character	Type
209			ν_4(SCl_2 bending)	A_1
280			ν_5(Torsion)	A_2
363			ν_7(Rocking)	B_1
388			ν_9(S−Cl asymmetric stretch)	B_2
403, 408			ν_3(S−Cl symmetric stretch)	A_1
556		577 vs	ν_8 (Rocking)	B_2
563		586 vs	ν_2(SO_2 bending)	A_1
578		595 m	$\nu_4+\nu_7$	B_1
		611 w	$\nu_4+\nu_9$	B_2
		619 w	$\nu_3+\nu_4$	A_1
		714 w	$2\nu_7$	A_1
		793 m	$\nu_3+\nu_4$, $\nu_4+\nu_8$	A_1, B_2
		946 w	$\nu_2+\nu_7$	B_1
		996 m	$\nu_3+\nu_5$, $\nu_2+\nu_3$	B_2, A_1
	1128 w			
	1160 s	1171 s	$2\nu_5$, $\nu_2+\nu_8$	A_1, B_2
1186	1196 s	1205 s	ν_1(S−O symmetric stretch)	A_1
1141	1419 s	1434 s	ν_6(S−O asymmetric stretch)	B_1
		2004 w	$\nu_2+\nu_5$, $\nu_1+\nu_3$	B_1, A
		2398 w	$2\nu_1$	A_1
		2632 m	$\nu_1+\nu_6$	B_1
		2869 w	$2\nu_6$	A_1

Some difficulty was encountered in resolving the two fundamentals whose Q branches are believed to be at 577 and 588. This is no doubt caused in part by the overlapping of bands due to the chlorine isotopes and the existence of absorption maxima from P and R branches. Moreover, a window band caused by the action of the gas on the KBr windows gave in this region a background which had to be subtracted from the observed spectrum. Nevertheless, the Raman data give assurance of two fundamentals in this region. The interpretation of the normal modes as given above agrees with that of Vogel-Hogler.[6]

SUMMARY

The infrared prism spectrum of $SOCl_2$ has been obtained and interpreted on the basis that the molecule possesses C_s symmetry. Such a model gains further support from the theory of directed valence, the electron diffraction data, and the majority of the Raman polarization data. There seems no question but that SO_2Cl_2 possesses C_{2v} symmetry and the infrared spectrum has been so interpreted.

ACKNOWLEDGMENTS

The authors are greatly indebted to Dr. Ernest A. Jones who not only made available experimental equipment but who participated in a large number of helpful discussions. One of us (D.E.M.) held a U. S. Atomic Energy Radiological Physics Fellowship at Vanderbilt University.

Lattice Parameters of the $FeFe_{(2-x)}Cr_xO_4$ Spinel System*

H. J. YEARIAN, J. M. KORTRIGHT, AND R. H. LANGENHEIM
Department of Physics, Purdue University, Lafayette, Indiana

(Received February 9, 1954)

Spinels of the $FeFe_{(2-x)}Cr_xO_4$, $0 \leqslant x \leqslant 2$, system have been made by reduction of the corresponding sesquioxide solid solution at 1180°C, 1100°C and 950°C and the lattice parameters determined at room temperature. The solutions of approximately stoichiometric composition have lattice parameters which vary with x in a nonlinear manner from 8.396±0.002A at $x=0$ to 8.376±0.002A at $x=2$. The four essentially linear segments comprising the total curve are interpreted as follows: from $x=0$ to $x=0.3$ the structure is completely inversed; from $x=1.28$ to $x=2.0$ it is completely normal; between these regions reversion from the inversed to the normal form occurs in two successive stages. Oxygen-rich spinels crystallized at 950°C show the same general variations of parameter but the region of complete inversion extends to approximately $x=0.6$.

DURING x-ray diffraction investigations of the oxides formed on chromium steels lattice parameters of the spinel type phases were observed which could not be interpreted satisfactorily on the basis of a linear variation of parameter in the solid solutions of $FeFe_2O_4$ and $FeCr_2O_4$. Deviations from Vegard's law might be anticipated in this system since it has been established by Verwey and Heilmann[1] that $FeCr_2O_4$ has the "normal" cationic arrangement whereas in $FeFe_2O_4$ the configuration is "inversed." In order to elucidate this situation, the spinels $FeFe_{(2-x)}Cr_xO_4$, $0 \leqslant x \leqslant 2$ have been synthesized and their lattice parameters determined.

PREPARATION OF MATERIALS

Appropriate proportions of reagent grade αFe_2O_3 and Cr_2O_3 (Baker's Analyzed) were intimately mixed by grinding, compacted in a molding press and sintered for several hours in air at temperatures of 1100°C to 1200°C. The rhombohedral solutions so formed gave excellent Debye-Scherrer diagrams which yielded lattice constants in good agreement with those determined by Wretblad.[2] The sintered ingots were crushed in a steel mortar and reduced to single phase spinels in a controlled $CO-CO_2$ atmosphere at temperatures of approximately 1180°C, 1100°C, and 950°C. At the conclusion of the reduction the sample was quenched by withdrawing it into a water cooled metal extension of the furnace tube proper. No appreciable differences were found between samples quenched in the reducing gas or in a nitrogen atmosphere. In the interest of obtaining a rapid quench, only small crucibles and samples were used.

It was observed during these experiments that the initial reduction product is poorer in Cr than the parent sesquioxide; the Cr content of the residual material therefore continues to increase and the final stages of the reaction involve the reduction of $Fe_2O_3-Cr_2O_3$ solutions approaching Cr_2O_3 in composition. At the lower temperatures this part of the process proceeds slowly even in strongly reducing atmospheres and could easily be misinterpreted as indicating a limited range of solubility in the spinel system. At 950°C spinels with an x larger than approximately 1.9 could not be attained as a single phase in 50 hours whereas at 1160°C $FeCr_2O_4$ was obtained free of the higher oxide in a few hours.

In addition to the single phase materials, spinels were prepared at 950°C in the metal-rich and oxygen-rich condition. No attempt was made to obtain two phase equilibria, but in each case the atmosphere was adjusted to give a rate of reduction or oxidation which would yield a few percent of the new phase in the one half to one hour reaction period. Immediately before quenching the sample the concentration of the reacting gas was increased by several percent to prevent a reversal of the reaction during cooling.

The oxidations were carried out in H_2O+H_2 for spinels of high x and in O_2+He for those of low x; the oxidation products were the oxygen-rich spinel and a sesquioxide solution which had a higher ratio of Cr to Fe than existed in the spinel. The reductions of all spinels except $x=2$ were carried out with $CO-CO_2$ mixtures, and gave the metal-rich spinel and FeO. Reduction of $FeCr_2O_4$ was effected with purified hydrogen dried in a trap cooled with liquid nitrogen. The reduced phase was a 2:1 solid solution of chromium and iron; it is not known whether this state was reached directly or by intermediate stages of reduction. The amount and composition of the precipitated phase was determined from the diffraction patterns and a correction made to obtain the x value of the residual spinel from the known value of the original spinel. No data are included herein for which the correction in x was larger than 0.05.

RESULTS

Lattice parameters were calculated from Debye-Scherrer diagrams obtained in 114.59 mm diameter cameras with filtered Cr radiation and calibrated by

* This research was conducted under the auspices of Project Squid, jointly sponsored by the U. S. Office of Naval Research and the Office of Air Research under contract N6-ori-104, and of the U. S. Office of Naval Research under contract N7-onr-39419.

[1] E. J. W. Verwey and E. L. Heilmann, J. Chem. Phys. **15**, 174 (1947).

[2] P. E. Wretblad, Z. anorg. u. allgem. Chem. **189**, 331 (1930).

the Straumanis technique. In some instances 57.3-mm cameras were used. Eccentricity and absorption errors were eliminated by graphical extrapolation,[3] giving an uncertainty in the result of ± 0.002A or less. The data obtained are plotted in Fig. 1. (In comparing these values with others in the literature it is to be noted that most of the latter are in *kX* units even when indicated as A units.)

It is evident that all of the single phase and metal-rich data are well represented by the same curve. This is understandable if it is assumed that the atmosphere used in order to reduce the sesquioxides at a convenient rate was sufficient to bring the spinel to, or near to, its metal-rich state, and further, that the composition of the metal-rich spinels does not change appreciably with temperature. In the case of Fe_3O_4 ($x=0$) it has been demonstrated[4] that the "metal-rich" compound has very nearly the stoichiometric composition. We therefore assume that the full curve represents the lattice parameter of essentially stoichiometric solutions.

That the curve for the oxygen-rich solutions lies below the one for stoichiometric solutions is to be expected from the generally accepted view that "oxygen-rich" actually corresponds to the presence of cation vacancies. This interpretation is in accord with the diffusion properties of Fe_3O_4.[5] Verwey and Haayman[4] have determined the lattice parameter of Fe_3O_4 at various stages of oxidation. Using their data, the observed displacement of the parameter of oxygen-rich Fe_3O_4 by 0.0065A below that for the stoichiometric compound corresponds to a maximum concentration at 950°C of 0.011 vacancies per molecule. The observed variation of parameter for $FeCr_2O_4$, although less than the probable experimental error, would correspond to 0.002 vacancies per molecule.

Longo[6] has made chemical analyses of the spinels which occur in the oxide scale formed on chromium steels oxidized in air at temperatures from 850° to 1000°C. These results confirm the general sigmoid type of curve found for the synthetic spinels, thus both sets of data disagree with the linear variation of parameter from 8.385A at $x=0$ to 8.344A at $x=2$ observed by Moreau.[7]

In making spinels of this solution system by reduction at 400°C Michel and Pouillard[8] report that complete solubility exists only below $x=0.36$. We have been able to prepare single phase oxides up to $x=0.75$, but not at $x=1.0$, in 50 to 100 hour reductions at 425°C. We believe the apparent solubility limit is a manifestation of the slow rate of reaction encountered even at higher temperatures, as described earlier. The lattice

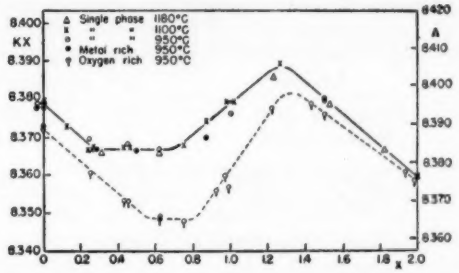

FIG. 1. Lattice parameter of the $FeFe_{(2-x)}Cr_xO_4$ solid solution system measured at room temperature. Full curve, stoichiometric solutions quenched from 1180°C, 1100°C and 950°C; dashed curve, oxygen-rich solutions quenched from 950°C.

parameters of the low-temperature preparations agreed with the metal rich curve of Fig. 1, to within ± 0.005A; the error of measurement of the patterns was large due to the considerable breadth of the lines.

DISCUSSION

By correlating lattice parameter differences of a large number of spinels with the structure determinations which they and others have made for some of them, Verwey and Heilmann[1] have shown that in all probability $FeCr_2O_4$ has the "normal" and $FeFe_2O_4$ the "inversed" structure. In the former structure the divalent cations occupy *A* sites (one per molecule) having oxygen ions in tetrahedral coordination and the trivalent cations are in *B* sites (two per molecule) having octahedral coordination. In the inversed structure half the trivalent cations are in *A* sites and the remaining half are distributed with the divalent cations over the *B* sites. The inversed structure of Fe_3O_4 has been verified by electrical conductivity measurements[9] and by neutron diffraction.[10] Verwey and Heilmann further show that the inversed ferrites have lattice parameters which are from 0.06A to 0.08A smaller than would be expected for a corresponding normal structure.

It is evident that the metal-rich and oxygen-rich curves of Fig. 1 can each be considered to be made up of four essentially linear regions which may be designated as regions 1 to 4 in the order of increasing x. When region 4 of the metal-rich (stoichiometric) solutions is extrapolated to $x=0$, the intercept is at 8.460A which lies 0.064A above the actual parameter of $FeFe_2O_4$. We assume, therefore, that region 4 represents solutions of the normal type, $Fe^{2+}[Fe^{3+}_{(2-x)}Cr^{3+}_x]O_4$, where the brackets indicate ions in *B* sites. The slope of the curve in region 1 is the same within the experimental error as in region 4. Since this would be expected if replacement of Fe^{3+} by Cr^{3+} were taking place in *B* sites, we assign completely inversed structures to these solutions, $Fe^{3+}[Fe^{3+}_{(1-x)}Cr^{3+}_xFe^{2+}]O_4$. According to the empirical rules of ion distribution[1] it can be assumed that none of the Cr^{3+} ions enter *A* sites. On the basis of

[3] M. J. Buerger, *X-Ray Crystallography* (John Wiley and Sons, Inc., New York 1942).
[4] E. J. W. Verwey and P. W. Haayman, Physica **8**, 979 (1941).
[5] Himmel, Mehl, and Birchenall, J. Metals **5**, 827 (1953).
[6] T. A. Longo, M.S. thesis, Physics Department, Purdue University, 1953.
[7] J. Moreau, Compt. rend. **236**, 85 (1953).
[8] A. Michel and E. Pouillard, Compt. rend. **227**, 194 (1948).
[9] E. J. W. Verwey and J. H. de Boer, Rec. trav. chim. **55**, 531 (1936). Verwey, Haayman, and Romeijn, J. Chem. Phys. **15**, 181 (1947).
[10] Shull, Wollan, and Koehler, Phys. Rev. **84**, 912 (1951).

TABLE I. Composition x, lattice parameter a, degree of inversion I, and molecular formula at the boundaries of the four regions of Fig. 1. O.R. and M.R. refer to oxygen-rich and metal-rich, respectively.

Boundary	x	$a(A)\pm0.002$	I	Formula
Region 1, M.R.	0	8.396	1.0	$Fe^{3+}[Fe^{2+}Fe^{3+}]O_4$
Region 1, O.R.	0	8.390	1.0	$^{a}Fe^{3+}[Fe^{2+}Fe^{3+}]O_4$
Region 1–2, M.R.	0.30	8.384	1.0	$Fe^{3+}[Fe^{2+}Fe^{3+}_{0.7}Cr^{3+}_{0.3}]O_4$
Region 1–2, O.R.	0.56	8.365	1.0	$^{a}Fe^{3+}[Fe^{2+}Fe^{3+}_{0.44}Cr^{3+}_{0.56}]O_4$
Region 2–3, M.R.	0.72	8.384	0.73	$Fe^{3+}_{0.27}Fe^{3+}_{0.73}[Fe^{2+}_{0.73}Fe^{3+}_{0.55}Cr^{3+}_{0.72}]O_4$
Region 2–3, O.R.	0.82	8.365	0.83	$^{a}Fe^{2+}_{0.17}Fe^{3+}_{0.83}[Fe^{2+}_{0.83}Fe^{3+}_{0.35}Cr^{3+}_{0.82}]O_4$
Region 3–4, M.R.	1.28	8.406	0	$Fe^{2+}[Fe^{3+}_{0.72}Cr^{3+}_{1.28}]O_4$
Region 3–4, O.R.	1.31	8.399	0	$^{a}Fe^{2+}[Fe^{3+}_{0.69}Cr^{3+}_{1.31}]O_4$
Region 4, M.R.	2.0	8.376	0	$Fe^{2+}[Cr^{3+}_{2.0}]O_4$
Region 4, O.R.	2.0	8.375	0	$^{a}Fe^{2+}[Cr^{3+}_{2.0}]O_4$

[a] Nominal. For v vacancies/molecule: decrease Cr^{3+} by $vx/3$; increase Fe^{3+} by $v(2+x/3)$; decrease Fe^{2+} by $3v$, where $x/(3-x)=Cr/Fe$.

these assignments, regions 2 and 3 represent two stages of reversion from the inversed to the normal form. It is clear that the presence of vacancies stabilizes the inversed structure to a remarkable degree.

If one defines the degree of inversion I as the fraction of A sites occupied by trivalent cations, the lattice parameter may be expressed, formally, as $a(A)=8.460-0.042x-0.064I$, and I can be determined for all points on the full curve. To treat the oxygen-rich curve it is assumed that the constant decrement due to vacancies in region 1 may be smoothly joined to the slightly smaller value at $x=1.35$. It is thereby implied that the maximum concentration of vacancies is essentially constant through regions 1, 2, and 3, i.e., as long as both Fe^{2+} and Fe^{3+} ions are present in B sites and decreases proportionally with Fe^{3+} concentration (in B sites) in region 4. These relations are consistent with the suggestion that vacancies occur in B sites preferentially.[4]

The values of I, x, and a at the limits of each of the four regions are collected in Table I, together with the corresponding molecular formulas. The rate of change of the degree of inversion, dI/dx, is zero in regions 1 and 4, -0.65 ($\cong 2/3$) in region 2, -1.31 ($\cong 4/3$) and -1.69 ($\cong 5/3$) in region 3 of the metal-rich and oxygen-rich curves, respectively. These values are to be compared with -0.5 which would obtain if the parameter variation were linear over the whole range of x. A random distribution of the iron ions over the A sites and available B sites, for which case $I_r=(2-x)/(3-x)$, occurs at $x=0.87$, $I=0.53$ and at $x=1.02$, $I=0.49$ for the metal-rich and oxygen-rich curves, respectively. For larger or smaller x values, Fe^{2+} or Fe^{3+} ions, respectively, take up A sites preferentially.

There are several known instances of spinel solid solutions in which the lattice parameter varies linearly. This is to be expected when the component spinels are both normal, as in the Zn aluminate–Co aluminate[11] and the Zn ferrite–Cd ferrite[11,12] systems, or when they are both inverse as in solutions of Fe_3O_4 in Ni or Co ferrite.[13] When, as in the present instance, one component is inversed and the other normal, irregularities may be expected. An interesting example has been investigated by Romeijn.[11] During the substitution of Cr^{3+} for Fe^{3+} in inversed Ni ferrite to form normal Ni chromite, the A sites remain completely occupied by Fe^{3+} ions and the structure remains completely inversed as long as this is structurally possible, i.e., to $x=1$. After B sites are devoid of Fe^{3+}, Ni^{2+} ions enter A sites, and the structure steadily reverts to the normal form at $x=2$. In the present case, with Fe^{2+} instead of Ni^{2+} as the common ion, the initial stage of substitution is similar, but at $x=0.30$ (or 0.56) Fe^{2+} begins to displace Fe^{3+} from A sites to B sites as reversion starts. This process continues at a constant rate, $dI/dx=-0.65$, in region 2, but in region 3 the rate of displacement increases to a higher value so that the normal structure is achieved before all of the Fe^{3+} has been replaced by Cr^{3+}. From this behavior it is clear not only that Fe^{2+} is a stronger competitor for A sites than is Ni^{2+}, but also that its strength is dependent upon the concentrations of the other ions and the vacancies present.

Romeijn[11] has attributed part of the stability of the inversed structure to a short-range order of divalent and trivalent ions in 1:1 proportions over the B sites. It is possible that some ordering process in different proportions is effective in region 2, since calculation shows that in this region the ratio of Fe^{2+} to Fe^{3+} in B sites is essentially constant at 7/5 and 12/5 for the metal-rich and oxygen-rich solutions, respectively.

[11] F. C. Romeijn, Philips Research Repts. I **8**, 304 (1953); II **8**, 321 (1953).

[12] L. Vegard and A. Borlaag, Avhandl. Norske Videnskaps.-Akad., Oslo, I. Mat. Nat. Natur. Kl. No. 5, 1–19 (Quoted in reference 11).

[13] J. Bénard, Ann. chim. **12**, 5 (1939).

Vibrational Spectrum of Bromotrifluoroethylene*

D. E. Mann, N. Acquista, and Earle K. Plyler
National Bureau of Standards, Washington, D.C.

(Received January 14, 1954)

The infrared spectrum of gaseous bromotrifluoroethylene $F_2C{:}CFBr$ has been investigated in the range 2–52μ. The assignment of fundamentals parallels that for chlorotrifluoroethylene very closely. The planar vibrational frequencies in cm^{-1} are 1783(ν CC), 1330(ν CF), 1203(ν CF), 1027(ν CF), 659(ν CBr), 510(δ CF_2), 370(δ CFBr), 311(ρ CF_2), 160(ρ CFBr), while the out-of-plane modes are assigned 538(β CF_2), 355(β CFBr), and 150(τ). A table of thermodynamic functions for the ideal gas is given.

INTRODUCTION

THE first paper in this series of reports on the vibrational spectra of the fluoroethylenes deals with the fundamental assignment for chlorotrifluoroethylene, $F_2C{:}CFCl$.[1,2] In order to study the spectral resemblances in this family of compounds, and also to provide some of the data needed for force constant calculations now in progress, the infrared vibrational spectrum of BTFE has been obtained and analyzed. The expected similarity of the BTFE spectrum to that of CTFE is remarkably close and provides added support for the proposed assignments.

EXPERIMENTAL

The sample of BTFE used in this work was provided by Dr. F. J. Honn of the M. W. Kellogg Company. Although no information about its purity was available, a comparison of its spectrum with that of a sample of CTFE of known purity suggests that it is probably quite high.

The infrared absorption spectrum of gaseous BTFE was measured from about 2 to 52μ. Prisms of LiF and CsI were employed with a Perkin-Elmer 12*C* spectrometer, NaCl with a Perkin-Elmer 21, and KBr with a Baird Associates instrument. Further details and references to the methods of measurement are given in the earlier paper on CTFE.[1]

For convenience in use the spectral curves have been presented in Fig. 1 with a scale linear in wave numbers. The wave numbers, relative intensities, and assignments of all the observed bands are listed in Table I. Raman data are not yet available.

INTERPRETATION

The most striking characteristic of the infrared spectrum of BTFE is its similarity to that of CTFE. This undoubtedly reflects a close correspondence in structures. Just as for the chloro compound, it may of course be supposed that BTFE is planar with C_s symmetry. Of the 12 fundamental vibrations the nine belonging to species a' are classified as planar modes while the three in a'' are out-of-plane motions. The latter give rise to type *C* infrared bands characterized mainly by very prominent *Q* branches. The a' vibrations result in hybrid bands which partake of the usual type *A* and *B* contours. All 12 fundamentals are infrared active, though it may be anticipated that two of them, the torsion and one of the rockings, will occur at wave numbers below the limit of about 190 cm^{-1} imposed by the cesium iodide prism. They should, however, be directly accessible in the Raman spectrum.

The earlier work on CTFE[1] and the evident similarity of its infrared spectrum to that of BTFE makes it quite easy to pick out most of the fundamentals. It is convenient to begin with the stretching modes. In CTFE these occur as strong bands at 1792, 1336, 1215, 1058, and 689 cm^{-1} for the CC, three CF, and CCl stretchings, respectively. Reference to Fig. 1 will show that for BTFE the corresponding bands occur at 1783, 1330, 1203, 1027, and 659 cm^{-1}.

The resemblances in the spectra of the chloro and bromo compounds are further emphasized by the location and appearance of the two bands in the region between 500 and 550 cm^{-1}. At 538 cm^{-1} there is clearly a type *C* band which must be assigned to the higher of the two wagging motions, β CF_2.† Just below the 538 cm^{-1} type *C* band there is at 510 cm^{-1} a mixed $A-B$ band which may at once be ascribed to the upper of the two deformation modes, δ CF_2. The corresponding bands in CTFE occur at 538 and 517 cm^{-1}, respectively.

It is in the region below 500 cm^{-1} that the few important differences between the spectra of CTFE and BTFE are most noticeable. First, the 463 cm^{-1} band of the former is entirely absent in the latter. Second, the 194 cm^{-1} band of CTFE is missing in BTFE. However, the group of bands around 300–375 cm^{-1} in the spectrum of the chloro compound appears to be only slightly shifted in frequency and altered in intensity in the curves for the bromo compounds. It will be seen that the proposed assignment which follows accounts for the character and magnitude of these changes in a satisfactory manner.

It will be convenient to dispose first of the low-frequency wagging mode, β CFBr. This was placed at 369

* This work has been supported in part by the U. S. Office of Naval Research under contract NAonr 112–51.

[1] Mann, Acquista, and Plyler, J. Chem. Phys. **21**, 1949 (1953).

[2] In accordance with the convention adopted previously chlorotrifluoroethylene will be abbreviated to CTFE, while its bromine analog will be represented by BTFE.

† For a discussion of the terminology and notation used in this paper to refer to the angular motions see reference 1.

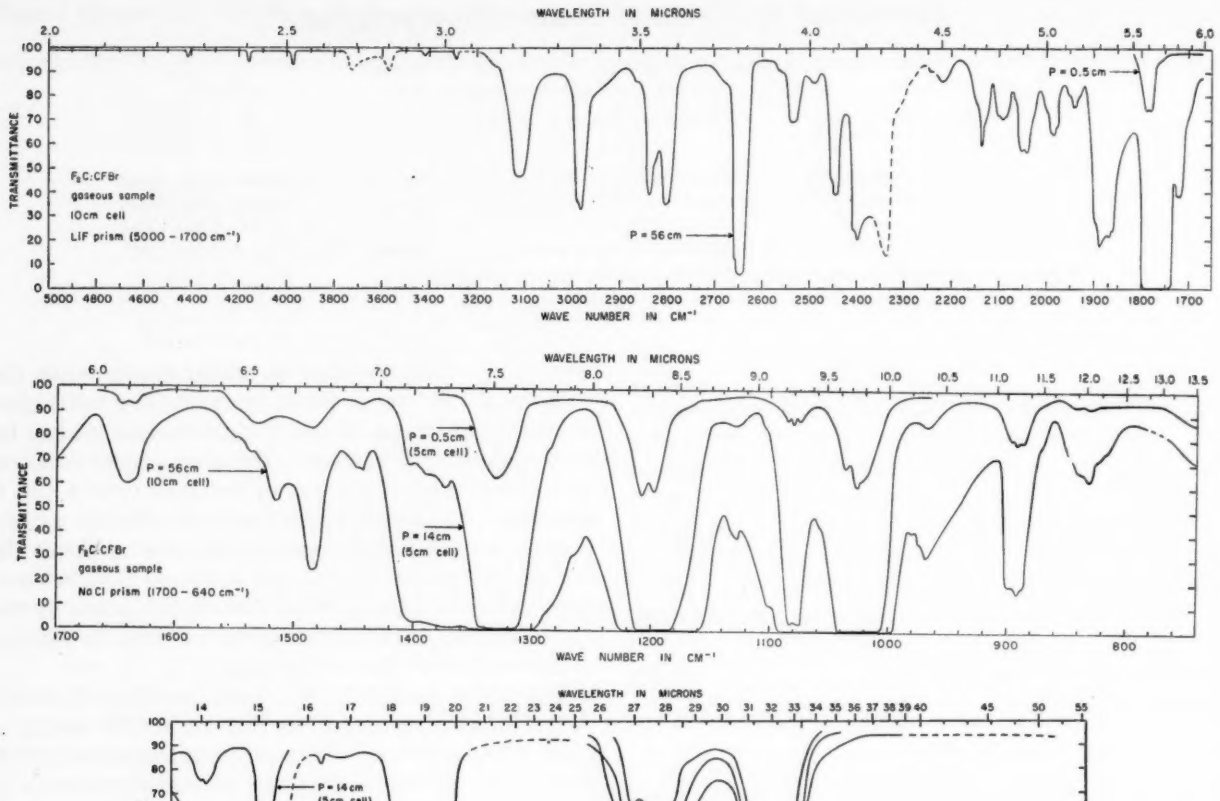
WAVELENGTH IN MICRONS
TRANSMITTANCE
F2C:CFBr
gaseous sample
10cm cell
LiF prism (5000 - 1700 cm⁻¹)
P = 0.5 cm
P = 56 cm
WAVE NUMBER IN CM⁻¹
P = 56cm (10cm cell)
P = 0.5cm (5cm cell)
P = 14cm (5cm cell)
NaCl prism (1700 - 640 cm⁻¹)
P = 14cm (5cm cell)
P = 56 cm (10cm cell to 640 cm⁻¹) (5cm cell, 640 - 390 cm⁻¹)
P = various (120cm cell, 390 - 190 cm⁻¹)
KBr prism (640 - 390 cm⁻¹)
CsI prism (390 - 190 cm⁻¹)

FIG. 1. Infrared spectrum of gaseous F_2C:CFBr from 2 to 52μ.

cm^{-1} in CTFE. As yet unpublished force constants calculations by Mann and Shimanouchi show that the frequency of this motion should be shifted only a little downward in BTFE. The band around 360 cm^{-1} in the bromo compound does in fact resemble that at 369 cm^{-1} in CTFE. The most convincing evidence in favor of the assignment of a band around 360 cm^{-1} to β CFBr is afforded by a comparison of the combination tones in which this vibration occurs with the corresponding sums in CTFE. The sums β CFBr$+\nu$ CC, β CFBr $+\beta$ CF_2, and $2\times\beta$ CFBr are especially significant in this regard since they parallel almost exactly their counterparts in CTFE in relative intensities as well as location. These considerations taken together lead quite directly to a frequency of about 355 cm^{-1} for β CFBr.

The same method of analysis may now be used to fix the frequencies of the remaining angular modes δ CFBr, ρ CF_2, and ρ CFBr, the torsion being excepted as a special problem to be dealt with subsequently. Although the lower of the two rocking vibrations may be expected to occur below the present limits of observation, the remaining rocking and the CFBr deformation are certainly between 200 and 400 cm^{-1}. It will be recalled that these vibrations were found in CTFE at 338 and 463 cm^{-1}, respectively. Inspection of this region in Fig. 1 reveals only the previously used band around 360 and a somewhat more intense band at 311 cm^{-1}. The envelope of the latter is similar to that of the 338 cm^{-1} band in CTFE. It is at once evident that the only reasonable interpretation of the observed spectrum requires the a'' band at 355 cm^{-1} to be overlapped by the upper of the two a' bands, *viz.*, δ CFBr, and leaves 311 cm^{-1} to be assigned to ρ CF_2. Correlation of combination tones in the manner described above now reveals this conclusion to be correct, and places δ CFBr at approximately 370 cm^{-1}.

It is to be expected that the shift in frequency from 463 cm^{-1} for δ CFCl to about 370 cm^{-1} for δ CFBr will also be reflected in the CFX rockings. Analysis and the correlation of combination tones reveals ρ CFBr at about 160 cm^{-1}. Unfortunately, there is not sufficient evidence to fix the frequency of the torsional mode.

TABLE I. Infrared spectrum of $F_2C{:}CFBr$ (gas).

Wave number (cm^{-1})	Intensity		Interpretation
306	~w−m[a]	*P*	
(311)$_c$[b]	~w−m		$\nu_8(a'; \rho\ CF_2)$[c]
316	~w−m	*R*	
360[d]	~w−m		$\nu_{11}(a''; \beta\ CFBr) = \sim 355\ cm^{-1}$
367–371	~w−m		$\nu_7(a'; \delta\ CFBr) = \sim 370\ cm^{-1}$
~507 sh	m	*P*	
510	m	*Q*	$\nu_6(a'; \delta\ CF_2)$
516	m	*R*	
533	m	*P*	
538	m	*Q*	$\nu_{10}(a''; \beta\ CF_2)$
545	m	*R*	
~595[b]	vvw		?
613	vw		2×311=622[c]
657	m	*P*	
(659)$_c$	m		$\nu_5(a'; \nu\ CBr)$
662	m	*R*	
~667 sh	~m		160+510=670; 311+355=666(A'')
709	m	*P*	
714	m	*Q*	2×355=710
~718 sh	m	*R*	
~818 sh	vw	*P*	
~822 sh	vw	*Q*	160+659=819
830	vw	*Q*	311+510=821
~840 sh	vw	*R*	
~877 sh	w		370+510=880
~888 sh	w	*P*	
892	w	*Q*	355+538=893
~896 sh	w	*R*	
~967 sh	w	*P*	
975	w	*Q*	311+659=970
~980 sh	w	*R*	
~1018 sh	vs	*P*	
1027	vs	*Q*	$\nu_4(a'; \nu\ CF)$
1036	vs	*R*	
~1059 sh	w		3×355=1065(A'')
1075	s	*P*	
1080	s	*Q*	2×538=1076
1085	s	*R*	
~1105 sh	~w		?
1129	w		160+311+659=1130; 2×311+510=1132
~1171 sh	m		510+659=1169
1198	vs	*P*	
(1203)$_c$	vs		$\nu_3(a'; \nu\ CF)$
1208	vs	*R*	
~1290 sh	~vw		2×311+659=1281
1330	vs		$\nu_2(a'; \nu\ CF)$
1374	w		2×355+659=1369
~1385	w		370+1027=1397; 355+1027=1382(A'')
1404	w		355+510+538=1403
1441	vw	*P*	370+2×538=1446
1449	vw	*R*	
~1473	w	*P*	
1484	w	*Q*	160+1330=1490
~1490	w	*R*	
1515	w		311+1203=1514
1529	w		510+1027=1537
~1536	vw		160+355+1027=1542(A'')
~1550	vw		355+538+659=1552
1634	w	*P*	
(1639)$_c$	w		311+1330=1641
1645	w	*R*	
~1695 sh	vw		370+1330=1700
1715	w	*P*	
(1720)$_c$	w		510+1203=1713
1724	w	*R*	
1779	vs	*P*	
(1783)$_c$	vs		$\nu_1(a'; \nu\ CC)$
1788	vs	*R*	
1862	m	*P*	
1867	m	*Q*	659+1203=1862
1887	m		355+510+1027=1892(A'')
~1934 sh	vw	*P*	
1939	vw	*Q*	160+1783=1943
~1949 sh	vw	*R*	
~1978 sh	vw	*P*	
1986	vw	*Q*	659+1330=1989
1992	vw	*R*	
1999	vw		311+659+1027=1997; 311+355+1330=1996(A'')
~2033 sh	vw		311+510+1203=2024
2043	vw	*P*	
(2047)$_c$	vw		2×1027=2054
2050	vw	*R*	
~2066 sh	vw		2×370+1330=2070; 355+510+1203=2068(A'')
~2085	vw	*P*	
~2092	vw	*Q*	311+1783=2094
~2099	vw	*R*	
~2132	vw	*P*	
2136	vw	*Q*	355+1783=2138(A'')
~2140	vw	*R*	
2221	vw		1027+1203=2230
~2245	vvw		160+311+1783=2254
~2336	m		1027+1330=2357
2399	w	*Q*	2×1203=2406
~2406 sh	w	*R*	
2445	w	*Q*	659+1783=2442
~2454 sh	w	*R*	
2487	vw		2×355+1783=2493
2532	vw		1203+1330=2533
~2567 sh	vvw		510+2×1027=2564
2648	m	*Q*	2×1330=2660
~2656 sh	m	*R*	
~2685 sh	vw		355+538+1783=2676; 370+538+1783=2691(A'')
2803	w		1027+1783=2810
2838	w		311+1203+1330=2844
~2863 sh	vw		2×538+1783=2859
2981	w	*Q*	1203+1783=2986
~2991 sh	w	*R*	
3109	w		1330+1783=3113
~3292	vvw		311+1203+1783=3297
~3411	vvw		311+1330+1783=3424
~3584	vvw		2×1783=3566; 3×1203=3609
~3731	vvw		2×1203+1330=3736
~3984	vvw		3×1330=3990
~4161	vvw		311+1203+2×1330=4174
~4417	vvw		2×1330+1783=4443

[a] The intensities of the bands observed in the cesium iodide region are uncertain relative to the remainder of the spectrum since the partial pressure of BTFE in the absorption cell was not determined.

[b] A wave number given in the form $(\cdots)_c$ is the measured value of the dip between the *P* and *R* branches. The designation 'sh' means shoulder, while 'b' stands for broad. The tilde (~) is used to indicate that the measured wave number or intensity may be more than normally uncertain.

[c] See reference 1 for a description of the notation used in this paper to describe the various modes.

[d] The text contains a discussion of the methods used to estimate the frequencies of the δ CFBr, β CFBr, and ρ CFBr modes. It must be emphasized that the values 370, 355, and 160 cm^{-1} for these vibrations, respectively, are only approximate though each is probably within five wave numbers of its true value.

[e] The species of the combination or overtone is understood to be A' unless A'' is given explicitly.

The force constant calculations alluded to previously in connection with the β CFBr vibration demonstrate in a convincing manner that the twisting frequency is probably between 145 and 150 cm^{-1}, and likely to be nearer the latter limit. Hence, for definiteness it is placed at 150 cm^{-1}. The Raman spectrum of BTFE may possibly reveal this fundamental directly.

The final assignment for BTFE is given in Table II together with that for CTFE.‡

THERMODYNAMIC FUNCTIONS

The molecular parameters used for BTFE parallel those assumed for CTFE.[1] The CC, CF, and CBr distances are taken to be 1.31A, 1.31A, and 1.90A, respectively. The FCF and FCBr angles are each estimated to be 114°. These constants lead to the moments of inertia 193.6, 591.4, and 785.0×10^{-40} g cm^2. These constants and the fundamental assignment given in Table II were used to compute the thermodynamic functions, to the rigid-rotator, harmonic-oscillator approximation, for BTFE in its ideal gaseous state. Table III is a condensed version of a more complete tabulation of the thermodynamic functions computed with the aid of the SEAC at the National Bureau of Standards.§

TABLE II. Fundamental vibration frequencies for F_2C:CFBr and F_2C:CFCl.

Species	Number	Designation	F_2C:CFCl	F_2C:CFBr
a'	1	ν CC	1792 cm^{-1}	1783 cm^{-1}
	2	ν CF	1336	1330
	3	ν CF	1215	1203
	4	ν CF	1058	1027
	5	ν CX[a]	689	659
	6	δ CF_2	517	510
	7	δ CFX	463	370
	8	ρ CF_2	338	311
	9	ρ CFX	194	160
a''	10	β CF_2	538	538
	11	β CFX	369	355
	12	τ	158	150

[a] The letter X represents either Cl or Br.

‡ The arguments pertaining to δ CFBr and ρ CF_2 make clear the necessity for interchanging the assignments given in reference 1 for the 463 and 338 cm^{-1} bands. The present Table II incorporates this minor revision.

TABLE III. Calculated thermodynamic functions for F_2C:CFBr in dimensionless units.

T°K	C_p^0/R	$(H^0-E_0^0)/RT$	$-(F^0-E_0^0)/RT$	S^0/R
200	8.584	5.998	30.456	36.454
300	10.349	7.174	33.118	40.292
400	11.603	8.132	35.318	43.450
500	12.537	8.924	37.220	46.144
600	13.240	9.588	38.908	48.495
700	13.770	10.149	40.429	50.578
800	14.173	10.628	41.816	52.444
900	14.483	11.040	43.092	54.132
1000	14.725	11.397	44.274	55.671
1100	14.915	11.708	45.376	57.084
1200	15.068	11.982	46.406	58.388
1300	15.192	12.224	47.375	59.599
1400	15.293	12.440	48.289	60.729
1500	15.377	12.633	49.154	61.787

ACKNOWLEDGMENTS

The authors are indebted to Dr. F. J. Honn of the M. W. Kellogg Company for providing us with the sample of BTFE.

§ Reference 1 contains a brief discussion of the uncertainties which may be encountered in a table of this type.

Rotational Magnet Moments of $KClFeCl_2$ and $KBrFeBr_2$†

P. KUSCH
Columbia University, New York, New York
(Received March 2, 1954)

The molecules $KClFeCl_2$ and $KBrFeBr_2$ have rotational magnetic moments much larger than those found in other heavy molecules with large moments of inertia. The maximum magnetic moment of the state of most probable J at a temperature of 935°K is about 72 nuclear magnetons for the first of the molecules and about 50 nuclear magnetons for the second of these molecules.

INTRODUCTION

THE rotational magnetic moments of the hydrogen molecules have been found[1,2] to be +0.88, +0.66, and +0.44 nuclear magneton for H_2, HD, and D_2, respectively, in the first rotational states. No observations of the rotational magnetic moments of other diatomic molecules have been made. It may, however, be surmised that the rotational magnetic moments of the alkali halides and of the homonuclear alkali molecules are very small, probably not greatly exceeding one nuclear magneton in the state for which $J=50$. This conclusion follows from the observation that the deflection, by an inhomogeneous magnetic field, of a beam of molecules evaporated from an oven at a temperature for which the most probable value of J is of the order of 50 may be accounted for by the nuclei in the molecule which have, themselves, a magnetic moment of the order of one nuclear magneton. In none of the polyatomic molecules which have heretofore been observed[3] in the molecular beam magnetic resonance method, is the rotational magnetic moment, in rotational states which are highly populated at a temperature in the neighborhood of 1000°K, large compared to the magnetic moment contributed by the nuclei.

The rotational magnetic moments of several polyatomic molecules have been measured by the methods of microwave spectroscopy.[4,5] Only in the cases of the molecules NH_3 and H_2O is a large rotational g factor found, of the order of one-half nuclear magneton per rotational quantum number. Jen[4] notes a trend to generally decreasing g values for heavy molecules with large moments of inertia. For both SO_2 and N_2O the g value is less than 0.1, where the moment is measured in nuclear magnetons and for OCS the g factor is, in magnitude, 0.025. We should, therefore, expect that very heavy molecules with large moments of inertia will have a very small rotational magnetic moment. It is the purpose of this paper to indicate, for two polyatomic molecules, $KClFeCl_2$ and $KBrFeBr_2$, the existence of much larger rotational moments than those observed in any other heavy polyatomic molecule.

METHOD OF DETERMINING ROTATIONAL g VALUES

The magnetic moment which characterizes the molecules in a molecular beam can be found from an observation of the deflection of the beam under the influence of an applied inhomogeneous magnetic field. It should be emphasized that such a determination is of low precision compared to the determination of magnetic moments by use of the several variations of the resonance technique. In the typical molecular beam apparatus the image of the beam in the plane of the detector has a trapezoidal distribution of intensity. For the purpose of determining the moment distribution of molecules in the beam from an observation of the change in the intensity distribution when the beam is deflected by an inhomogeneous magnetic field, it is convenient to replace the trapezoidal distribution by an "equivalent" rectangular distribution whose width is $2b$, where $2b$ is also the width of the trapezoidal beam at half-intensity. The beam is detected on a wire whose width is $2d$, where, in the present case, $d<b$.

If the beam consists of molecules with a magnetic moment μ, the deflection in the z direction of molecules with the most probable velocity, $\alpha=(2kT/m)^{\frac{1}{2}}$, in the oven is

$$S_\alpha=(\partial H/\partial z)\mu G/4kT=\gamma\mu i, \qquad (1)$$

where G is a fixed function, for any particular apparatus, of the various distances along the direction of propagation of the beam. Over one of these distances there exists $\partial H/\partial z$, the gradient of the field in a direction perpendicular both to the plane of the beam and its direction of propagation. $\partial H/\partial z$ is proportional to the field H at any position within the gap of a magnet which produces the field and H is, in turn, proportional to the current i in the coils of the magnet. γ then depends on fixed properties of the magnet and on the temperature of the source.

The effect of the deflecting field is to broaden the originally trapezoidal intensity distribution in the plane of the detector. By intensity as the term is used

† This research was supported in part by the U. S. Office of Naval Research.
[1] N. F. Ramsey, Phys. Rev. **58**, 226 (1940).
[2] N. J. Harrick and N. F. Ramsey, Phys. Rev. **88**, 228 (1952).
[3] Discussions of experiments involving the following polyatomic molecules occur in the published papers originating in the molecular beams laboratory of Columbia University: NaOH, KOH, NaCN, KCN, RbCN, $NaBO_2$, KBO_2, $Li_2B_4O_7$, $Na_2B_4O_7$, $K_2B_4O_7$, $NaFBeF_2$, $KFBeF_2$, $NaClAlCl_3$, $KClAlCl_3$. It seems unnecessary to give detailed references.
[4] C. Jen, Phys. Rev. **81**, 197 (1951).
[5] J. R. Eshbach and M. W. Strandberg, Phys. Rev. **85**, 24 (1952).

here, we mean that fraction of the total intensity intercepted by the detector at a position which remains fixed at the center of the undeflected beam. Suppose that I_0 is the intensity of an undeflected beam in which the molecules are characterized by a single value of the magnetic moment. I, the intensity of the beam when a deflecting field is applied, is then found to be

$$I=\tfrac{1}{2}I_0\{(1+b/d)\exp[-S_\alpha/(b+d)] + (1-b/d)\exp[-S_\alpha/(b-d)]\}. \quad (2)$$

Suppose, now, that the magnetic moments of the particles in the beam have a virtually continuous distribution. In the case of a diatomic molecule this would occur if the molecule is characterized by a g_J, where the most probable value of J, the rotational quantum number, is high and the contribution to the total moment of the nuclear magnetic moments is small. For any m_J the magnetic moment is then $m_J g_J$. The contribution to the intensity of the undeflected beam by molecules lying within any interval dJ, dm_J is

$$d^2I_0=I_0a^2\exp(-a^2J^2)dJdm_J \quad (3)$$

where $a^2=h^2/8\pi^2AkT$ and A is the moment of inertia of the molecule. The intensity contributed by molecules whose moments lie between $|\mu|$ and $|\mu+d\mu|$ is

$$dI_0=(\pi^{\frac{1}{2}}I_0a/g_J)[1-\Phi(a\mu/g_J)]d\mu, \quad (4)$$

where Φ is the error function.

The most probable value of J, $\bar{J}$, is $\sqrt{2}/2a$ and the maximum value of the magnetic moment in the rotational state with the most probable value of J is $\bar{\mu}=g_J\bar{J}$. The intensity at the detector, when the inhomogeneous field is applied, is then:

$$I/I_0=[(2\pi)^{\frac{1}{2}}/4\gamma d\bar{\mu}i][4bd-(b+d)^2\{1-\Phi(\rho_1)\} \times\exp\rho_1{}^2+(b-d)^2\{1-\Phi(\rho_2)\}\exp\rho_2{}^2], \quad (5)$$

where $\rho_1=\gamma\bar{\mu}i/\sqrt{2}(b+d)=\gamma g_J i/2a(b+d)$ and $\rho_2=\gamma\bar{\mu}i/\sqrt{2}(b-d)=\gamma g_J i/2a(b-d)$.

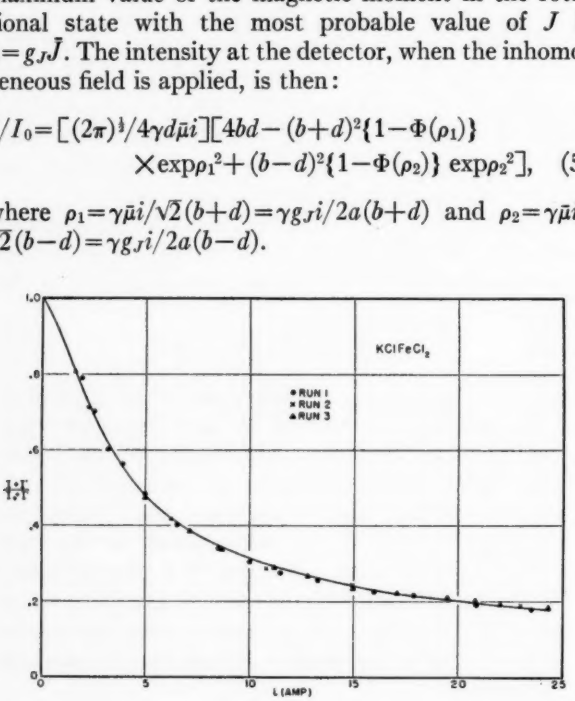

FIG. 1. The intensity of a beam, obtained by heating equimolar proportions of KCl and $FeCl_2$, as a function of the current through the coils of a magnet which produces an inhomogeneous magnetic field.

If the molecule has an unknown configuration it is necessary to make two assumptions in order to analyze the available data. The first of these is that the molecule is spherical, that is, that the moment of inertia about any axis through the center of mass is equal to A. All levels with the same J but different K coincide. For sufficiently large values of J, the contribution to the intensity of the undeflected beam by molecules lying within the interval dJ, dm_J is then

$$d^2I_0=I_02Ja^3\pi^{-\frac{1}{2}}\exp(-a^2J^2)dJm_J, \quad (6)$$

where a is defined as before. The second assumption, that the magnetic moment produced by unit angular momentum about any axis through the center of mass of the molecule is the same, is not a necessary consequence of the first assumption. The molecule is then characterized by a g_J and for any m_J, the magnetic moment is $m_J g_J$. The most probable value of J, $\bar{J}$, is now $1/a$ and $\bar{\mu}=g_J\bar{J}$ where $\bar{\mu}$ is the maximum value of the magnetic moment in the state of most probable J. It can then be shown that the intensity at the detector, when an inhomogeneous field is applied is:

$$I/I_0=\tfrac{1}{2}[(1+b/d)\{1-\Phi(\rho_1)\}\exp\rho_1{}^2 + (1-b/d)\{1-\Phi(\rho_2)\}\exp\rho_2{}^2], \quad (7)$$

where $\rho_1=\gamma\bar{\mu}i/2(b+d)=\gamma g_J i/2a(b+d)$ and $\rho_2=\gamma\bar{\mu}i/2(b-d)=\gamma g_J i/2a(b-d)$.

All quantities in (5) and (7) are known with the exception of $\bar{\mu}$ and it should then be possible to determine the value of $\bar{\mu}$ by fitting a calculated curve to an experimentally determined curve which relates the intensity of the beam at the position of the undeflected beam to the current in a deflecting magnet. It is not possible by the method of these experiments alone to determine the value of g_J unless other data permit calculation of the constant a. In the cases here under consideration we have ignored the contribution to the total magnetic moment of the various nuclei within the molecule since their contribution is small compared to the magnetic moment due to the rotation which has ultimately been found.

It is always possible, and there is evidence of this in the present experiment, that the beam which issues from the oven consists of more than one molecular species which is detectable on the detector. If one of these species has a large rotational magnetic moment and the other species the more usual rotational magnetic moment of the order of a nuclear magneton, then the second of the molecular species will not be significantly deflected at fields which have a large effect on the first of the molecular species. If the molecule of small moment contributes an intensity I' at all fields, the ratio $(I+I')/(I_0+I')$ is experimentally determined. Evidently it is then necessary in fitting an observed curve to adjust not only the value of $\bar{\mu}$ but also the value of I'/I_0.

APPARATUS

The molecular beam apparatus used in the present experiments has previously been described.[6] It was originally designed to give an easily detectable differential deflection at the highest available field gradients for molecules which differ in moment by considerably less than one nuclear magneton. The ratio of the gradient $\partial H/\partial z$ in the gap of the deflecting magnet and the field H is about 8 cm^{-1}. Since the magnet is operated far below saturation of the iron, the integral of the field in the gap is found from the current in the field coils. From the known configuration of the pole faces, it was then found that $\partial H/\partial z = 920i$ gauss cm^{-1}, at the position of the beam in the gap. The deflecting magnet is 50.8 cm long and the geometrical factor is 4520 cm^2. Both of the beams investigated in the present experiments were produced at a temperature of about 935°K, so that $S_a = 6.98\times10^{-2}\ \mu i$ cm where μ is expressed in Bohr magnetons. The total width of the detector was 0.0025 cm and the width of the undeflected beam at half intensity was about 0.006 cm.

RESULTS

The observation of a molecule with unusual magnetic properties first occurred in the attempt to observe the nuclear resonances of the silver isotopes in the molecule KClAgCl. Equimolar proportions of KCl and AgCl were heated in an iron oven; it was at once apparent that the mean magnetic moment was much greater than that to be expected from the nuclei alone but also less than the characteristic electronic moment of any state other than a $^1\Sigma$ state. Subsequent investigation indicated that silver played no role in the phenomenon and that a replacement of the silver in the molecule by the iron of the oven was essential to the production of the molecule in question. An equimolar mixture of KCl and dry $FeCl_2$ or KBr and $FeBr_2$ heated in either an iron or a silver oven gave molecules of the indicated properties.

In Fig. 1 is shown the observed variation of the intensity of a beam, produced by heating equimolar proportions of KCl and $FeCl_2$, on a detector at the center of the undeflected beam as the current in the deflecting field is varied. The data of three separate runs are shown. The solid curve is one calculated from Eq. (7) which applies to a spherical molecule, where it has been assumed that $\bar{\mu}=72$ nuclear magnetons and that $I'/I_0=0.10$. The latter quantity corresponds to a fraction of the total beam of 9.1 percent which is not significantly deflectable in moderate gradients. The curve in Fig. 1 may be fitted quite as well by use of Eq. (5) which applies to a diatomic molecule. In that case $\bar{\mu}$ is found to be 66 nuclear magnetons and I'/I_0 to be 0.08. For each calculation the fit is quite sensitive to the assumed values of $\bar{\mu}$ and of I'/I_0. A change in $\bar{\mu}$ of 5 nuclear magnetons makes the calculated curve deviate significantly from the observed data for all values of I'/I_0.

[6] H. Taub and P. Kusch, Phys. Rev. **75**, 1481 (1949); Logan, Cote, and Kusch, Phys. Rev. **86**, 280 (1952).

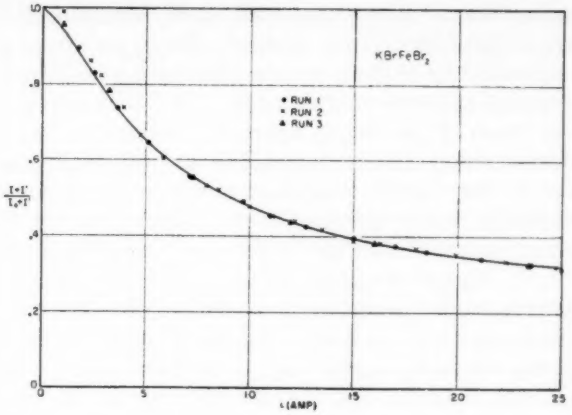

FIG. 2. The intensity of a beam, obtained by heating equimolar proportions of KBr and $FeBr_2$, as a function of the current through the coils of a magnet which produces an inhomogeneous magnetic field.

The data obtained when equimolar proportions of KBr and $FeBr_2$ are heated in the oven are shown in Fig. 2. If a spherical molecule is assumed, $\bar{\mu}$ is 50 nuclear magnetons and I'/I_0 is 0.25. The solid curve in Fig. 2 is obtained from this assumption. If a diatomic molecule is assumed, $\bar{\mu}$ is 46 nuclear magnetons and I'/I_0 is 0.22.

It is not possible to fit the experimental data on the basis of the assumption that only the moments $\pm\mu$ occur in the molecules. It is clear, however, that an excellent fit can be obtained by a distribution of moments among a relatively small number of values rather than over a continuous range. However, the fact that it was not possible, in these experiments, to observe radiofrequency transitions suggests that the g value associated with the magnetic moment is small and that the angular momentum associated with the moment is large to give rise to the large observed moment. This is so because to keep molecules of large moment on a trajectory which refocuses at the detector, it is necessary to apply only moderate field gradients. In the presence of a limited gradient, as was applied here, the observation of g values of less than 5 (where μ is measured in nuclear magnetons) would be difficult and it may be assumed that no large fraction of the molecules had a g value greater than 5. Accordingly, it seems reasonable that the observed moments are associated with large angular momenta. Finally, it should be noted that it is not possible to ascribe to the molecule an electronic configuration which, by virtue of the electronic moments alone, would yield magnetic moments as low as those here observed.

The occurrence of some fraction of molecules which possess no large magnetic moments is to be expected. In the present experiments it is possible to detect only molecules that contain at least one alkali atom. At the temperatures at which both the bromine and chlorine

bearing beams were evaporated, both KBr and KCl have a significant vapor pressure. Hence an excess of these molecules in the oven or a dissociation pressure of a complex molecule containing KCl or KBr would give some beam of the simple potassium halide. Abundant evidence exists that both the KCl and KBr molecules have a very small magnetic moment which arises principally from the statistical distribution of the nuclear magnetic moments which are themselves small.

R. C. Miller[7] of Columbia University is developing methods to determine the composition of beams by a velocity analysis. An analysis of the beam produced by heating equimolar proportions of KCl and $FeCl_2$ in an iron oven indicates that the observed velocity distribution curve can be accurately described by assuming a beam composed of 84.6 percent of $KClFeCl_2$ and 15.4 percent of KCl. The agreement with the 9.2 percent of KCl obtained from the data in Fig. 1 is good, especially in view of a difference in temperature in the two cases. The large rotational magnetic moment is, therefore, to be ascribed to the molecule $KClFeCl_2$ and, most probably, to $KBrFeBr_2$.

DISCUSSION

No data are available on the structures of the two molecules here investigated. Reasonable values of the ionic radii of the component atoms and any one of several conceivable molecular models yield for the most probable value of J at the temperature of the source, about 140 for $KClFeCl_2$ and 200 for $KBrFeBr_2$. The magnetic moment is then of the order of 0.5 and 0.25 nuclear magnetons for unit rotational quantum number for $KClFeCl_2$ and $KBrFeBr_2$, respectively. It is to be noted that the result is only approximate, since the assumptions which are made have a limited validity. In particular, it would be most surprising if the rotational magnetic moment per unit rotation were not significantly dependent on the axis of rotation. Nevertheless, the fact has been established that the molecules $KClFeCl_2$ have rotational magnetic moments much larger than those observed in other molecules of comparable mass and moment of inertia.

The theory of the rotational magnetic moment of $^1\Sigma$ molecules has been discussed in several papers.[4,5,8] In the absence of extensive data relating to the structure of the molecules in question and to the electronic states in which they may occur, it is not possible to apply the theory to detailed analysis of the effects here observed. The contribution of the electrons in the molecule to the rotational magnetic moment involves the ratio of the square of the matrix elements of an angular momentum operator between the ground state $^1\Sigma$ for which the moment is being found and the excited states of the molecule to the energy difference between the states. It is, presumably, through terms of this sort that the net contributions of the electron becomes abnormally large in the present cases. Low-lying paramagnetic levels of the molecules induce in the ground state a large magnetic moment, not to be expected if the molecule is in a $^1\Sigma$ state, far removed from molecular states with a net resultant electronic moment. That there should be low-lying paramagnetic states in these molecules is not at all surprising in view of the large number of low-lying states of the iron atom itself.

ACKNOWLEDGMENT

I wish to thank Mr. Thomas Eck for his aid in taking the data of these experiments. Professors Townes and Halford have given valuable advice about molecular and chemical questions related to these experiments.

[7] Mr. Miller will give a detailed discussion of the analysis of beams by a velocity analysis in another connection. I am grateful to him for making the analysis which is here quoted.

[8] G. C. Wick, Z. Physik **85**, 25 (1933); Phys. Rev. **73**, 51 (1948).

The Fluorescence of Biacetyl Vapor at 4358A*

NATHAN A. COWARD† AND W. ALBERT NOYES, JR.
Department of Chemistry, University of Rochester, Rochester, New York

(Received January 22, 1954)

The fluorescence efficiency of biacetyl vapor when excited by radiation of wavelength 4358A is independent of the number of quanta absorbed per cubic centimeter per second, almost if not quite independent of biacetyl pressure, and decreases with increase in temperature but there seems to be a transition from one type of variation with temperature to another between 60° and 100°. Oxygen quenches the fluorescence strongly, and isobutylene quenches the fluorescence little or not at all.

The marked difference in fluorescence behavior of biacetyl when excited by 4358A radiation from that when excited by 3660A radiation as pointed out by previous authors makes desirable an attempt to correlate fluorescence with photochemical behavior. Some suggestions are made with regard to mechanism.

BIACETYL vapor shows an abnormal behavior at 3660A in that increase in pressure causes an increase in fluorescence efficiency,[1,2] whereas at 4358A a decrease in fluorescence efficiency with increasing pressure is observed.[3] Since it has been suggested[2] that the behavior at 3660A may be due to the presence of a predissociation limit such that molecules excited to energies higher than that limit can fluoresce only if stabilized by collisions, it would be desirable both to have additional fluorescence data at 4358A and to have a detailed photochemical study at both wavelengths so that an attempt could be made to correlate the photochemical and fluorescence behaviors. The work herein reported supplies additional fluorescence data at 4358A. The photochemical data are not complete, and at the present writing, the nature of any ultimate correlation is not apparent. Brief mention will be made of these data in the present article.

EXPERIMENTAL

The incident beam from either a S100 Hanovia Alpine burner or a General Electric Company AH-6 arc passed through (1) an ultraviolet sharp cut-off filter (Corning 3387), (2) a collimating lens, (3) a blue filter (Wratten 47B), (4) a shutter, and (5) an adjustable diaphragm. This produced a narrow beam of 4358A radiation incident on the cell face. After passing through the cell, the light was focused by a lens on the photocathode of a G.E. 929 tube. The amplified current was balanced with a Leeds and Northrup student potentiometer, using a wall-type galvanometer as a null point indicator. Neutral density filters were placed in front of the G.E. 929 tube for the high intensities from the AH-6 arc. The amplifier circuit was stable and reproducible.

The fluorescent light emerged from the side arm of a *T*-shaped cell and passed through (1) a diaphragm, (2) a rotating sector which chopped the beam 30 times a second, (3) a diaphragm, (4) a cut-off filter to remove reflected exciting light (Corning 3387 for the S100 arc and a Wratten 16 filter for the AH-6 arc), a lens which focused the beam on the photocathode of an IP21 photomultiplier tube. The details of the circuit and the method of operation have been described.[4,5] The fluorescence amplifier was not as stable as might have been desired and showed considerable drift with time. To provide calibration, a radium-activated phosphor disk was mounted behind the cell so that when the cell was raised, the light from the phosphor would fall on the IP21 tube. The position of the phosphor relative to the phototube was quite critical so that the mounting was of necessity quite rigid. The calibration left something to be desired but the relative fluorescence efficiency is probably accurate to about five percent.

The purification of the biacetyl has been described.[5] The oxygen purification has also been described.[4] Tank isobutylene was admitted to a storage bulb through a trap held at the temperature of dry ice. After freezing with liquid nitrogen the isobutylene was repeatedly outgassed.

In some instances the various gases were mixed by means of a magnetically driven glass stirrer, but results were found to be just as reproducible by allowing mixing through diffusion. When oxygen was used it was admitted to the cell with the biacetyl frozen and the pressure measured. When isobutylene was used it was first admitted to the cell and the pressure measured, after which it was condensed into a storage bulb. The biacetyl was then admitted, the pressure measured, the cutoff to the storage bulb lowered, and both gases condensed into the fluorescence cell with liquid nitrogen.

The following measurements were made with the biacetyl condensed by liquid nitrogen: (1) I_0, the incident intensity (measured by moving the cell out

* This work was supported in part by contract between the U. S. Office of Naval Research, United States Navy, and the Department of Chemistry, University of Rochester.

† Hanovia Chemical and Manufacturing Company Fellow at the University of Rochester 1952–1953.

[1] F. C. Henriques, Jr., and W. A. Noyes, Jr., J. Am. Chem. Soc. **62**, 1038 (1940).

[2] G. M. Almy and P. R. Gillette, J. Chem. Phys. **11**, 188 (1943).

[3] Almy, Fuller, and Kinzer, J. Chem. Phys. **8**, 37 (1940).

[4] G. W. Luckey and W. A. Noyes, Jr., J. Chem. Phys. **19**, 227 (1951).

[5] H. J. Groh, Jr., J. Chem. Phys. **21**, 674 (1953).

of the light beam); (2) I_t^0, the light transmitted by the empty cell; (3) I_p, the intensity of the standard phosphor. The biacetyl (with or without foreign gas) was then vaporized in the cell and the following measurements made: (4) I_0, as above; (5) I_t, the transmitted light; (6) I_f, the intensity of the fluorescence. I_f^0, the intensity of extraneous fluorescence and scattered radiation, was very small and virtually constant so that it was not measured each time. The inverse of the fluorescence efficiency $1/Q$ was calculated from the following equation:

$$1/Q=\frac{I_0}{I_f-I_f^0}\times\left(\frac{I_t^0\,I_t}{I_0\,I_0}\right)^{\frac{1}{2}}\ln(I_t^0/I_t), \qquad (1)$$

Equation (1) assumes that the number of quanta absorbed per unit volume per second in the center of the fluorescence cell opposite the window through which the fluorescence emerges is proportional to the geometrical mean of the intensity entering the cell and the intensity emerging from the cell. This assumption is approximately correct as long as the fraction of the radiation absorbed is not large. This error could not exceed five percent in the present experiments. Values obtained by Eq. (1) are purely relative. When absolute values were desired they were calculated by comparison with the absolute values given by Almy and Gillette.[2]

RESULTS

It should be emphasized that the quenching studies herein reported relate only to the "green" fluorescence of biacetyl and neglect the weak "blue" fluorescence. This is unavoidable because of the difficulty of reducing scattered 4358 radiation and of obtaining color filters which would permit measurement of the blue fluorescence without including scattered radiation.

It has already been reported[3] that the fluorescence efficiency of biacetyl excited at 4358A is independent of the intensity of the exciting light. This is confirmed in the present work by varying the intensity more than 100 fold. The facts that the mean lifetime of the fluorescence decreases with increasing intensity[6] and that the rate of photochemical decomposition at this wavelength apparently depends on some power higher than one of the intensity[7] must be correlated with the lack of effect of intensity on fluorescence efficiency.

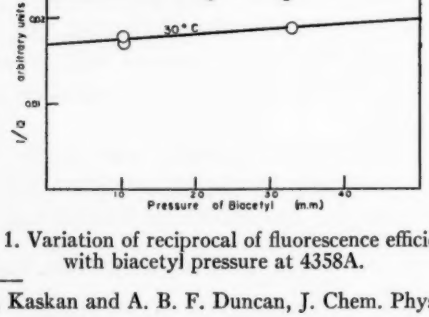

FIG. 1. Variation of reciprocal of fluorescence efficiency with biacetyl pressure at 4358A.

It has also been reported that self quenching is small or negligible in biacetyl at 4358A.[2] This is confirmed at 30° and also now found to be true at 70°. (See Fig. 1.) Behavior at 4358A is in marked contrast with that at 3660A where increase in pressure caused an increase in fluorescence efficiency. It may be mentioned that effects of pressure on the ratio of carbon monoxide to ethane in the photochemical reaction are different at the two wavelengths.[7] These facts should be correlated with the fluorescence data if possible.

The change in fluorescence efficiency with pressure of added oxygen was investigated at 28° and at 100° (Fig. 2). The pressure for half-quenching at 28° is found to be 0.023 mm, somewhat larger than the value of 0.013 found by Almy *et al.*[3] The slope of the $1/Q$ *vs* (O_2) plot at 100° is within experimental error of the same as at 28°. However $1/Q$ is higher at the higher temperature (i.e., the fluorescence efficiency in pure biacetyl is lower at the higher temperature just as it is at 3600A) so that the oxygen pressure for half-quenching is higher at 100° than at 28°. This agrees with the decrease in lifetime at higher temperatures.[6]

Two runs, one with and the other without oxygen, may be compared as follows: run 1: biacetyl pressure

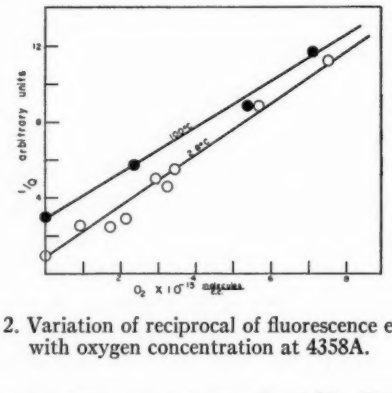

FIG. 2. Variation of reciprocal of fluorescence efficiency with oxygen concentration at 4358A.

$=10.7$ mm, oxygen pressure$=0$, $1/Q=7.2$; run 2: biacetyl pressure$=20.8$ mm, oxygen pressure$=5$ mm, $1/Q=400$. Temperature$=28°$ in both runs. These results indicate that the fluorescence being studied in these experiments is almost exclusively from the long-lived state[5] and that errors due to reflected light and extraneous fluorescence are negligible.

In view of the effect of intensity on the fluorescence lifetime[6] and the fact that a peculiar variation of photochemical yield with intensity at 4358A seems probable, it was desirable to add some gas which would

[6] W. E. Kaskan and A. B. F. Duncan, J. Chem. Phys. 18, 427 (1950).

[7] G. F. Sheats and E. D. Becker (unpublished work), University of Rochester. We are indebted to Professor F. E. Blacet of the University of California at Los Angeles for private communications on this subject.

remove the radicals resulting from the photochemical dissociation (presumably methyl and acetyl radicals)[8] from the system. Isobutylene was chosen both because of its physical properties and because the simple olefins are known to react with free radicals. Table I presents the results.

The quenching by isobutylene is, therefore, negligible.

The course of the photochemical reaction at 4358A changes markedly as the temperature is increased from 30° to 100°. A careful study of the effect of temperature on the fluorescence seemed to be essential. The data are presented graphically in Fig. 3. A plot $\ln(1/Q-1)$ *vs* $1/T$ was chosen as the best means of portraying the data because it should give a straight line if there are two competing simple unimolecular processes, *viz.* fluorescence and internal degradation of energy without fluorescence (see below). There are therefore, peculiarities in the fluorescence behavior in the same temperature region where the photochemical behavior shows abnormalities.

TABLE I. Quenching of biacetyl fluorescence by isobutylene at 4358A.

P(biacetyl) mm	*P*(isobutylene) mm	Temp	*I/Q*
11	0	30°	7.2
11	182	30°	7.6
35	0	30°	7.6
35	36	30°	8.0
18	0	95°	17.2
18	47	95°	16.9

($I/Q=7.2$ at 11 mm is taken from Almy and Gillette as a standard.)

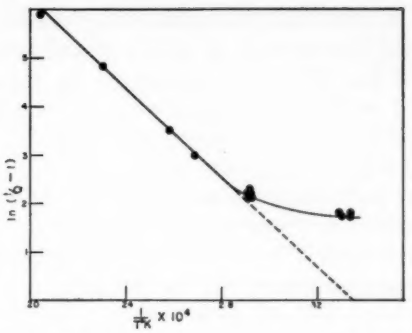

FIG. 3. Effect of temperature on quenching of biacetyl fluorescence at 4358A.

The significant results may be summarized briefly: (a) The "green" fluorescence is far more intense than the "blue" fluorescence at this wavelength, the ratio being impossible to determine but it is certainly 25:1 or more; (b) the fluorescence efficiency is independent of intensity (this is not true at 3660A)[9] and nearly independent of biacetyl pressure; (c) oxygen quenches the fluorescence strongly, the pressure for half quenching being higher, the higher the temperature; (d) isobutylene quenches the fluorescence little or not at all; (e) the fluorescence efficiency varies in a more or less normal way with temperatures above 90°, but at lower temperatures the behavior is different and shows a less rapid variation with temperature.

DISCUSSION

The detailed correlation between the fluorescence and the photochemical phenomena must await sufficient photochemical data. It is possible, however, to make certain comparisons between behaviors at 3660A and at 4358A.

The most striking difference between the two wavelengths is the almost complete lack of pressure effect on the quenching at the longer wavelength and the increase in fluorescence efficiency with increase in pressure at the shorter of the two wavelengths. The increase in fluorescence efficiency at 3660A is not at the expense of dissociation since quantum yields of products also increase with pressure at both wavelengths. There are two important photochemical differences, however: (1) the quantum yields of the photochemical reaction are independent of intensity at all temperatures at 3660A whereas at room temperature they are roughly proportional to intensity at 4358A and only become independent of intensity at temperatures toward 100°; (2) the ratio CO/C_2H_6 in the products decreases with increasing pressure at 3660A but is virtually independent of pressure at 4358A.[7]

These facts strongly suggest a fundamental difference in the photochemical primary process at the two wavelengths, at least at room temperature. As suggested by Groh,[5] the photochemical reaction at 3660A resembles that at 2654A as described by Blacet and Bell[8] and the primary dissociation can well be into two acetyl radicals. Quantum yields are very low but since both these yields and the fluorescence yield increase with pressure, there is no apparent simple correlation with the suggestion by Almy and Gillette[2] of prevention of predissociation by collision.

At 4358A at room temperature it is apparently necessary to assume that the photochemical reaction results either from collision between two excited molecules or between excited molecules and free radicals. If the lifetime of the excited state is as long as reported by Kaskan and Duncan[6] there could be enough collisions between excited molecules to give the observed yields. In any case either the photochemical loss of excited molecules is negligible compared to other losses or the states involved are different from the fluorescing states since at 4358A there is no dependence of fluorescence efficiency on intensity.

It cannot be proved conclusively, owing to experimental difficulties, that the ratio of shortlived (blue) to longlived (green) fluorescence at 4358A is much

[8] F. E. Blacet and W. E. Bell, Discussions Faraday Soc. No. 14, 70 (1953).
[9] H. J. Groh, Jr., Ph.D. thesis, University of Rochester, 1952.

less than at 3660 but this seems to be almost certain. Most of the fluorescence at 4358A would arise, therefore, from the B^{**} state postulated by Groh.[5] This is assumed to be formed rapidly by collision from the state formed initially by absorption of radiation.

The quantity of fluorescence emitted by B^{**} is dependent only on temperature and on intensity but is independent of pressure. The fluorescence efficiency is, however, only about 0.15.[2] Hence there are competing processes either for the formation of for the destruction of B^{**} or both. The ratios of the rates would be nearly independent of pressure but would be dependent on temperature. B^{**} must be destroyed by collision with oxygen molecules, unless oxygen prevents its formation.

It is possible to derive a simple expression which will account for the variation of $1/Q$ with temperature. This expression may be based essentially on the mechanism proposed by Groh[5] except that certain steps are unnecessary because of the lower energy absorbed. A smaller number of steps cannot be used.

$$B+h\nu=B' \tag{2}$$

$$B'(+B)=X(+B) \tag{3}$$

$$B'(+B)=Y(+B) \tag{4}$$

$$B'(+B)=B^{**}+B \tag{5}$$

$$B^{**}=B+h\nu \tag{6}$$

$$1/Q-1=k_3/k_5+k_4/k_5. \tag{7}$$

Equations (3), (4), and (5) must involve the same function of the concentration of B in their rates as otherwise $1/Q$ would be a function of pressure, in disagreement with the facts. If one of the activation energy differences E_3-E_5 or E_4-E_5 is about 9000 calories per mole and the other is very much lower the variation will agree with that shown in Fig. 3.

The following expression for $1/Q$ is found from the data shown in Fig. 3:

$$1/Q=5+3\times10^6\exp(-9000/RT). \tag{8}$$

To explain the photochemical data with this mechanism either X or Y must be a state capable of dissociation with a relatively small probability of doing so. In addition there must be a small amount of decomposition at room temperature with a rate dependent on the square of the concentration of some active species, perhaps X or Y. Neither type of dissociation can be the main cause for decrease in fluorescence efficiency with increase in temperature. It is probably significant that both the fluorescence and the photochemical kinetics at 4358A change character between 60° and 90°.

Absorption of 4358A corresponds to about 69 000 calories per mole. If vibration energy is lost prior to fluorescence so that active molecules possess energy equivalent to the long wave limit of the absorption spectrum (4670A) there would be available about 62 000 calories per mole. Bond energies in biacetyl are not well known, but probably neither of these energy values is sufficient to cause rupture of a carbon-carbon bond. Hence an activation energy for formation from the active species of a state capable of dissociation is probable. Such an activation energy is suggested by the data on acetone.[10] It is not possible to state whether the activation energy of 9000 calories derived from the slope of the line in Fig. 3 is related in any way to dissociation or not, but the possibility certainly exists.

Isobutylene does not quench the fluorescence by more than the experimental error (Table I) and hence its effective cross section for quenching must be very small. It does have a small but definite effect on the course of the photochemical reaction, mainly by causing a decrease in the CO/C_2H_6 ratio in the products. Isobutylene does not appear to be very effective in removal of methyl radicals from the system.

The quenching effect of oxygen on the green fluorescence needs further investigation. It is not certain that it is due to a simple deactivation by collision. It may be due to a reaction between the active molecules and oxygen. Either process could lead to a Stern-Volmer type of quenching (Fig. 2). From the data shown in Fig. 2 one can calculate an effective cross section for quenching if one uses the mean lifetime found by Kaskan and Duncan[6] (1.8×10^{-3} sec at 25° and 1.3×10^{-3} sec at 79°). The result is about 1.6×10^{-16} cm² at 30° and 3.1×10^{-16} cm² at 100°. The latter is based on an estimated 10^{-3} sec for the mean life at 100°. Thus there is a fairly efficient quenching by oxygen at both temperatures and little change with temperature. Put in another way, the "steric factor" for the quenching process is about 0.1. It should be pointed out, however, that instead of destroying the fluorescing state, oxygen may destroy the state from which the fluorescing state is derived. In either case the effective cross section for quenching would be the same provided oxygen does not change the ratio of the rates for the disappearance of this parent state (e.g. does not change $k_3:k_4:k_5$ in the mechanism).

It is evident that a study of the photochemical reactions in the biacetyl-oxygen system is necessary to provide information on some of these points. No data of this type are at present available.

[10] W. A. Noyes, Jr., and L. M. Dorfman, J. Chem. Phys. 16, 788 (1948).

Nuclear Quadrupole Resonances in Solid Bromine in Iodine Compounds

A. L. SCHAWLOW
Bell Telephone Laboratories, Inc., Murray Hill, New Jersey
(Received January 13, 1954)

Pure quadrupole resonances of bromine or iodine nuclei have been observed in paradibromo- and paradiiodo-benzene; the tetrabromides of carbon, silicon, germanium and tin; germanium and tin tetraiodides; sodium, potassium, and cesium bromates; antimony tribromide and iodide; and cyanogen bromide. For most of these compounds, measurements were made at room temperature and at liquid nitrogen temperature. The results are correlated with chemical bonding and crystal structure data.

NUCLEAR quadrupole resonances in solids have been reported for at least eleven elements, but have been extensively studied only in chlorine compounds. Measurements have therefore been made in a number of bromine and iodine compounds and are compared with those in the analogous chlorine compounds.

APPARATUS

The resonance detector was a superregenerative oscillator using a single type 6AF4 triode. The circuit is similar to those used as local oscillators in some ultra-high-frequency television converters (Fig. 1).[1]

A vibrating condenser permits frequency modulation at a rate which is usually around 60 cycles per second for searching, and around 18 cycles for measuring the line frequency. The oscillator is swept over a range which need be only somewhat greater than the line width; 30 kilocycles might be a typical value.

The oscillator becomes a superregenerative detector by the application of a quenching voltage. This voltage, which turns the oscillations on and off every 10^{-5} second or so, may be applied either to the midpoint of the two grid resistors or to the top of the cathode resistor. Usually the cathode connection was employed. The cathode resistor was adjustable to set the operating point for optimum signal-to-noise ratio.

Superregenerative detectors are especially well adapted for detecting quadrupole resonances because of their simplicity and relatively high sensitivity.[2] Moreover, they permit large radio-frequency amplitudes to be applied to the sample during the peak of the oscillator quench cycle. This is advantageous for quadrupole resonance lines at high frequencies, as these lines are not easily saturated.

Superregenerative detectors do have a disadvantage in that the lines are accompanied by several sidebands separated from the main line by the quench frequency. The main line can usually be distinguished by changing the quench frequency which moves the sidebands but not the main line. In some substances, such as carbon tetrabromide, several closely spaced lines are present and it is very difficult to distinguish the lines from sidebands with certainty.

The particular oscillator circuit employed does not seem to be critical; several have been used with comparable results. The circuit of Fig. 1 performs well, but to cover a frequency range of more than about 100 megacycles the radio-frequency choke coils may have to be adjusted.

Line frequencies were measured by superimposing a signal from a standard frequency oscillator on the line. As the shapes of the nuclear resonance and frequency standard pulses are different, they undergo different time delays in passing through the audio amplifiers.[3] To compensate for this, the final measurement is an average of the value obtained for a sweep upward and a sweep downward in frequency. The discrepancy between the two directions in not large for low sweep rates, but it must be eliminated for good accuracy.

MEASUREMENTS

Table I shows the measured frequencies of the lines observed. For bromine compounds only the Br^{81} resonance is listed in the table; usually the Br^{79} resonance was also observed. The ratio of resonance frequencies of the two isotopes is discussed below. For iodine, there is only one stable isotope (I^{127}), but since its spin is 5/2, two resonances differing in frequency by a ratio close to 2:1 are to be expected. Only the lower of these came within the tuning range of this apparatus and is tabulated for these compounds.

If it is assumed that the electric field gradient tensor at the halogen nucleus is cylindrically symmetrical,

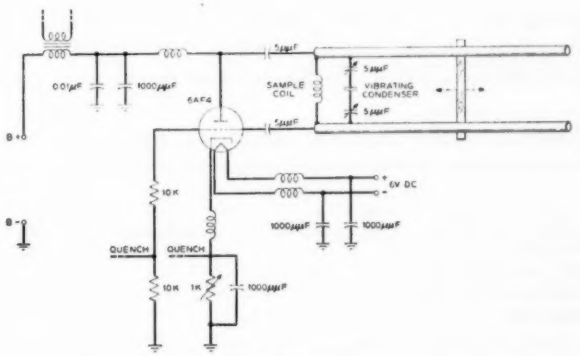

FIG. 1.

[1] See, for instance, N. Edwards, Radio and Television News **48**, 47 (July, 1952).
[2] H. G. Dehmelt, Z. Physik **130**, 356 (1951).
[3] D. K. Coles, Advances in Electronics **II**, 299 (1950).

TABLE I. Frequencies of quadrupole resonance lines—Br^{81} or I^{127}.

Substance	Room temperature Temperature (°C)	Room temperature Frequency (Mc)	Liquid nitrogen Frequency (Mc)
$pC_6H_4Br_2$	24.8	223.788	226.494
$pC_6H_4I_2$	24.2	276.684	280.243
$SnBr_4$*	21.0	157.618 160.934 160.480 160.347	162.032 165.208 165.401 165.270
$GeBr_4$	23.7	171.572 171.839	175.584 175.949
$SiBr_4$			147.511 147.576
CBr_4			More than 4 lines around 268 Mc.
GeI_4	24.0	218.992 220.656	222.660 226.103
SnI_4†			207.682 209.127
$NaBrO_3$	24.1	149.375	151.909
$KBrO_3$	28.4	144.354	149.361
$CsBrO_3$	23.9	142.735	145.662
$SbBr_3$	24.0	135.56	
SbI_3			174.509
BrCN	13.0	285.483	296.247

* Resonances in $SnBr_4$ have also been observed by Kojima, Tsukada, Ogawa, and Shimauchi, J. Chem. Phys. 21, 1415 (1953).
† Measured previously at room temperature by H. G. Dehmelt (see reference 2).

the quadrupole coupling constant eqQ can be derived from the resonance frequencies. For bromine, which has a nuclear spin I of 3/2, we then obtain $eqQ=2\nu$, where ν is the resonance frequency. For iodine $I=5/2$, and so $eqQ=20/3\nu$, where ν is the lower of the two resonance frequencies, i.e., the frequency listed in Table I. If the higher-frequency iodine resonance were measured, the field gradient asymmetry could also be deduced.[2]

The value of the quadrupole coupling constant is related to the bond structure of the compound (see, for instance, C. H. Townes and B. P. Dailey).[4,5] In a completely ionic bond, the halogen atom acquires an electron to complete its outer p shell, so that the electron distribution near the nucleus is spherically symmetric. Then the field gradient q and hence the quadrupole coupling are zero. For a purely covalent bond, on the other hand, the halogen atom lacks just one p electron of having a complete outer shell. The quadrupole coupling is large, and has a value characteristic of the free atom so that it can be obtained from atomic beam resonance measurements.[6] These lead to the following quadrupole couplings in purely covalent bonds: for Cl^{35}, $eqQ=109.746$ Mc; for Cl^{37}, $eqQ=86.510$ Mc; for Br^{79}, $eqQ=384.878$ Mc; for Br^{81}, $eqQ=321.516$ Mc; and for I^{127}, $eqQ=2292.430$ Mc. From these, the resonance frequencies ν_0 for a purely covalent bond are:[7] Cl^{35}, 54.873 Mc; Cl^{37}, 43.255 Mc; Br^{79}, 384.9 Mc; Br^{81}, 321.5 Mc; I^{127}, 343.9 and 687.7 Mc.

TABLE II. Nuclear quadrupole resonances in *para*-dihalobenzenes.

	Cl^{35}	Br^{81}	I^{127}
ν(Mc) (at 77°K)	34.780	226.494	280.243
$f=100\nu/\nu_0$	63	70	82
Electronegativity difference (carbon-halogen)	0.5	0.3	−0.1

If the bond can be properly described as a superposition of pure ionic and covalent structures, the percentage of covalent character is given directly by $f=100\nu/\nu_0$, where ν is the observed resonance frequency. However, Townes and Dailey's analysis of quadrupole couplings in a number of halogen compounds shows that if the bond is appreciably ionic, i.e., more than about 5 percent ionic, it is also appreciably s hybridized.[8] It may usually be assumed that if the bond has more than 5 percent ionic character, it has about 15 percent s-hybrid character. As an s bond contributes nothing to the quadrupole coupling, the percentage of covalent p bond is $f/0.85$.

The fraction of covalent character would be expected to be small when there is a large electronegativity difference between the halogen and the atom to which it is bonded. If f does not vary monotonically with electronegativity difference, then some of the compounds have more complicated bond structures. When several structures are involved in the bond, measurement of a single resonance is not enough to determine their relative importance, but may serve to confirm structures postulated from other considerations.

Table II summarizes the frequencies, ν, observed for the *para*-dihalobenzenes of chlorine, bromine, and iodine at liquid air temperature and their corresponding values of $f=100\nu/\nu_0$. It is seen that in this case f does increase as the electronegativity difference decreases, so that the changes in f may reasonably be interpreted as changes in the percentage covalent character.

Table III shows the measured values of f for the tetrahalides and the corresponding electronegativity differences. Again the value of f increases in going from corresponding chlorine to bromine to iodine compounds, as would be expected from the decreasing electronegativity. A similar trend is observed in going from tin to germanium to carbon, but the value of f is less for the silicon compounds than for any of the others. In this case a decrease in f cannot be interpreted simply as caused by increasing ionicity with increasing electronegativity difference.

Silicon halides are also known to have unusually short bond lengths.[8–10] For instance, the Si-Cl distance in

[4] C. H. Townes and B. P. Dailey, J. Chem. Phys. **17**, 282 (1949).
[5] C. H. Townes and B. P. Dailey, J. Chem. Phys. **20**, 35 (1951).
[6] V. Jaccarino and J. G. King, Phys. Rev. **83**, 471 (1953), and private communication.
[7] H. G. Dehmelt and H. Krüger, Z. Physik **129**, 401 (1951).
[8] C. H. Townes and B. P. Dailey, private communication.
[8] M. W. Lister and L. E. Sutton, Trans. Faraday Soc. **37**, 393 (1941).
[9] L. E. Sutton, Ann. Repts. Chem. Soc. **37**, 36 (1940).
[10] P. W. Allen and L. E. Sutton, Acta Cryst. **3**, 46 (1950).

$SiCl_4$ is 2.00A, which is 0.16A less than the sum of the single-bond covalent radii of the silicon and chlorine atoms. The Si-Br distance is likewise 0.16A shorter than the sum of the single-bond radii. In other halides of group IV elements, the discrepancy is somewhat less. This shortness of the silicon-halogen bond in these and the related XYH_3 compounds has been attributed[11,12] to partial double bonding. It is possible to use the measured bond lengths to estimate the fraction of double-bond character.[12,13] Then the quadrupole coupling constants are used to deduce the fraction of ionic character in the bond. In so doing, it is necessary to make assumptions about the degree of hybridization. Following Townes and Dailey's analysis, it is assumed here that bonds which have more than 5 percent ionic character have 15 percent s hybridization.

The procedure is first to express the quadrupole couplings as percentages f of the coupling for a single unbalanced p electron. The percentage of double-bond character y is derived from the bond lengths by using Pauling's relation[12,13]

$$y=100(r_1-r_0)/(r_1+2r_0-3r_2),$$

and from it, f_2, the double-bond contribution to f, is determined.[12] By subtracting f_2 from f one obtains the part f_1 of the quadrupole coupling which must be ascribed to the single-bond structure. All these f's are fractions of the quadrupole coupling for the halogen atom with a pure p bond. The ionic structure contributes nothing to f_1, and so the percentage of single covalent bond is deduced by dividing f_1 by 0.85 to take into account hybridization. Finally, the percentage ionic bond is 100 minus the sum of the percentages of double bond and single covalent bonds.

Table IV gives the percentages obtained in this way. The measured bond lengths r_0 are taken from the review paper by Allen and Sutton.[10] Most of these bond lengths are close to those measured by microwave spectroscopy in the XYH_3 molecules. The Ge-Cl bond appears to be an exception: the bond length in $GeCl_4$ is 2.08A, while in GeH_3Cl it is 2.148A. In Table IV the limits listed for the bond percentages are simply those arising from the stated uncertainties of the bond lengths. More serious errors might arise if the assumptions are not valid. In particular it has been suggested that bond shortening can be produced by ionic character as well as by double bond.[14,15] If some of the shortening were attributed to ionic character, the double-bond percentages would be decreased somewhat, with the single and especially the ionic bond percentages being increased correspondingly.

[11] L. Pauling, *Nature of the Chemical Bond* (Cornell University Press, Ithaca, 1940), Chap. 7.
[12] J. Mays and B. P. Dailey, J. Chem. Phys. **20**, 1695 (1952).
[13] See reference 11, p. 175.
[14] V. Schomaker and D. P. Stevenson, J. Am. Chem. Soc. **63**, 37 (1941).
[15] Gordy, Smith, and Trambarulo, *Microwave Spectroscopy* (John Wiley and Sons, Inc., New York, 1953), p. 318.

TABLE III. Nuclear quadrupole resonance in tetrahalides (averages of line groups at 77°K)

		C	Si	Ge	Sn
Cl_4	frequency (Mc)[a]	40.6	20.4	25.7	24.1
	f	74	37	47	43
	electronegativity difference	0.5	1.2	1.3	1.3
Br_4	frequency (Mc)	268	147	176	164
	f	83	46	55	51
	electronegativity difference	0.3	1.0	1.1	1.1
I_4	frequency (Mc)			224	208
	f			65	62
	electronegativity difference			0.7	0.7

[a] R. Livingston, J. Phys. Chem. **57**, 496 (1953).

The general reasonableness of the scheme used here is supported by the fact that, if we except Ge-Cl in which the bond length seems anomalous, the ionic character increases gradually and steadily in going from carbon to tin. As would be expected, there is no dip in ionic character at silicon.

INTERMOLECULAR BINDING AND CRYSTAL STRUCTURES

In interpreting the quadrupole couplings it has been assumed that intermolecular bonding has a small effect on the coupling. This is reasonable in view of the smallness of intermolecular binding energy in molecular crystals like the tetrahalides. Intermolecular forces give rise to a small displacement of quadrupole resonance lines so that sometimes several lines are observed, each line corresponding to a different nonequivalent position of the halogen atom in the crystal lattice. In molecular crystals the spacing between lines is never very large; in the tetrahalides it is never more than about 3 percent. This splitting is a measure of the magnitude of the intermolecular effects and indicates strongly that they are small. Thus the measured quadrupole couplings are probably close to those which would be obtained if they could be measured in the free molecules.

TABLE IV. Bond structures of tetrahalides deduced from bond lengths and quadrupole couplings.

	Single-bond radius r_1A	Double-bond radius r_2A	Observed radius r_0	% double bond	% covalent single bond	% ionic bond
C-Cl	1.76	1.56	1.765±0.015	0	81	19
C-Br	1.91	1.70	1.91±0.02	0	92	8
Si-Cl	2.16	1.96	2.02±0.02	45±12	22±8	33±4
Si-Br	2.31	2.11	2.15±0.02	60±15	24±8	16±7
Ge-Cl	2.21	2.01	2.08±0.03	41±16	34±8	25±8
Ge-Br	2.36	2.16	2.29±0.02	16±6	57±3	27±3
Ge-I	2.55	2.35	2.50±0.03	11±7	70±4	19±3
Sn-Cl	2.39	2.19	2.30±0.03	22±11	40±6	38±5
Sn-Br	2.54	2.34	2.44±0.02	25±8	47±4	28±4
Sn-I	2.73	2.53	2.64±0.04	21±11	62±6	17±5

The number of lines observed gives directly the number of nonequivalent lattice positions. In $SiBr_4$, $GeBr_4$, GeI_4, and SnI_4, two lines were observed in accordance with the known crystal structures. $SiCl_4$, $GeCl_4$, $SnCl_4$, and $SnBr_4$, have four-line patterns. CBr_4 shows more than four lines, with a pattern too complicated to resolve completely with a super-regenerative detector in which sidebands can be confused with the main lines. CCl_4 has at least fifteen and probably sixteen lines.[16] The number of lines permits a grouping of these compounds into several families of related crystal structures.

Two phases were noted in *p*-diiodobenzene at room temperature. In a sample which had been standing at room temperature for some time, a resonance was observed at 276.560 Mc (at 31°C). If the sample was melted and then allowed to return to the same temperature, the resonance occurred at 275.905 Mc, a displacement of 0.655 Mc. A phase transition marked by a volume change has been observed to occur at 50°C.[17] The nuclear quadrupole resonance observations show that the high-temperature phase can be supercooled at least 20°C.

Some indication of a metastable phase in $SnBr_4$ was obtained in samples which had been melted and quickly frozen. The low-frequency line (for each isotope) was observed at the same position as in annealed samples, but the higher-frequency group was replaced by a single line at 192.53 Mc (Br^{79} at 24.0°C). This structure was not very stable and was not found at all for those samples which had the highest purity as indicated by the highest melting point.

The quadrupole coupling in BrCN is slightly larger in the solid (582 Mc at 77°K) than in the gaseous molecule (573 Mc).[18] In ICN the coupling is 10 percent greater in the solid. There it has been attributed to bonding between molecules which are arranged in long chains.[5] The effect in BrCN is smaller, and unfortunately its crystal structure is not known.

TABLE V. Quadrupole coupling ratio of the bromine isotopes.

Compound	Ratio $(eqQ)_{79}/(eqQ)_{81}$ Room temperature	Liquid nitrogen
$NaBrO_3$	1.19705	1.19707
$KBrO_3$	1.19711	1.19704
$CsBrO_3$	1.19703	1.19703
$GeBr_4$	1.19712	
$SnBr_4$	1.19703	
$pC_6H_4Br_2$	1.19711	1.19706
Average 1.19707±0.00003		

[16] R. Livingston, J. Phys. Chem. **57**, 496 (1953).
[17] K. Ueberreiter and H. J. Orthmann, Z. Naturforsch. **5a**, 101 (1950).
[18] Townes, Holden, and Merritt, Phys. Rev. **74**, 1113 (1948).

QUADRUPOLE COUPLING RATIO OF THE BROMINE ISOTOPES

If the electronic structure of the molecule, and hence q, is unchanged by substituting one isotope for another, then the ratio of the quadrupole couplings for two isotopes is just the ratio of their quadrupole moments. The coupling ratio was measured in several compounds at room and at liquid nitrogen temperatures. The results are given in Table V. Individual measurements are believed accurate to about 0.00010; the mean is probably more precise, and the average deviation of individual measurements from the mean is 0.00003. The final value is in excellent agreement with the ratio of the bromine quadrupole moments measured with an atomic beam.[19] It also confirms, with increased precision, the previous values from microwave spectroscopy[15] and quadrupole resonance.[20]

A small variation in the coupling ratio with temperature and with change of compound is to be expected because of the effect of nuclear mass on zero-point vibrations. In chlorine the ratio varies by one or two parts in 10 000[21] and the variation expected in bromine would be several times smaller. The accuracy needed to detect such a small shift would require an oscillator with less frequency flutter than the one used in this investigation. Such stability is difficult to achieve in a superregenerative detector.

However, some of the lines appear to be sharp enough to permit more precise measurements if desired. Sodium bromate in particular gives a very strong, sharp line, having a half-width at half-maximum of about 1.5 kc, in 150 Mc, corresponding to an effective Q of the order of 50 000. It is noteworthy that the corresponding chlorine compound, $NaClO_3$, gives the sharpest chlorine quadrupole resonance.

Such sharp resonances would be suitable for use as frequency standards,[22] except that they usually have negative temperature coefficients of the order of 100 parts per million per degree C. This almost universal temperature coefficient is in qualitative agreement with the theory of Dehmelt and Krüger, as developed by Bayer.[7,23] Further refinements would be needed to fit the temperature curves closely.

The author wishes to thank A. N. Holden and C. E. Miller for chemical advice and for the preparation of most of the compounds investigated. He would also like to acknowledge the assistance of J. G. Caruso and G. E. Devlin in the construction and operation of the apparatus.

[19] J. G. King and V. Jaccarino, Phys. Rev. **91**, 209 (1953).
[20] H. G. Dehmelt and H. Krüger, Z. Physik **129**, 401 (1951); H. G. Dehmelt, Z. Physik **130**, 480 (1951); Manring, Brown, and Williams, Phys. Rev. **90**, 348 (1953).
[21] Wang, Townes, Schawlow, and Holden, Phys. Rev. **86**, 809 (1952).
[22] H. Lyons, Ann. N. Y. Acad. Sci. **55**, 831 (1952).
[23] H. Bayer, Z. Physik **130**, 227 (1951).

Heterogeneous Nucleation of Crystals from Vapor*

G. M. POUND, M. T. SIMNAD, AND LING YANG
Metals Research Laboratory, Carnegie Institute of Technology, Pittsburgh, Pennsylvania
(Received February 15, 1954)

A rate equation is derived for heterogeneous nucleation of crystals from the vapor on the basis of an adsorption, surface diffusion, and statistical fluctuation mechanism. It should be emphasized that the term surface diffusion as used in this development does not imply the existence of a gradient. Rather it refers to random movement of absorbed atoms on the subtrate surface. It is shown that this mechanism results in a rate at least 10^2 to 10^3 times greater than that calculated on the basis of direct addition of atoms to the critical nucleus from the vapor phase. The equation describes the temperature dependence of existing critical supersaturation data for heterogeneous nucleation. Analysis of the existing data by this treatment permits an evaluation of the standard free energy of adsorption. Particular attention is given to heterogeneous nucleation from atomic beams.

INTRODUCTION

SOME fairly precise data are available on the supersaturation required for appreciable heterogeneous nucleation rate of metal crystals from the vapor phase. In general, the better data were obtained using a thermal beam technique in which the intensity of the atomic beam impinging on a substrate was increased until appreciable nucleation rate of crystals was observed. This intensity, expressed in terms of supersaturation, gives the critical supersaturation for heterogeneous nucleation. In 1925, Estermann[1] studied the condensation of cadmium on various substrates in the temperature range of $-83°C$ to $-111°C$ and found that cadmium condensed at lower supersaturations on silver than on copper, while glass was the least effective in starting the condensation. In 1928, Cockcroft[2] made a careful study of critical supersaturation for the condensation of cadmium on copper at six different target temperatures between $-92°C$ and $-155°C$ and also the condensation of cadmium on silver, copper, and glass at $-137°C$. He could not find any difference in the critical supersaturations for condensation on these different substrates, and suggested that this was due to the existence of gas films on the surfaces of these substrates which masked the true surface forces. Recently, the present authors[3] investigated the heterogeneous nucleation of sodium on various substrates at low temperatures and hypothesized that the surfaces were partially masked by adsorbed gas films. In all of these investigations the observed critical supersaturation ratios were high, i.e., of the order of 10^{10} to 10^{20}, and decreased appreciably with increase in substrate temperature.

In spite of the possible masking of true surface forces by adsorbed gas films in the above experiments, it is of interest to describe the temperature dependence of critical supersaturation. Also, it is of interest to decide whether the nucleation occurs primarily by an adsorption and surface diffusion mechanism or by direct addition of an atom from the vapor phase to the critical nucleus.[4–11] These matters are considered in the following treatment.

Burton, Cabrera, and Frank[12] have shown conclusively that crystal growth from the vapor proceeds by a mechanism of adsorption and surface diffusion to the edge of an advancing monatomic layer. Inasmuch as the probability of a direct hit by an atom from the vapor on the advancing edge is low relative to the probability of adsorption on the surrounding area and diffusion to the edge or the line sink, it is clear that surface diffusion is a fundamental process in crystal growth. However, in the present application, the critical nucleus on the substrate surface presents some area to the vapor phase. Thus, it is not immediately clear whether addition of an atom to the critical nucleus can occur more rapidly by direct impingement from the vapor phase or by surface diffusion to the critical nucleus edge.‡[13]

The theory of heterogeneous nucleation of crystals from the supercooled liquid has been successfully treated by Turnbull,[4,14,15] Hollomon,[4,11] and Fisher.[14]

* The research described in this paper was sponsored by the U. S. Office of Naval Research.

[1] I. Estermann, Z. Elektrochem. **31**, 441 (1925).
[2] J. D. Cockcroft, Proc. Roy. Soc. (London) **A119**, 293 (1928).
[3] Yang, Birchenall, Pound, and Simnad "Heterogeneous Nucleation of Sodium Crystals from Atomic Beams," Acta Metallurgica (to be published).
[4] J. H. Hollomon and D. Turnbull, *Progress in Metal Physics* IV (Interscience Publishers, Inc., New York, 1953), pp. 333–388
[5] V. K. La Mer, Ind. Eng. Chem. **44**, 1270 (1952).
[6] G. M. Pound, Ind. Eng. Chem. **44**, 1278 (1952).
[7] Howard Reiss, Ind. Eng. Chem. **44**, 1284 (1952).
[8] R. Smoluchowski, *Phase Transformations in Solids* (John Wiley and Sons, Inc., New York, 1951), pp. 149–183.
[9] R. S. Bradley, Quart. Revs. **5**, 315 (1951).
[10] D. Turnbull and J. H. Hollomon, *The Physics of Powder Metallurgy* (McGraw-Hill Book Company, Inc., New York, 1951), pp. 109–143.
[11] J. H. Hollomon, *Thermodynamics in Metallurgy* (American Society for Metals, New York, 1950), pp. 161–177.
[12] Burton, Cabrera and Frank, Phil. Trans. Roy. Soc. (London) **243A**, 299 (1951).
‡ Cabrera and Burton assumed a surface diffusion mechanism in deriving an expression for two-dimensional nucleation in crystal growth.
[13] N. Cabrera and W. K. Burton, Discussions Faraday Soc. No. 5, 33 (1949).
[14] D. Turnbull, and J. C. Fisher, J. Chem. Phys. **17**, 71 (1949).
[15] D. Turnbull, J. Appl. Phys. **21**, 1022 (1950).

Adsorption and surface diffusion are not operative in such transformations involving only condensed phases.

Turnbull and Vonnegut[16] have derived an interesting relationship between the critical free energy of transformation per unit volume ΔF_v^*, defined as the free energy change per unit volume needed for a nucleation rate of one per cm^2 per second, and the lattice misfit δ between the substrate and the substance deposited on it. The derivation is based on Turnbull's equation for the rate of heterogeneous formation of crystalline nuclei and the dislocation model of interphase boundaries developed by Van der Merwe and by Brooks. By taking into consideration the strain energy in the nucleus, these authors conclude that in the heterogeneous transformation of liquid to solid, there is a parabolic relationship between $|\Delta F_v^*|$ and δ if the nucleus forms coherently on the substrate, where

$$\delta=\frac{(a_0)\text{ substrate}-(a_0)\text{ nucleus}}{(a_0)\text{ nucleus}},$$

a_0 being the lattice parameter. When the nucleus forms incoherently, the relationship is not parabolic but linear. These conclusions have not yet been tested by systematic experiments.

DERIVATION OF THE RATE EQUATION

The kinetics of nucleation of metal crystals on the substrate may be analyzed on the assumption that every atom from the atomic beam that strikes the substrate surface is, temporarily at least, adsorbed there. This assumption is believed to be correct for the usual source and target temperatures.[1]§ It means that no incident atoms are reflected from the surface by semielastic collision. All incident atoms are adsorbed and come to thermal equilibrium with the substrate surface. These adsorbed atoms may then diffuse at random over the surface until they join a growing subcritical embryo or leave the surface by evaporation. The equilibrium concentration of nuclei of critical size (comprised of i^* atoms) is given by[4–15]

$$n(i^*)=n(1)\exp(-\Delta F^*/kT), \tag{1}$$

where $n(1)$=equilibrium concentration of adsorbed single atoms, number/cm^2, and is much larger than $n(i^*)$, ΔF^*=standard free energy of formation of the critical nuclei, k=Boltzmann's constant, and T=absolute temperature of substrate.

$n(1)$ is determined, in accordance with the usually unknown adsorption characteristics of the particular system, by the equivalent partial pressure of the metal atoms at the surface. The equivalent partial pressure depends on the rate at which atoms from the beam strike the substrate surface. The rate of collision is given by[1]

$$p_0/(2\pi mkT_0)^{\frac{1}{2}}\times f_0/\pi l^2 \tag{2}$$

where p_0=the vapor pressure of the pure metal at source temperature T_0, m=mass of metal atom, f_0=area of the effusion orifice, and l=distance between orifice and target (substrate). Thus the equivalent partial pressure of metal vapor giving the same collision rate at substrate temperature T is

$$p'=p_0f_0/\pi l^2\times(T/T_0)^{\frac{1}{2}}. \tag{3}$$

Equating the rate of arrival of atoms to the substrate surface to the rate of evaporation:

$$n(1)=p'/\nu(2\pi mkT)^{\frac{1}{2}}\cdot\exp(-\Delta F_{ad}^0/kT), \tag{4}$$

where ν=vibration frequency of substrate surface atoms, about 10^{13} sec^{-1}, and ΔF_{ad}^0=the standard free energy of adsorption per atom ($-$).

In order to arrive at an expression for ΔF^*, one must assume that ordinary thermodynamic concepts can be applied to small aggregates of the order of magnitude of 10 atoms.[3] This assumption does not as yet have a firm basis but must be used for want of a better approach.[4–15,17]‖ Also, the shape of the critical nucleus cannot be calculated from the Gibbs-Wulff theorem,[12] because the required interfacial free energies are not known. Accordingly, it would appear expedient to follow Volmer[18] and Hollomon and Turnbull[4] in assuming a spherical-cap nucleus shape. The formula for the free energy of formation then becomes:

$$\Delta F^*=16\pi\gamma^3f(\theta)/3\Delta F_v^2, \tag{5}$$

where γ=free energy/unit area of crystal-vapor interface, $f(\theta)$=a function of crystal-substrate contact angle θ (in general, θ is not known), and ΔF_v=free energy change accompanying the transformation/unit volume of crystal$=(-RT/V)\ln p'/p$, p being the equilibrium vapor pressure of the bulk metal at substrate temperature T and V the molar volume.

This equation for ΔF^* has received some substantiation through kinetic studies of solidification of liquid metals. It described the data of Pound and LaMer[19] on supercooled tin droplets, and the data of Turnbull[20] for various mercury dispersions.

Subject to the usual equilibrium assumption in physico-chemical rate theory, the nucleation frequency

[16] D. Turnbull and B. Vonnegut, Ind. Eng. Chem. **44**, 1292 (1952).

§ The mean translational kinetic energy ($3kT_0/2$) of the atoms in the atomic beam is probably small relative to the standard free energy of adsorption under the usual experimental conditions.

[17] F. P. Buff, J. Chem. Phys. **19**, 1591 (1951).

‖ It would be highly desirable to evaluate ΔF^* by a method that does not assume macroscopic thermodynamic concepts, e.g., the treatment by J. E. Lenard-Jones, Proc. Phys. Soc. (London) **49**, 140 (1937), and E. T. S. Appleyard, Proc. Phys. Soc. (London) **49**, 118 (1937), for estimating the free energies of clusters on surfaces. However, such methods are not yet sufficiently developed for quantitative comparison with critical supersaturation data.

[18] M. Volmer, Z. Elektrochem. **35**, 555 (1929).

[19] G. M. Pound and V. K. La Mer, J. Am. Chem. Soc. **74**, 2323 (1952).

[20] D. Turnbull, J. Chem. Phys. **20**, 411 (1952).

per unit area of substrate is simply related to the equilibrium concentration of critical nuclei $n(i^*)$ by

$$I=\mu n(i^*) \tag{6}$$

where μ is the rate at which adsorbed metal atoms join the critical nuclei, thus allowing them to grow to macroscopic dimensions. In the present case, μ equals the circumference[11] of the critical sphere segment of radius r^* intersected by the substrate surface times the frequency c per unit length with which atoms diffusing on the surface impinge on the circumference: $\mu=2\pi r^* c$. Eliminating r^* by means of the Gibbs-Thompson formula,

$$\mu=(-4\pi\gamma \sin\theta/\Delta F_v)c. \tag{7}$$

Assuming that the metastable limit has not been transgressed, i.e., that the nucleation rate is not rapid, and that the adsorbed atoms occupy only a small fraction of the sites available on the surface, c may be evaluated in terms of elementary random-walk considerations. Imagine two parallel straight lines of unit length and separation a_0 (the lattice parameter) drawn on the substrate surface. The population of adsorbed atoms between the lines is $n(1)a_0$, and the frequency J with which these atoms jump to another site on the surface, is

$$J=\nu' \exp(-\Delta F_D^*/kT), \tag{8}$$

where ν' is the vibrational frequency of adsorbed atoms, and ΔF_D^* is the free energy of activation for surface diffusion. The probability that an atom will jump in a direction such that it will cross a specified line is $\frac{1}{4}$, to a first and perhaps sufficient approximation.[21] Accordingly,

$$c=(n(1)a_0/4)\nu' \exp(-\Delta F_D^*/kT), \tag{9}$$

and from Eq. (7),

$$\mu=(-\pi\gamma \sin\theta n(1)a_0\nu'/\Delta F_v) \exp(-\Delta F_D^*/kT). \tag{10}$$

Actually, this expression for μ should include a condensation coefficient α, which refers to the fraction of impinging atoms that become attached to the embryo, but α is usually taken to be unity.[4] Thus from Eqs. (6), (10), (1), and (4), the nucleation frequency I becomes

$$I=(\gamma \sin\theta a_0/2mk\nu)(p'^2/-\Delta F_v T) \times\exp[-(2\Delta F_{ad}^0+\Delta F_D^*+\Delta F^*)/kT], \tag{11}$$

if it is assumed that $\nu'=\nu$.[12] The Zeldovich factor,[7] which takes into account possible dissociation of atoms from the embryos and nonequilibrium concentration of critical nuclei, is omitted here because it assumes values not appreciably different from unity in cases where it has been evaluated.[4,14]

[21] Taylor and I. Langmuir, Phys. Rev. 44, 423 (1933).

COMPARISON OF THE SURFACE DIFFUSION MECHANISM WITH A MECHANISM INVOLVING DIRECT ADDITION FROM THE VAPOR

It can be readily shown[4,11] that a mechanism requiring direct addition of an atom from the vapor to the critical nucleus leads to the expression

$$I=\pi r^{*2}[p'/(2\pi mkT)^{\frac{1}{2}}]n(1) \exp(-\Delta F^*/kT). \tag{12}$$

Eliminating $n(1)$ by Eq. (4), this becomes

$$I=(\pi r^{*2}/\nu)(p'^2/2\pi mkT) \times\exp[-(\Delta F_{ad}^0+\Delta F^*)/kT]. \tag{13}$$

Rearranging Eq. (11), which represents the surface diffusion mechanism, with the help of the Gibbs-Thomson formula:

$$I=(\pi r^* a_0/2\nu)[p'/(2\pi mkT)^{\frac{1}{2}}]^2 \times\exp[-(2\Delta F_{ad}^0+\Delta F_D^*+\Delta F^*)/kT]. \tag{14}$$

Inasmuch as r^* and a_0 are approximately equal,[3,4] the coefficients of Eqs. (13) and (14), are of the same order of magnitude. However, the nucleation frequency given by Eq. (14) is greater by a factor $\exp[-(\Delta F_{2d}^0+\Delta F_D^*)/kT]$. ΔF_{ad}^0 is negative as defined here, and ΔF_D^* is characteristically positive. Also, it is generally considered[12] that $\Delta F_D^*<|\Delta F_{ad}^0/2|$. Thus for a typical value[3] of $\Delta F_{ad}^0(=\frac{1}{5}$ the heat of sublimation $=5000$. cal/g-atom) and a substrate temperature of 200°K, the surface diffusion mechanism leads to a rate that is higher by a factor of 10^2 to 10^3. This comparison does not consider the effect of atoms from a thermal beam which have a higher mean translational kinetic energy than ordinary vapor atoms whose energy corresponds to the substrate temperature T. Such atoms from a thermal beam would be expected to have a more disruptive effect in direct impingement on the embryos than ordinary vapor atoms. This would result in a lower condensation coefficient for the case of direct addition from the vapor and would tend to favor the surface diffusion mechanism in atomic beam experiments.

COMPARISON OF THEORY WITH EXPERIMENT

p', the equivalent partial pressure of metal vapor, is the only quantity in the coefficient of Eq. (11) that is subject to appreciable change within the scope of normal experimental conditions. Substituting reasonable numerical values (Table I) for the other quantities in the coefficient and assuming $\Delta F_D^* \ll |2\Delta F_{ad}^0|$ or ΔF^*, one gets

$$I=6\times10^7 p'^2 \exp[-(2\Delta F_{ad}^0+\Delta F^*)/kT], \tag{15}$$

TABLE I. List of numerical values used to evaluate the kinetic coefficient in Eq. (11).

a_0	4×10^{-8} cm
$\gamma/\Delta F_v$	3×10^{-8} cm
$\sin\theta$	1
m	$23/6\times10^{23}$ gm
ν	10^{13} sec^{-1}
T	200°K

TABLE II. Values of γ, θ, and $\Delta F_{ad}{}^0$ obtained from correlation of the critical supersaturation data in terms of Eq. (16).

	γ[a] ergs/cm²	θ, degrees	$-\Delta F_{ad}{}^0$ cal/gm-At
Sodium deposition on metals	350	101	5750
Sodium deposition on CsCl	350	81	4220
Cadmium deposition on copper	760	99	10 300

[a] γ is independently calculated, see reference 3, using Turnbull's relationship between the gram atomic interfacial energy and the gram atomic heat of fusion in conjunction with data on the surface tension of the liquid metals and Neumann's formula.

where p' is expressed in dynes/cm². Because of the strong dependence of I on $\Delta F_v = (-RT/V)lnp'/p$, as indicated by Eqs. (5) and (11), it is permissible to define the critical supersaturation as the ratio of p'/p required to make $I=1$ cm^{-2} sec^{-1} or $lnI=0$.[22,6] Rearranging Eq. (15) to describe the conditions for critical supersaturation,

$$(1/\Delta F_v{}^*)^2 = 2kT(9+lnp')/B\phi(\theta) - 2\Delta F_{ad}{}^0/B\phi(\theta), \quad (16)$$

where $\Delta F_v{}^* = (-RT/V)ln(p'/p)_{crit}$, and $B=16\pi\gamma^3/3$. This equation should provide a satisfactory description of the temperature dependence of $\Delta F_v{}^*$.

Figures 1 and 2 show the correlation of critical supersaturation data as a function of temperature in terms of Eq. (16). It is seen that reasonably linear plots are obtained. $B\phi(\theta)$ may be evaluated from the slopes, and $\Delta F_{ad}{}^0$ may be computed from the intercepts. From Table II it is seen that the data are fitted by reasonable values of γ, θ, and $\Delta F_{ad}{}^0$. The data of Figs. 1 and 2 are discussed in greater detail in reference 3.

Although Eq. (16) describes the data very well, this agreement does not constitute experimental proof of the surface diffusion mechanism. Equation (13) for the direct impingement mechanism could be adapted to fit the data equally well. However, it was important to decide (by theoretical means as done in the preceding section) on the actual mechanism in order to know whether to interpret the intercepts of the plots as $\Delta F_{ad}{}^0/B\phi(\theta)$ or $2\Delta F_{ad}{}^0/B\phi(\theta)$.

The mathematical treatment presented in this paper assumes uniform substrate surfaces. However, it is thought that preferred sites for nucleation, such as dislocations, cracks, impurity particles, etc., would not detract appreciably from the usefulness of Eq. (16). Consider that the presence of preferred sites would merely reduce the kinetic coefficient and the free energy of activation ΔF^*. The kinetic coefficient would be proportional to the fraction of surface area covered by the preferred sites. If only 10^{-8} of the total substrate surface is responsible for the nucleation, the quantity

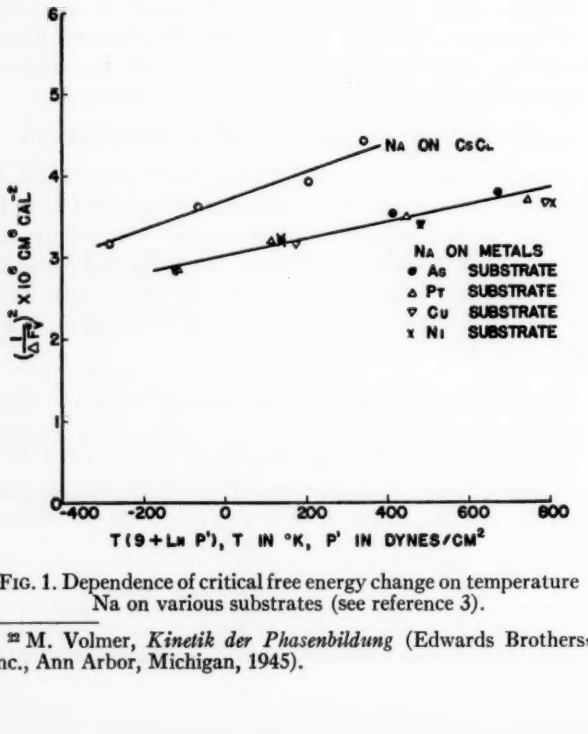

FIG. 1. Dependence of critical free energy change on temperature Na on various substrates (see reference 3).

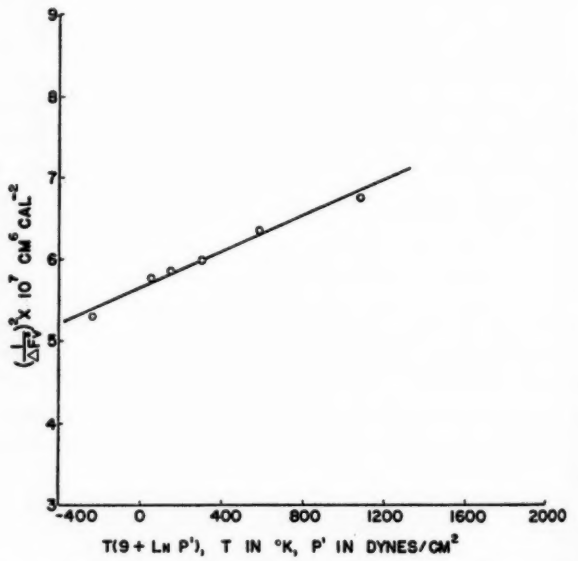

FIG. 2. Dependence of critical free energy change on temperature. Cd on Cu (data of Cockcroft) (see reference 2).

$(9+lnp')$ in Eq. (16) would reduce to (lnp'). However, the present data are not linearly fitted by a plot of $(1/\Delta F_v{}^*)^2$ *vs* $Tlnp'$. Accordingly, one would conclude that the nucleation is not caused by a few active centers, but is random over a large fraction of the substrate surface. This is consistent with the hypothesis[3] that the substrate surfaces are coated with films of absorbed gas in the case of the present data.

NOMENCLATURE

ΔF^* = standard free energy of formation of a critical nucleus. (+)

$\Delta F_{ad}{}^0$ = standard free energy of adsorption per atom. (−)

ΔF_v = bulk free energy change accompanying the transformation per unit volume of condensed phase. (−)

[22] M. Volmer, *Kinetik der Phasenbildung* (Edwards Brothers, Inc., Ann Arbor, Michigan, 1945).

ΔF_v^* = bulk free energy change per unit volume needed for a nucleation frequency of $1/cm^2/sec$. $(-)$

ΔF_D^* = free energy of activation for surface diffusion. $(+)$

θ = crystal-substrate contact angle.

$\phi(\theta) = (2+\cos\theta)(1-\cos\theta)^2/4$.

γ = free energy per unit area of crystal-vapor interface.

$B = 16\pi\gamma^3/3$.

p' = equivalent partial pressure of vapor giving the same collision rate at substrate temperature T (Eq. 3).

ACKNOWLEDGMENT

The authors would like to express their sincere thanks to Dr. Robert F. Mehl for many helpful discussions.

THE JOURNAL OF CHEMICAL PHYSICS VOLUME 22, NUMBER 7 JULY, 1954

Studies of Ionization Efficiency. Part IV. The Electron Spectra of Some Simple Molecules

J. D. MORRISON

Chemical Physics Section, Division of Industrial Chemistry, Commonwealth Scientific and Industrial Research Organization, Melbourne, Australia

(Received November 3, 1953)

The second differential ionization efficiency curves for a number of simple molecule-ions have been recorded using a new technique of measurement. A close correlation can be drawn between the results and spectroscopic data, confirming in most respects the interpretation of ionization efficiencies made in Part III. It proves possible to detect the presence of upper ionic states at energies corresponding to extreme ultraviolet radiation. The factors which affect line shape in optical spectra are shown to apply also to the second differential ionization efficiency curves, which are termed electron spectra. It is shown that the ionization efficiency curves for fragment ions can also be interpreted in a similar manner, and the types of electron spectra to be expected for different kinds of dissociation processes are discussed.

INTRODUCTION

IN Part III of this series[1] it was demonstrated that if the energy spread in the ionizing electron beam were removed, the probability of ionization to one electronic level of a singly charged rare gas ion was a linear function of the excess electron energy for a few volts above the excitation threshold, at least within the limit of the experimental error. This has been found also by Fox and co-workers[2] using an entirely different experimental approach.

Taken over the whole range of ionizing electron energies, the ionization probability for normal transitions to a single level is some function of the energy such that its second differential has a low value except at the ionization potential. An actual ionization efficiency is made up by the linear superposition of the ionization probabilities for each electronic state of the ion. If these probabilities are all of the same form, the second differential of the ionization efficiency will consist of a set of peaks at the energy states of the ion. This was found to be the case for the two lowest electronic states in the rare gases Ne, A, Kr, and Xe, and seemed to apply also for a few polyatomic molecules which were examined.

The method used to produce the differential ionization efficiency curves on which this interpretation was based, was unsatisfactory in that the scatter in the values increased rapidly with energy above the ionization threshold, and the detection of structural details with certainty was made difficult. In the present work, a new technique of measurement has been employed which enables the second differential ionization efficiency curves to be produced directly, with a much greater accuracy than was previously possible. In the method used formerly, the mass spectrometer system was adjusted to collect ions of the desired mass, and the ion current recorded at each value of the ionizing electron energy gave the relative ionization efficiency at that energy. In the new method, a sine wave signal of small amplitude ΔV and frequency f is superposed on the steady value of the ionizing electron voltage V. An ion current detecting system is used which responds only to ac of frequency $2f$, and which is phase-sensitive. This detector gives an output which is proportional to the second differential of the ionization efficiency at electron energy V, and in which the instrumental noise has been largely removed, leaving only the statistical noise due to the discrete nature of the ion current. By varying V at a rate slow compared with f, the second differential ionization efficiency curve is traced out. In order that there should be obtained a reasonably close approximation to the true derivative, ΔV should be small. When this is so, the statistical noise in the ion currents recorded makes it necessary to use corre-

[1] J. D. Morrison. J. Chem. Phys. **21**, 1767 (1953).
[2] Fox, Hickam, and Kjeldaas, Phys. Rev. **89**, 555 (1953).

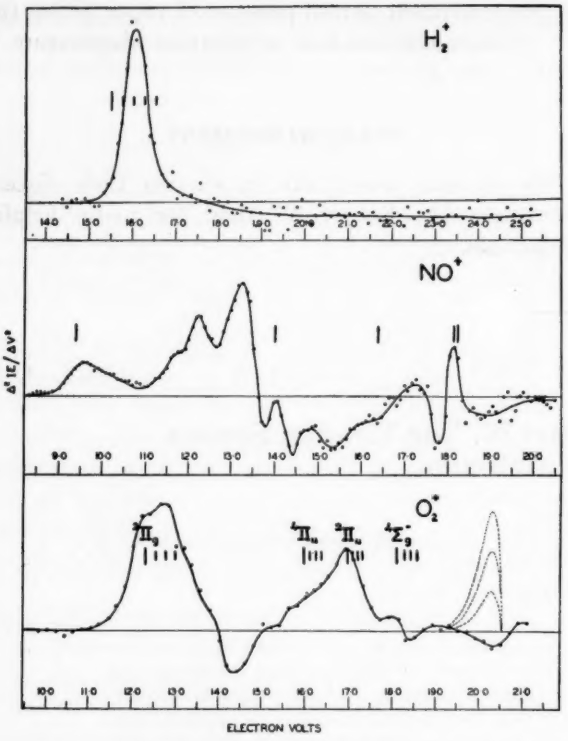

FIG. 1. Second differential ionization efficiency curves for H_2^+, NO^+, and O_2^+. $\Delta V = 0.1$ v rms. The presence of electronic states and vibrational levels are shown by long and short lines, respectively. Reversed Maxwellian distributions for 2500°K of different amplitudes are superposed on the figure for comparison with the observed peaks. The energy scale for H_2^+ cannot be calibrated accurately, so that the position of the energy levels on the curve is uncertain. From the relative positions of the potential curves for H_2 and H_2^+ it is to be expected that the most probable transitions occur to the vibrational levels $v' = 2, 3, 4$.

lation in order to improve the signal-to-noise ratio. The ac outputs corresponding to the second differential are rectified, and sampled every $\frac{1}{3}$ second. A section of an ionization efficiency curve is scanned every 20 seconds, and the recorded totals are correlated arithmetically. A more complete description of this technique and apparatus is published elsewhere.[4]

A difficulty which still remains is due to the fact that the electron beam used to produce the ionization is not monoenergetic, but is found to possess an energy distribution which is very close to Maxwellian. The effect of this energy distribution on the second differential ionization efficiency curves is to spread out the peaks into distributions similar to that of the electron beam, but reversed on the energy scale. A lower limit is set therefore in practice to the resolution of structure at about 0.2–0.3 ev, which places a serious restriction on the accurate study of the ionization efficiencies of polyatomic molecules, where the energy levels are much more closely spaced than in the rare gases. Nevertheless, there is a sufficient correlation between the mass spectrometric results and spectroscopic data to show that the interpretation of ionization efficiencies made in the previous paper is substantially correct.

[4] J. D. Morrison, J. Chem. Phys. **21**, 1767 (1953); Rev. Sci. Instr. (to be published).

EXAMINATION OF RESULTS

The mass spectra of the substances for study were used as a criterion of their degree of purity. In all cases except H_2 and He, krypton was introduced with the sample gas and its second differential ionization efficiency curve measured immediately after that of the sample.* The energy scale was then adjusted to bring the maximum of the krypton $^2P_{\frac{3}{2}}$ peak to 14.02 ev. The amount of the adjustment varied between 1.30 and 1.50 ev for most of the gases measured. The error in the absolute voltage scale is estimated to be ± 0.1 ev.

For helium, the second energy level lies 40.8 ev above the lowest ionic state, after which a series of levels tend to the second ionization potential at 78.98 ev.[5] The other rare gases are similar, in that the two lowest $^2P_{\frac{3}{2}}$ and $^2P_{\frac{1}{2}}$ states of the ions are separated from the next levels by at least 10 ev. In all cases, the second differential ionization efficiency curves consist of a large single or double peak at the lowest energy states of the ions, and no indication is found of any peaks at the higher energy states. If peaks are present at these states, their heights must be less than 10 percent of the peak at the lowest ionized state.

For the other molecules examined, a more satisfactory correlation can be obtained. In Fig. 1 are shown the curves for H_2^+, NO^+, and O_2^+. The H_2^+ curve is very similar to those for the monatomic gases. For oxygen four known energy states of the molecule ion are superposed on the figure; each is associated with a peak in the curve. The curve for NO^+ shows more detail than any other. No spectroscopic data on the electronic states of the ion are available, but the limits of four Rydberg series are shown, which also can be related to peaks in the curve. There are several other peaks present, for which no energy states are known.

It may be noted that the peaks in the second differential ionization efficiency curves are much broader than the reversed Maxwellian distribution which would be expected for a single level, if the assumptions made previously were correct. One explanation would be that the ionization probabilities for these processes do not increase linearly. If, however, the vibrational levels for each electronic state are superposed on the O_2^+ curve, and if it is assumed that transitions to each one of these levels gives rise to a reversed Maxwellian peak, then the observed shape of the second differential is accounted for.

The curves for N_2^+ and CO_2^+ are shown in Fig. 2, in which known states of these molecular ions are superposed on the curves. In neither of these cases is the agreement quite so good, although a peak is always

* The mass spectrometer used in this work was a somewhat modified Consolidated Engineering Corporation Model 21.102.

[5] C. E. Moore, Atomic energy levels, Natl. Bur. Standards Circ. (U. S.) **1** (1949).

found at 0.5–1.0 ev above a known level. This may be attributed to the difference in equilibrium interatomic spacings between the ground state of the neutral molecules and the various states of the ions (although the difference in the case of N_2^+ seems rather large). The lowest electronic state of CO_2^+ would appear to contain an extended series of vibrational levels due to this cause.

In Fig. 3 are given the curves for $C_2H_2^+$ and $C_6H_6^+$. In acetylene, there are three maxima which can probably be associated with electronic states, although only the first has been observed spectroscopically. For benzene, two ionized states are known, which are associated with peaks in the curve. The peak at the lowest ionized state has a double maximum, which may be due to a second state 0.5 ev above the lowest. This may be the explanation for the fact that the ionization potentials of benzenoid molecules measured by ordinary electron impact methods are consistently higher than the spectroscopic figures.[6] Other peaks are present at higher energies.

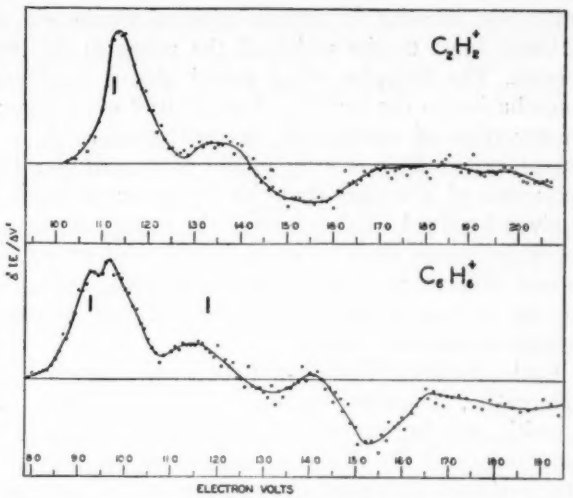

FIG. 3. Second differential ionization efficiency curves for acetylene and benzene, showing the presence of upper states. $\Delta V = 0.1$ v rms.

LINE BREADTHS AND ELECTRON SPECTRA

Sufficient evidence on ionization probabilities has now been accumulated to justify a more detailed consideration of the factors on which the probability function depends. All of the experimental data is consistent with the view that the ionization probability for the production of an ion in a single discrete energy level is very close to a linear function of the excess energy above the threshold, for a range of a few volts at least. As measured at present, the second differential ionization probability curve consists of a positive peak of the same width and shape as the electron energy distribution, followed by a broad shallow negative region extending over a range of from 10 to 30 ev above the ionization potential. The width of this region becomes less, the more complex the molecule-ion. At energies above this negative region, the curves become very slightly positive again, then fall asymptotically towards zero at very high electron energies. The effects of the distribution of ionizing electron energies, and the amplitude of the ionizing electron voltage wave form which is used to produce the second differential ionization probability curve, may be considered together as analogous to that of slit widths in conventional spectroscopy. As the energy spread in the electron beam is reduced, for a constant beam current, the positive peak in the second differential ionization probability curve will increase in height and decrease in width so that the area beneath the peak remains constant. Provided that the wave form used to produce the differential is greater in amplitude than the width of the electron energy distribution curve in volts, decreasing it will increase the height of the positive peak with respect to the following broad negative and positive regions.[7] As both are decreased, the second differential ionization probability curve will become more and more closely similar to a line in optical spectroscopy. Hence, for convenience, the second differential ionization efficiency curve will be referred to as an electron spectrum. If the ionization probability were perfectly linear, the peak in the spectrum would tend towards a δ function.

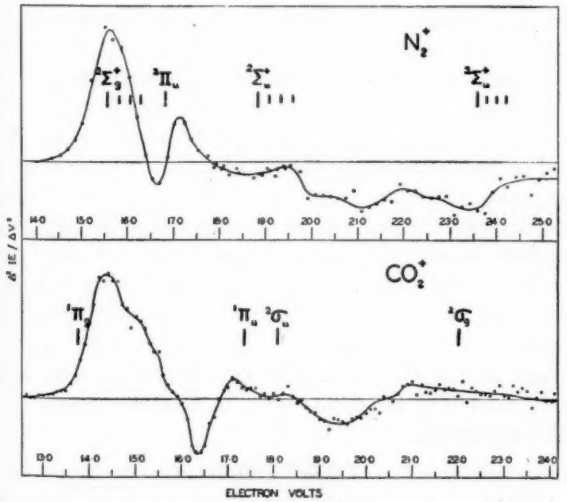

FIG. 2. Second differential ionization efficiency curves for N_2^+ and CO_2^+. $\Delta V = 0.1$ v rms. Known electronic states are superposed on the figure.

Although, in practice, the electron energy spread (half-width 0.3 ev) is at present by far the dominant factor in determining line breadth, even if this were removed, the same factors which operate to cause

[6] J. D. Morrison and A. J. C. Nicholson, J. Chem. Phys. **20**, 1021 (1952).

[7] The effect of a finite differential is discussed by B. van der Pol and H. Bremmer, *Operational Calculus* (Cambridge University Press, Cambridge, 1950), p. 293.

finite line breadth in optical spectra would set an ultimate limit to the width of the peaks in electron spectra. The Doppler effect would give a maximum contribution to the breadth of about 0.02 ev, although conservation of momentum in electron-molecule collisions may reduce this by orders of magnitude. The deduction of Wannier[8] that the ionization probability is given by the 1.127th power of the energy above the threshold would seem to have the effect of giving the second differential "line" a finite breadth, analogous to the natural radiation line breadth, but of much greater magnitude (~0.02 ev).

Each of these effects, electron energy spread, finite differential, Doppler broadening, and natural line breadth, can be represented by probability sampling functions, and the observed differential peak can be obtained from their product integrated over all energies. The area under the peak corresponding to a given transition will be proportional to the square of the matrix component for that transition between the neutral ground state and the ionized level. Transitions to ionized states can be assumed to be vertical, so that the relative probabilities of excitation of the various vibrational levels will be determined in each case by the positions of the potential curves for the states involved. Where the Franck-Condon region intersects repulsive potential curves, the electron spectrum of the fragment ion would consist of diffuse maxima, each produced by the reflection of the ground-state probability function in the curve of an upper state.

THE ELECTRON SPECTRA OF FRAGMENT IONS

Since it has proved possible to obtain the electron spectrum of molecule ions in the manner described above, an attempt can be made to interpret the electron spectra of fragment ions similarly. To a rough approximation, the levels of the spectrum of a fragment ion will be displaced along the energy axis by an amount equal to the dissociation energy of the bond broken, and there will be present, in addition, levels corresponding to transitions where the other fragment formed in the dissociation is in excited states.

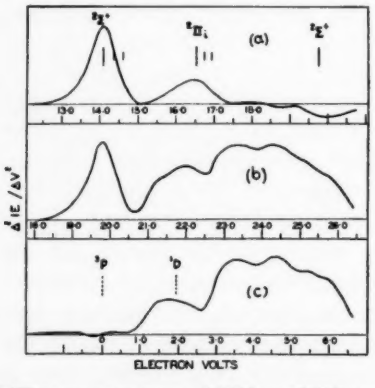

FIG. 4. (a) Electron spectrum of CO^+_{CO} with known electronic states superposed. (b) Electron spectrum of $CO^+_{CO_2}$. (c) Plot of the difference between the electron spectra for $CO^+_{CO_2}$ and CO^+_{CO}. The ^3P and ^1D states of the oxygen atom are shown.

The processes $NO_2 \rightarrow NO^+ + O + e$ and $CO_2 \rightarrow CO^+ + O + e$ were chosen as being good subjects for a preliminary examination, as the spectra of NO^+ and CO^+ can be measured directly, and the fragment ions are abundant and easy to measure.

The curve for NO^+ from NO_2 is unusual, in that the electron spectrum agrees in every detail with that for NO^+ from NO. The amount of correction necessary for the energy scale differs for the two gases, and when this is taken into account the curves appear to lie at the same position on the energy scale. The only explanation would seem to be that the NO_2 is very largely dissociated into NO and O before the electron impact and that the ionization efficiency of NO^+_{NO} is much greater than that for $NO^+_{NO_2}$.† This requires further examination.[9]

The curves for CO^+_{CO} and $CO^+_{CO_2}$ are shown in (a) and (b) of Fig. 4. The agreement between the CO^+_{CO} curve and the two known lowest states of the ion is good, but there is no sign of the third state. Vibrational levels may be present in both states, but are not resolved. In the $CO^+_{CO_2}$ curve the first large peak lies at 5.6 ev above the similar one in CO^+_{CO} and presumably corresponds to the production of CO^+ and O in their lowest $^2\Sigma^+$ and ^3P states, respectively. This is in agreement with a figure of 5.5 v quoted elsewhere.[9] The heights of the CO^+_{CO} and $CO^+_{CO_2}$ curves and their position on the energy scale were now adjusted to make the first peaks coincide, and the difference between the curves was plotted in (c). The first peak is entirely removed, and the first maximum in this curve lies at about 1.9 v higher on the energy scale. This will correspond to the production of CO^+ in its lowest $^2\Sigma^+$ state and O in its $'D$ state which is 1.96 ev above the ^3P state. At higher energies a broad maximum occurs in the curve. As might be expected, this simple subtractive approach breaks down when any attempt is made to carry it further, as the potential curves for higher ionized states will be displaced relative to the ground state of the neutral molecule, and the broad peak remaining at higher energies may be due to the intersection of the Franck-Condon region with a steeply rising upper state potential energy curve. In fact, it is surprising that the formation of CO^+ and O in their lowest states is apparently unaccompanied by appreciable kinetic energy of the products. The electron spectra of fragment ions will be dealt with in greater detail in a following paper.

CONCLUSION

The idea of competition between entirely different ionization processes, and between processes of excita-

[8] G. H. Wannier, Phys. Rev. 9, 817 (1953).

† The parent peak for NO_2 was found to be about 35 percent of the peak at mass 30.

[9] See E. C. G. Stueckelberg and H. D. Smyth, Phys. Rev. 36, 478 (1930).

tion and ionization, which was earlier postulated to account for the presence of certain sharp negative peaks in the electron spectra of ions such as Hg^+ and A^+, may require modification. At present it is difficult to decide whether a particular negative region in a curve is a negative peak, as suggested earlier, or the trough between two positive peaks. If the idea of competition were carried to its logical conclusion, the various electronic states of a single ion could compete with each other in a similar fashion. This would mean that each positive peak in the spectrum would be simultaneously accompanied by a negative peak, with the net result that all the peaks above the first would appear to be less than their true value. The possibility must be considered that there are processes of ionization where the probability is other than a linear function of the energy above the threshold. The X-type peaks referred to by Bates *et al.*[10] may afford one such example. Autoionization may be expected to occur in some cases[11] and the probability of ionization due to this process will presumably be proportional to the probability of excitation of the neutral level from which the autoionization takes place.

These processes should give rise to additional peaks in the second differential curves, and with the present low resolution be confused with the normal peaks in the spectrum. This may account for some of the discrepancies between the electron spectra and the spectroscopic term schemes.

These matters should be clarified if an electron beam with a smaller velocity spread can be obtained. The results obtained to date are interesting, and if extended may perhaps prove of value to ionosphere physics in that conditions in the spectrometer ion chamber are very similar to those in the upper atmosphere. If the resolution of the method can be increased, the measurement of the electron spectra of fragment ions should provide an excellent method for the determination of bond dissociation energies. Detailed information on the potential energy surfaces for upper states should be forthcoming, in an energy region which is inaccessible by other methods.

[10] Bates, Fundaminsky, Leech, and Massey, Trans. Roy. Soc. (London) **A243**, 127 (1950–51).

[11] G. Herzberg, *Spectra of Diatomic Molecules* (D. Van Nostrand and Company, Inc., New York, 1952), second edition, p. 414. Fox, Hickam, and Kjeldaas Jr., Phys. Rev. **89**, 555 (1953).

THE JOURNAL OF CHEMICAL PHYSICS VOLUME 22, NUMBER 7 JULY, 1954

The Effect of Ring Substituents on the Isotope Effects in Reactions of Carbonyl-C^{14} Esters and Ketones*

GUS A. ROPP AND VERNON F. RAAEN
Chemistry Division, Oak Ridge National Laboratory, Oak Ridge, Tennessee

(Received July 20, 1953)

The variations of the isotope fractionation factor k_{14}/k_{12} with changes in ring substituents, reaction temperature, solvent, concentration, and the alcohol group have been studied for the saponification of ethyl benzoates (α-carbon-14). The variations of the k_{14}/k_{12} ratio with changes in temperature and ring substituents have been studied for the formation of the 2,4-dinitrophenylhydrazones of acetophenones (α-carbon-14).

I. INTRODUCTION

In a recent communication[1] some isotope effect ratios were reported for the saponification at 25° of a series of ethyl benzoates labeled with carbon-14 in the carbethoxy group:

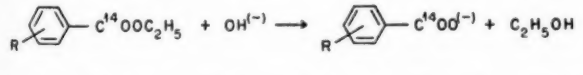

($R = p-OCH_3, p-Cl, p-CH_3, H, m-Cl$, and $m-NO_2$).

The details of this study which has now been considerably extended are presented here. A second series of reactions, the formation of the 2,4-dinitrophenylhydrazones of α-carbon-14 acetophenones:

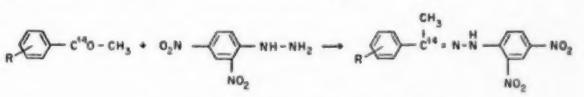

($R = p-OCH_3$, H, $m-NO_2$)

has been included. The previously noted effect of the ring substituents on the k_{14}/k_{12} ratio in the ester series appears to be borne out in the series of three labeled ketone reactions. In addition the effect on k_{14}/k_{12} of temperature changes, solvent changes, concentration changes, and changes in the carbethoxy group of an ester have been evaluated in one or both reaction series. Attempts have been made to explain the results obtained making use of current theory of the isotope effect.[2]

* This document is based upon work performed under Contract No. W-7405-eng-26 for the U. S. Atomic Energy Commission at the Oak Ridge National Laboratory.

[1] G. A. Ropp and V. F. Raaen, J. Chem. Phys. **20**, 1823 (1952).

[2] J. Bigeleisen, J. Chem. Phys. **17**, 675 (1949).

II. THE ISOTOPE EFFECTS IN THE SAPONIFICATION OF ETHYL BENZOATES (α-CARBON-14)

A. Method of Measuring the Isotope Effects

The general method of measuring the carbon isotope effects in these saponifications has been discussed earlier.[1,3] The method was believed to be the simplest available method which would permit rapid and precise determination of k_{14}/k_{12} ratios. It involved determining S_3 and S_{100}, the specific activities, respectively, of the acid produced by 3 percent and 100 percent saponification of a given sample of a carboxyl-labeled ester. Then k_{14}/k_{12} was calculated in each case as S_3/S_{100}. The method was believed to be particularly well suited to determining the effect of changing the reaction conditions on the isotope effect for a given ester as the following relation holds in which the errors in S_{100} cancel:

$$\frac{(k_{14}/k_{12})\text{ condition A}}{(k_{14}/k_{12})\text{ condition B}}=\frac{(S_3)\text{ A}}{(S_3)\text{ B}}.$$

It was necessary to make certain that all the carbon-14 labeled esters used in this study were chemically pure. The esters were very carefully tested for freedom from the corresponding organic acid, since traces of the acid, if present, could cause appreciable error in the value of S_3. Tests were also devised to prove that no isotopic exchange took place between any of the esters and the corresponding free acids under the conditions used for the ester saponifications. As a further check on the validity of the S_3 values, the specific activity, S_6, of the acid obtained by 6 percent saponification of an ester was usually measured and compared with the corresponding S_3 value. Good agreement between S_3 and S_6 values was expected and usually found, although in theory the S_6 value should be slightly closer to S_{100} than should the S_3. It was recognized that in theory the true value of k_{14}/k_{12} should be given by S_0/S_{100}. However S_3 was taken as a practical and satisfactory approximation for S_0 from which it might differ by about 0.2 percent. Furthermore, any error caused by the approximation that $S_3=S_0$ would probably cancel in the present study, where the primary objective was to determine the relative values of several isotope effect ratios for different esters or for the same ester under different conditions. The radioassay methods and their precision have been discussed earlier.[3]

B. Isotope Effect Ratios at 25°C for Various Ring-Substituted Esters

In Table I are reported the S values in μc per mg and the values of S_3/S_{100}, (k_{14}/k_{12}) for six ethyl benzoates at 25°C. In the runs from which these data were obtained, 67 *mmo/S* of ester, 210 ml 90 percent ethyl alcohol, and sufficient sodium hydroxide to give the desired percent reaction were used.

[3] V. F. Raaen and G. A. Ropp, Anal. Chem. **25**, 174 (1953).

TABLE I. Isotope effect data for saponification of various esters at 25°C.

Substituent	S_3 μc/mg	S_6 μc/mg	S_{100} μc/mg	S_3/S_{100}	Mean S_3/S_{100}
$p-OCH_3$	0.01329	0.01332	0.01451	0.916	
	0.01293	0.01301	0.01413	0.915	0.916
$p-Cl$	0.00648	0.00649	0.00702	0.923	
	0.02099	0.02091	0.02266	0.927	
	0.01966	0.01957	0.02122	0.926	0.925
$p-CH_3$	0.01864	0.01861	0.02006	0.929	
	0.01903	0.01902	0.02054	0.926	
	0.01804	···	0.01944	0.928	0.928
None	0.02473	···	0.02664	0.928	
	0.00731	0.00730	0.00785	0.931	
	0.02432	···	0.02621	0.928	0.929
$m-Cl$	0.01120	0.01123	0.01201	0.933	
	0.01120	0.01117	0.01201	0.933	0.933
$m-NO_2$	0.01440	0.01447	0.01537	0.937	
	0.04466	0.04462	0.04765	0.937	0.937

C. Discussion of the Isotope Effect Data of Table I

Theoretically a correlation of these isotope effect data in terms of the Hammett equation[4] should be possible. Ingold and Nathan[5] have measured rate constants for the saponification of *para*-substituted ethyl benzoates which can be fitted to a Hammett-type plot. With the exception that ethyl *p*-nitrobenzoate has been replaced here by ethyl *m*-nitrobenzoate, the ring substituents employed in the present study of isotope effects were the same as those involved in the rate studies of Ingold and Nathan. Their rate studies were performed in 85 percent ethanol solution at 25°. It should be possible to write two Hammett equations which differ in the values of rho:

For the reaction of the series of unlabeled ester molecules, i.e.,

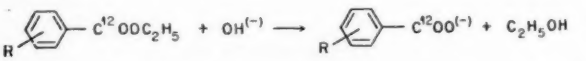

the Hammett equation is

$$\log[k_{12}/k_{12}^0]=\rho_{12}\sigma. \quad (1)$$

For the reaction of the series of labeled ester molecules, i.e.,

the Hammett equation is

$$\log[k_{14}/k_{14}^0]=\rho_{14}\sigma. \quad (2)$$

Since the C^{14} label is at the reaction center, different rho values must apply in Eqs. (1) and (2). The same

[4] L. P. Hammett, *Physical Organic Chemistry* (McGraw-Hill Book Company, Inc., New York, 1940), Chap. VII.

[5] Ingold and Nathan, Trans. Chem. Soc. **1936**, 222 (1936).

substituent constants should, of course, apply to both Eq. (1) and Eq. (2). Subtracting Eq. (1) from Eq. (2) and rearranging gives

$$\log[k_{14}/k_{12}]-\log[k_{14}^0/k_{12}^0]=(\rho_{14}-\rho_{12})\sigma. \quad (3)$$

If the terms with zero superscripts, which apply to the unsubstituted esters, are treated as constants, Eq. (3) becomes

$$\log[k_{14}/k_{12}]=(\rho_{14}-\rho_{12})\sigma+\text{Constant}. \quad (4)$$

Thus $\rho_{14}-\rho_{12}$, the difference between the reaction constants for saponification of the two isotopic species of esters at 25°C, should be given as the slope when $\log[k_{14}/k_{12}]$ is plotted against the substituent constant σ.

An attempt to correlate the ester saponification isotope fractionation ratios using Eq. (4) resulted in the points indicated by rings in the lower half of Fig. 1. Scattering of the points about the line is to be expected because of the limited precision with which the fractionation factors can be measured. Figure 1 does indicate that the plot of points in the ester series roughly parallels the plot in the ketone series which is discussed below.

Bigeleisen[6] has discussed the isotope fractionation in the saponification of ethyl benzoate-α-C^{14} with the view that the observed isotope effect is the product of two factors: (a) the effect of the isotope on an equilibrium, and (b) the effect of the isotope on the subsequent rate controlling step. However, his arguments are weakened by the fact that his predicted fractionation factor ($k_{12}/k_{14}=ca$ 1.15) is far greater than the actual factor reported here ($k_{12}/k_{14}=1.076$), although in agreement with the earlier value observed by Stevens and Attree.[7]

Following Bigeleisen[6] the effect of a nuclear substituent on the carbon isotope fractionation in the ethyl

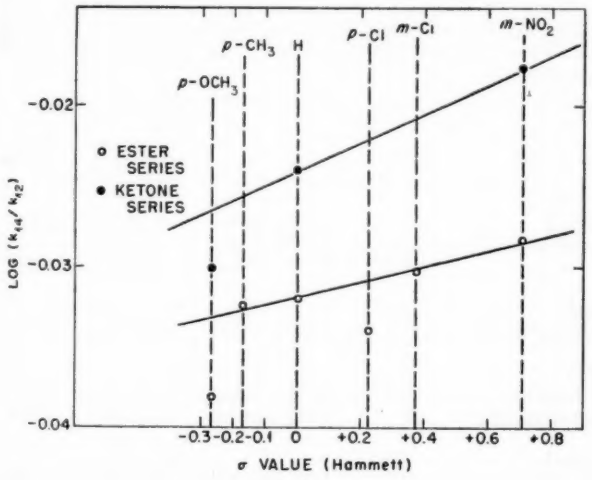

FIG. 1.

benzoate-α-C^{14} saponification could be considered as the resultant of the effects of the substituent (a) on isotope fractionation in an equilibrium process and (b) an isotope fractionation in the subsequent step. However, the authors prefer the following as a possible way of explaining qualitatively the variations in degree of isotope fractionation in this series of ester reactions.

The isotope effect ratios have been measured in the present work with enough precision to indicate that in the saponification of ethyl p-methoxy-benzoate-α-C^{14}, and to a lesser extent ethyl p-chlorobenzoate-α-C^{14}, greater carbon isotope fractionation occurs than in saponification of the other esters. As previously discussed[1] this may be due to the capacity of these two esters to partake of resonance forms with double bonds between the labeled carboxyl group and the aromatic ring:[8]

I 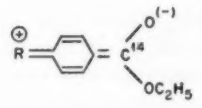

Several assumptions are made: (1) that the isotopic zero point energy levels of the unactivated ester molecule are the more widely separated the greater the contribution of structures like I; structures like I are assumed to involve tighter bonding of a carbon atom in the labeled position; (2) that a corresponding effect of the substituent on the separation of the isotopic levels in the activated state does not occur if the activated state is something like the following structure:

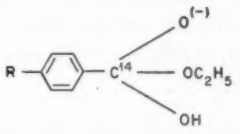

Then as a result of (1) and (2) the difference between the activation energies for the two isotopic species $E_{14}-E_{12}$ should be greatest for the saponification of those esters in which the ring substituent promotes the greatest contribution of structures like I.

As an extension of the foregoing picture, it seems possible that the apparent decrease in the degree of isotope fractionation in the direction—p−methyl>unsubstituted>m−chloro>m−nitro ester, may also be due to a decreasing tendency of these esters to partake of resonance structures with a double bond between the carboxyl group and the ring. In view of the limited precision in determining the values of these isotope effect ratios, some of the apparent differences between the ratios for different esters are too small to be accepted as real differences. Yet there seems to be little doubt that ethyl p-methoxy-benzoate-α-C^{14} shows the greatest isotope fractionation, that ethyl m-nitro-benzoate-α-C^{14} shows the least fractionation, and that the other esters lie between these limits. It seems possible that in the

[6] J. Bigeleisen, J. Chem. Phys. **56**, 823–31 (1952).

[7] (a) W. Stevens and R. Attree, Can. J. Chem. **B27**, 807 (1949). (b) In a communication to the present authors, W. H. Stevens expressed the belief that the k_{12}/k_{14} ratio reported in 1949 for the saponification of ethyl benzoate-α-C^{14} was high.

[8] A. E. Remick, *Electronic Interpretations of Organic Chemistry* (John Wiley and Sons, Inc., New York, 1949), second edition.

cases of the *meta*-substituted esters, structures such as

could make such large contributions to the normal state of the esters that structures of type I could become relatively unimportant. This might then explain the fact that these *meta*-substituted esters show the least carbon isotope fractionation in the saponification reaction.

An alternative explanation of the presently observed effect of ring substituents on the degree of carbon isotope fractionation might lie in the identity of the rate-controlling step.[9] The isotope effect on a reaction rate is usually considered to result largely from the effect of isotopic substitution on the rate of the rate controlling process. If, in the ester saponification, each of two steps were partially rate controlling and if the relative rate-controlling effect of each depended upon the ring substituent, then the observed dependency of the isotope effect on the substituent might result.

It is also of interest to note that in the series of ester saponifications studied, those reactions which were slowest generally showed the greatest degree of carbon isotope fractionation. This fact may possibly be related to a somewhat similar observation of Urry[10] with reactions of deuterium labeled compounds.

D. The Effect of Varying Reaction Conditions and the Alcohol Group on the Isotope Effect in Ethyl Benzoate-α-C^{14} Saponification

The data listed in Table II indicate an increase of the k_{14}/k_{12} ratio with decreasing reaction temperature which is in accord with theory.[2] This variation of isotope effect with temperature corresponds to a difference of approximately 46 calories per mole between the Arrhenius activation energies[11] for the reactions of the two isotopic species of ethyl benzoate. This value of ΔE seems reasonable since it results in a ratio of frequency factors A_{14}/A_{12} for the Arrhenius equations for the two isotopic species of essentially unity. The data of Table II also show little or no variation of the saponification isotope effect when the solvent is changed to 56 percent acetone or when the concentration of the ester in the solvent is increased fivefold. Apparently, therefore, the solvent has little effect on those vibrational frequencies of the bonds to the labeled carbon atom which are presumed to be of critical importance in isotope effect calculations. Table II does show that changing the alcohol group in ethyl benzoate-α-C^{14} from the ethyl group to the *t*-butyl group decreases the isotope effect in the saponification. Since the *t*-butyl ester saponifies far more slowly than the ethyl ester under identical conditions, the previously mentioned observation that those esters which saponified most slowly gave the greatest degree of isotope fractionation is not borne out in this case. Since the alcohol group in the ester is considerably closer to the labeled reaction center than any *meta* or *para* substituent, it is not surprising that changing to the *t*-butyl group alters the degree of isotope fractionation.

The facts that (a) basic hydrolysis of *t*-butyl benzoate-α-C^{14} is accompanied by isotope fractionation and (b) acid hydrolysis of this ester shows no isotope effect[7b] are in accord with the accepted ideas that the former involves cleavage between the oxygen and the carbonyl carbon while the latter involves cleavage between the oxygen and the alkyl group.[12] An isotope effect is usually to be expected when the bond to the labeled position is altered.

III. THE ISOTOPE EFFECTS IN THE ACID-CATALYZED FORMATION OF 2,4-DINITROPHENYLHYDRAZONES OF ACETOPHENONES (α-CARBON-14)

A. Method of Measuring the Isotope Effects

It was the purpose of the study of the isotope effects in the ring-substituted ketones to check further the effect of ring substituents on the degree of carbon isotope fractionation. A somewhat different method of measuring the isotope effects was employed in the ketone series. Here the specific activity, S, of the 2,4-dinitrophenylhydrazone formed by 5 percent, 10 percent, or 30 percent reaction of the ketone was divided by the specific activity, S_{100}, of the same derivative formed by 100 percent reaction of the ketone by the use of excess reagent solution of 2,4-dinitrophenylhydrazine

TABLE II. Effect of varying temperature, solvent, ester concentration and the alkyl group on the isotope effect in ethyl benzoate-α-C^{14} saponification and ethyl *p*-methoxy benzoate-α-C^{14} saponification.

Ester	Temp. °C	Solvent	Ester concentration in solvent	$S_2/S_{100} = k_{14}/k_{12}$
Ethyl benzoate-α-C^{14}	0°	90% ethanol	0.32 M	0.918
	25°	90% ethanol	0.32 M	0.929
	78.5°	90% ethanol	0.32 M	0.939
Ethyl benzoate-α-C^{14}	25°	56% acetone	0.32 M	0.928
Ethyl *p*-methoxy benzoate-α-C^{14}	25°	90% ethanol	0.32 M	0.916
	25°	56% acetone	0.32 M	0.917
Ethyl benzoate-α-C^{14}	25°	90% ethanol	1.60 M	0.926
t-Butyl benzoate-α-C^{14}	25°	56% acetone	0.32 M	0.939

[9] C. A. Bunton and D. R. Llewellyn, Research **5**, 443 (1952).

[10] W. H. Urry, "Structural influences in the reactions of free radicals in solution," presented at the Organic Chemistry Symposium, Denver, June, 1951.

[11] Ropp, Weinberger, and Neville, J. Am. Chem. Soc. **73**, 5573 (1951).

[12] S. Cohen and A. Schneider, J. Am. Chem. Soc. **63**, 3382 (1941).

sulfate. The ratio, k_{14}/k_{12}, was calculated from S/S_{100} and the known percent reaction which produced the 2,4-dinitrophenylhydrazone having the specific activity S. For rapid calculation the equation of Stevens and Attree[7] was employed in graphical form.

For the formation of the ketone 2,4-dinitrophenylhydrazones, a procedure similar to that given by Shriner and Fuson,[13] Procedure 15, was employed except that a constant temperature bath at the desired temperature was used. For the formation of the acetophenone-α-C^{14}-2,4-dinitrophenylhydrazone at −75°, dry-ice-acetone cooling was used while the desired amount of 2,4-dinitrophenylhydrazine solution in sulfuric acid was added over ninety minutes with stirring. The mixture was kept at −75° overnight, then worked up. The 2,4-dinitrophenylhydrazones were recrystallized from ethyl alcohol and ethyl acetate to sharp melting points.

B. Tabulation of Isotope Effect Data for the Formation of 2,4-Dinitrophenylhydrazones of Acetophenones (α-Carbon^{14})

Table III presents the details of the data for a number of runs with the three acetophenones.

C. Discussion of the Isotope Effect Data of Table III

The isotope effect ratios reported in Table III for the formation of 2,4-dinitrophenylhydrazones of ketones bear out, in general, the trends found in the ester saponification series. In Fig. 1 the points corresponding to a Hammett plot in the ketone series are shown as dark circles. For the formation of the 2,4-dinitrophenylhydrazone of acetophenone-α-C^{14}, the reported values of k_{14}/k_{12} at three temperatures correspond to a value of 49 cal per mole for the difference between the Arrhenius activation energies for the reactions of the two isotopic species. This value of ΔE corresponds to a ratio of A_{14}/A_{12} of 1.027 at 25°. However this deviation of the ratio from unity is somewhat uncertain, as it depends on only five isotope effect determinations. The trend in isotope fractionation ratios in the ketone reactions may result from circumstances similar to those mentioned under IIC even though the mechanisms of the ester and ketone reactions are undoubtedly quite different.

[13] R. L. Shriner and R. C. Fuson, *Identification of Organic Compounds* (John Wiley and Sons, Inc., New York, 1940), second edition, p. 171.

TABLE III. Isotope effect data for the individual reactions forming 2,4-dinitrophenylhydrazones of three ring-substituted acetophenones (α-carbon-14).

Substituent	Temperature °C	Percent reaction of ketone	$10^3\times$ specific activity in μc per mg	S/S_{100}	k_{14}/k_{12}	Mean k_{14}/k_{12}
$p-OCH_3$	25°	100	4.209	0.947	0.936	
		30	3.984			
	25°	100	4.341	0.935	0.931	
		10	4.060			
	25°	100	4.303	0.936	0.932	0.933
		10	4.028			
None	−75°	100	9.09	0.910	0.908	0.908
		5	8.27			
	25°	100	8.97	0.945	0.943	
		5	8.48			
	25°	100	8.94	0.951	0.949	0.946
		10	8.50			
	78°	100	8.97	0.966	0.959	
		30	8.67			
	78°	100	9.15	0.965	0.958	0.959
		30	8.83			
$m-NO_2$	25°	100	6.95	0.962	0.960	0.960
		10	6.68			

ACKNOWLEDGMENT

The authors wish to thank Dr. W. H. Stevens for information included in the communication referred to in this paper.

Infrared Spectrum and Thermodynamic Functions of Formamide

J. C. EVANS*
The Edward Davies Chemical Laboratories, University College of Wales, Aberystwyth, Wales
(Received September 8, 1953)

The infrared spectra of formamide in the vapour and liquid states, and in solutions in $CHCl_3$, CCl_4, CH_3CN, H_2O, and D_2O, and of sodium formamide and formamide hydrochloride were observed between 650 cm^{-1} and 3800 cm^{-1}. The effect of association on the bands was examined, where possible, in solution and in the vapor state. These infrared results were taken in conjunction with the available Raman data and an assignment of the frequencies to the fundamental modes of vibration of the molecule has been made. Thermodynamic functions have been calculated.

INTRODUCTION

THE infrared spectrum of formamide in the vapor state has not previously been reported, possibly because of its low vapor pressure at room temperature and the necessity for using a cell of long path length even at high temperatures. An additional complication is that formamide decomposes to an appreciable extent above 160°C.[1] On the other hand, the infrared spectrum of liquid formamide has been examined between 500 cm^{-1} and 1700 cm^{-1} by Lecomte and Freymann,[2] while Kahovec and Wasmuth[3] and Saksena[4] have thoroughly investigated the Raman spectrum of the liquid and solid. Kahovec and Wasmuth also proposed an assignment of the frequencies which does not differ greatly from that arrived at here.

EXPERIMENTAL

Formamide was purified by the method recommended by Smith[5] until of freezing point 1.5°C (uncorrected), i.e., with approximately 0.5 percent of water. It was decided that further drying would not be justifiable since the formamide would be unavoidably exposed to the atmosphere, if only for a short time, while the solutions were prepared or the cells filled.

The solvents used, CCl_4 (Analar), $CHCl_3$ (Analar), and CH_3CN (British Drug House) were dried and redistilled.

The measurements were made using a Grubb Parsons *S*3 spectrometer fitted with SiO_2 and NaCl prisms. The uncertainties in the band center frequencies were estimated to be within ± 2 cm^{-1} at 1000 cm^{-1}, ± 4 cm^{-1} at 1700 cm^{-1}, and ± 5 cm^{-1} at 3500 cm^{-1}. The spectral slit widths are shown on the diagrams.

The Vapor Spectrum

A multiple reflection cell, based on an optical arrangement described by White[6] was built for this work. The surface-aluminized concave mirrors were of 15-cm focal length, thus providing path lengths of 60 cm, 120 cm, 180 cm, etc. The 120-cm path was found to be suitable for all the observations, the radiation transmitted by the empty cell being then approximately 40 percent. The cell was placed between the radiation and spectrometer units. To facilitate the ready removal and replacement of the cell heater, each surface of the rectangular cell was separately heated by a flat, asbestos-covered coil. A controlled, dry nitrogen stream bubbling through a little liquid maintained a constant partial pressure of formamide within the cell, which was not vapor tight. The vapor concentration in the cell could be varied by changing the temperature of the oil bath in which the bubbler was immersed; the latter was kept at least 10°C below the cell temperature so as to preclude condensation of liquid in the cell.

The effects of temperature and pressure changes on the vapor bands were examined to determine whether there was any association of the molecules. This was best studied in the 3μ region where, in solution, the well-defined NH_2 stretching frequencies were accompanied by several strong association peaks.[7] No such bands appeared for the vapor in our observations between 130°C and 160°C and estimated partial pressures of 20 mm and 95 mm in the cell. None of the other vapor absorptions showed any signs of association occurring. At a temperature of 160°C in the cell, some peaks were detected near 10μ arising from traces of ammonia produced by decomposition. Such records were discarded.

The Liquid Spectrum

Capillary films of unknown thickness were used to record the strongest bands. The very weak bands at 1190 cm^{-1} and 1090 cm^{-1} required a thickness of 0.025 mm. These films were found to scatter the radiation markedly, whilst the strong bands, e.g., at 1310 cm^{-1}, were then very broad. A noteworthy point, which the doublet structure of the absorption due to the $\nu(C=0)$ vibration suggested, was that, even in the liquid state, complete association does not occur; the component of

* Present address; Pure Chemistry Division, National Research Council of Canada, Ottawa.

[1] Schwab, Z. anorg. u. allgem. Chem. **262**, 41 (1950).
[2] J. Lecomte and R. Freymann, Bull. soc. chim. **8**, 612 (1941).
[3] Kahovec and Wasmuth, Z. physik. Chem. **48B**, 70 (1941).
[4] Saksena, Chem. Abstracts **34**, 6882 (1940).
[5] G. F. Smith, J. Chem. Soc. **1931**, 3257.
[6] J. U. White, J. Opt. Soc. Am. **32**, 285 (1942).
[7] Mansel Davies and J. C. Evans, J. Chem. Phys. **20**, 342 (1952).

higher frequency is at the same value as the monomer absorption in dilute solutions.

Solution Spectra

As much as was possible of the spectrum was investigated with solutions in CCl_4 and $CHCl_3$. The main restriction on the use of these inert solvents was the limited solubility of formamide. With $CHCl_3$, however, it was possible to reach an appreciable degree of association, so that the behavior of some of the bands when the degree of association was varied could be followed. Other spectral regions not accessible in the above solvents were examined in CH_3CN.

Solutions of formamide in H_2O and D_2O were examined in the hope that the results of deuterium substitution could be obtained without separating the pure substituted compounds. The results did not prove to be of great value in the frequency assignment because of (a) the unknown influence of hydration effects on the formamide molecule, (b) the presence of HDO absorptions which might be confused with those of formamide, and (c) the inevitably incomplete spectra in these solvents and the frequently unknown mass factor influence on the frequencies.

Sodium Formamide and Formamide Hydrochloride

Some aid in making the frequency assignment was derived from the results of measurements on the sodium derivative of formamide, HCO—NHNa, which was examined as a powdered-solid film immersed in CCl_4. Formamide hydrochloride was investigated as a suspension in $CHCl_3$.

GENERAL FEATURES

It is to be expected that the four atoms

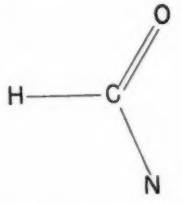

will be coplanar. Of the various alternatives for the orientation of the NH_2 group, including, presumably, coplanarity with the foregoing[8]—it can be stated that the results indicate with considerable probability, that the NH_2 group is symmetrically disposed about, but not in, this plane. The point group is then C_s and the twelve fundamental modes are distributed as $8A'+4A''$. No direct experimental data on the molecular dimensions of formamide appear to be available. The values used have been chosen after a detailed consideration of the best data in related molecules (methylamine, ammonia, formic acid, formaldehyde) and the differences likely to exist between them and formamide.[9] In the present paper none of the deductions, except the values of the thermodynamic functions, are dependent upon the precision of these estimates. These values are:

$(H-C)=1.08A$, $(C=O)=1.22A$, $(C-N)=1.40A$, $(N-H)=1.00A$, angle $HCO=122°$, angle $OCN=122°$, angle $HCN=116°$, and $114°$ for the NH_2 group angle. The principal moments of inertia were calculated: $A=14, B=72, C=82$ (in 10^{-40} g cm^2). The B axis is very nearly parallel to the H—C bond; A is perpendicular to it in the OCN plane, and C is perpendicular to that plane. The types of band structures to be expected for dipole moment changes parallel to these axes can be deduced from Badger and Zumwalt's curves.[10] The A type should have two strong peaks with an intermediate weak one, the B type merely a well-defined doublet, and the C type should give a strong central peak flanked by two weaker peaks. Many of the absorptions will necessarily be hybrids of these types.

FREQUENCY ASSIGNMENTS

The frequency assignment is given in Table I; see also Fig. 1. The normal vibrations are designated in order of decreasing frequencies by the numbers 1 to 12.

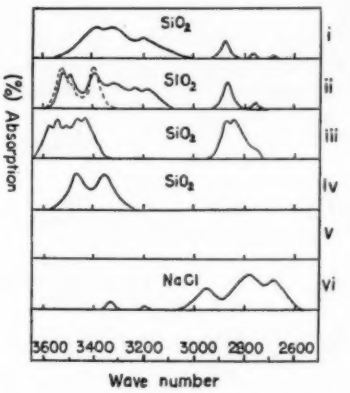

FIG. 1(a). For key, see Fig. 1(b).

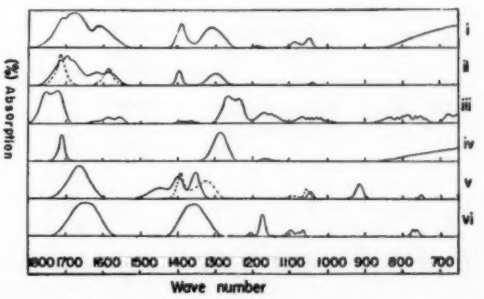

FIG. 1(b). (i) Liquid. (ii) $CHCl_3$ solutions (—— saturated solution; ------ $\frac{1}{8}$ saturated solution). (iii) Vapor. (iv) CH_3CN solutions. (v) D_2O solutions ——; ----- H_2O solutions. (vi) HCONHNa mull in CCl_4.

[8] L. Pauling and R. B. Corey, Proc. Natl. Acad. Sci. **37**, 285 (1951).

[9] J. C. Evans, Ph.D. thesis, University of Wales, 1953.

[10] R. M. Badger and Z. R. Zumwalt, J. Chem. Phys. **6**, 711 (1938).

TABLE I.[a,b]

Descriptive assignment	INFRA-RED RESULTS: Vapour Type	Vapour Intens.	Vapour cm^{-1}	Liquid cm^{-1}	Liquid Intens.	Solutions $CHCl_3$	Solutions CH_3CN	Solutions H_2O	Solutions D_2O	Sodium formamide cm^{-1}	RAMAN DATA[c] Liquid cm^{-1}	Liquid Intens.
$\nu_a NH_2, \nu_1$	C	m.s.	3580 3545 3515	3388 3328	m.s. m.s.	3524(m)	3471					
$\nu_s NH_2, \nu_2$	B	m.s.	3466 3435	3207	m.	3403(m)	3357			3345 3195		
$\nu CH, \nu_3$	B	m.s.	2870 2834	2881	m.	2863				2950 2780 2680	2884	(3b)
$2\nu_6$	?	v.w.	2730	2763	v.w.	2754					2772	(0)
$\nu_6+\nu_7$				2685	v.w.							
$2\nu_{10}$				2170	v.w.							
$\nu CO?, \nu_4$	A,B	v.s.	1756 1734 1723	1713(m) 1681(a)	sh. v.s.	1709(m) 1686(a)	1709		1665	1654	1674	(4b)
$\nu_{10}+\nu_{12}$	B(?)	v.w.	1640 1628									
$\delta NH, \nu_5$	B	m.w.	1589 1555	1611(a)	m.	1612(a) 1583(m)					1588	(2b)
(HOD)									1450		1489	(00)
$\delta CH, \nu_6$	A	v.w.	1395 1378 1362	1391	s.	1395		1392	1397		1390	(10)
ν_5									1353			
$\nu CN, \nu_7$	A,B	s.	1267 1255 1237	1309	s.	1299	1280	1324		1358	1312	(6b)
$\gamma NH_2, \nu_8$	B,A	m.	1167 1152	1190	v.w.		1160			1207		
WNH_2, ν_9	B,A	w.	1065 1053	1087	w.			1090		1173 1098	1096	(4)
$\delta CH, \nu_{10}$	C	w.	1044 1030 1019	1050	w.	1044		1055	1048	1077 1065	1050	(1)
$\nu_4-\nu_{11}$	B(?)	v.w.	1004 989								1002	(1)
ν_{10}	?	v.w.	866						920			
$\nu_5-\nu_{11}$	Appreciable C-character m.w.		833 816 803	Steadily increasing absorption			Steadily increasing absorption					
$\tau NH_2, \nu_{11}$	Appreciable C-character m.		787 765 756						750	770 764		
$\nu_4-\nu_{10}$	?	v.w.	735								690	(0)
$\delta OCN, \nu_{12}$	B,A(?)	m.	675 ?	595(centre)							605	(?)

[a] (m) = monomer; (a) = associated; sh = shoulder.
[b] The vertical bars show regions where conditions of solubility, solvent absorption, etc., are unsuitable for study.
[c] Raman data of Kahovec and Wasmuth, with intensities in brackets.

ν_1 and ν_2 at 3545 and 3450 cm^{-1}

These bands undoubtedly arise from the asymmetric and symmetric vibrations of the NH_2 group. In the vapor, ν_1 was a *C*-type band and ν_2 a *B*-type band (see Fig. 2). The only geometrical arrangement of the NH_2 group compatible with this result is that in which the two hydrogen atoms are symmetrically disposed about the molecular plane with the three nitrogen valence bonds at angles not far removed from the value in ammonia. The results of solution studies on the bands have already been reported.[7] In the liquid state the broad region of absorption was not very well resolved.

ν_3 at 2852 cm^{-1}

This, again without doubt, is due to the stretching vibration of the C—H bond. The structure of the vapor band, Fig. 1, conforms to expectations from the molecular configuration described above.

ν_4 at 1740 cm^{-1}

This may safely be assigned to the asymmetric stretching mode of the OCN group where the vibration is largely confined to the C=O bond. The vapor-band structure, an *A* type with a small *B* component—solution studies, and the liquid spectrum all support this assignment.

ν_5 at 1572 cm^{-1}

This band is rather weak relative to its neighbor, ν_4. It is now fairly well established that the in-plane bending vibration of the NH_2 group lies in the 1500–1600 cm^{-1} region. The behavior of the band on changing the degree of association provided strong evidence for this assignment in formamide; the wave numbers found in various phases were: liquid 1611: $CHCl_3$ solution 1612 (assoc.); 1583 (monomer): vapor 1572. A difficulty arises in discussing the vapor-band structures for the deformation modes of the NH_2 group. It is uncertain to what extent the oscillation of the nitrogen lone-pair electrons contributes to the dipole moment change during the vibration. In this particular bending mode however, it makes little difference whether the lone-pair oscillation is considered or not, since in either case the expectation would be a band of the *B*-type structure, as observed. On deuterium substitution, this frequency disappeared completely.

TABLE II.

	Liquid	Vapor	In $CHCl_3$	In CH_3CN	In H_2O	Sodium formamide
ν_4	1681	1740	1710	1708	1665 (D_2O)	1654
ν_7	1309	1255	1299	1280	1324	1358
$\nu_4+\nu_7$	2990	2995	2999	2988	2989	3012

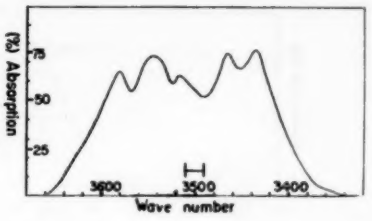

FIG. 2. Formamide vapor absorption: effective cell length 120 cm: temperature 135°C: approximate pressure 40 mm.

ν_6 at 1378 cm^{-1}

This has been assigned to the in-plane deformation mode of the C—H bond. The band was sharp and remarkably constant in frequency in liquid formamide and in solutions in CCl_4, $CHCl_3$, and H_2O (1390 cm^{-1}). In D_2O the band was reduced in intensity but did not disappear completely. In the sodium formamide spectrum, a very broad band, centered at 1360 cm^{-1}, obscured this region and the presence or absence of the 1390 cm^{-1} center could not be ascertained. In the vapor, the band structure (*A* type) was in agreement with this assignment, but its intensity was now very remarkably reduced. Further support was drawn from the presence of bands at much the same frequency in *N*-methyl formamide,[11] formaldehyde[12] and in the formate ion.[13]

ν_7 at 1253 cm^{-1}

ν_7 was the second most intense band in the spectrum under all conditions. It was somewhat sensitive to the environment of the molecule and its behavior seemed to be complementary to that of ν_4, the asymmetric mode of

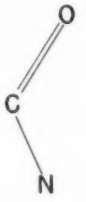

(see Table II).

The band has been assigned to the symmetrical stretching mode of the

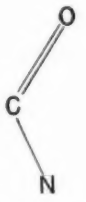

group. The structure of the vapor band, Fig. 3, conforms to that for a vibration producing a dipole change with a main *A* component and a smaller *B* component. The frequency shifts in the band between formamide

[11] Randall, Fowler, Fuson, and Dangl, *Infra-Red Determination of Organic Structures* (D. Van Nostrand Company Inc., New York, 1949), p. 146.
[12] J. C. Morris, J. Chem. Phys. **11**, 230 (1943).
[13] R. Newman, J. Chem. Phys. **20**, 1663 (1952).

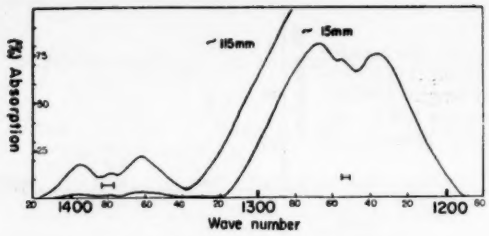

FIG. 3. Formamide vapor absorption; effective cell length 120 cm; temperature 155°C; approximate pressures indicated.

and sodium formamide, 1309–1358 cm^{-1}, and between formamide and formamide hydrochloride, 1309–1340 cm^{-1}, are in accord with the probable changes in the nature of the C—N bonds between these substances. In D_2O, the band disappeared and its new location could not be determined.

The five remaining fundamental modes are not so readily assigned. They may be represented as the twisting mode of the NH_2 group, $\gamma(NH_2)$; the wagging mode of the NH_2 group, $\omega(NH_2)$; the torsional NH_2 mode, $\tau(NH_2)$;

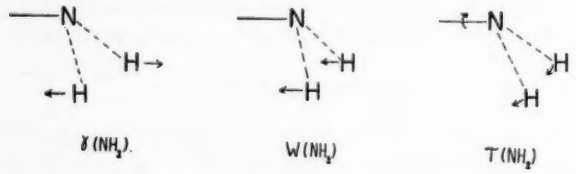

the out-of-plane deformation C—H mode; and the skeletal deformation mode

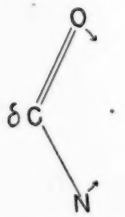

The expected order of the NH_2 frequencies is $\gamma > \omega > \tau$.

A rather ill-defined band of medium intensity of 1160 cm^{-1} in the vapor, Fig. 4, has been correlated with very weak absorptions at 1190 cm^{-1} in the liquid and at 1160 cm^{-1} in the CH_3CN solution, and assigned to $\gamma(NH_2)$. The band was detected in the liquid and solution only under conditions which produced a considerable spread of the neighboring strong absorption, ν_7; it was, thus,

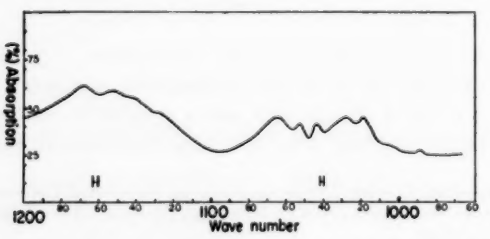

FIG. 4. Formamide vapor absorption; effective cell length 120 cm; temperature 135°C; approximate pressure 45 mm.

observed as a shoulder at the foot of the latter. The band-center shift between vapor and liquid is consistent with the assignment, but conclusive support cannot be drawn from the vapor-band contour. It can at least be said that the observed band structure is not at variance with the assignment.

The out-of-plane δ(C—H), a *C*-type vibration, is expected to appear near 1050 cm^{-1} (see HCOOH and $HCOO^-$). Formamide vapor in this region, Fig. 4, shows a broad absorption with five well-defined peaks, at 1065, 1053, 1044, 1030, and 1019 cm^{-1}, while the liquid shows a weak band at 1050 cm^{-1} and a very weak band at 1087 cm^{-1}. Solution studies were difficult in this region, and in $CHCl_3$ only the stronger band, now at 1044 cm^{-1}, was detected. Conditions were more favorable with H_2O and two bands, at 1090 and 1055 cm^{-1}, were observed. Solutions in D_2O did not show the 1090 cm^{-1} band, and the behavior of the 1050 cm^{-1} feature in these solutions was reminiscent of that of ν_6, the in-plane C—H deformation mode; the band decreased in intensity but did not disappear entirely as the degree of deuterium substitution increased. Accompanying this change was the increase in intensity of a new band at 915 cm^{-1}.

The band at 1050 cm^{-1} in the liquid, at 1055 cm^{-1} in H_2O and at 1044 cm^{-1} in $CHCl_3$, is assigned to the out-of-plane δ(C—H). The expectation, which arises from the consideration of the frequency shift of 1050–1044 cm^{-1} between liquid and chloroform solution, that the vapor band lies at still lower frequency, is in agreement with the observation that the three peaks in the vapor absorption which most closely resemble a *C*-type band are the peaks at 1044, 1030, and 1019 cm^{-1}, and these features are assigned to δ(C—H) in the vapor. The remaining two vapor peaks at 1065 cm^{-1} and 1053 cm^{-1} are appropriately allocated to $\omega(NH_2)$, which appears in the liquid at 1087 cm^{-1} (Raman value 1096 cm^{-1}) and in the solid at 1134 cm^{-1} (Raman).

The assignment of the skeletal mode δOCN is made by comparison with the frequencies of similar modes in other molecules; HCOOH at 658 cm^{-1} and $H \cdot COO^-$ at 775 cm^{-1},[14] $H \cdot CO \cdot CH_3$ at 510 cm^{-1}.[15] A strong band appears in the infrared spectrum of liquid formamide at 595 cm^{-1},[16] and a line of lower intensity occurs in the Raman spectrum at 605 cm^{-1}. In the vapor, a band which could not be observed completely because of the prism limit, but which was estimated to be centered at 660 cm^{-1}, was examined. These absorptions have been assigned to δOCN, ν_{12}.

One more mode, the torsional NH_2 mode, remains to be assigned. The vapor spectrum, Fig. 5, contains two bands of similar forms with an appreciable *C* component, one centered at 816 cm^{-1}, the other at 765 cm^{-1}. The direction of dipole moment change during this NH_2

[14] W. J. O. Thomas, Discussions Faraday Soc. **9**, 339 (1950).
[15] H. W. Thompson and G. P. Harris, Trans. Faraday Soc. **38**, 37 (1942).
[16] Private communication to Dr. Mansel Davies from Dr. G. G. Cannon, British Nylon Spinners, Pontypool.

TABLE III.[a]

Liquid		$CHCl_3$ solution		Suggested assignment using the fundamental frequencies in $CHCl_3$ solution.
cm^{-1}	Intensity	cm^{-1}	Intensity	
8350	v.w.			
		6984	v.w.	$\nu_a(NH_2) + \nu_s(NH_2)$
6565	m.	6799	m.	$2\nu_a(NH_2)$.
6138	sh.	6702	m.	$2\nu_s(NH_2)$.
5592	w.			$2\nu(CH)$.
5673	sh.			
5015	s.	5085	s.	$\nu_a(NH_2) + \delta(NH_2)$.
		4974	w.	$\nu_s(NH_2) + \delta(NH_2)$.
4752	m.	4816	m.	$\nu_a(NH_2) + \nu(CN)$.
4544	v.s.	4610	v.s.	$\nu_a(NH_2) + W(NH_2)$. (liquid value.)
4194	m.w.			
4025	w.			

[a] The intensities quoted are relative to the strongest band.

torsional oscillation is uncertain, but it must undoubtedly have a component in the *C*-axis direction, so that the structures of the two bands are not incompatible with the assignment of either to this mode. Assignment of the more intense 765-cm^{-1} band to $\tau(NH_2)$ allows the other to be explained as a difference tone; 1572 (bending NH_2) − 765 (τNH_2) = 807 cm^{-1}. The bands were resolved neither in the liquid nor in $CH_3 \cdot CN$ solution. In both these cases, an absorption commences at approxlmately 850 cm^{-1} and increases steadily until the rocksalt prism limit is reached at 650 cm^{-1}. Some support for this torsional assignment may be drawn from the assignments of similar modes in other molecules; Hadzi and Sheppard[17] place the out-of-plane O−H deformation mode in dimeric carboxylic acids at 935 cm^{-1}, while in trifluoracetic acid the similar monomeric frequency is placed at 904 cm^{-1}.[18]

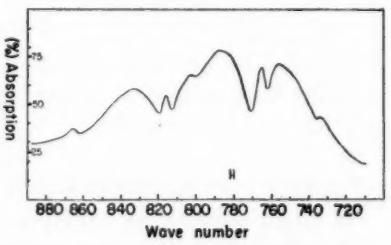

FIG. 5. Formamide vapor absorption; effective cell length 120 cm; temperature 150°C; approximate pressure 75 mm.

[17] D. Hadzi and N. Sheppard, Proc. Roy. Soc. (London) **A216**, 247 (1953).

[18] Fuson, Josien, Jones, and Lawson, J. Chem. Phys. **20**, 1627 (1952).

OVERTONES AND COMBINATION TONES

Some very weak features in the vapor and in the liquid spectra have been assigned to overtones and combination tones (see Table I). The overtone region above 4000 cm^{-1} was examined in the case of the liquid and chloroform solutions. The liquid films required were of thicknesses 0.1 and 0.8 mm, while the saturated solution in chloroform was examined in a 10-mm cell. There is only poor correspondence between the spectra, due to association in the liquid, and it is not surprising that a clearer assignment of the bands is possible in the solution spectrum (see Table III).

THERMODYNAMIC FUNCTIONS

On the basis of the following value for the fundamental vibrational frequencies (in cm^{-1}), 3545, 3450, 2852, 1740, 1572, 1378, 1253, 1160, 1060, 1030, 765, 660, the vibrational contributions to the thermodynamic functions were obtained over the temperature range

TABLE IV.[a]

Absolute temperature	C_p^0	$\frac{E^0 - E_0^0}{T}$	$\frac{-(F^0 - E_0^0)}{T}$	S^0
273.16	10.24	6.48	50.15	58.61
298.16	10.84	6.65	50.89	59.53
300	10.88	6.67	50.95	59.60
400	13.43	7.54	53.55	63.08
600	17.82	9.61	57.80	69.40

[a] There are no published data with which these figures can be directly compared.

273.16···600°K using the tables given by Aston[19] and Torkington.[20] The rotational and translational contributions were determined using the equations given by Wagman *et al.*,[21] assuming $I_A \cdot I_B \cdot I_C$ to be 81.7×10^{-117} g^3 cm.[6] The total contributions are collected in Table IV, in terms of calories per mole per degree. These values relate, of course, to formamide vapor in the ideal gas state.

[19] J. C. Aston in *Treatise on Physical Chemistry*, by H. S. Taylor and S. Glasstone (Macmillan and Company, New York, 1942), third edition, Vol. 1.
[20] P. Torkington, J. Chem. Phys. **18**, 1373 (1953).
[21] Wagman, Kilpatrick, Taylor, Pitzer, and Rossini, J. Research Natl. Bur. Standards **34**, 143 (1945).

ACKNOWLEDGMENTS

The author wishes to thank Dr. Mansel Davies for his constant encouragement and many helpful discussions in directing this work.

The Department of Scientific and Industrial Research is also thanked for the provision of a Maintenance Award.

THE JOURNAL OF CHEMICAL PHYSICS VOLUME 22, NUMBER 7 JULY, 1954

The Application of the Debye-Hückel Theory to Polyions. Part I. The Range of Applicability of the Debye Limiting Law

H. J. G. HAYMAN
The Department of Physical Chemistry, The Hebrew University, Jerusalem, Israel
(Received November 3, 1953)

The Debye limiting law has been used to deduce an expression for the electrical work which must be done to build up a polyion from the corresponding single ions in extremely dilute solutions containing various (appreciable) concentrations of 1−1 electrolyte. The case of an infinite straight rigid polyion having charges at equal intervals along its length was treated in greater detail, and a corrected expression was obtained for the above-mentioned electrical work, which makes allowance for the finite size of the polyion charges and takes some account of the steric effects due to the remainder of the polyion molecule. The error due to the high electric potential ψ surrounding such a polyion which invalidates the Debye approximation of replacing $\sinh(\epsilon\psi/kT)$ by $\epsilon\psi/kT$ was evaluated by numerical integration of the Poisson-Boltzmann equation. The integration was started at a considerable distance from the polyion on the assumption of cylindrical symmetry and continued at closer distances on the assumption of spherical symmetry surrounding each polyion charge. The results obtained indicated that the error involved in using the simple Debye limiting law formula would seldom be more than a few percent, provided the concentration of the 1−1 electrolyte was rather low (not more than about $N/100$).

1. INTRODUCTION

THE free energies of various polyions have been calculated by a number of workers on the basis of the Poisson-Boltzmann equation,[1,2] using certain simplifying assumptions. The commonest of these is that the electric potentials are small enough to permit the use of the Debye (linear) form of the Poisson-Boltzmann equation, but the validity of this assumption has been questioned because of the high electric potentials in the immediate vicinity of a polyion.[3]

If the applicability of the Debye limiting law (point charges) is assumed, the expression for the electrical work required to build up a *rigid* polyion from the corresponding single ions (hereafter referred to as the "polyionic work") takes a particularly simple form.[4] The object of this paper will be to examine the order of magnitude of the errors arising from the application of this expression to the case of an infinite straight rigid polyion having charges at equal intervals along its length. These errors are due to the finite size of the polyion atoms and to the high electric potentials prevailing. The latter source of error, which is the more difficult to estimate, was evaluated by a series of numerical integrations of the Poisson-Boltzmann equation, the method being similar to that used by Müller[5] for the case of single (spherically symmetric) ions. Unfortunately, this method cannot be expected to give much more than the order of magnitude of the error involved, since the Poisson-Boltzmann equation is self-consistent only for low electric potentials.[6]

[1] J. J. Hermans and J. Th. G. Overbeek, Rec. Trav. Chim. **67**, 761 (1948). O. Künzle, Rec. Trav. Chim. **68**, 699 (1949). A. Katchalsky, J. Polymer Sci. **7**, 393 (1951). T. L. Hill, J. Chem. Phys. **20**, 1259 (1952). A. Katchalsky and S. Lifson, J. Polymer Sci. **11**, 409 (1953). S. Lifson and A. Katchalsky, J. Polymer Sci. **13**, 43 (1954).
[2] Fuoss, Katchalsky, and Lifson, Proc. Natl. Acad. Sci. U. S. **37**, 579 (1951). Alfrey, Jr., Berg, and Morawetz, J. Polymer Sci. **7**, 543 (1951).
[3] Kimball, Cutler, and Samelson, J. Phys. Chem. **56**, 57 (1952).
[4] See Eq. (3), below; compare T. L. Hill, Discussions Faraday Soc. **13**, 132 (1953).
[5] H. Müller, Physik. Z. **28**, 324 (1927).
[6] H. S. Harned and B. B. Owen, *The Physical Chemistry of Electrolytic Solutions* (Reinhold Publishing Corporation, New York, 1950), second edition, p. 34. R. Fowler and E. A. Guggenheim, *Statistical Thermodynamics* (Cambridge University Press, Cambridge, 1949), second impression, p. 409.

2. THE DEBYE LIMITING LAW FORMULA

The polyionic work, being equal to the difference between the electrical work required to charge the polyion by a Güntelberg charging process and that required to charge the corresponding single ions, can easily be calculated in the case of a rigid polyion in a salt solution of known concentration provided the Debye limiting law is applicable, since in this case the electric potentials due to the various ionic atmospheres will be additive.

Consider a polyion being charged by a Güntelberg charging process and having charges $\lambda_D\epsilon$ at each of the points A, B, C, ...I, ...J, ... (Whenever the Debye approximation is assumed, the degree of charging λ will be denoted by λ_D). According to the Debye limiting law, the potential ψ_{IJ} at I due to the charge $\lambda_D\epsilon$ at J, distant l_{IJ} from I, will be given by

$$\psi_{IJ}=\frac{\lambda_D\epsilon}{Dl_{IJ}}e^{-\kappa l_{IJ}}, \tag{1}$$

where κ is the Debye parameter corresponding to the concentration of salt present in the solution, and D is the dielectric constant of water.

The additional work required to charge the Ith ion of the polyion over that needed to charge the corresponding single ion will therefore be

$$\int_0^1 [\sum_{J\neq I}\psi_{IJ}]\epsilon d\lambda_D=(\epsilon^2/2D)\sum_{J\neq I}(1/l_{IJ})e^{-\kappa l_{IJ}}, \tag{2}$$

so that the polyionic work will be[6a]

$$(\epsilon^2/2D)\sum_I\sum_{J\neq I}(1/l_{IJ})e^{-\kappa l_{IJ}}. \tag{3}$$

In the case of a straight infinite linear polyion, having charges at equal intervals l, the right-hand side of Eq. (2) can be written

$$\frac{\epsilon^2}{D}\sum_{n=1}^{\infty}\frac{1}{nl}e^{-n\kappa l}=-\frac{\epsilon^2}{Dl}\ln(1-e^{-\kappa l})=\frac{\epsilon^2\kappa}{2D}A(\kappa l) \quad \text{(say)}. \tag{4}$$

Since all the charges are equivalent, Eq. (4) also gives the polyionic work per charge.

3. EFFECT OF FINITE DIAMETER OF CHARGES

Owing to the finite size of the constituent atoms of the polyion and of the ions of the dissolved salt, the polyion will be surrounded by a certain region into which the salt ions cannot penetrate. For the moment we shall make the rather drastic simplifying assumption that this region consists of a series of spheres of radius a surrounding the various polyion charges, a being the "mean distance of closest approach" of the salt ions.

[6a] This result can also be obtained using a Debye charging process, see H. J. G. Hayman, Bull. Res. Counc. of Israel, **3** (1954), (In the press, Einstein Issue).

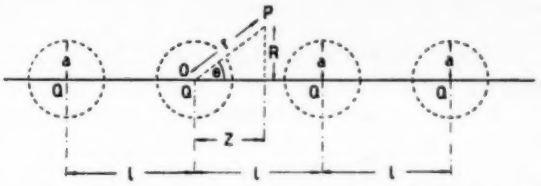

FIG. 1. Hypothetical infinite polyion consisting of a series of point charges Q spaced at equal intervals l.

We now show how Eq. (4) can be modified to allow for this effect.

Consider a hypothetical infinite straight rigid polyion consisting of *point* charges Q at equal intervals l, and assume that the charge density of the ionic atmosphere surrounding this polyion is given everywhere by the Debye limiting law. In order that the charge distribution of the ionic atmosphere surrounding a polyion having spherically symmetric charges of magnitude ϵ and of finite diameter shall be the same as that of the corresponding part of the ionic atmosphere surrounding the above hypothetical polyion, we must assume, not only that the *total* charge inside an imaginary sphere of radius a surrounding each of the point charges Q must be equal to ϵ, but also that that part of the ionic atmosphere inside this sphere of radius a has spherical symmetry. The latter assumption will be more nearly correct the smaller the value of a.

In the course of a Güntelberg charging process, when the point charges on our hypothetical polyion are λ_DQ, the overall potential ψ_P at P (Fig. 1) will be given according to the Debye limiting law by

$$\psi_P=\frac{\lambda_DQ}{D}\sum_{n=-\infty}^{\infty}\frac{e^{-\kappa l_n}}{l_n}, \tag{5}$$

where l_n, the distance of P from the nth charge, is given by

$$l_n=(n^2l^2+r^2-2nlr\cos\theta)^{\frac{1}{2}}. \tag{6}$$

The average potential $\bar{\psi}_r$ at a distance r from O will be given by

$$\bar{\psi}_r=\int_0^{\pi/2}\psi_P(r,\theta)\sin\theta d\theta$$
$$=\frac{\lambda_DQ}{D}\sum_{n=-\infty}^{\infty}\int_0^{\pi/2}\frac{e^{-\kappa l_n}}{l_n}\sin\theta d\theta. \tag{7}$$

If $r\leq l$, this leads to

$$\bar{\psi}_r=\frac{\lambda_DQ}{D}\left[\frac{e^{-\kappa r}}{r}+\frac{A}{r}\sinh\kappa r\right], \tag{8}$$

where A is defined by Eq. (4).

Since the charge density ρ of the ionic atmosphere at P is $-(D\kappa^2/4\pi)\psi_P(r,\theta)$, the charge of the ionic atmosphere contained in a spherical shell of radius r and thickness dr will be $-D\kappa^2r^2\bar{\psi}_r dr$. The *total* charge contained within the sphere of radius a surrounding the point

charge $\lambda_D Q$ at O will therefore be

$$\lambda_D Q - D\kappa^2 \int_0^a r^2 \bar{\psi}_r dr = \lambda_D Q[\mu(a) - A\eta(a)], \quad (9)$$

where

$$\mu(a) = (1+\kappa a)e^{-\kappa a},$$

and

$$\eta(a) = \kappa a \cosh\kappa a - \sinh\kappa a.$$

From Eq. (9) we see that if $Q = \epsilon/[\mu(a) - A\eta(a)]$, the total charge contained within the sphere of radius a will reach the required value of ϵ at the conclusion of the charging process when $\lambda_D = 1$.

The average potential $\bar{\psi}_r(a)$ on the surface of the sphere of radius a surrounding the polyion charge of magnitude $\lambda_D\epsilon$ is obtained by putting

$$Q = \epsilon/[\mu(a) - A\eta(a)]$$

and $r = a$ in Eq. (8); this gives

$$\bar{\psi}_r(a) = \frac{\lambda_D \epsilon}{Da(1+\kappa a)} + \frac{\lambda_D \epsilon \kappa A}{D\mu(a)[\mu(a) - A\eta(a)]}. \quad (10)$$

Since the first term on the right-hand side of Eq. (10) is equal to the potential on the surface of a sphere of radius a surrounding a single charge $\lambda_D\epsilon$, the second term must be the difference between the potential on a polyion charge $\lambda_D\epsilon$ and that on the corresponding single ion. Hence, using a Güntelberg charging process, we see that the polyionic work per charge will be

$$\int_0^1 \frac{\lambda_D \epsilon \kappa A}{D\mu(a)[\mu(a) - A\eta(a)]} \epsilon d\lambda_D = \frac{\frac{1}{2}\epsilon^2 \kappa A}{D\mu(a)[\mu(a) - A\eta(a)]}. \quad (11)$$

For finite values of a, this expression is always larger than the Debye limiting law formula, Eq. (4).

A. Effect of Size of Remainder of Polyion Molecule

The expression obtained in Eq. (11) takes account of the finite diameter of the polyion charges, but ignores the steric effect due to the remainder of the polyion, namely the existence of a region between the polyion charges into which the salt ions cannot penetrate. We have only succeeded in treating this problem by making the simplifying assumption that the above-mentioned region between the polyion charges is spherical in shape.

Consider a hypothetical polyion consisting of alternate point charges Q and q at equal intervals $l/2$ along its length. In order that the ionic atmosphere surrounding this polyion shall be similar to that surrounding the real polyion, we assume that the total charge inside imaginary spheres of radii a and a' surrounding the point charges Q and q are equal to ϵ and zero respectively. The expression for the polyionic work per charge now becomes

$$\frac{\frac{1}{2}\epsilon^2\kappa\{A[\mu(a') - A\eta(a')] + B^2\eta(a')\}}{D\mu(a)\{[\mu(a) - A\eta(a)][\mu(a') - A\eta(a')] - B^2\eta(a)\eta(a')\}}, \quad (12)$$

where

$$B = (2/\kappa l) \ln \coth \tfrac{1}{4}\kappa l,$$

and the functions A, μ and η have the same meaning as before.

For small values of a' (i.e., when $\kappa a' \ll 1$), expression (12) will be given approximately by

$$\frac{\frac{1}{2}\epsilon^2\kappa A}{D\mu(a)[\mu(a) - A\eta(a)]}\left(1 + \frac{B^2\mu(a)\kappa^3 a'^3}{3A[\mu(a) - A\eta(a)]}\right), \quad (13)$$

so that, under these circumstances, the polyionic work per charge will be larger than that given by Eq. (11) by an amount which is proportional to the *volume* of the (spherical) region between the polyion charges into which the salt ions cannot penetrate. Hence, in order to make use of expression (12), we choose a' so as to make the *volume* of the above-mentioned hypothetical spherical region of radius a' equal to that of the actual non-spherical region which it represents.

4. EFFECT OF THE HIGH POTENTIALS SURROUNDING A POLYION

The expressions so far obtained for the polyionic work are based on the validity of the Debye form of the Poisson-Boltzmann equation. The possibility that these expressions may be good approximations is suggested by the success of the Debye-Hückel theory for ordinary (single) ions in dilute solution, in spite of the fact that the potentials in the immediate neighborhood of such ions are too high for the Debye approximation to be valid there. In the case of single ions, the success of the Debye-Hückel theory appears to be due to the fact that nearly all the ionic atmosphere surrounding a particular ion is at a potential low enough to justify the Debye approximation.[7]

In the case of a polyion, the electric potentials are considerably higher than those surrounding a single ion and it therefore appears doubtful whether the Debye approximation is permissible. In order to examine this question, we used a modification of the method used by Müller[5] to evaluate the deviations from the Debye-Hückel theory for simple (spherically symmetric) ions. Müller's method consisted of a series of stepwise integrations of the exact Poisson-Boltzmann equation, starting from a point sufficiently far from the central ion for the Debye assumption to be justified.

We shall confine ourselves to the case of an infinite straight rigid polyion having charges of finite diameter at equal intervals l along its length, and shall neglect steric effects due to the uncharged atoms of the polyion

[7] G. S. Hartley, Trans. Faraday Soc. (London) **31**, 31 (1935).

molecule. We assume as before that the polyion is present at infinite dilution in a solution of 1−1 electrolyte of known concentration.

At a considerable distance from the polyion, the ionic atmosphere will have cylindrical symmetry (i.e., its density will depend only on the distance from the polyion axis), whereas, at closer distances, the alternative assumption that the ionic atmosphere has spherical symmetry round each of the polyion charges will be more correct. We therefore start our stepwise integrations at a point far away from the polyion on the assumption of cylindrical symmetry and, at a suitable stage, continue them on the alternative assumption of spherical symmetry until we reach the inner boundary of the ionic atmosphere at a distance a from a polyion charge.

In general we shall use capital letters to denote functions calculated on the assumption of cylindrical symmetry and the corresponding small letters to denote these functions calculated on the assumption of spherical symmetry. Furthermore, functions calculated on the basis of the Debye approximation will be indicated by the suffix D.

A. Stepwise Integrations Assuming Cylindrical Symmetry

The Poisson-Boltzmann equation for cylindrical symmetry takes the form

$$\frac{1}{R}\frac{\partial}{\partial R}\left(R\frac{\partial\Psi}{\partial R}\right)=-\frac{4\pi\rho}{D}=\frac{\kappa^2 kT}{\epsilon}\sinh\frac{\epsilon\Psi}{kT}, \tag{14}$$

where R is the distance from the axis of the polyion.

On putting $\Phi=\epsilon\Psi/kT$ and $u=\ln\kappa R$, we obtain

$$\Phi^{II}=e^{2u}\sinh\Phi, \tag{15}$$

roman numerals being used as superscripts to indicate derivatives with respect to u. If the Debye approximation is assumed, this becomes

$$\Phi_D{}^{II}=e^{2u}\Phi_D. \tag{16}$$

The relevant solution of Eq. (16) can be expressed in terms of Bessel functions[8] by

$$\Phi_D=CK_0(e^u)=CK_0(\kappa R), \tag{17}$$

and

$$\Phi_D{}^I=-Ce^uK_1(e^u), \tag{18}$$

where C is a parameter depending on the charge density of the polyion.

Returning to the hypothetical point-charge polyion of section 3, we recall that if the Debye approximation is assumed, the potential at P will be given by Eq. (5). Also, l_n, the distance of P from the nth charge, can be expressed in terms of the cylindrical coordinates, R and Z, by

$$l_n=[R^2+(nl-Z)^2]^{\frac{1}{2}}. \tag{19}$$

The average potential $\bar{\psi}_R$ at a distance R from the polyion will therefore be given by

$$\bar{\psi}_R=\frac{1}{l}\int_0^l\psi_P(R,Z)dZ=\frac{\lambda_D Q}{Dl}\int_{-\infty}^{\infty}\frac{1}{l_0}e^{-\kappa l_0}dZ. \tag{20}$$

The integral can be evaluated by putting $Z=R\sinh\omega$ when we obtain[9]

$$\bar{\psi}_R=(2\lambda_D Q/Dl)K_0(\kappa R). \tag{21}$$

Now for large values of R, this average potential $\bar{\psi}_R$ must be the same as the potential Ψ_D calculated from Eq. (17) on the assumption of cylindrical symmetry and the Debye approximation, namely

$$\Psi_D=(kT/\epsilon)\Phi_D=(CkT/\epsilon)K_0(\kappa R). \tag{22}$$

This will be the case (for all values of R) if

$$2\lambda_D Q/Dl=CkT/\epsilon, \tag{23}$$

thus determining C.

We now put

$$\Gamma=\Phi-\Phi_D, \tag{24}$$

so that

$$\Gamma^I=\Phi^I-\Phi_D{}^I. \tag{25}$$

Also, using Eqs. (15) and (16), we obtain

$$\Gamma^{II}=\Phi^{II}-\Phi_D{}^{II}=e^{2u}[\sinh(\Phi_D+\Gamma)-\Phi_D]. \tag{26}$$

When u is large, the absolute values of the correction terms Γ and Γ^I will be small, but will increase as u decreases.

By using the asymptotic expansions[10] for $K_0(e^u)$ and $K_1(e^u)$ when u is very large, it can be shown that in this region

$$\Gamma\sim(C^3/48)K_0{}^3(e^u), \tag{27}$$

and

$$\Gamma^I\sim-(C^3/16)e^uK_0{}^3(e^u). \tag{28}$$

In order to carry out the stepwise integration of Eq. (26), we choose as starting point a suitable large value of u, calculate the corresponding values of Γ and Γ^I from Eqs. (27) and (28), and continue the integration as far as required, or until Φ is large enough for us to put $\sinh\Phi=\frac{1}{2}e^\Phi$ when an exact solution is possible.[2] It can be shown that only in the early stages of the stepwise integration when $\Gamma\ll\Phi\ll1$ will Γ and Γ^I remain proportional to C^3; it is therefore necessary to carry out the later stages of the integration separately for each value of the parameter C required. Further details are given in Appendix I.

The total charge inside unit length of the cylinder of radius R surrounding the polyion, being equal in mag-

[8] Compare Abramson, Moyer, and Gorin, *Electrophoresis of Proteins* (Reinhold Publishing Corporation, New York, 1942), p. 126; Abramson, Gorin, and Moyer, Chem. Rev. **24**, 345 (1939).

[9] G. N. Watson, *Theory of Bessel Functions* (Macmillan Company, New York, 1948), second edition, p. 185.

[10] G. N. Watson, *Theory of Bessel Functions* (Macmillan Company, New York, 1948), second edition, p. 202.

nitude but opposite in sign to the corresponding charge of the ionic atmosphere *outside* the above cylinder, will be given by

$$-\int_R^\infty 2\pi R\rho dR=\frac{D}{2}\int_R^\infty \frac{\partial}{\partial R}\left(R\frac{\partial\Psi}{\partial R}\right)dR$$

$$=-\tfrac{1}{2}DR\frac{\partial\Psi}{\partial R}=-\frac{DkT}{2\epsilon}\Phi^I. \quad (29)$$

B. Stepwise Integrations Assuming Spherical Symmetry

The Poisson-Boltzmann equation for spherical symmetry takes the form

$$\frac{1}{r^2}\frac{\partial}{\partial r}\left(r^2\frac{\partial\psi}{\partial r}\right)=\frac{\kappa^2kT}{\epsilon}\sinh\frac{\epsilon\psi}{kT}. \quad (30)$$

On putting $\phi=\epsilon\psi/kT$ and $\chi=1/\kappa r$, we obtain

$$\phi''=\chi^{-4}\sinh\phi, \quad (31)$$

primes being used to indicate derivatives with respect to χ. If the Debye approximation is assumed, this becomes

$$\phi_D''=\phi_D/\chi^4. \quad (32)$$

We now return to our hypothetical point-charge polyion and assume for the moment that the Debye approximation is justified. We introduce spherical symmetry by making the simplifying assumption that the potential ψ_D at all points distant r from one of the charges λ_DQ is constant and equal to the average potential $\bar{\psi}_r$ at this distance, given by Eq. (8). It follows that

$$\phi_D=\frac{\epsilon\psi_D}{kT}=\frac{\epsilon\bar{\psi}_r}{kT}=\frac{\lambda_DQ\epsilon\kappa}{DkT}\left[\chi e^{-1/\chi}+A\chi\sinh\frac{1}{\chi}\right]. \quad (33)$$

It should be noted that Eq. (33) is a particular solution of Eq. (32).

On combining Eqs. (23) and (33) we obtain

$$\phi_D=\tfrac{1}{2}C\kappa l\left[\chi e^{-1/\chi}+A\chi\sinh(1/\chi)\right]=Cf(\kappa l,\chi) \text{ (say)}, \quad (34)$$

so that

$$\phi_D'=Cf'(\kappa l,\chi)=\tfrac{1}{2}C\kappa l\left[\left(1+\frac{1}{\chi}\right)e^{-1/\chi}\right.$$

$$\left.-A\left(\frac{1}{\chi}\cosh\frac{1}{\chi}-\sinh\frac{1}{\chi}\right)\right]. \quad (35)$$

We now put

$$\gamma=\phi-\phi_D, \quad (36)$$

so that

$$\gamma'=\phi'-\phi_D'. \quad (37)$$

Also, using Eqs. (31) and (32), we obtain

$$\gamma''=\phi''-\phi_D''=\chi^{-4}[\sinh(\phi_D+\gamma)-\phi_D]. \quad (38)$$

The stepwise integration of Eq. (38) had to be carried out separately for each value of C and κl required. For particular values of C and κl (and hence of A) the appropriate starting values of χ, γ, and γ' were calculated by the method described below (Sec. 4C), and γ and γ' evaluated for a series of increasing values of χ.

According to the inverse square law, the total charge inside the sphere of radius r will be

$$-Dr^2\frac{\partial\psi}{\partial r}=\frac{DkT}{\epsilon\kappa}\phi'(\chi). \quad (39)$$

C. The Transition from Cylindrical Symmetry to Spherical Symmetry

We denote the values of u and χ when the stepwise integrations on the assumption of cylindrical symmetry should be replaced by integrations on the assumption of spherical symmetry by u_t and χ_t respectively.

The most reasonable assumptions for evaluating u_t and χ_t are firstly that the corresponding potentials, $\Psi(u_t)$ and $\psi(\chi_t)$, are equal so that

$$\Phi(u_t)=\phi(\chi_t), \quad (40)$$

and secondly that the enclosed charges are equal, i.e., the charge enclosed in a length l of the cylinder corresponding to u_t must equal that enclosed in the sphere corresponding to χ_t. Using Eqs. (29) and (39), this assumption can be expressed by

$$-\tfrac{1}{2}\kappa l\Phi^I(u_t)=\phi'(\chi_t). \quad (41)$$

In the initial stages of the Güntelberg charging process the Debye approximation is justified, so that Eqs. (40) and (41) become

$$\Phi_D(u_t)=\phi_D(\chi_t), \quad (42)$$

and

$$-\tfrac{1}{2}\kappa l\Phi_D{}^I(u_t)=\phi_D'(\chi_t). \quad (43)$$

Using Eqs. (17) and (34), we transform Eq. (42) into

$$K_0(e^{u_t})=f(\kappa l,\chi_t) \quad (44)$$

while Eqs. (18) and (35) are used to transform Eq. (43) into

$$e^{u_t}K_1(e^{u_t})=\left(1+\frac{1}{\chi_t}\right)e^{-1/\chi_t}$$

$$-A\left(\frac{1}{\chi_t}\cosh\frac{1}{\chi_t}-\sinh\frac{1}{\chi_t}\right). \quad (45)$$

For a given value of κl (and hence of A) Eqs. (44) and (45) are used to determine u_t and χ_t. Since these equations do not involve the parameter C, u_t and χ_t will be independent of the degree of charging as long as the Debye approximation is justified.

We now make the additional assumption that, for the higher values of the degree of charging, when the Debye approximation is no longer justified, it is still permissible to carry out the transition from cylindrical

symmetry to spherical symmetry at these same values of u_t and χ_t, namely those determined from Eqs. (44) and (45).

The values of $\gamma(\chi_t)$ and $\gamma'(\chi_t)$ can easily be determined, since, on subtracting Eq. (42) from Eq. (40) and simplifying the result by means of Eqs. (24) and (36) we obtain

$$\gamma(\chi_t)=\Gamma(u_t); \tag{46}$$

similarly, Eqs. (25), (37), (41), and (43) give

$$\gamma'(\chi_t)=-\tfrac{1}{2}\kappa l\Gamma^I(u_t). \tag{47}$$

D. Procedure

The ranges of the various parameters used in the calculations were chosen on the basis of known experimental data on polyelectrolytes. The calculations were confined to aqueous solutions at 25°C.

(i) The distance of closest approach (a)

Calculations were carried out for three values of a, namely 3.5, 4.5, and 5.5A.

(ii) The Debye radius ($1/\kappa$)

Five values of $1/\kappa$ ranging from 43 to 9.6A were used, corresponding to $N/200$, $N/100$, $N/50$, $N/20$, and $N/10$ salt solutions.

(iii) The distance between the polyion charges (l)

Our assumption of a spherically symmetric ionic atmosphere in the immediate neighborhood of each polyion charge limits l to values greater than $2a$. For each value of κ we carried out calculations for five or six different values of l, the largest of which was usually around 45A.

(iv) The product κl

Nine different values of κl, ranging from about 0.2 to 3.2 were used in order to cover the above-mentioned ranges for $1/\kappa$ and l.

(v) The parameter C

For each value of l, we required two or three values of C which would lead to values of the degree of charging, λ, between about 0.5 and 1.3. By making the simplifying assumptions of putting $Q=\epsilon$ and $\lambda=\lambda_D$ in Eq. (23) we obtained appropriate values of C in advance. Altogether seven different values of C were used, ranging from 0.18 to 2.00.

Pairs of values of u_t and χ_t were evaluated as follows. For a particular value of χ_t and a series of trial values for κl, we obtained a series of values of e^{u_t} from Eq. (45) and tested them in Eq. (44) until sufficient agreement was obtained, when we calculated the corresponding value of u_t. We repeated the process for a number of values of χ_t, such that the corresponding values of κl were in the required range. Further details are given in Appendix II.

For each value of χ_t there were two solutions for κl; for one solution, the volume of a length l of the cylinder corresponding to u_t was almost exactly equal to that of the sphere corresponding to χ_t, while for the other it was appreciably larger. We therefore considered only the first solution for which both κl and e^{u_t} were almost exactly inversely proportional to χ_t. This reduced the labor of the calculations very considerably, and enabled us to choose values for χ_t leading to values of κl of the required size.

For a particular value of κl, and each relevant value of C, we evaluated $\Gamma(u_t)$ and $-\Gamma^I(u_t)$, obtained $\gamma(\chi_t)$ and $\gamma'(\chi_t)$ by means of Eqs. (46) and (47), and continued our stepwise integrations on the assumption of spherical symmetry. Then, for a particular value of κ and each of the corresponding values of C we evaluated γ and γ' at the inner surface of the ionic atmosphere given by $\chi=1/\kappa a$ for each value of a.

E. The Güntelberg Charging Process

The degree of charging, λ, of the polyion can be obtained from Eq. (39) by putting $\chi=1/\kappa a=\chi_a$ (say). This gives

$$\lambda=(DkT/\epsilon^2\kappa)\phi'(\chi_a). \tag{48}$$

It follows from Eqs. (48) and (35) that if the Debye approximation were everywhere justified, the degree of charging would be

$$\lambda_D=(DkT/\epsilon^2\kappa)\phi_D'(\chi_a)=(CDkT/\epsilon^2\kappa)f'(\kappa l,\chi_a), \tag{49}$$

while, according to Eqs. (34) and (49), the potential at the inner surface of the ionic atmosphere would be

$$\psi_D(\chi_a)=\frac{kT}{\epsilon}\phi_D(\chi_a)=\frac{\lambda_D\epsilon\kappa f(\kappa l,\chi_a)}{Df'(\kappa l,\chi_a)}. \tag{50}$$

Hence, if the Debye approximation were justified, the potential at the inner surface of the ionic atmosphere, corresponding to the degree of charging given by Eq. (48), would be equal to

$$\frac{kT\phi'(\chi_a)f(\kappa l,\chi_a)}{\epsilon f'(\kappa l,\chi_a)},$$

instead of to the value $(kT/\epsilon)\phi(\chi_a)$ actually existing.

It can be shown, using Eqs. (34), (35), (36), and (37), that the decrease, δ, in the potential due to the deviations from the Debye-Hückel theory will be given by

$$\delta=\frac{kT}{\epsilon}\left[\frac{\gamma'(\chi_a)f(\kappa l,\chi_a)}{f'(\kappa l,\chi_a)}-\gamma(\chi_a)\right]. \tag{51}$$

Using a Güntelberg charging process, we see that the deviations from the Debye-Hückel theory will lead to too high a value for the polyionic work per charge by

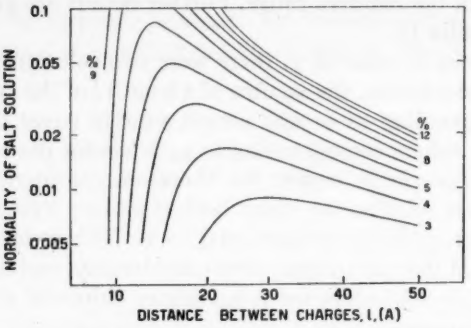

FIG. 2. Error due to nonvalidity of the Debye approximation. The contour lines show the percentage error in the evaluation of the polyionic work for a straight polyion, the distance of closest approach of the salt ions to the polyion charges being 4.5A.

an amount I given by

$$I=\int_0^1 \delta\epsilon d\lambda. \tag{52}$$

Now when C is small, $\lambda\sim\lambda_D$. Hence, from Eq. (49), we see that under such circumstances λ will be proportional to C. Furthermore, for small values of C, it can be shown that δ is proportional to C^3 and hence to λ^3.

We now define

$$P(\lambda^2)=\delta\epsilon/4\lambda^3, \tag{53}$$

and should expect it to be given by a power series in λ^2, i.e.,

$$P(\lambda^2)=A_0+A_2\lambda^2+A_4\lambda^4+A_6\lambda^6+\cdots. \tag{54}$$

If the coefficients of λ^4 and higher powers of λ were all zero, I would be given exactly by

$$I=P(\tfrac{2}{3}), \tag{55}$$

that is, by the value of $P(\lambda^2)$, when $\lambda^2=\frac{2}{3}$.

If Eq. (55) is not sufficiently accurate we have to include two more terms in our expression for $P(\lambda^2)$. In this case I will be given exactly by

$$I=\left(\frac{1}{2}-\frac{\sqrt{6}}{18}\right)P\left(\frac{6-\sqrt{6}}{10}\right)+\left(\frac{1}{2}+\frac{\sqrt{6}}{18}\right)P\left(\frac{6+\sqrt{6}}{10}\right)$$
$$=0.364P(\lambda_1^2)+0.636P(\lambda_2^2), \tag{56}$$

where $\lambda_1^2=0.355$, and $\lambda_2^2=0.845$.

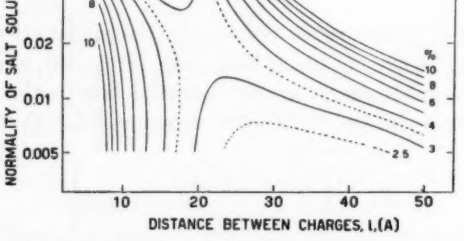

FIG. 3. Net error resulting from use of the Debye limiting law. The contour lines show the net percentage error in the polyionic work for a hypothetical straight polyion consisting only of charges of finite size. The distance of closest approach of the salt ions to the polyion charges was taken as 3.5A.

In general, $P(\lambda^2)$ was found to be a nearly linear function of λ^2 and in many cases, I was obtained with sufficient accuracy from Eq. (55) by evaluating $P(\frac{2}{3})$ by linear interpolation between two values of $P(\lambda^2)$. In other cases, we plotted $P(\lambda^2)$ against λ^2 for the three values of λ for which figures were available, read off the values of $P(\lambda_1^2)$ and $P(\lambda_2^2)$, and calculated I from Eq. (56).

Finally, we expressed this error, I, as a percentage of the polyionic work per charge as calculated from the Debye limiting law formula, Eq. (4).

5. DISCUSSION

The calculations described in section 4 were based on the simplest possible model, that of a hypothetical infinite straight rigid polyion having charges of finite diameter at equal intervals along its length; we shall discuss this case first, before considering that of a real polyion in which the uncharged atoms also occupy a finite volume.

If Eq. (11) is used to calculate the polyionic work per charge for such a hypothetical polyion, the result obtained will be too high owing to the high electric potentials prevailing. On the other hand, if, for the sake of simplicity, we use the Debye limiting law formula (Eq. (4)) instead of Eq. (11), then, apart from this positive error, we also introduce a negative error due to neglecting the finite size of the charges.

Both of these errors inherent in Eq. (4) were calculated and plotted against l, the distance between adjacent polyion charges, for a number of different concentrations of the 1−1 electrolyte present. Using these curves we then plotted the errors against the electrolyte concentration for a number of values of l. These two sets of graphs were then used to obtain Figs. 2, 3, 4, and 5, in which contour lines indicate the percentage error as a function of both the electrolyte concentration and the value of l.

The contour lines in Fig. 2 show the percentage error in the evaluation of the polyionic work according to Eq. (11), due to the nonvalidity of the Debye approxi-

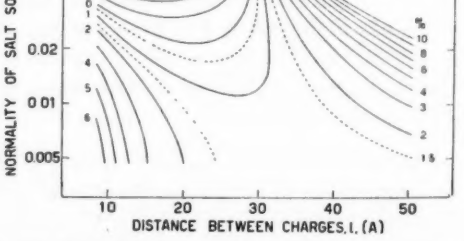

FIG. 4. Net error resulting from use of the Debye limiting law. The contour lines show the net percentage error in the polyionic work for a hypothetical straight polyion consisting only of charges of finite size. The distance of closest approach of the salt ions to the polyion charges was taken as 4.5A.

mation for the higher potentials. The high values of this percentage error occurring for small values of l can be attributed to the very high potentials existing near the polyion, whereas those occurring when l is large are due to the smallness of the polyionic work per charge under such circumstances. The contour lines in Fig. 2 were drawn assuming the distance of closest approach (a) of the salt ions to the polyion charges to be 4.5A; for larger values of a these errors will be smaller and *vice versa*, but the general shape of the contour diagram will remain unchanged.

Contour lines, corresponding to the net percentage error in the Debye limiting law value for the polyionic work, are shown in Figs. 3, 4, and 5 which are drawn for values of a of 3.5, 4.5, and 5.5A respectively. These diagrams indicate that the net error involved in the use of Eq. (4) will be relatively unimportant (amounting to not more than a few percent at the most) over a rather large range of l provided the electrolyte concentration is not too high. For high electrolyte concentrations we cannot generalize, since the net percentage error is then markedly dependent on the values of a and l.

In the case of a *real* polyion, the negative error, associated with the use of the Debye limiting law formula and the consequent neglect of steric effects, can be calculated approximately using expression (12). This error will be larger than the corresponding error in the case of the hypothetical polyion considered above consisting only of charges of finite size, but the difference will only become significant for the more concentrated electrolyte solutions. The general conclusions drawn above regarding the applicability of the Debye limiting law formula in dilute solutions of electrolyte will therefore remain unchanged. This is exemplified by Fig. 6 which shows the net percentage error in the Debye limiting law value for the polyionic work for the case of a *real* polyion of cylindrical form carrying charges at equal intervals l along its length. The distance of closest approach of a salt ion to the axis was taken as 4.5A.

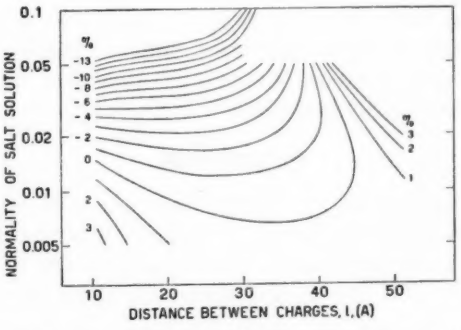

FIG. 5. Net error resulting from use of the Debye limiting law. The contour lines show the net percentage error in the polyionic work for a hypothetical straight polyion consisting only of charges of finite size. The distance of closest approach of the salt ions to the polyion charges was taken as 5.5A.

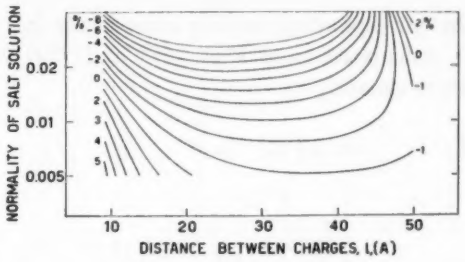

FIG. 6. Net error resulting from use of the Debye limiting law. The contour lines show the net percentage error in the polyionic work for a real polyion of cylindrical form, carrying charges at equal intervals along its axis. The distance of closest approach of the salt ions to the axis was taken as 4.5A.

It must be stressed that Figs. 2, 3, 4, 5, and 6 cannot be expected to provide much more than a general qualitative picture of the errors involved, owing to the large number of simplifying assumptions which have been made, the most serious of which may well be the use of the Poisson-Boltzmann equation itself.

ACKNOWLEDGMENTS

The author wishes to thank Prof. A. Katchalsky and Dr. J. Gillis of the Weizmann Institute of Science, Rehovoth, Israel, for helpful discussions, and Mr. H. Tabor of the Research Council of Israel for the use of a calculating machine.

APPENDIX I. FURTHER DETAILS OF STEPWISE INTEGRATIONS

The stepwise integration of Eq. (26) was carried out by means of the recurrence formulas

$$\Gamma_a(u)=\Gamma(u+\Delta u)-(\Delta u)\Gamma^I(u+\Delta u)+\tfrac{1}{2}(\Delta u)^2\Gamma_a{}^{II}(u+\Delta u), \quad (57)$$

and

$$-\Gamma^I(u)=-\Gamma^I(u+\Delta u)+\tfrac{1}{2}(\Delta u)\Gamma_a{}^{II}(u+\Delta u)+\tfrac{1}{2}(\Delta u)\Gamma_a{}^{II}(u). \quad (58)$$

In these equations, $\Gamma_a(u)$ represents an approximate value of $\Gamma(u)$ which is later corrected by the equation

$$\Gamma(u)=\Gamma_a(u)+\tfrac{1}{3}(\Delta u)^2[\tfrac{1}{2}\Gamma_a{}^{II}(u)-\tfrac{1}{2}\Gamma_a{}^{II}(u+\Delta u)], \quad (59)$$

while $\Gamma_a{}^{II}(u)$ represents the corresponding approximate value of $\Gamma^{II}(u)$ which is actually a sufficiently good approximation not to need subsequent correction.

By considering the terms omitted in Eqs. (57) and (58), involving higher powers of Δu, it can be shown that the relative error in the increment in $-\Gamma^I(u)$, calculated from Eq. (58), will be given approximately by

$$\frac{(\Delta u)^2}{12}\cdot\frac{\Gamma^{IV}(u)}{\Gamma^{II}(u)}=\frac{1}{12}\cdot\frac{\Delta^2[\tfrac{1}{2}\Gamma^{II}(u)]}{\tfrac{1}{2}\Gamma^{II}(u)}, \quad (60)$$

while the corresponding relative error in the increment in $\Gamma(u)$, calculated from Eqs. (57) and (59) will be given approximately by

$$\frac{(\Delta u)^3}{24}\cdot\frac{\Gamma^{IV}(u)}{\Gamma^{I}(u)}=\frac{\Delta u}{12}\cdot\frac{\Delta^2[\frac{1}{2}\Gamma^{II}(u)]}{\Gamma^{I}(u)}$$

$$=(\Delta u)\left(\frac{\frac{1}{2}\Gamma^{II}(u)}{\Gamma^{I}(u)}\right)\left(\frac{1}{12}\cdot\frac{\Delta^2[\frac{1}{2}\Gamma^{II}(u)]}{\frac{1}{2}\Gamma^{II}(u)}\right); \quad (61)$$

in these expressions, $\Delta^2[\frac{1}{2}\Gamma^{II}(u)]$ signifies the second difference in our tabulated values of $\frac{1}{2}\Gamma^{II}(u)$.

It should be noted that whereas the relative error in the increment in $-\Gamma^{I}(u)$ is proportional to $(\Delta u)^2$, that in the increment in $\Gamma(u)$ is proportional to $(\Delta u)^3$.

Equations (60) and (61) enabled us to verify that the value of Δu used at any stage was not too large to give the required accuracy. [The maximum permissible error in the increments in $\Gamma(u)$ and $-\Gamma^{I}(u)$ was taken as 3 parts per thousand.]

The stepwise integration of Eq. (38) was carried out in a similar manner.

APPENDIX II. THE NUMERICAL EVALUATION OF u_t AND χ_t

In order to facilitate the numerical evaluation of pairs of values of u_t and χ_t corresponding to a series of values of κl, Eq. (44) was written in the form

$$F(e^{u_t})-\log(e^{u_t})-\tfrac{1}{2}y\chi_t e^{-1/\chi_t}-\tfrac{1}{2}Ay\chi_t\sinh(1/\chi_t)=0, \quad (62)$$

where

$$F(e^{u_t})=(\log e)K_0(e^{u_t})+\log(e^{u_t}), \quad (63)$$

and

$$y=\kappa l\log e. \quad (64)$$

On eliminating κl from Eq. (4) by means of Eq. (64) we obtain

$$\tfrac{1}{2}Ay=y-\log[(\text{antilog}y)-1]. \quad (65)$$

The advantage of Eq. (62) over Eq. (44) lies in the fact that $F(e^{u_t})$ can be evaluated more accurately by linear interpolation than $K_0(e^{u_t})$.

For a given value of χ_t, a trial value for y was chosen and $\frac{1}{2}Ay$ and A evaluated from Eq. (65). The corresponding value of e^{u_t} was then obtained from Eq. (45) and tested in Eq. (62). The process was repeated until sufficient agreement was reached, when κl and u_t were evaluated.

THE JOURNAL OF CHEMICAL PHYSICS VOLUME 22, NUMBER 7 JULY, 1954

The Structure and Internal Motion of Hexachloroethane

D. A. Swick, I. L. Karle, and J. Karle
U. S. Naval Research Laboratory, Washington 25, D. C.

(Received June 18, 1953)

The equilibrium interatomic distances and their average amplitudes of vibration were determined for C_2Cl_6 by means of the microphotometer method in electron diffraction. Internal rotation was investigated, and the interdependence of the effects of the torsional mode and other modes of vibration on the *gauche* Cl—Cl distance is presented graphically.

An electron diffraction investigation of the structure of hexachloroethane has been performed by a microphotometer method,[1] which permitted a study of the nature of the internal motion of this molecule. In particular the effect of hindered rotation was of interest. An estimate of 10–15 kcal/mole for the potential barrier hindering internal rotation has been made by Morino and Iwasaki[2] using the visual method of electron diffraction. A more detailed study of the effect of the internal rotation is now possible due to the formulation of a theory which takes into account not only the effect of the torsional mode on the scattered electron intensity, but also that of the over-all vibration of the molecular frame.[3]

The structure of hexachloroethane has been studied previously by means of infrared and Raman spectroscopy,[4] x-ray,[5] and electron[2,6] diffraction. The molecule was found to be in the staggered position in the vapor and in the solid states, and the values of the equilibrium distances are in fair agreement with the results of this investigation.

PROCEDURE

The sample of cp hexachloroethane was obtained from the Eastman Kodak Company. Electron diffraction pictures were taken of the vapor, using a nozzle heated to 200–210°C. The camera distance was about

[1] (a) I. L. Karle and J. Karle, J. Chem. Phys. **17**, 1052 (1949). (b) J. Karle and I. L. Karle, J. Chem. Phys. **18**, 957 (1950). (c) I. L. Karle and J. Karle, J. Chem. Phys. **18**, 963 (1950).
[2] Y. Morino and M. Iwasaki, J. Chem. Phys. **17**, 216 (1949).
[3] J. Karle, J. Chem. Phys. **22**, 1246 (1954).
[4] See Landolt-Börnstein, *Zahlenwerte und Funktionen aus Physik, Chemie, Astronomie, Geophysik und Technik* (Springer-Verlag, Berlin, 1951), 1 Band, 2 Teil, p. 281; 3 Teil, p. 361.
[5] Y. Sasada and M. Atoji, J. Chem. Phys. **21**, 145 (1953).
[6] O. Hassel and H. Viervoll, Arch. Math. Naturvidenskab **B47**, 13 (1944).

11 cm, and the wavelength about 0.06A. The apparatus and the methods have been described in previous publications.[1] The experimental molecular scattering curve is shown at the top of Fig. 1. From the scattering curve, a radial distribution curve $f(r)$ was computed using Eq. (1) of reference 1(c). This was decomposed into individual peaks for each interatomic distance, and is shown in Fig. 2. The areas under the individual peaks multiplied by their respective equilibrium distances were made proportional to the coefficients in the theoretical scattering curves, and the peaks were made Gaussian in shape.[1] The positions of the maxima of the decomposed peaks indicate the equilibrium interatomic distances, while the widths of the peaks are related to the average amplitudes of vibration between pairs of atoms.

ANALYSIS

According to the decomposition of the radial distribution curve, Fig. 2, the equilibrium distances are

TABLE I. Equilibrium distances and average amplitudes of vibration.

	$r(A)$	$\langle l^2\rangle_{Av}^{\frac{1}{2}}(A)$[a]
C−C	$1.57+\alpha\pm0.06$	0.02 assumed
C−Cl	1.74 ± 0.01	<0.03
C−Cl	$2.70+\alpha\pm0.02$	0.03 ± 0.02
Cl−Cl	2.84 ± 0.01	$l_0\pm0.01$
Cl−Cl	$3.19+1/2\alpha\pm0.01$	see Fig. 5
Cl−Cl	$4.27+1/2\alpha\pm0.01$	0.08 ± 0.03

$<CCCl=109°40'-25\alpha°\pm30'$

where $l_0=\langle l^2\rangle_{Av}^{\frac{1}{2}}$ for 1, 1′−Cl atoms

$=0.06\begin{cases}+0.04\\-0.01\end{cases}$

and $\alpha=l_0-0.06$.

[a] The values for the average amplitudes of vibration may be compared with the theoretical values of Morino, Kuchitsu, Takahashi, and Maeda, J. Chem. Phys. 21, 1927 (1953).

~1.55A (C−C), 1.74A (bonded C−Cl), ~2.68A (nonbonded C−Cl), 2.84A ($Cl_1-Cl_{1'}$), 3.19A (*gauche* Cl−Cl), and 4.27A (*trans* Cl−Cl). The corresponding amplitudes of vibration were also obtained from the radial distribution curve. The *gauche*-peak will be discussed in detail later. Molecular intensity curves for assumed models, using reasonably exhaustive variations in all parameters, were computed using Eq. (34) of reference 1(b), and were compared with the experimental curve. The temperature factors for the acceptable models were varied as much as was required to produce a curve which differed significantly from the experimental curve, thus giving rise to the acceptable range reported in Table I. These curves served to establish the limits of error and the final results thus obtained were essentially the same as the values obtained from the radial distribution curve, i.e., each of the models with acceptable intensity curves can be fitted within the experimental limits of the radial distribution

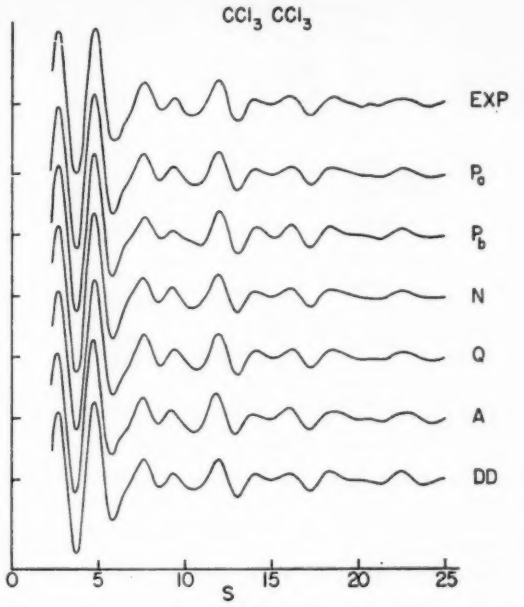

FIG. 1. Experimental and theoretical intensity curves.

curve. Some of the computed intensity curves are shown in Fig. 1. In the parameter chart, Fig. 3, each type of line separates models for which the computed curves are acceptable in a particular feature from those which are unsatisfactory or doubtful in that feature. Certain additional criteria used for rejecting intensity curves are discussed below but are not included in Fig. 3.

Curve P_a of Fig. 1 is that of the best model. Its agreement with the experimental curve is quite good, except in the vicinlty of the minimum at $s=5.8$. All computed curves show this minimum narrower and deeper than the experimental curve. This region is one of lower accuracy in the background line which represents atomic scattering.[1b] In the region $7<s<25$ the coefficients C_{ij} in the theoretical scattering curve are essentially constant, and were so considered.

Curve P_b is to be discussed below. An examination of the remaining curves in Fig. 1 reveals sets of borderline deviations from the experimental curve. They illustrate some of the particular features which determined the limits of the acceptable region of Fig. 3. In none of the rejected or borderline models could a combination of vibrational amplitudes be found which would substantially improve the agreement with the experimental

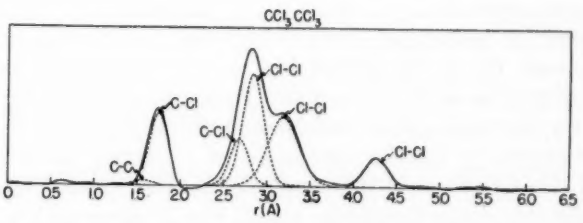

FIG. 2. Radial distribution curve. The dashed lines indicate the individual peaks for each interatomic distance.

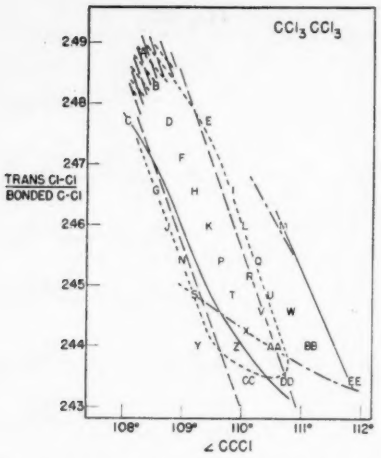

FIG. 3. Parameter chart. The positions of the letters indicate the parameters of the models for which intensity curves were computed. The various types of lines indicate the borderline of the acceptable region for certain particular features.

curve. The solid line of Fig. 3 concerns the height of the maximum at $s=7.66$, relative to the minimum at 8.62 which is too low in model N. The — — line concerns the region $8<s<10$. The maximum at 9.4 is too high relative to adjacent minima in N and in A, while the minimum at 8.6 is too deep in Q relative to adjacent maxima. The shape and depth of the next minimum, at $s=10.4$ are represented by the - - - - line of Fig. 3. Model Q shows this minimum distorted towards the right, while in A it is too deep and is distorted slightly towards the right; in DD it is too shallow. The weak maximum at $s=20.5$ is missing in curve N. The region $13.5<s<16.5$ is unsatisfactory in models Q, A, and DD. The maximum at $s=22.54$ has shifted to a higher s value in model A. The - - - - - line of Fig. 3 concerns the maximum at $s=11.92$, which is too shallow in DD. The region $s>18$ is also unsatisfactory in DD. The average deviation from the average s/s_{exp} ratio for the maxima and minima increases from ± 0.006 and ± 0.007 for models T and P to ± 0.009 and ± 0.010 for A and B.

The parameters of the model reported as their best by Morino and Iwasaki[2] fall between those of models X, Z, and AA of Fig. 3, while those of Hassel and Viervoll's[6] model lie roughly between Y and CC.

The results of this investigation are shown in Table I, where the $\langle l^2\rangle_{Av}^{\frac{1}{2}}$ are the rms amplitudes of vibration projected on the line connecting a pair of atoms at equilibrium,[1(b)] and have been corrected for spread of gas sample during exposure to the electron beam.[1(c)] The effect of uncertainty in the vibrational amplitudes is to extend the acceptable region of Fig. 3. Whereas the limits of error shown in Table I are all interdependent, this interrelationship was ignored except for the strong dependency on the amplitude of vibration between 1, 1′—Cl atoms. If this amplitude is large, models near the top of the parameter chart, Fig. 3, agree with experiment. If the 1, 1′—Cl distance is more rigid, the experimental data is satisfied only by models in the lower portion of the acceptable region of Fig. 3. This dependency is indicated by the quantity α in Table I.

Although the magnitude of α is determined by comparisons of intensity curves, the dependence of the errors on the amplitude of vibration of the 1, 1′—Cl atoms is apparent in the ambiguity which arises in the decomposition of the second large peak in the radial distribution curve, Fig. 2. It is possible to fit this peak, consistent with the criteria of area and shape, by covering a range of amplitudes for the 1, 1′—Cl vibration with associated changes in the two adjacent equilibrium distances. Although the uncertainty in the vibration of the 1, 1′—Cl atoms is large, the corresponding equilibrium interatomic distance is essentially constant within the region of acceptable models.

INTERNAL ROTATION

The theory of the combined effects of restricted internal rotation and over-all vibration of the molecular frame has been applied to C_2Cl_6. Those portions of the radial distribution curve, Fig. 2, which are related to interatomic distances affected by the torsional oscillation were fitted to a new function, $t(r)$, (Eq. (26), or Eq. (38) of reference 3.

The effect of the torsional oscillation on the *trans* Cl—Cl distance in C_2Cl_6 is quite small owing to the high potential barrier. As a consequence, (26) of reference 3 is essentially Gaussian in shape, and it is not possible to distinguish the contribution to the *trans* Cl—Cl vibration of the torsional mode from that of the other modes.

The effect of the torsional oscillation on the *gauche* distance is much more pronounced. Nevertheless the effects of the two types of motion in C_2Cl_6 cannot be separated within the accuracy of the experiment. Only the combined effect can be observed, and only the functional dependence of the possible combinations of vibrational modes can be presented.

The height of the potential barrier hindering internal rotation in hexachloroethane has been variously estimated to be of the order of 10 kcal/mole. With a barrier as large as 10 kcal/mole, Eq. (38) of reference 3, which was used to fit the *gauche* Cl—Cl peak of the radial distribution curve, is experimentally indistinguishable from a Gaussian function. It is, however, much broader than the Gaussian obtained[1] using the same values of

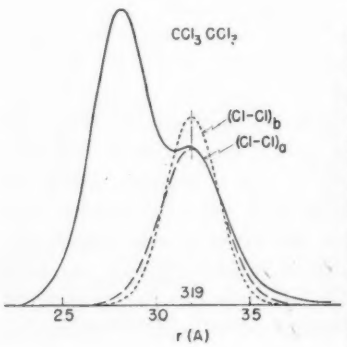

FIG. 4. An enlarged portion of the radial distribution curve. Curve $(Cl-Cl)_a$ was computed from an assumed potential barrier of 10 kcal and an over-all amplitude of 0.08A. Curve $(Cl-Cl)_b$ was computed by omitting the torsional oscillation and using only the amplitude of 0.08A. It is possible for either the torsional oscillation or the over-all vibration to independently satisfy the experimental data.

the other parameters but omitting the internal rotation. An additional difficulty arises from the fact that a portion of the *gauche*-peak in Fig. 2 is obscured by an adjacent peak in the experimental radial distribution curve. The Gaussian curve fitted to the *gauche* Cl—Cl peak in the radial distribution curve is much broader than the Gaussian curves for each of the other peaks. This broadness can be attributed either to a very large amplitude of vibration or to some internal rotation in addition to vibration or to internal rotation alone. In Fig. 4 the solid line is an enlarged portion of the experimental radial distribution curve. Curve $(Cl-Cl)_a$ was computed using Eq. (38) of reference 3 with an assumed potential barrier of 10 kcal and an over-all amplitude of 0.08A. Curve $(Cl-Cl)_b$ is a Gaussian drawn with the same area as curve $(Cl-Cl)_a$ for the same value of the over-all vibration, but no internal rotation. The intensity curve P_b of Fig. 1, corresponding to $(Cl-Cl)_b$ is quite unacceptable. The parameters of P_b are identical with those of P_a, except for the vibrational factor for the *gauche*-distance.

It is possible for a very large contribution from the over-all vibration to account independently for the experimental results. So, too, it is possible for a low potential barrier to independently account for the experimental results. This interdependence is illustrated graphically in Fig. 5 which was obtained in the following way.

A sine-like potential function was assumed which for small angles of rotation ϕ becomes

$$V=(9/4)V_0\phi^2, \tag{1}$$

where V_0 is the barrier height. The function $t(r)$ [Eq. (38) of reference 3] was approximated by

$$t'(r)=\exp[-G(\Gamma_e-\Gamma)^2], \tag{2}$$

where

$$G=Hb^2\Big/\left[\left(\frac{c_2S}{2\Gamma_e}\right)^2H+b^2\right] \tag{3}$$

and is determined by the experimental curves to be $18\pm2A^{-2}$. H is related[1] to the projected rms amplitude of vibration, $\langle l^2\rangle_{Av}^{\frac{1}{2}}$, and

$$b^2=-\frac{9}{4}\frac{V_0}{kT}, \tag{4}$$

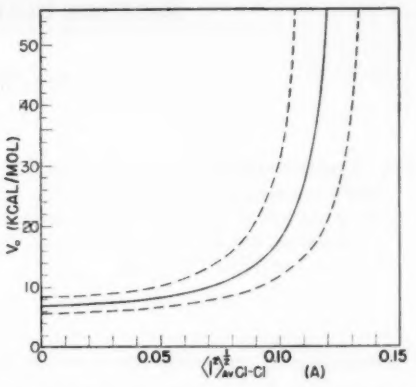

FIG. 5. Graph showing the corresponding values of the potential barrier hindering rotation and the rms projected amplitude from all modes except the torsional mode which would satisfy the experimental data for the *gauche* Cl—Cl distance.

where k is Boltzmann's constant, and T is the absolute temperature. The quantity c_2 involves[7] the largest and smallest possible distances of approach of 1,2—Cl atoms if the rotating groups could rotate freely, and is equal to $5.38A^2$, $S=\sin120°$, and $r_e=3.19A$. The errors introduced by this approximation are, in the case of hexachloroethane, less than the experimental error in G.

If the values of the parameters are substituted in (3), we obtain

$$V_0=HG/4.39(H-G). \tag{5}$$

This result is plotted in Fig. 5, where the dashed lines indicate the limits of experimental error. The minimum possible value of the potential barrier is 7 ± 1 kcal/mole, and the maximum possible value of the projected amplitude of vibration is $0.125\pm0.015A$.

An attempt to separate the two types of motion by performing the experiment at higher temperatures would not succeed since the temperature dependencies of the two effects are very similar for molecules with high potential barriers. This technique may succeed for molecules with smaller barriers.

We wish to thank Mr. Peter O'Hara of the Computation Laboratory of the Bureau of Standards for his cooperation with regard to the IBM computations required for this paper.

[7] J. Karle, J. Chem. Phys. **15**, 202 (1947).

Electron Scattering and Internal Rotation

J. KARLE
U. S. Naval Research Laboratory, Washington, D. C.
(Received June 18, 1953)

Theoretical functions are developed which facilitate the analysis of electron-scattering data from molecules which undergo internal rotation. The probability distributions for distances whose equilibrium positions occur anywhere on the circle of rotation are derived taking into account the combined effect of the over-all vibration of the molecular frame and the torsional motion. The extremes of small oscillations and free rotation are treated in detail.

THE possibility of studying the internal motion of gas molecules by means of a direct analysis of electron-scattering data was pointed out by P. Debye[1] in 1941. Debye showed that the Fourier transform of the molecular-scattering function, corrected for the variable atomic-scattering factors, gives the probability distribution for the distances between the pairs of atoms in a molecule. Methods for obtaining accurate molecular diffraction data by use of a rotating sector[2,3] and microphotometer have been developed in Norway,[4,5] and more recently the treatment of the data has been improved to permit the interpretation of the Fourier transform in terms of the vibrational motion of the molecule.[6–8] In order to facilitate the analysis of the Fourier transform, it is desirable to develop theoretical functions for the probability distributions describing the interatomic vibrations. In this paper we are concerned with the probability distributions associated with restricted internal rotation. In addition to this torsional oscillation, it is necessary to include the over-all vibration of the molecular frame. An analysis which includes both these types of motion has already been made[9] for the molecular configuration in the *trans*-position. This will be extended for any equilibrium position on the circle of rotation. The probability distribution associated with free rotation will also be derived. Since simple formulas, which avoid numerical integration, are obtained only for the extremes of free rotation and small vibrations, a knowledge of the character of both these extremes is helpful for the analysis of molecules falling in the intermediate range.

Generalized probability distributions which are comparable with those that arise from internal torsional motion have been studied and tabulated by Bauer and Coffin[10] and can be used for analyzing radial distribution curves. These were not based on a specific theoretical model for the potential barrier. In this paper a model for the potential barrier is assumed whose potential energy is a quadratic function of the angle of oscillation for small oscillations. The usual sine-like potential function falls into this class. The theory presented here has been applied to C_2Cl_6 in the previous paper. Its application to C_2F_6 and Si_2Cl_6 will be published in the near future.

THE PROBABILITY DISTRIBUTION FOR RESTRICTED ROTATION

It has been shown by James[11] that the probability distribution $\pi(r)$ for the distance r between a pair of atoms in a molecule, is of Gaussian form, assuming small vibrations and Hooke's law forces. The probability of finding an interatomic distance between r and $r+dr$ as a consequence of the general vibration of the molecular frame is, therefore,

$$\pi(r)dr=(h/\pi)^{\frac{1}{2}}\exp[-h(r-r_0)^2]dr, \quad (1)$$

where h is some constant and r_0 is an equilibrium or reference distance. In order to introduce the additional effect of internal rotation, it is plausible to assume that the contribution of the motion from the molecular frame does not vary significantly with small changes in the position of the atoms on the circle of internal rotation. We may thus preserve the form of (1) and define r_0 as various possible reference distances corresponding to positions on the circle of rotation that are governed by a probability law. We have for r_0, as a function of the angle of rotation ϕ,

$$r_0(\phi)=[c_1+c_2\cos(\phi_e+\phi)]^{\frac{1}{2}}, \quad (2)$$

where ϕ_e is an equilibrium angle on the circle of rotation, $c_1=(l_2^2+l_1^2)/2$ and $c_2=(l_2^2-l_1^2)/2$ and where l_2 is the maximum possible value of r_0 in the course of a complete rotation (*trans*-position) and l_1 is the smallest possible value of r_0 (*cis*-position). Equation (2) applies where the axis of rotation for each rotating end of a molecule is rigidly held on the same straight line. The probability, $P(r)dr$, of finding an interatomic distance r between r and $r+dr$ as a consequence of the over-all vibration of the molecular frame and the internal rotation is from (1) and (2), assuming independence of the probability functions,

$$P(r)dr=(h/\pi)^{\frac{1}{2}}\int_{-\infty}^{\infty}\exp\{-h[(c_1+c_2\cos(\phi_e+\phi))^{\frac{1}{2}}-r]^2\}\times P'(\phi)d\phi dr, \quad (3)$$

[1] P. Debye, J. Chem. Phys. **9**, 55 (1941).
[2] C. Finbak, Avhandl. Norske Videnskaps-Akad. Oslo, I. Mat. Naturv. Kl. No. 13 (1937).
[3] P. P. Debye, Physik. Z. **40**, 66, 404 (1939).
[4] H. Viervoll, Acta Chem. Scand. **1**, 120 (1947).
[5] O. Hassel and H. Viervoll, Acta Chem. Scand. **1**, 149 (1947).
[6] I. L. Karle and J. Karle, J. Chem. Phys. **17**, 1052 (1949).
[7] J. Karle and I. L. Karle, J. Chem. Phys. **18**, 957 (1950).
[8] I. L. Karle and J. Karle, J. Chem. Phys. **18**, 963 (1950).
[9] J. Karle and H. Hauptman, J. Chem. Phys. **18**, 875 (1950).
[10] K. P. Coffin, thesis, Cornell University, 1951.
[11] R. W. James, Physik. Z. **33**, 737 (1932).

where $P'(\phi)d\phi$ is the probability of finding ϕ between ϕ and $\phi+d\phi$. $P'(\phi)$ will now be evaluated.

It is assumed that the potential function hindering internal rotation has the form for small angles ϕ,

$$V=K\phi^2, \tag{4}$$

where K is some constant. It follows that the probability function for small oscillations $P'(\phi)$ which neglects the effect of the general vibration of the frame, is given by[12]

$$P'(\phi)d\phi=(b/\pi^{\frac{1}{2}})\exp(-b^2\phi^2)d\phi, \tag{5}$$

where b^2 is defined according to quantum theory by

$$b^2=\alpha\tanh(h\nu/2kT). \tag{6}$$

The quantity h is Planck's constant [not to be confused with the constant in (1)], k is Boltzmann's constant, T is the absolute temperature, $\alpha^2=8K\pi^2I/h^2$, $\nu^2=K/2I\pi^2$, and I is the reduced moment of inertia equal to $I_1I_2/(I_1+I_2)$, where I_1 and I_2 are the moments of inertia of the groups rotating at the ends of the molecule about the molecular axis. When $h\nu$ is small compared to kT, (6) reduces to the classical value[13]

$$b^2=K/kT. \tag{7}$$

We are now in a position to derive a theoretical function, $t(r)$, expressed in terms of the parameters associated with the internal rotation and the over-all vibration of the molecular frame, which may be compared with the Fourier sine transform of the experimental data. The function $t(r)$ is defined[6]

$$t(r)=\frac{c}{4}(\pi/a)^{\frac{1}{2}}\int_{-\infty}^{\infty}\frac{P(\rho)}{\rho}\exp[-(\rho-r)^2/4a]d\rho, \tag{8}$$

where c is a constant related to the interatomic distance under consideration, ideally the product of the atomic numbers of the pair of atoms involved, and a is a number chosen[6] so that the Fourier integral involving the molecular scattering intensity will converge rapidly.

The substitution of (3) and (5) into (8) gives

$$t(r)=\frac{bc}{4r_e}(h/\pi a)^{\frac{1}{2}}\int_{-\infty}^{\infty}\int_{-\infty}^{\infty}\times\exp\{-h[(c_1+c_2\cos(\phi_e+\phi))^{\frac{1}{2}}-\rho]^2-b\phi^2-(\rho-r)^2/4a\}d\rho d\phi, \tag{9}$$

where the approximation

$$\rho\sim r_e=(c_1+c_2\cos\phi_e)^{\frac{1}{2}} \tag{10}$$

has been introduced into the denominator of the integrand. Expression (9) becomes

$$t(r)=\frac{bcH^{\frac{1}{2}}}{2r_e}\int_{-\infty}^{\infty}\times\exp\{-H[(c_1+c_2\cos(\phi_e+\phi))^{\frac{1}{2}}-r]^2-b^2\phi^2\}d\phi, \tag{11}$$

where

$$H=h/(4ah+1). \tag{12}$$

The fitting of $t(r)$ to that portion of the Fourier transform of the experimental data which is associated with the internal rotation permits an evaluation of the parameters H and b which define this motion. The quantity h, which determines the contribution to the probability distribution (3) due to the general vibration of the molecular frame, is obtained from (12) from the evaluation of H and the known value of a. The quantity b which determines the contribution of the torsional motion to the probability distribution is obtained directly from the fitting of (11) to the experimental data. Except for large values of b, the fitting of $t(r)$ is performed by numerical integration of (11) for sets of values of unknown parameters. In the case of small $b(b<2)$, it should be recognized that the oscillations become much larger as b decreases and Eq. (5) will be in error. There will also be interaction between the torsional mode and the rest of the vibrational modes. The applicability of (11) decreases below $b=2$, the region of almost free rotation or low-barrier heights. For estimating the height of an assumed potential barrier which is quadratic at small angles, it is useful in the range of low-barrier heights to interpolate between the contribution of free rotation, to be derived below, and the contribution from (11) in the region $b=2$ or 3. For large values of $b(b>3)$ the integral of (11) can be evaluated to a good approximation and this will now be considered. These approximations have been developed, bearing in mind the geometry of the molecules to which this theory might be applied.

The exponent in the integrand of (11) is expanded about the point $\phi=0$, giving

$$t(r)=\frac{bcH^{\frac{1}{2}}}{2r_e}\exp[-H(r_e-r)^2]\int\times\exp(f_1\phi-f_2\phi^2+f_3\phi^3-f_4\phi^4)d\phi, \tag{13}$$

where

$$f_1=Hc_2S(r_e-r)/r_e, \tag{14}$$

$$f_2=Hc_2^2S^2/4r_e^2-H(r_e-r)\times(c_2^2S^2/4r_e^3+c_2C/2r_e)+b^2, \tag{15}$$

$$f_3=-Hc_2^3S^3/8r_e^4-Hc_2^2SC/4r_e^2-H(r_e-r)(c_2S/6r_e-c_2^2CS/4r_e^3-c_2^3S^3/8r_e^5), \tag{16}$$

$$f_4\sim 3Hc_2^3CS^2/16r_e^4+Hc_2^2C^2/16r_e^2-Hc_2^2S^2/12r_e^2, \tag{17}$$

and

$$S=\sin\phi_e,\quad C=\cos\phi_e. \tag{18}$$

[12] J. Karle, J. Chem. Phys. **15**, 202 (1947).

[13] For the potential function, $V=V_0(1-\cos3\phi)/2$, we have $b^2=9V_0/4kT$ since $V=9V_0\phi^2/4$ for small angles. Thus, for this potential barrier, we have at room temperature $b^2=3.8V_0$, affording an estimate of b^2 and the applicability of the equations to be derived on the basis of anticipated values for the barrier height, V_0 (in kcal).

The first approximation to (13) involves expanding the exponential of the first and third powers of the polynomial in the exponent of the integrand. From the transformation $f_4\phi^4=w^4$ (13), becomes

$$t(r)=\frac{bc}{2r_e}(H/f_4^{\frac{1}{4}})^{\frac{1}{2}}\exp[-H(r_e-r)^2]\int \times\exp(Pw+2Qw^2+Rw^3-w^4)dw, \quad (19)$$

where

$$P=f_1/f_4^{\frac{1}{4}}, \quad (20)$$

$$2Q=-f_2/f_4^{\frac{1}{2}}, \quad (21)$$

$$R=f_3/f_4^{\frac{3}{4}}. \quad (22)$$

Taking the Maclaurin expansion of $\exp(Pw+Rw^3)$ leads to a form for (19) which may be evaluated. The number of terms which are used in the application of the formula is determined as usual by the rapidity of the convergence of the series for the parameters of interest. If a large number of terms are involved, the computation of this formula may be more tedious than the direct numerical evaluation of (11). An evaluation of (19) will be presented below for a three term expansion of $\exp(Pw+Rw^3)$ giving a formula which is useful for large b in the vicinities of $\phi_e=0$ (*trans*-position) and $\phi_e=\pi$ (*cis*-position). This formula may be readily extended for more terms in the expansion of the exponential if desired.

The first three terms of the Maclaurin expansion of $\exp(Pw+Rw^3)$ are taken and odd powers of w are ignored, since they lead to an odd integrand whose integral is equal to zero. This gives for (19)

$$t(r)=\frac{bc}{2r_e}(H/f_4^{\frac{1}{4}})^{\frac{1}{2}}\exp[-H(r_e-r)^2]\times\int_{-\infty}^{\infty}(1+Pw^2/2+PRw^4+R^2w^6/2)\times\exp(2Qw^2-w^4)dw. \quad (23)$$

From the value of the integral[14]

$$\int_{-\infty}^{\infty}\exp(2Qw^2-w^4)dw=(Q^2/4)^{\frac{1}{4}}\exp(Q^2/2)K_{\frac{1}{4}}(Q^2/2), \quad Q<0 \quad (24)$$

and its successive derivatives with respect to Q, (23) may be readily evaluated to give,

$$t(r)=\frac{bc}{2r_e}(Q^2/4)^{\frac{1}{4}}(H/f_4^{\frac{1}{4}})^{\frac{1}{2}}\exp[-H(r_e-r)^2+Q^2/2]\times\{K_{\frac{1}{4}}(Q^2/2)+P^2Q[K_{\frac{1}{4}}(Q^2/2)-K_{\frac{3}{4}}(Q^2/2)]/4+PR[(1+2Q^2)K_{\frac{1}{4}}(Q^2/2)-2Q^2K_{\frac{3}{4}}(Q^2/2)]/4+R^2[(5Q+4Q^3)K_{\frac{1}{4}}(Q^2/2)-(3Q+4Q^3)K_{\frac{3}{4}}(Q^2/2)]/16\}. \quad (25)$$

[14] D. R. Hartree and S. Johnston, Manchester Memoirs **83**, 183 (1938–39).

Equation (25) is useful within about 10° of the *cis*- and *trans*-positions for large b.

If equilibrium occurs in the *trans*-position, i.e., $\phi_e=0$, we obtain from (25)

$$t_{\phi_e=0}(r)=bc(H^{\frac{1}{2}}/2c_2l_2)^{\frac{1}{2}}(Q^2)^{\frac{1}{4}}\times\exp[-H(l_2-r)^2+Q^2/2]K_{1/4}(Q^2/2), \quad Q<0, \quad (26)$$

where

$$Q=H^{\frac{1}{2}}(l_2-r)-2l_2b^2/H^{\frac{1}{2}}c_2. \quad (27)$$

A comparison of formula (26) with (26) of reference 9 shows that the two formulas are the same to a satisfactory approximation for the values of the parameters arising in practice. This is of significance since the function in reference 9 was derived in a somewhat different fashion than was employed here.

To cover the intermediate range $10°<\phi_e<170°$ we make a second type of approximation to (13) which involves keeping a second power in the exponential and expanding the exponential of the remaining powers. The following transformation is made on (13),

$$f_1\phi-f_2\phi^2=-(E+F\phi)^2+G, \quad (28)$$

giving

$$E=-f_1/2f_2^{\frac{1}{2}}, \quad (29)$$

$$F=f_2^{\frac{1}{2}}, \quad (30)$$

$$G=f_1^2/4f_2. \quad (31)$$

Making the further substitution into (13),

$$v=E+F\phi, \quad (32)$$

leads to

$$t(r)=\frac{bc}{2r_e}(H/f_2)^{\frac{1}{2}}\times\exp[-H(r_e-r)^2+E^2-f_3E^3/F^3-f_4E^4/F^4]\times\int\exp(k_1v-k_2v^2+k_3v^3+k_4v^4)dv, \quad (33)$$

where

$$k_1=3f_3E^2/F^3+4f_4E^3/F^4, \quad (34)$$

$$k_2=1+3Ef_3/F^3+6E^2f_4/F^4, \quad (35)$$

$$k_3=f_3/F^3+4Ef_4/F^4, \quad (36)$$

$$k_4=-f_4/F^4. \quad (37)$$

The exponential $\exp(k_1v+k_3v^3+k_4v^4)$ is now expanded and (33) is evaluated. The first four terms of the expansion are considered here. The result, on integrating between infinite limits, is

$$t(r)=\frac{bc}{2r_e}(H\pi/k_2f_2)^{\frac{1}{2}}\times\exp[-H(r_e-r)^2+E^2-f_3E^3/F^3-f_4E^4/F^4]\times\{1+3k_4/4k_2^2+(k_1^2/k_2+3k_1k_3/k_2^2+15k_3^2/4k_2^3+105k_4^2/8k_2^4)/4+15k_4(k_1^2/k_2^3+7k_1k_3/k_2^4+63k_3^2/4k_2^5+231k_4^2/8k_2^6)/16\}. \quad (38)$$

Expression (38) is useful for large b in the range $10°<\phi_e<170°$. Equations (25) and (38) can be applied when $b<3$. In this case the curve fit should be checked by a numerical integration of (11). [Note previous discussion on applicability of (11) for $b<2$.]

INTENSITY FUNCTION FOR RESTRICTED ROTATION

The contribution to the molecular scattering from a restricted rotator is

$$i_m=c\int P(r)(\sin sr/sr)dr, \tag{39}$$

where $P(r)$ is defined by (3). From (3) and neglecting the small variation of r in the denominator of the integrand of (39), we have

$$i_m=\frac{c}{s}\{h/[\pi(c_1+c_2\cos\phi_e)]\}^{\frac{1}{2}}\int_{-\infty}^{\infty}\int_{-\infty}^{\infty}P'(\phi)\sin sr \times\exp\{-h[(c_1+c_2\cos(\phi_e+\phi))^{\frac{1}{2}}-r]^2\}drd\phi. \tag{40}$$

Substituting the transformation,

$$Y=[c_1+c_2\cos(\phi_e+\phi)]^{\frac{1}{2}}-r \tag{41}$$

and (5) into (40) and evaluating the resulting integral gives,

$$i_m=\frac{bc}{s}\{1/[\pi(c_1+c_2\cos\phi_e)]\}^{\frac{1}{2}}\exp(-s^2/4h) \times\int_{-\infty}^{\infty}\sin\{s[c_1+c_2\cos(\phi_e+\phi)]^{\frac{1}{2}}\} \times\exp(-b^2\phi^2)d\phi. \tag{42}$$

If we define r_e as in (10), we have the following Maclaurin expansion,

$$[c_1+c_2\cos(\phi_e+\phi)]^{\frac{1}{2}} =r_e-c_2S\phi/2r_e-c_2(C+c_2S^2/2r_e^2)\phi^2/4r_e+\cdots \tag{43}$$

$$=r_e+T\phi+U\phi^2+\cdots, \tag{44}$$

where

$$T=-c_2S/2r_e, \tag{45}$$

$$U=-c_2(C+c_2S^2/2r_e^2)/4r_e. \tag{46}$$

We thus have on substituting (44) into (42)

$$i_m=\frac{bc}{sr_e\pi^{\frac{1}{2}}}\exp(-s^2/4h)\int_{-\infty}^{\infty} \times\exp(-b^2\phi^2)\sin(sr_e+sT\phi+sU\phi^2)d\phi, \tag{47}$$

which is equal to[12]

$$i_m=\frac{c}{sr_e}(\cos\theta)^{\frac{1}{2}}\exp(-s^2/4h-s^2T^2\cos^2\theta/4b^2) \times\sin(sr_e-sT^2\sin^2\theta/4U+\theta/2), \tag{48}$$

where

$$\tan\theta=sU/b^2. \tag{49}$$

PROBABILITY DISTRIBUTION FOR FREE ROTATION

From (3) and the fact that

$$P'(\phi)d\phi=d\phi/2\pi \tag{50}$$

for free rotation, we have for the probability of finding an interatomic distance between r and $r+dr$ as a consequence of the over-all vibration of the molecular frame and the free rotation,*

$$P(r)dr=(h/\pi)^{\frac{1}{2}}\int_0^{2\pi} \times\exp\{-h[(c_1+c_2\cos\phi)^{\frac{1}{2}}-r]^2\}drd\phi/2\pi. \tag{51}$$

The substitution of (51) into (8) and integrating over ρ gives

$$t(r)=\frac{c}{4}(H/\pi)^{\frac{1}{2}}\int_0^{2\pi}(\exp\{-H[(c_1+c_2\cos\phi)^{\frac{1}{2}}-r]^2\}/ (c_1+c_2\cos\phi)^{\frac{1}{4}})d\phi, \tag{52}$$

where the variable ρ in the denominator of (8) is replaced by $(c_1+c_2\cos\phi)^{\frac{1}{2}}$. The main contribution to (52) occurs in the vicinity of $(c_1+c_2\cos\phi)^{\frac{1}{2}}=r$, or, when this relation cannot be fulfilled, the main contribution occurs in the vicinity of the closest approach of $(c_1+c_2\cos\phi)^{\frac{1}{2}}$ to the value of r. In order to evaluate (52), we therefore expand $(c_1+c_2\cos\phi)^{\frac{1}{2}}$ about the point ϕ_r where ϕ_r is defined as follows:

Case (a), $r\leq l_1$, $\phi_r=\cos^{-1}-1$,

Case (b), $l_1<r<l_2$, $\phi_r=\cos^{-1}[(r^2-c_1)/c_2]$,

Case (c), $r\geq l_2$, $\phi_r=\cos^{-1}1$.

Case (a)

The Taylor expansion of $(c_1+c_2\cos\phi)^{\frac{1}{2}}$ about ϕ_r for case (a) is,

$$(c_1+c_2\cos\phi)^{\frac{1}{2}}=l_1+c_2(\phi-\pi)^2/4l_1-\cdots. \tag{53}$$

We make the transformations

$$w_1=(\phi-\pi)(c_2H^{\frac{1}{2}}/4l_1)^{\frac{1}{4}}, \tag{54}$$

$$q_1=-H^{\frac{1}{2}}(l_1-r), \tag{55}$$

and substitute (53) into (52), obtaining

$$t(r)=(cH^{\frac{1}{2}}/(4\pi l_1c_2)^{\frac{1}{2}})\int_{-\infty}^{\infty}\exp[-(q_1-w_1^2)^2]dw_1, \tag{56}$$

where the limits on the integral have been changed to infinity with negligible error. We thus obtain[14]

$$t(r)=(cH^{\frac{1}{2}}/(16\pi l_1c_2)^{\frac{1}{2}})(-2q_1)^{\frac{1}{2}}K_{1/4}(q_1^2/2) \times\exp(-q_1^2/2),\quad q_1\leq 0 \tag{57}$$

which should be used when $r\leq l_1$.

* In this treatment it is assumed that the contribution from the frame is independent of the angle of rotation ϕ.

Case (b)

The Taylor expansion of $(c_1+c_2\cos\phi)^{\frac{1}{2}}$ about ϕ_r for case (b) is

$$(c_1+c_2\cos\phi)^{\frac{1}{2}} = r-c_2\sin\phi_r(\phi-\phi_r)/[2(c_1+c_2\cos\phi_r)^{\frac{1}{2}}] - (c_2^2\sin^2\phi_r/[4(c_1+c_2\cos\phi_r)^{\frac{3}{2}}]+c_2\cos\phi_r/[2(c_1+c_2\cos\phi_r)^{\frac{1}{2}}])(\phi-\phi_r)^2/2+\cdots. \quad (58)$$

We set $w_2=\phi-\phi_r$, substitute (58) into (52), and obtain

$$t(r)=\frac{c}{4r}(H/\pi)^{\frac{1}{2}}\int_{-\infty}^{\infty}\exp[-(mw_2+nw_2^2)^2]dw_2, \quad (59)$$

where

$$m=H^{\frac{1}{2}}c_2\sin\phi_r/[2(c_1+c_2\cos\phi_r)^{\frac{1}{2}}], \quad (60)$$

and

$$n=H^{\frac{1}{2}}(c_2^2\sin^2\phi_r/[8(c_1+c_2\cos\phi_r)^{\frac{3}{2}}] +c_2\cos\phi_r/[4(c_1+c_2\cos\phi_r)^{\frac{3}{2}}]). \quad (61)$$

The evaluation of (59) gives[14]

$$t(r)=\frac{c}{8r}(\pi Hq_2/|n|)^{\frac{1}{2}}[I_{-\frac{1}{4}}(q_2^2/2)+I_{\frac{1}{4}}(q_2^2/2)] \times\exp(-q_2^2/2), \quad q_2\geq 0, \quad n\neq 0, \quad (62)$$

where

$$q_2=m^2/4|n|. \quad (63)$$

Expression (62) should be used when $l_1<r<l_2$.

Case (c)

The Taylor expansion of $(c_1+c_2\cos\phi)^{\frac{1}{2}}$ about ϕ_r for case (c) is,

$$(c_1+c_2\cos\phi_r)^{\frac{1}{2}}=l_2-c_2\phi^2/4l_2+\cdots. \quad (64)$$

We make the transformations,

$$w_3=(H^{\frac{1}{2}}c_2/4l_2)^{\frac{1}{2}}\phi, \quad (65)$$

$$q_3=H^{\frac{1}{2}}(l_2-r) \quad (66)$$

and substitute (64) into (52), obtaining

$$t(r)=(cH^{\frac{1}{2}}/(4\pi c_2l_2)^{\frac{1}{2}})\int_{-\infty}^{\infty}\exp[-(q_3-w_3^2)^2]dw_3. \quad (67)$$

We obtain

$$t(r)=(cH^{\frac{1}{2}}/(16\pi c_2l_2)^{\frac{1}{2}})(-2q_3)^{\frac{1}{2}}K_{1/4}(q_3^2/2) \times\exp(-q_3^2/2), \quad q_3\leq 0 \quad (68)$$

which should be used when $r\geq l_2$.

INTENSITY FUNCTION FOR FREE ROTATION

The contribution to the molecular scattering from a free rotator is obtained from (3), (39), and (50). We obtain

$$i_m=c(h/\pi)^{\frac{1}{2}}\int_0^{2\pi}\int_{-\infty}^{\infty}(\sin sr/[s(c_1+c_2\cos\phi)^{\frac{1}{2}}]) \times\exp\{-h[(c_1+c_2\cos\phi)^{\frac{1}{2}}-r]^2\}drd\phi/2\pi, \quad (69)$$

where the variable r in the denominator has been replaced to a good approximation by its equilibrium value for a given ϕ. We obtain from the integration with respect to r,

$$i_m=c\exp(-s^2/4h)\int_0^{2\pi}(\sin[s(c_1+c_2\cos\phi)^{\frac{1}{2}}]/[s(c_1+c_2\cos\phi)^{\frac{1}{2}}])d\phi/2\pi. \quad (70)$$

This integral has been evaluated[1,15] and the result is asymptotically,

$$i_m\sim\frac{c\exp(-s^2/4h)}{(\pi p)^{\frac{1}{2}}x^{\frac{3}{2}}}[S(x,p,\pi/4)\sigma_1(p)+C(x,p,\pi/4)\sigma_2(p) +S(x,-p,-\pi/4)\sigma_1(-p) +C(x,-p,-\pi/4)\sigma_2(-p)], \quad (71)$$

where

$$\begin{matrix}S\\C\end{matrix}(x,p,\pi/4)=\begin{matrix}\sin\\\cos\end{matrix}[x(1-p)^{\frac{1}{2}}+\pi/4]/(1-p)^{\frac{1}{4}}, \quad (72)$$

$$\sigma_1(p)=1-3b_2/4x^2+\cdots, \quad (73)$$

$$\sigma_2(p)=b_1/2x-15b_3/8x^3+\cdots, \quad (74)$$

$$b_1=(2-3p)/[4p(1-p)^{\frac{1}{2}}], \quad (75)$$

$$b_2=(12-20p+11p^2)/[32p^2(1-p)], \quad (76)$$

$$b_3=(40-132p+166p^2-79p^3)/[128p^3(1-p)^{\frac{3}{2}}], \quad (77)$$

$$p=c_2/c_1, \quad x=sc_1^{\frac{1}{2}}. \quad (78)$$

Graphs of the intensity function for free rotation modulated by harmonic motions of the molecular frame may be found in the thesis of Coffin.[10]

[15] J. Karle, J. Chem. Phys. **13**, 155 (1945).

Virial Expansion of the Osmotic Pressure in the Donnan Membrane Equilibrium*

TERRELL L. HILL
Naval Medical Research Institute, Bethesda, Maryland
(Received March 22, 1954)

Two methods for refining the usual Donnan treatment of the Donnan membrane equilibrium are introduced and compared. One method is to apply the McMillan-Mayer solution theory while the second method involves modifying the Donnan treatment to include Debye-Hückel corrections to activity coefficients and osmotic pressure expressions.

ON one side (the "outside") of a semipermeable membrane we have an aqueous solution of an electrolyte, the jth species of which has a valence z_j and a concentration (molecules/cc) c_j^0. On the other side (the "inside") of the membrane, the jth species has a concentration c_j. In addition, there is (on the inside) an ion of valence z and concentration ρ which cannot pass through the membrane. Let ψ be the membrane potential.

If the inside and outside solutions are assumed ideal, one finds by the Donnan method (equating inside and outside electrochemical potentials of diffusible ions) the well-known results

$$\epsilon\psi/kT=(\rho z/\sum^{(2)})+\cdots \tag{1}$$

$$B_2=z^2/2\sum^{(2)}=2\pi\epsilon^2z^2/DkT\kappa^2 \tag{2}$$

where B_n is the nth virial coefficient in the osmotic pressure expansion (in powers of ρ), $\epsilon=|\text{electronic charge}|$ and

$$\sum^{(n)}=\sum_j c_j^0 z_j^n \tag{3}$$

$$\kappa^2=4\pi\epsilon^2\sum^{(2)}/DkT. \tag{4}$$

Two refinements (assuming point charges) of this usual treatment are the following: (1) use the McMillan-Mayer method[1] with the Debye-Hückel limiting potential of average force between a pair of nondiffusible ions immersed in the outside solution:

$$W(r)=z^2\epsilon^2e^{-\kappa r}/Dr; \tag{5}$$

(2) use the Donnan method but assume the Debye-Hückel limiting law is followed (for activity coefficients and osmotic pressure) in the inside as well as in the outside solution.

In the McMillan-Mayer case (1) it is easy to calculate the first few virial coefficients to linear terms in $\alpha=\epsilon^2\kappa/DkT$:

$$B_2-(z^2/2\sum^{(2)})-(z^4\alpha/8\sum^{(2)}), \tag{6}$$

$$B_3=z^6\alpha/24(\sum^{(2)})^2, \tag{7}$$

$$B_4=-3z^8\alpha/128(\sum^{(2)})^3. \tag{8}$$

Although Eqs. (6)–(8) are correct *for the potential of Eq. (5)*, it cannot be assumed that these equations are exact as leading terms for a system of point charges, since, as Mayer has pointed out in another connection,[2] higher terms not included in Eq. (5) might affect higher virial coefficients. In fact, one can show[1] that the third and higher virial coefficients are certainly not exact in this sense. The first term in Eq. (6) [deduced from Eq. (5)] agrees with Eq. (2) (deduced without use of the Debye-Hückel theory). This may be regarded as a confirmation of the Debye-Hückel limiting law. Incidentally, for the potential

$$W(r)=+\infty \quad r<a$$
$$=z^2\epsilon^2e^{-\kappa(r-a)}/Dr(1+\kappa a) \quad r\geqslant a \tag{9}$$

one finds [including terms in $(1/kT)^{\frac{1}{2}}$]

$$B_2=\frac{2\pi a^3}{3}+\frac{z^2}{2\sum^{(2)}}-\frac{z^4\alpha}{8(1+\kappa a)^2\sum^{(2)}} \tag{10}$$

$$B_3=\frac{5\pi^2a^6}{18}+\pi^2a^5\left[\frac{z^2\epsilon^2}{DkT(1+\kappa a)}\right]\left(\frac{11}{15}-\frac{19}{90}\kappa a+\cdots\right)$$
$$+\frac{8\pi^2a^3}{3}\left[\frac{z^2\epsilon^2}{DkT(1+\kappa a)}\right]^2\frac{e^{2\kappa a}}{\kappa}(1+\cdots)$$
$$+\frac{2\pi^2}{3}\left[\frac{z^2\epsilon^2}{DkT(1+\kappa a)}\right]^3\frac{e^{-\kappa a}}{\kappa^3}. \tag{11}$$

Equation (9) is the limiting potential if all ions have a hard core of diameter a. It is also an *approximate* potential for a pair of large, nondiffusible particles of uniform surface charge z and diameter a, with the diffusible ions considered as point charges.[3] It seems

* Summarized at a Gordon Research Conference on Proteins and Nucleic Acids, New Hampton, N. H., August 25, 1953. A much more detailed account of this work is available as Naval Medical Research Institute Report NM 000 018.06.35 by T. L. Hill. See also T. L. Hill in *Ion Transport Across Membranes* (Academic Press, New York, 1954), edited by H. T. Clarke.

[1] W. G. McMillan and J. E. Mayer, J. Chem. Phys. **13**, 276 (1945). A review of the McMillan-Mayer solution theory is available as Naval Medical Research Institute Report 54-2 by T. L. Hill.

[2] J. E. Mayer, J. Chem. Phys. **18**, 1426 (1950), p. 1427.

[3] E. J. W. Verwey and J. Th. G. Overbeek, *Theory of the Stability of Lyophobic Colloids* (Elsevier Publishing Company, Amsterdam, 1948).

probable that when the correct potential of average force is used for any pair of molecules with a fixed charge z, regardless of how dilute or concentrated the outside solution, B_2 will consist of the first term in Eq. (6) (which is independent of T, D, molecular size and shape, etc.) plus other terms (not independent of these factors). See, for example, Eq. (10).

In the Donnan case (2), above, it is also certain that the third and higher virial coefficients are not exact in the sense mentioned since in special cases the third virial coefficient turns out to be negative,* which is impossible with strictly repulsive forces between non-diffusible ions. One finds, instead of Eqs. (1) and (2) ($\alpha=0$),

$$\frac{e\psi}{kT}=\left[\frac{z}{\sum^{(2)}}+\frac{\alpha\sum^{(3)}}{4(\sum^{(1)})^2}\left(z^2-z\frac{\sum^{(3)}}{\sum^{(2)}}\right)\right]\rho+\cdots \quad (12)$$

$$B_2=\frac{z^2}{2\sum^{(2)}}-\frac{\alpha}{8\sum^{2)}}\left(z^2-z\frac{\sum^{(3)}}{\sum^{2)}}\right)^2. \quad (13)$$

The second terms in Eqs. (6) and (13) agree whenever $\sum^{(3)}=0$; it is difficult to decide which second term, if either, is exact for point charges when $\sum^{(3)}\neq 0$ without having available an exact extension of the Debye-Hückel theory to higher concentrations.

THE JOURNAL OF CHEMICAL PHYSICS VOLUME 22, NUMBER 7 JULY, 1954

A Note on the Flow of Gases through Very Fine Tubes

G. W. SEARS
General Electric Research Laboratory, Schenectady, New York

(Received November 24, 1953)

It is shown that Knudsen's laws of flow for rarefied gases must be modified for very fine tubes. Gas flow occurs by diffusion of molecules in the adsorbed layer on the tube walls as well as in the gas phase. When the tube dimension is comparable to the mean free path in the gas film, the two flow mechanisms become comparable in effectiveness.

EARLY experimenters[1,2] discovered that rarefied gases do not obey Poisseuille's law of viscous flow. However, Knudsen[3] in 1909 first quantitatively derived and experimentally verified the laws of flow for rarefied gases. These laws are valid when the mean free path of gas molecules exceeds the least cross-sectional dimension of the tube through which gas is flowing. Knudsen's derivation was based on classical kinetic theory of gases with the additional postulate that gas molecules are reflected from the tube walls according to the cosine law and independently of their direction before impact. In effect, the reflected molecules forget their direction of motion before impact. It is the purpose of the present paper to point out that the accepted reflection mechanism leads to a significantly modified law of gas flow through very fine tubes.

Knudsen[3] assumed that the cosine reflection law was caused by irregular roughness of the tube surface on an atomic scale. However, the work of Langmuir[4,5] and Volmer and Estermann[6] demonstrated that gas molecules are not reflected at solid surfaces by a simple impact and rebound mechanism. Rather, gas molecules are adsorbed on impact and after a surface lifetime τ_s, they are evaporated. Every surface, no matter how smooth, will reflect gas molecules according to a cosine law. There are a very few exceptions to the adsorption-evaporation reflection mechanism. Estermann and Stern,[7] for example, have demonstrated the wave nature of He atoms and H_2 molecules by diffraction at a LiF cleavage surface. The same mechanism is valid for both condensable and noncondensable gases. The root mean square distance, λ_x traversed by an adsorbed molecule in its lifetime τ_s, is given by

$$\lambda_x^2=2D_s\tau_s \quad (1)$$

where D_s is the coefficient of surface diffusion. Equation (1) was derived by Einstein[8] in his earliest paper on Brownian motion.

Returning to Knudsen's equation for the rate of molecular flow, it is apparent that a significant modification must be made for tubes, whose least cross-sectional dimension b approaches λ_x for adsorbed gas molecules on the solid surface. If it is assumed that the adsorbed film is in equilibrium with the gaseous phase, then surface diffusion and molecular flow are driven by the same free energy gradient and if

$$\lambda_x=b, \quad (2)$$

a given molecule travels as far in the adsorbed phase as in the gaseous phase in its passage through the tube.

[1] A. Kundt and E. Warburg, Pogg. Ann. **155**, 337 and 525 (1875).
[2] E. Warburg, Pogg. Ann. **159**, 399 (1876).
[3] M. Knudsen, Ann. Physik **28**, 75 (1909).
[4] I. Langmuir, Phys. Rev. **8**, 149 (1916).
[5] I. Langmuir, J. Am. Chem. Soc. **38**, 2250 (1916).
[6] M. Volmer and I. Estermann, Z. Physik **7**, 13 (1921).
[7] I. Estermann and O. Stern, Z. Physik **61**, 95 (1930).
[8] A. Einstein, Ann. Physik **17**, 549 (1905).

Clausing[9] has previously postulated a similar model for the molecular flow of gases through very fine tubes. His analysis was unsatisfactory because his mechanism of surface diffusion is at variance with experimental evidence. In passing it should be noted that Flood and co-workers[10] and Carman[11] have proposed a flow contribution of the adsorbed layer. They were concerned with higher pressure flow and their treatment is unrelated to the analysis in this paper.

If the principle of microscopic reversibility is valid, the same number of gas molecules are adsorbed and desorbed per unit time for any element of tube length. The assumption of microscopic reversibility and the cosine law of reflection are sufficient to insure that the laws of molecular flow are valid for the flow of molecules in the gas phase. The rate $\dot{n}$ at which molecules pass a given cross section in steady state flow is given by:

$$\dot{n}=-D_s\cdot o\cdot\frac{\partial\sigma}{\partial X}-\frac{8}{3}\left(\frac{2}{\pi mkT}\right)^{\frac{1}{2}}\frac{A^2}{o}\frac{\partial p}{\partial X} \tag{3}$$

where σ is the surface concentration of *ad* atoms, ρ is the gas density, A is the tube cross-sectional area, o is the cross-sectional periphery, and m is the mass of a molecule. A relation between surface concentration and pressure may be established by equating the rate of impingement to the rate of evaporation for adsorbed molecules

$$\frac{\sigma}{\tau_s}=\frac{p}{(2\pi mkT)^{\frac{1}{2}}}. \tag{4}$$

Combining Eqs. (3) and (4) after differentiating the latter with respect to length gives the equation:

$$\dot{n}=\left\{-\frac{D_s\tau_s\cdot o}{(2\pi mkT)^{\frac{1}{2}}}-\frac{8}{3}\left(\frac{2}{\pi mkT}\right)^{\frac{1}{2}}\frac{A^2}{o}\right\}\frac{\partial p}{\partial X}. \tag{5}$$

Introducing Eq. (1) into Eq. (5) and simplifying yields the equation:

$$\dot{n}=-\left\{o\frac{\lambda X^2}{2}+\frac{16}{3}\frac{A^2}{o}\right\}\left\{\frac{2\pi mkT}{l}\right\}^{-\frac{1}{2}}\frac{\partial p}{\partial X}. \tag{6}$$

For steady-state flow, the pressure gradient is constant over the length of the tube and Eq. (6) may be written:

$$\dot{n}=\left\{o\frac{\lambda X^2}{2}+\frac{16}{3}\frac{A^2}{o}\right\}\left\{\frac{2\pi mkT}{l}\right\}^{-\frac{1}{2}}_{(p_2-p_1)} \tag{7}$$

where l is the length of the tube and p_2-p_1 is the pressure drop. The two cross sections of interest are circular and rectangular. For the former:

$$\dot{n}=\left\{\pi r\lambda_X{}^2+\frac{8}{3}\pi r^3\right\}\left\{\frac{2\pi mkT}{l}\right\}^{-\frac{1}{2}}_{(p_2-p_1)}. \tag{8}$$

The rectangular cross sectional is of interest for width w and thickness δ when $w\gg\delta$. Equation (7) may be written:

$$\dot{n}=\left\{w\lambda_X{}^2+\frac{8}{3}w\delta^2\right\}\left\{\frac{2\pi mkT}{l}\right\}^{-\frac{1}{2}}_{(p_2-p_1)}. \tag{9}$$

An exact dimension may now be calculated for which motion of molecules in the surface layer becomes equal in effect to motion in the gas phase:

$$\delta=3/8\lambda_X;\quad r=3/8\lambda_X. \tag{10}$$

These results are of interest in several respects. Equation (9) predicts that a gas should flow through a fine channel more rapidly than would be calculated by Knudsen's equations of molecular flow. It is implied that Graham's law is valid for molecules differing only in isotopic composition. There is no *a priori* reason to expect two different molecules to have the same mean free path between adsorption and re-evaporation. For large enough channels, however, Graham's law is still valid for all molecules.

By studying the flow of gases through rectangular channels constructed of optical glass flats coated with various films it would be possible to study diffusion in adsorbed films. Both λ_X and its temperature coefficient for a given gas on a number of substrates, or a number of gases on a given substrate could be measured.

[9] P. Clausing, Ann. Physik **7**, 489 (1930).
[10] Flood, Tomlinson, and Leger, Can. J. Chem. **30**, 348 (1952).
[11] P. C. Carman and P. Malherbe, Proc. Roy. Soc. (London) **A203**, 165 (1950).

Letters to the Editor

THIS section will accept reports of new work, provided these are terse and contain few figures, and especially few half-tone cuts. The Editorial Board will not hold itself responsible for opinions expressed by the correspondents. Contributions to this section should not exceed 600 words in length and must reach the office of the Editor not later than the 15th of the second month preceding that of the issue in which the Letter is to appear. No proof will be sent to the authors. A publication charge of $10.00 per Letter is made which, when honored, will entitle the Institution to 100 free reprints.

The Calculation of the Free Volumes of Liquids from Measurements of Sonic Velocity

F. C. COLLINS AND M. H. NAVIDI
Department of Chemistry, Polytechnic Institute of Brooklyn, Brooklyn, New York
(Received March 23, 1954)

EQUATIONS have been proposed by Eyring and Kincaid[1] and by Kittel[2] for relating the free volume of liquids to the velocity of sound. The Eyring-Kincaid equation was derived using a geometrical, rather than a thermodynamic, interpretation of the propagation of sound in a liquid, while Kittle used a very approximate form of the free volume equation of state in obtaining the relationship. In the following, a more exact equation is derived and is compared numerically with those mentioned above in the cases of several liquids.

The velocity of sound at low frequencies in an isotropic elastic medium is given by the Rayleigh equation as

$$u_s=[-v(\partial p/\partial v)_s/\rho]^{\frac{1}{2}}, \tag{1}$$

where $-v(\partial p/\partial v)_s$ is the adiabatic compressibility. Equation (1) may be put into the more convenient form

$$u_s=\left[\frac{vC_p/\rho}{C_p(\partial v/\partial p)_T+T(\partial v/\partial T)_p{}^2}\right]^{\frac{1}{2}}. \tag{2}$$

The free volume equation of state[3] is

$$pv=kT/[1-(v_0/v)^{\frac{1}{3}}], \tag{3}$$

where v_0 is the incompressible volume of the liquid per molecule. The use of Eq. (3) in Eq. (2) leads to the following equation for the velocity of sound in terms of molecular dimensions:

$$u_s=\frac{1-\frac{2}{3}(v_0/v)^{\frac{1}{3}}}{1-(v_0/v)^{\frac{1}{3}}}\left\{\frac{C_pRT/M}{C_p[1-\frac{2}{3}(v_0/v)^{\frac{1}{3}}]-R}\right\}^{\frac{1}{2}}. \tag{4}$$

Equation (4) is most readily solved for the ratio $(v_0/v)^{\frac{1}{3}}$ by the method of successive approximation using $(v_0/v)^{\frac{1}{3}}=0.9$ as the zeroth-order approximation. A value correct to 0.1 percent will usually result upon the third iteration. It will be seen that Eq. (4) is the ratio of the incompressible volume to the molecular volume rather than the free volume directly; thus the necessity of assigning an arbitrary geometry to the free volume is avoided. Table I gives values of $(v_0/v)^{\frac{1}{3}}$ calculated from Eq. (4) for several organic liquids at two temperatures using values of sonic velocity at 3 megacycles per second measured by one of us (M.H.N.). The table also shows that the resulting values of the incompressible volume v_0 are nearly independent of the temperature. The sonic interferometer described by Weissler[4] was used for the measurements. The values of the density and heat capacity required for the calculation were taken from the International Critical Tables. The sonic velocity at 3 megacycles is assumed to differ but little from that at low frequencies for the particular liquids studied.

TABLE I. Sonic velocities u_s at 3 megacycles, the calculated ratios $(v_0/v)^{\frac{1}{3}}$ and the incompressible volumes v_0 for various liquids at two temperatures.

Substance	u_s, M/sec 15°C	u_s, M/sec 25°C	$(v_0/v)^{\frac{1}{3}}$ 15°C	$(v_0/v)^{\frac{1}{3}}$ 25°C	$v_0\times10^{22}$ cm³ 15°C	$v_0\times10^{22}$ cm³ 25°C
Benzene	1348.3	1299.9	0.91119	0.90610	1.1098	1.1044
Chlorobenzene	1306.2	1268.4	0.92522	0.92149	1.3311	1.3279
Bromobenzene	1185.2	1153.4	0.93071	0.92741	1.3990	1.3967
Iodobenzene	1127.5	1099.2	0.93663	0.93360	1.5131	1.5110
Carbon tetrachloride	953.4	921.4	0.91045	0.90547	1.2018	1.1961
Toluene	1348.9	1304.0	0.91984	0.91557	1.3682	1.3637
Chloroform	1018.7	983.7	0.90320	0.89771	0.9743	0.9689
Bromoform	941.0	918.4	0.93027	0.92619	1.1642	1.1594

TABLE II. Experimental values of the ratio $(a/v^{\frac{1}{3}})$ for various liquid elements. X-ray diffraction data for a and ν from Gringrich[a] and density data for v from the International Critical Tables (ν=number of nearest neighbors).

Element	Temp. °C	ν	$a\times10^8$ cm	$(a/v^{\frac{1}{3}})$
Sodium	100	...	3.83	1.109
Aluminum	200	10.6	2.96	1.113
Argon	−188.8	(10.5)	(3.79)	1.053
Potassium	70	...	4.64	1.082
Potassium	375	...	4.76	1.082
Zinc	460	10.8	2.94	1.152
Cadmium	350	8.3	3.06	1.070
Tin	390	8.9	3.38	1.107
Mercury	ca 20	...	3.23	1.109

[a] See reference 5.

The molecular free volume is given by

$$v_f=\alpha(v^{\frac{1}{3}}-v_0^{\frac{1}{3}})^3. \tag{5}$$

The constant α has been assumed by Eyring and Hirschfelder[3] to be approximately $(4\pi/3)(a^3/v)$, where a is the average distance between nearest neighbors. The ratio $(a/v^{\frac{1}{3}})$ depends upon the form assumed for the liquid quasi lattice and is $2^{1/6}$ for the face-centered cubic case. The distance a has been calculated by Gringrich[5] from x-ray diffraction data for a number of liquid elements. Table II presents the values of the ratios $a/v^{\frac{1}{3}}$ calculated from these data and the densities. While the calculated ratios differ somewhat among themselves, their average, 1.097, is not greatly different from $2^{1/6}=1.122$.

TABLE III. Comparison of free volumes calculated according to Kincaid Eyring [Eq. (32)], Kittel [Eq. (39)], and the present method [Eqs. (46) and (47)]. Units are cc/molecule $\times10^{24}$.

Substance	Kincaid-Eyring 15°C	Kincaid-Eyring 25°C	Kittel 15°C	Kittel 25°C	Present method 15°C	Present method 25°C
Benzene	0.361	0.429	0.0846	0.1001	0.590	0.706
Chlorobenzene	0.301	0.357	0.0593	0.0687	0.404	0.472
Bromobenzene	0.258	0.298	0.0492	0.0566	0.332	0.384
Iodobenzene	...	0.264	...	0.0466	...	0.311
Carbon tetrachloride	0.417	0.493	0.0941	0.1108	0.657	0.782
Toluene	0.347	0.408	0.0754	0.0881	0.520	0.614
Chloroform	0.450	0.532	0.0981	0.1159	0.689	0.821
Bromoform	0.203	0.232	0.0420	0.0480	0.282	0.324

The free volume calculated from Eqs. (4) and (5) is to be compared with that obtained from the equation

$$u_s=\left(\frac{v}{v_f}\right)^{\frac{1}{3}}\left(\frac{C_pRT}{C_vM}\right)^{\frac{1}{2}} \tag{5'}$$

of Kincaid and Eyring's[1] geometric interpretation, and that of Kittel[2]

$$u_s=\frac{1}{3}\left(\frac{v}{v_f}\right)^{\frac{1}{3}}\left(\frac{C_v+3R}{C_v}\right)^{\frac{1}{2}}\left(\frac{3RT}{M}\right)^{\frac{1}{2}} \tag{6}$$

which was derived using the approximate free volume equation of state

$$p(v-v_0)=3kT. \tag{7}$$

Table III compares the values of the free volume obtained by the three methods. A value of 1.110 was assumed for the ratio $(a/v^{\frac{1}{3}})$

in all cases. It will be readily seen that although the free volumes calculated by the three methods are not in simple ratio to each other, their order of magnitude does not differ widely. The relative order of magnitude depends somewhat upon the value selected for the constant α in Eq. (5) for calculating the free volume from values of $(v_0/v)^{\frac{1}{3}}$ from Eq. (4).

Where only a value of (v_0/v) is required, the present method of calculation is preferable because it leads directly to this ratio without introducing assumptions as to the form of the liquid quasi lattice and the average geometry of the free volume.

[1] J. F. Kincaid and H. Eyring, J. Chem. Phys. **6**, 620 (1938).
[2] C. Kittel, J. Chem. Phys. **14**, 614 (1946).
[3] H. Eyring and J. O. Hirschfelder, J. Phys. Chem. **41**, 249 (1937).
[4] A. Weissler, J. Am. Chem. Soc. **70**, 1634 (1948).
[5] N. S. Gringrich, Revs. Modern Phys. **15**, 90 (1943).

Surface Tension of High-Polymer Solutions

FUMIO OOSAWA AND SHO ASAKURA
Department of Physics, Faculty of Science, Nagoya University, Nagoya, Japan
(Received February 25, 1954)

LET us consider a flat surface of a solution of chain polymers. In the neighborhood of the surface, the micro-Brownian motion of these polymers is restricted and their configurational entropy is decreased. Consequently, if they have no other energetic interactions with the surface, their concentration is decreased near it. Such a decrease of concentration results in the increase of the surface tension.

If inter- and intramolecular interactions of chain polymers are neglected, the total change of their configurational entropy, S, due to a flat surface of the solution per unit area is expressed as

$$S=k\int_0^\infty N(x)\,\ln W(x)dx, \tag{1}$$

$$W(x)=(2/\pi^{\frac{1}{2}})\int_0^{\sqrt{(3/2)}\cdot x/<r>}\exp(-y^2)dy, \tag{2}$$

where x is the distance from the surface and $N(x)$ the number concentration of polymers with their ends at x. $\langle r\rangle$ denotes the mean end-to-end distance of polymers in the free space. Equation (2) is obtained by applying a diffusion equation under suitable boundary conditions to the calculation of acceptable configurations of polymers near the surface. The mixing free energy of polymers and solvent molecules, F, may be approximately written as:

$$F=\int_0^\infty N(x)\cdot\mu_p(x)dx+\int_0^\infty n(x)\cdot\mu_s(x)dx. \tag{3}$$

$n(x)$ is the number concentration of solvent molecules. $\mu_p(x)$ and $\mu_s(x)$ are chemical potentials of polymers and solvent molecules, respectively, in the bulk solution, whose concentration is $N(x)$.

The total free energy of the solution is composed of these two parts, and its minimum condition gives the equilibrium $N(x)$ as a function of the concentration of the whole solution, N_∞ $(=N(\infty))$, through the following relation:

$$\mu_p(x)-kT\cdot\ln W(x)-z\cdot\mu_s(x)=\mu_p(\infty)-z\cdot\mu_s(\infty). \tag{4}$$

z is the molecular volume ratio of polymers and solvent molecules. The surface tension increment of the solution, $\Delta\sigma$, is derived from the Gibb's thermodynamic absorption equation.

In dilute solutions, $\Delta\sigma$ is given by

$$\Delta\sigma=\int_0^{P\infty}\int_0^\infty(1-\theta)dx\,dP_\infty, \tag{5}$$

and Eq. (4) is rewritten as

$$\theta\cdot\exp(2\alpha(\theta-1))=W, \tag{6}$$

where $\theta=N(x)/N_\infty=c(x)/c_\infty$ and $\alpha=A_2Mc_\infty$. P_∞ is the osmotic pressure of the solution with the concentration N_∞, expressed as $RT\cdot(c_\infty/M+A_2c_\infty^2)$.[1] A_2 is the second virial coefficient, c the concentration of polymers in g/cc and M their molecular weight. From these equations, the final result becomes

$$\Delta\sigma=(2/3\pi)^{\frac{1}{2}}\cdot RT\cdot(c_\infty/M)\cdot\langle r\rangle\cdot f(\alpha). \tag{7}$$

$f(\alpha)$ is a function increasing with α and is expanded as

$$f(\alpha)=1+\left\{\int_0^\infty(1-W)^2dx\right\}\Big/\left\{\int_0^\infty(1-W)\cdot dx\right\}\cdot\alpha+\cdots$$
$$=1+0.58\cdot\alpha+\cdots. \tag{8}$$

This result shows that the Θ point of the solution,[2] where $\alpha=0$ and $\langle r\rangle\propto M^{\frac{1}{2}}$, $\Delta\sigma$ is proportional to $M^{-\frac{1}{2}}$ at constant values of c_∞.

If M and A_2 are determined experimentally, for example, by the osmotic pressure, measurements of the surface tension will make it possible to pursue the change of $\langle r\rangle$ with the concentration, the temperature, etc., and to compare it with theoretical results.

The surface tension of polymer solutions is often smaller than that of the solvent, owing to the energetic adsorption of polymers by the surface. In such cases also, if the adsorption is not so strong, Eqs. (3) to (6) are employed and the problem is reduced to the derivation of a new W from the adsorption potential.[3,4]

The authors wish to express their sincere thanks to Professor P. J. Flory, who kindly suggested them to treat this problem and has given valuable criticisms throughout this work.

[1] W. G. McMillan, Jr., and J. E. Mayer, J. Chem. Phys. **13**, 276 (1945); P. J. Flory, J. Chem. Phys. **10**, 51 (1942).
[2] P. J. Flory and T. G. Fox, Jr., J. Am. Chem. Soc. **73**, 1904 (1951); P. J. Flory, J. Chem. Phys. **17**, 303 (1949).
[3] Simha, Frisch, and Eirich, J. Phys. Chem. **57**, 584 (1953).
[4] A. Katchalsky and J. Miller, J. Phys. and Colloid. Chem. **55**, 1182 (1951).

On Interaction between Two Bodies Immersed in a Solution of Macromolecules

SHO ASAKURA AND FUMIO OOSAWA
Department of Physics, Faculty of Science, Nagoya University, Nagoya, Japan
(Received February 25, 1954)

IT is the purpose of this note to point out that between two bodies immersed in a solution of macromolecules an interaction appears owing to characteristics of the medium.

Let us consider two parallel and large plates of the area A immersed in a solution of rigid spherical macromolecules. If the distance between these plates a is smaller than the diameter of solute molecules d, none of these molecules can enter between the plates. Then this region becomes a phase of the pure solvent, while the solution outside the plates is little affected by them. Therefore, a force equivalent to the osmotic pressure of the solution of macromolecules acts inwards on each plate.

When the medium is a very dilute and monodisperse solution, the force P between two bodies in it, can be given by:

$$P=kTN\partial\,\ln Q/\partial a, \tag{1.1}$$

$$Q=\int_V\exp(-w(x,a)/kT)dx; \tag{1.2}$$

where N denotes the total number of solute molecules and V the total volume of the solution. $w(x,a)$ is the potential energy of a solute molecule situated at x, being due to its interaction with the bodies. The negative P corresponds to the attractive force.

Applying these formulas to the following three cases, we get the results shown in Figs. 1 and 2; (i) the above-mentioned case; (ii) two parallel plates in a solution of thin rodlike macromolecules of the length l $(l^2\ll A)$; (iii) two spherical bodies of the diameter D in the same solution as the first case. In every case the force is attractive, being proportional to the osmotic pressure of the medium, $p_0(=kTN/V)$, and its range is of the order of the dimension of the solute molecules. For example, in the third case, P is

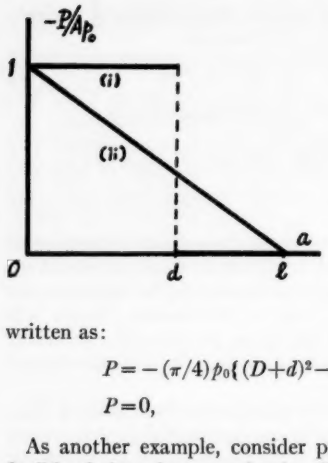

FIG. 1. The force between two parallel plates in a solution of (i) spherical and (ii) rod-like macromolecules.

written as:

$$P=-(\pi/4)p_0\{(D+d)^2-a^2\}, \quad D<a<D+d; \tag{2.1}$$

$$P=0, \qquad a>D+d. \tag{2.2}$$

As another example, consider parallel plates in a solution of flexible chain polymer molecules. The configurational entropy of chain molecules is decreased in the neighborhood of the plates and this effect is regarded as the source of $w(x,a)$. We can approximately calculate such an entropy decrement by reducing this problem to that of the diffusion in a vessel with walls which absorb diffusing particles.[1] The final result is:

$$P=-Ap_0\{(1-f)-a\partial f/\partial a\}, \tag{3.1}$$

$$f=(8/\pi^2)\sum_{\nu=1,3,5,\cdots}(1/\nu^2)\exp\{-(\nu^2\pi^2/6)(\langle r\rangle/a)^2\}; \tag{3.2}$$

$\langle r\rangle$ is the mean end-to-end distance of the chain molecules in the free space. The first term of (3.1), $(1-f)$, is the attraction due to the osmotic effect and the second term, $a\cdot\partial f/\partial a$, is the repulsion

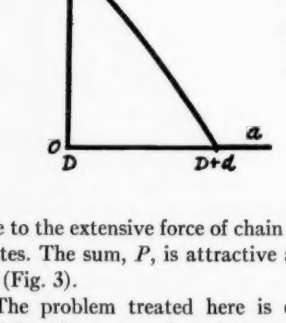

FIG. 2. The force between two spherical bodies in a solution of spherical macromolecules.

due to the extensive force of chain molecules confined between the plates. The sum, P, is attractive and its range is of the order of $\langle r\rangle$ (Fig. 3).

The problem treated here is considered as special cases of deriving the average force between solute particles in solutions.[2,3] The attractive force concluded from the above typical examples will have great influence on the behavior of suspended particles, for instance, on their coagulation, in solutions of macromolecules. If the medium is a solution of macro-ions, the force will become stronger and of longer range. Such a force perhaps plays an important role in biophysical problems, because the medium in

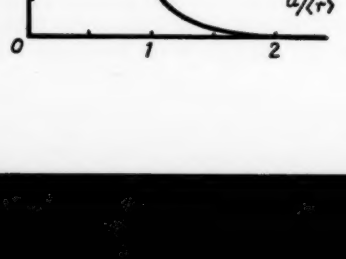

FIG. 3. The force between two parallel plates in a solution of chain polymers.

biological systems may be regarded as solutions of macromolecules, i.e., of various proteins.

The authors wish to express their sincere thanks to Professor P. J. Flory, who kindly read the manuscripts and has given them advice and many valuable criticisms.

[1] H. S. Carslaw, *The Conduction of Heat* (Macmillan and Company, Ltd., London, 1921), p. 158.
[2] W. G. McMillan, Jr., and J. E. Mayer, J. Chem. Phys. **13**, 276 (1945).
[3] J. H. de Boer, Repts. Progr. in Phys. **12**, 305 (1948).

Polarization of π-Electron Transitions in Aromatic Molecules

DONALD S. MCCLURE
Department of Chemistry and Chemical Engineering, University of California, Berkeley
(Received April 16, 1954)

THE recent theoretical work of Moffitt[1] on the electronic spectra of the catacondensed hydrocarbons appears to explain all of the major features of these spectra where data are available. Three properties of the electronic transitions are needed for comparison with the theory, namely, the frequency, the intensity, and the polarization. Positive proof of the polarization has been lacking for naphthalene and azulene, and independent checks of the polarization are desirable in the other cases. These data have been obtained in this laboratory in a number of ways and the results will be given here. Details will be reported in later papers. The results are in complete agreement with Platt's semi-empirical theory[2] and with Moffitt's new theoretical work.

Naphthalene.—Attempts to determine the polarization of the transitions in the naphthalene molecule by using the pure crystal[3] must be questioned because the first two electronic states are badly scrambled by intermolecular resonance.[4] In dilute solid solution of naphthalene in durene, the naphthalenes are clamped by the durene matrix with their short axes along the c' direction of the crystal, and the long axes perpendicular to the c' direction. The absorption and fluorescence at 20°K from the bc' face of such a crystal show that the o—o band occurs only along the b axis (long molecular axis) for the first transition. The total absorption is somewhat greater in the short axis direction because of vibrational-electronic interactions with b_{1g} vibrations. Thus the first transition must be $A_g-B_{3u}(L_b)$. The second transition is entirely polarized in these solid solutions along the c' axis, and must therefore be $A_g-B_{2u}(L_b)$.

Azulene.—Pure azulene crystal shows large intermolecular resonance interaction as does naphthalene, but the mixing of states is less, and it appears that the first transition is short-axis polarized. This is confirmed by the solid solution of azulene in naphthalene where the azulene lines of the first two transitions are extremely sharp at 20°K. The first transition is short-axis polarized, the second long-axis polarized. Vibrational electronic interaction plays only a minor part in changing the polarization direction in either case. Thus the lowest excited state is L_b, the next L_a.

Anthracene.—The fluorescence of single anthracene crystals has been used to show that the first transition is short-axis polarized.[5] In order to eliminate the possible complications arising from the very strong intermolecular resonance in the first electronic band of the crystal, a one mole percent solid solution of anthracene in phenanthrene was used. The bc face of a single crystal of the solution was examined under absorption and fluorescence, and the results confirmed the previous conclusion that the transition is short-axis polarized. The lowest excited state is thus L_a.

Phenanthrene.—The fluorescence work recently reported[6] shows that the first transition is short-axis polarized. This work was repeated at 20°K, and the absorption of single crystals was also examined at 20°K in order to see if a situation similar to that in the pure naphthalene crystal could exist. The conclusion was that although intermolecular resonance is strong, the second electronic

state is too far away to change the polarization of the first, and that the results using the pure crystal are probably valid. The lowest excited level is therefore L_b.

It seems to this author that these results remove the last objections to a complete acceptance of the semiempirical correlations made by Platt, at least for the lowest electronic states.

[1] W. Moffitt, J. Chem. Phys. **22**, 320 (1954).
[2] J. R. Platt, J. Chem. Phys. **17**, 484 (1949).
[3] D. P. Craig and L. E. Lyons, J. Chem. Phys. **20**, 1949 (1952); O. Schnepp and D. S. McClure, J. Chem. Phys. **21**, 959 (1953).
[4] D. S. McClure and O. Schnepp (to be published).
[5] Ganguly and Choudhury, J. Chem. Phys. **19**, 617 (1951).
[6] Ganguly and Choudhury, J. Chem. Phys. **21**, 554 (1953).

The Microwave Spectrum of Vinyl Iodide*

C. D. Cornwell† and R. L. Poynter‡§
Department of Chemistry, The State University of Iowa, Iowa City, Iowa
(Received May 6, 1954)

SINCE the carbon-halogen bond in the vinyl compounds C_2H_3X exhibit some double bond character, a complete study of this group of molecules would be of interest. The molecules C_2H_3Cl and C_2H_3Br have been studied recently.[1,2] In order to complete the study of the vinyl halide series, the study of vinyl iodide was undertaken.

A recording Stark effect type spectrometer utilizing a square wave modulation frequency of 100 kc and phase-sensitive detection was used for all measurements reported here. Spectral frequencies were measured by the use of a microwave frequency standard which multiplied the output from a 5-mc crystal oscillator up to the K-band region. The frequency measuring system was designed to produce frequency markers on the recorder charts at intervals of 1.25 mc.

Of 69 transitions which have been observed in the 24 600-mc to 25 800-mc region of the microwave spectrum of vinyl iodide, 28 have been assigned as the $J=3\rightarrow4$ transitions $3_{03}\rightarrow4_{04}$, $3_{13}\rightarrow4_{14}$, and $3_{12}\rightarrow4_{13}$. A prediction of the location of these lines, based on rotational parameters calculated from electron diffraction data,[3] indicated that the seven $J=3\rightarrow4$ groups of transitions should fall in the region of 25 to 26 kmc. A careful scanning of the region from 24 to 27 kmc yielded a group of lines falling between 24.6 and 25.8 kmc which could be tentatively assigned to this transition. Confirmation of this assignment was obtained from the quadrupolar hfs, Stark effect, temperature coefficient of intensity, and relative intensities of the various lines.[4]

Although first-order perturbation theory was adequate to predict the general form of the quadrupolar hfs pattern, it was necessary to take into account second order effects to obtain a precise agreement between observed and calculated frequencies. The assignments were refined by the method of least-squares and by the method of successive approximations. The molecular and quadrupolar constants obtained from these assignments are given in Table I.

The quadrupolar constants for the two transitions with $K_{-1}=1$ agree reasonably well, so that on this basis the average value of these constants could be taken as $\chi_{aa}=-1645\pm5$ mc and $\chi_{bb}=+764\pm9$ mc. The apparent disagreement of the χ_{aa}, χ_{bb} values for the $3_{03}\rightarrow4_{04}$ transition with those for the two $K_{-1}=1$ transitions is not surprising when one observes that the first order quadrupolar energy terms are quite insensitive to χ_{bb} for this transition. No attempt was made to determine the magnetic interaction constants for the $3_{03}\rightarrow4_{04}$ transition, since the six quadrupolar multiplet levels which exist do not provide a well overdetermined set of equations suitable to this purpose.

From the observed quadrupole coupling constants, the components of $eQ\nabla^2V$ along the C–I bond are computed as $\chi_{zz}=-1869$ mc, $\chi_{yy}=+988$ mc, and $\chi_{xz}=+882$ mc, where y and z are in the molecular plane. In terms of these components, Bragg's asymmetry parameter,[5] η, which is a measure of the bonds' deviation from cylindrical symmetry, has a value of 0.057 for vinyl iodide. This is of the same order of magnitude as is found for vinyl chloride,[1] and vinyl bromide.[2]

TABLE I. Rotational and quadrupolar constants for vinyl iodide.

Transition	$3_{03}\rightarrow4_{04}$	$3_{13}\rightarrow4_{14}$	$3_{12}\rightarrow4_{13}$
χ_{aa}	−1679.2 mc	−1644.7 mc	−1646.2 mc
χ_{bb}	764 mc	755.1 mc	772.8 mc
$\nu_{rot.}$	25 295.40 mc	24 916.68 mc	25 684.77 mc
a		−0.06 mc	0.06 mc
b		0.012 mc	0.019 mc
$b-c$		192.02 ±0.04 mc	
$b+c$		6325.52 ±0.04 mc	
$a-c$		41 540 ±100 mc	
		$\delta=$ 0.004461 (±0.00001)	
		$\kappa=-0.991079$ (±0.00001)	

We wish to thank Professor George Glockler for his continued interest in this problem, Dr. Kenneth McCulloh for his advice, and Mr. Randolph Phillips and Mr. Jack Althouse for their help with the electronic equipment.

* The Research reported in this publication was supported in part by the U. S. Office of Naval Research, Contract No. N8-onr-79400.
† Present address: Department of Chemistry, The University of Wisconsin, Madison, Wisconsin.
‡ Present address: Department of Physics, The Ohio State University, Columbus, Ohio.
§ Du Pont Predoctoral Fellow.
[1] J. H. Goldstein and J. K. Bragg, Phys. Rev. **75**, 1453 (1949).
[2] C. D. Cornwell, J. Chem. Phys. **18**, 1118 (1950).
[3] Hugill, Coop, and Sutton, Trans. Faraday Soc. **34**, 1518 (1938).
[4] R. L. Poynter, State University of Iowa, U. S. Office of Naval Research Progress Report, June, 1951.
[5] J. H. Goldstein and J. K. Bragg, Phys. Rev. **78**, 347 (1950).

Conductivity of Supercritical Solutions of Sodium Chloride and Water

James T. Corwin and Gwilym E. Owen
Antioch College, Yellow Springs, Ohio
(Received May 7, 1954)

DILUTE solutions of NaCl in water between 375° and 400°C show clear evidence of two phases, a liquid-like phase which has a conductivity which is relatively unaffected by changes in pressure and another phase above this whose conductivity is greatly affected by changes in pressure and density. The electrical conductivity of the liquid-like phase changes with temperature in a smoothly continuous way that gives no indication of a sudden change at the critical temperature. The other phase, that which is the vapor phase below the critical temperature, shows a very sharp break in the conductivity-temperature curve as the temperature passes through the critical.[1]

In their report in this Journal "On the conductivity of supercritical solutions of NaCl and water," February, 1954,[2] Fogo, Benson, and Copeland have calculated specific conductivities on the assumption that only one phase exists. Since they vigorously agitated the oven before taking readings they have undoubtedly found a sort of average value. At very high values of charge in the measuring cell, i.e., when the cell is nearly full at room temperature this average value will not differ much from the value found for each phase separately. At small charges the liquid-like phase has a very much higher conductivity than the other phase. In their report the final clause of paragraph 2, column 2, page 213, ". . . the initial resistances at 1000 cps have been used for calculation of specific conductances" implies that the initial values differed from later ones. This would be consistent with results we obtained after agitation when the resistance changed as though one phase were settling to the bottom.

[1] Swinnerton, Owen, and Corwin, Discussions Faraday Soc. No. 5, 172 (1949).
[2] Fogo, Benson, and Copeland, J. Chem. Phys. **22**, 212 (1954).

Isolation of HO_2 from the Hydrogen, Oxygen Diffusion Flame*

J. D. McKinley, Jr.
Chemical Kinetics Group, The James Forrestal Research Center, Princeton University, Princeton, New Jersey
(Received April 23, 1954)

A TECHNIQUE for the isolation and identification of intermediate species in diffusion flames has been described by Stadnik.[1-3] Reactive products are absorbed in a film of water flowing close to the flame, and are later identified by appropriate analyses. In the case of the hydrogen, oxygen flame a reducing substance was isolated[3] which reacted slowly with potassium permanganate, and after the permanganate titration, liberated large quantities of iodine from potassium iodide. Stadnik attributed this behavior to the presence of hydrogen peroxide and larger amounts of hydrogen superoxide, H_2O_4, resulting from the absorption of HO_2 from the flame. A slow decomposition of the H_2O_4 to oxygen and hydrogen peroxide was believed to account for the analytical results.

Because of the importance of HO_2 in mechanisms proposed for various chain reactions involving hydrogen and oxygen, and the scarcity of direct experimental evidence for its existence, an attempt has been made to repeat and extend these experiments. The results indicate that nitrous acid from the oxidation of atmospheric nitrogen is present in the absorbing solutions, and that hydrogen peroxides are not present; it appears that the evidence attributed to hydrogen superoxide can be adequately explained in terms of nitrous acid.

An apparatus similar in design to that described in detail by Stadnik[3] was used. The reaction vessel, a tin plated copper tube (130 mm long by 20 mm i.d.) is mounted vertically and equipped with shallow overflow dishes at the top and bottom. A sample of cool (15°C) water, recirculated by a small glass pump, pours continually down the inner walls of the tube. Oxygen enters the reaction zone through small perforations in the upper wall of the tube, and hydrogen is introduced through a 5 mm i.d. quartz tube mounted coaxially with the reaction tube; the flame burns at the hydrogen inlet and extends to within 2 mm of the flowing water surrounding it. In all experiments a 30 percent excess of oxygen was used; 400 cc of water was recirculated at a rate between 400 and 600 cc per minute, and 50 cc aliquots were analyzed after 0.8 to 1.0 moles of hydrogen had burned.

The recirculated solutions gave a positive test for nitrite in a modified form of the Griess-Illosvay method.[4] When mixed with acidified titanium sulfate, the solutions failed to show the yellow color characteristic of the peroxytitanic complex.

The uv absorption spectrum of a recirculated solution showed increasing absorption below 2200A and a maximum in the vicinity of 3600A. The absorption near the visible corresponds to that reported for nitrous acid[5] between 3100A and 3900A. No maximum in this region occurs in the spectrum of dilute aqueous hydrogen peroxide.

On titration with 0.01 *N* permanganate, the reactions were slow and the analyses less precise than corresponding titrations with ceric ion. The slow reaction with permanganate is characteristic of nitrous acid. After a permanent permanganate end point had been reached, the samples were freed of oxygen, treated with potassium iodide, and left overnight in sealed flasks; no iodine in excess of that corresponding to the permanganate blank was liberated. The large quantity of liberated iodine found by Stadnik could arise from a slight undertitration with permanganate (caused by slowness of the MnO_4^-, NO_2^- reaction) and incomplete removal of traces of oxygen from the sealed flasks, since nitrite is known to be an effective catalyst for the oxygen, iodide reaction.

The interfering nitrogen probably comes from the atmosphere around the apparatus, although 0.1 percent of nitrogen in the hydrogen or oxygen supplies if completely burned would be sufficient to cause these results. Addition of 3 percent nitrogen to the oxygen supply caused a fourfold increase in the nitrous acid concentration of the final solution. Saturating the water sample with nitrogen at 1 atmos served to increase the final nitrous acid concentration by about 30 percent.

Since nitrous acid would destroy any hydrogen peroxides that might be dissolved, this method will be inapplicable to the study of flame intermediates unless it is modified to insure exclusion of atmospheric nitrogen from the reaction.

* This research was supported by the United States Air Force under Contract No. AF 33(038)-23976 monitored by the Air Research and Development Command, and has been reported fully in Technical Note No. 9, OSR-TN-54-34.

[1] P. M. Stadnik, Dopovidi Akad. Nauk Ukr. R. S. R. **1950**, 201.
[2] P. M. Stadnik and O. K. Bodnya, Zhur. Fiz. Khim. **26**, 1173 (1952).
[3] P. M. Stadnik, Doklady Akad. Nauk S.S.S.R. **87**, 445 (1952).
[4] B. J. Rider and M. G. Mellon, Ind. Eng. Chem., Anal. Ed. **18**, 96 (1946).
[5] G. Porter, J. Chem. Phys. **19**, 1728 (1951).

s-Triazine. IV. The Mass Spectrum

C. M. Judson, R. J. Francel, and J. A. Weicksel
Stamford Research Laboratories, American Cyanamid Company, Stamford, Connecticut
(Received May 15, 1954)

THE mass spectrum of *s*-triazine has been obtained using a Consolidated Engineering Corporation, model 21-103-A mass spectrometer. A vapor sample of *s*-triazine, which is a solid with a vapor pressure of a few mm of mercury at room temperature, can be readily obtained after pumping out air at dry ice temperature. The spectrum obtained is shown in Table I, with formulas for the expected fragments at each mass.

Table I. Mass spectrum of *s*-triazine.

Mass/charge	Pattern (%)	Fragments
12	7.9	C
13	7.2	CH
14	2.1	N
24	2.0	C−C(*R*)
25	1.6	CH−C(*R*)
26	6.4	C−N
27	56.1	HC−N
28	83.3	(HC−N)H or N−N(*R*)
29	1.4	(*I*)
38	5.1	C−N−C
39	4.3	CH−N−C
40	3.3	CH−N−CH
41	0.5	N−CH−N
52	2.6	C−N−C−N
53	18.9	CH−N−C−N or C−N−CH−N
54	84.7	CH−N−CH−N
55	2.5	(*I*)
81	100.0	$C_2N_3H_2$
82	4.4	(*I*)

(*R*) = rearrangement; (*I*) = isotopic. Spectrum obtained at 270°C., 97.5 μA ionizing current, low amplifier gain, metastable suppressor out, 70 volts ionizing potential, mass 58 recorded at 714 volts. Sensitivity of mass 81 in *s*-triazine = 40.5 div./μ. Sensitivity of mass 43 in butane = 39.1 div./μ; butane pattern, 58/43 = 12.5 percent, 29/43 = 42.6 percent.

The mass spectrum of *s*-triazine is characterized by a large parent peak at mass 81, relatively large peaks corresponding to fragments of the C_2N_2 and CN groups, small peaks of C_2N, CN_2, C and N fragments, other small peaks due to rearrangements, and complete absence of C_2N_3 and C_3N_2 fragments. The spectrum differs from that of benzene in the greater importance of the CN and C_2N_2 fragments in *s*-triazine in comparison with the analogous C_2 and C_4 fragments in benzene, and in the absence of C_2N_3 and C_3N_2 fragments, while C_5 fragments are obtained in benzene.

The peaks at masses 24 and 25 are believed to be due, not to impurities, but to rearrangement. It is well known that rearrangement peaks are frequently encountered in mass spectra, particularly in compounds containing oxygen and nitrogen.[1-3] In some cases such peaks may be the largest in the spectrum.[2] However, the types of rearrangement which are commonly observed can be explained by rearrangements of hydrogen atoms and do not re-

quire any rearrangement in the skeleton of the molecule. The rearrangement peaks at masses 24 and 25 in *s*-triazine require a rearrangement in the skeleton of the molecule. The peak at mass 28 may be due to a hydrogen atom rearrangement to form CNH_2^+ or to a skeleton rearrangement to form N_2^+. Other peaks may involve contributions from rearrangements even though the peak can be explained by the expected fragments formed without rearrangement; for example, mass 26 may be due in some part to $C_2H_2^+$.

It has been shown[4] that the mass 26 peak in the benzene spectrum is due to a split into $CH{\equiv}CH^+$ and $2CH{\equiv}CH$. If *s*-triazine splits analogously into 3 fragments instead of the usual 2 fragments, the appearance of C−C fragments, which apparently requires the formation of at least 3 fragments, might not be too surprising. The distance between atoms in the potential C−C bond in *s*-triazine is short enough so that a C−C bond can be formed[5] without requiring change in the position of the *C* atoms, and thus appearance of C−C fragments does not violate the Franck-Condon principle.[2,6] Stevenson[7] has concluded from studies with C^{13} tagged propane and butanes that individual carbon atoms tend to lose their identity in the process of fragmentation on electron bombardment. However, because the stripped C−C fragment has a very low abundance in the propane and butane spectra, it was not possible to show that the rearrangement in C^{13} tagged propane and butane involved skeleton rearrangements. The evidence for skeleton rearrangements presented in this paper contributes further to the idea that the individual atoms lose their identity in the process of fragmentation.

[1] Catalog of Mass Spectra, American Petroleum Institute.
[2] A. Langer, J. Phys. Coll. Chem. **54**, 618 (1950).
[3] J. Collin, Bull. Soc. Roy. Sci. Liege **21**, 446 (1952).
[4] J. L. Franklin and F. H. Field, J. Chem. Phys. **21**, 2082 (1953).
[5] G. Herzberg, *Spectra of Diatomic Molecules* (D. Van Nostrand Inc., New York, 1950), second edition, p. 454.
[6] H. D. Hagstrum, *Mass Spectroscopy in Physics Research*, Natl. Bur. Standards Circ. 522, p. 193, U. S. Government Printing Office, 1953.
[7] D. P. Stevenson, J. Chem. Phys. **19**, 17 (1951).

A Theoretical Study of the Colored Alkali Oxides

INGA FISCHER-HJALMARS AND BARBRO GRABE
Institute of Theoretical Physics, University of Stockholm, Stockholm, Sweden
(Received May 3, 1954)

THERE are three kinds of oxides, common to all the alkali metals: Me_2O, Me_2O_2, and MeO_2. Furthermore, the sesquioxides $Me_4(O_2)_3$ have been prepared from at least Rb and Cs. The crystal structures of all these oxides have been determined by Helms and Klemm.[1] The sesquioxides are characterized by a dark color, whereas the other oxides are almost colorless. This feature of the sesquioxides can hardly be attributed to any of the separate ions. Most probably, the color depends on the structure of the crystal lattice.

In the present study an attempt has been made to describe the electron distribution of the sesquioxides in terms of semilocalized orbitals. By means of this description an explanation of the dark color has been suggested.

The computations have been carried out using the parameters of the $Rb_4(O_2)_3$ crystal, but analogous results could obviously be obtained in the case of $Cs_4(O_2)_3$.

We have considered an Rb atom and the three nearest O atoms, O_α, O_β, and O_γ, as an entity. Let φ_{Rb}, φ_α, φ_β, and φ_γ be suitable atomic orbitals of Rb, O_α, O_β, and O_γ. We have assumed that the valence electron of Rb can be assigned to an orbital:

$$\varphi = a\varphi_{Rb} + b(\varphi_\alpha + \varphi_\beta + \varphi_\gamma).$$

The energy has been calculated from the expression

$$E = \int \varphi^* H \varphi d\tau,$$

where H is the Hamiltonian of the electron in the field from the whole crystal. The parameters a and b of φ have been determined by variation of E with respect to a and b. This computation has been carried out using two different approximations of the potential energy. The results are collected in Table I. The column a/b shows that in the lower state the main contribution to φ comes from the oxygen orbitals, and in the higher state φ is almost a pure Rb orbital. The last two columns give the difference in energy ΔE between the two states and the corresponding wavelength λ, which is seen to belong to the visible part of the spectrum. Our suggestion is, therefore, that a transition between these two states gives rise to the color of the crystal.

TABLE I.

Approx.	a/b	E	ΔE	λ
I	0.3	−0.296 a.u.	0.07 a.u.	6500A
	−5.7	−0.226 a.u.		
II	0.6	−0.314 a.u.	0.06 a.u.	7500A
	−4.1	−0.253 a.u.		

Full details will be published by one of us (B. G.) in *Arkiv för Fysik*.

[1] A. Helms and W. Klemm, Z. anorg. u. allgem. Chem. **242**, 201 (1939).

Color Centers in Synthetic Quartz*

GEORGE W. ARNOLD, JR.
Naval Research Laboratory, Washington, D. C.
(Received May 12, 1954)

RECENTLY, Cohen[1] has reviewed some of the literature on the absorption maxima in fused and crystalline quartz. In particular, the work of Yokota,[2,3] was discussed and some doubt indicated as to the reality of the absorption maximum reported by Yokota at 2.67 ev (462 mμ) in x-irradiated α quartz.

This note is written to report an absorption maximum in x-irradiated synthetic quartz at 2.64 ev (470 mμ). Samples of synthetic quartz cut perpendicular to the *c* axis were employed. The quartz used was cut from crystals grown by the Bell Telephone Laboratories, Inc., and by the Brush Development Company. Quartz from both sources yielded the 2.64 ev maximum when

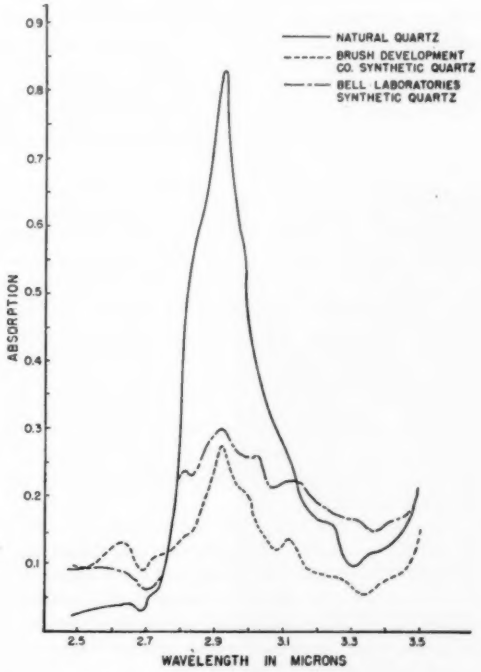

FIG. 1.

x-irradiated by means of a tungsten tube operated at 45 kv at 15 ma for periods from 24–44 hours.

It is believed that this maximum is the same as that observed by Yokota and that the mechanism of color center formation by electron trapping at oxygen vacancies advanced by Yokota is correct. The explanation advanced by Niira[4] to account for the shift in frequency of the color centers in fused and crystalline α quartz seems to be reasonable.

Further evidence for oxygen vacancy trapping is given by spectroscopic investigations of the absorption maximum found in quartz at 2.92μ. In Fig. 1 this maximum is shown for 10.0 mm thicknesses of natural quartz and for the two types of synthetic quartz. For other regions of the spectrum investigated (0.2μ to 15μ) the absorption of these samples is very nearly identical. Saksena[5] has analyzed the Raman and infrared spectra of quartz and has assigned the characteristic absorption maxima in the infrared at wavelengths of 8.7μ, 12.8μ, and 27.5μ. It is believed that the 2.92μ wavelength is due to the third harmonic of the frequency at 8.7μ which, according to Saksena, arises from the valence bond oscillation of the oxygen atoms. On this basis the reduced absorption for the synthetic quartz at 2.92μ is ascribed to oxygen vacancies and such vacancies are believed to be responsible for the trapping of electrons in color center formation.

* This material was presented at the 8th Annual Frequency Control Symposium, Asbury Park, New Jersey, 12 April 1954.

[1] A. J. Cohen, J. Chem. Phys. **22**, 570 (1954).
[2] R. Yokota, J. Phys. Soc. (Japan) **7**, 222 (1952).
[3] R. Yokota, J. Phys. Soc. (Japan) **7**, 316 (1952).
[4] K. Niira, Busseiron Kenkyu **50**, 17 (1952); Chem. Abstracts **46**, 7421c (1952).
[5] B. Saksena, Proc. Indian Acad. Sci. **A12**, 93 (1940).

Influence of Intramolecular Repulsion on Bond Energies

NORBERT W. LUFT
Cheadle Hulme, Cheshire, England
(Received March 8, 1954)

ALTHOUGH the decrease of "standard bond energies" in polyatomic molecules, e.g., upon substitution of methyl groups for hydrogen atoms, is a well-established experimental fact,[1,2] its explanation has been the subject of much controversy.[3–5] In general, the lowering effect upon dissociation energies of radical substituents is mainly attributed to resonance stabilization of or hyperconjugation in the radicals formed by the dissociation process. Occasionally reference is made to other factors, in particular electrostatic or steric repulsion,[6] polarization of adjacent bonds,[7] and some bond strengthening by resonance in the undissociated molecule,[5] e.g., NC−CN, $\phi CH_2-CH_2\phi$.

Recent experimental results on poly-substituted aryl ethanes[6] have made it very probable that the oversimplified resonance theory is not quite adequate and that repulsion plays a major part in bond weakening. By nature the repulsive forces responsible for bond weakening are identical with those stabilizing the staggered or *trans*-configuration in molecules with internal rotation. In a number of calculations[8] on methyl-substituted ethanes the electrostatic repulsive energies were found to be considerably larger than the threefold barriers themselves. Such high values seem quite reasonable, however, in view of the exponential falling-off of experimental repulsive interactions with distance[9] and the usual increase of torsional barrier height V_0 with decreasing multiplicity n; e.g. barrier increments for individual bonds are higher for $n=1$ than for $n=3$.

From the point of electrostatic interactions the dissociation energy is made up of the true electron pair bond energy D^0, whose variation with nuclear separation may be approximated by a Morse potential function, and the change in interaction energies, ΔW, between nonadjacent bonds, which vanish after dissociation. Thus in a series of homologs bond energy variations would simply represent differences in ΔW and should correlate with barrier heights, V_0, of internal rotation in these molecules. Figure 1

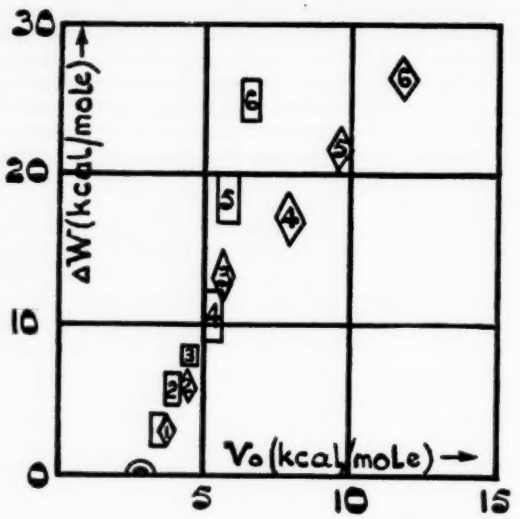

FIG. 1. Correlation between bond weakening, $\Delta W = D(H_3C-CH_3) - D_h$, and height of threefold torsional barrier, V_0, in methyl (□) and chlorine (◇) substituted ethanes.

shows that for chlorinated and methyl substituted ethanes with threefold torsional barriers this correlation is quite satisfactory. For poly-methyl ethanes the repulsive interactions include also those with the bond which undergoes fission.

It appears that in these and similar cases electrostatic repulsions in the original molecules are the decisive factor in bond weakening. But one might still be in doubt as to whether or not the (positive) resonance energy of radicals is, at least formally, equivalent to the (negative) repulsive energy in molecules from which they are formed. Recent experimental results,[10,11] however, on CH bond energies in hydrocarbon molecules with extended side-chains are at variance with predictions[12] by the resonance principle, whereas the repulsion theory gives numerical agreement, *viz.* roughly a classification according to primary, secondary, and tertiary CH bonds.

The different way of reasoning along the two lines is particularly instructive in the case of diamond. Roberts and Skinner[12] assumed that its CC-bonds, of length $r_e=1.54$A, are ethane-like bonds with increased strength. Thus, the heat of sublimation is

$$L=2D_0(\text{C}-\text{C};\ \text{diamond})=2\{D_0(H_3C-CH_3)+X\} \quad (1)$$

$=176.4$ kcal/mole with $D(H_3C-CH_3)=83$ and $X=5.2$ kcal/mole.[12] On the other hand, according to the repulsion theory the diamond lattice may be regarded as a fully branched and completely substituted paraffin, so that

$$L=2\{D^0(\text{C}-\text{C})-W_c\}_{r=r_e}\approx 2\{D_0(H_3C-CH_3)+W_h-W_c\}, \quad (2)$$

where W_h, ~25 kcal/mole, is the repulsion between CH bonds in ethane. The repulsive energy, per CC bond, between nonadjacent bonds in the diamond lattice may be estimated by reference to methyl substituted ethanes, *viz.* $W_c\sim 20$ kcal/mole. Thus, $L\sim 176$ kcal/mole from Eq. (2), and since no reorganization energy is included in this figure, it refers to excited ^5S carbon atoms.

[1] M. Szwarc, Chem. Revs. **47**, 75 (1950); Discussions Faraday Soc. **10**, 336 (1951).
[2] E. Wicke in Landolt-Börnstein, *Zahlenwerte und Funktionen* (Springer Publishing Company, Inc., New York, 1951), I, 2, p. 55.
[3] M. G. Evans, Discussions Faraday Soc. **10**, 1 (1951).
[4] E. Wicke, Naturwiss. **35**, 335 (1948).
[5] M. Szwarc, J. Chem. Phys. **18**, 1660 (1950).
[6] W. A. Waters, *The Chemistry of Free Radicals* (Oxford University Press, New York, 1946).
[7] A. D. Walsh, Trans. Faraday Soc. **43**, 60 (1947).
[8] N. W. Luft, Trans. Faraday Soc. **49**, 118 (1953).
[9] J. W. Linnett, and D. F. Heath, Trans. Faraday Soc. **48**, 592 (1952).
[10] D. P. Stevenson, J. Chem. Phys. **19**, 778 (1951).
[11] A. F. Trotman-Dickenson, Discussions Faraday Soc. **10**, 111 (1951).
[12] J. S. Roberts, and H. A. Skinner, Trans. Faraday Soc. **45**, 339 (1949).

An Experimental Value of the Force Constant of the SH Radical

SYDNEY LEACH
Laboratoire de Chimie-Physique, University of Paris, France
(Received May 11, 1954)

IN a recent note in this Journal,[1] Mitra has examined the data on the force constants k_e(MH) of the diatomic hydrides MH of the second and third periods of the periodic table of elements. He finds that the experimental k_e(MH) values of the various hydrides can be fitted into an empirical formula of the form

$$k_e^{\frac{1}{2}} = A + Bn, \tag{1}$$

where A and B are constants for the particular period and n is the number of electrons in the outermost shell of the element M considered.

Mitra gives experimental k_e values for every hydride of the first two periods except SH. Formula (1) predicts $k_e(\mathrm{SH}) = 4.154 \times 10^5$ dynes/cm.

A second relation was found by Mitra as follows:

$$\frac{k_e(\text{III period})}{k_e(\text{II period})} = R, \tag{2}$$

where R is a constant whose mean value is found to be $R = 0.53714$. From relation (2), Mitra predicts $k_e(\mathrm{SH}) = 4.184 \times 10^5$ dynes/cm, in good agreement with the value predicted by Eq. (1).

I wish to report an experimental value for the SH ground electronic state force constant: $k_e(\mathrm{SH}) = 4.192_9 \times 10^5$ dynes/cm. This value has been found from a spectroscopic analysis of the $^2\Sigma - {}^2\Pi$ system of both SH and SD observed in emission in the near ultraviolet. It is in excellent agreement with the values predicted by Mitra, and also with the value $k_e(\mathrm{SH}) = 4.15 \times 10^5$ dynes/cm predicted by Sheline.[2]

Preliminary reports on the analysis of the SH and SD emission spectra have appeared elsewhere.[3,4] A fuller account of this work is to be published in the near future.[5]

[1] Mitra, J. Chem. Phys. **22**, 564 (1954).
[2] R. K. Sheline, J. Chem. Phys. **18**, 927 (1950).
[3] S. Leach, Compt. rend. **230**, 2181 (1950).
[4] S. Leach, Boll. sci. fac. chim. ind. Bologna **10**, 9 (1952).
[5] S. Leach, Thése Paris (1953); to be published in J. de Physique (1954)

Spectroscopic Examination of the $NH_3 - HNO_3$ and $NH_3 - NO_2$ Diffusion Flames*

MILTON FARBER AND ALFRED J. DARNELL
Jet Propulsion Laboratory, California Institute of Technology, Pasadena, California
(Received February 25, 1954)

A SPECTROSCOPIC study of the gaseous NH_3—liquid HNO_3 (red fuming nitric acid containing 12 percent excess NO_2 hereinafter referred to as RFNA) and gaseous NH_3—gaseous NO_2 diffusion flames has been made with a 1.5-meter visible and ultraviolet spectrograph.

Gaydon and Wolfhard[1] have investigated the reactions of the $NH_3 - O_2$ diffusion flame and from an identification of the species have stated that the decomposition of NH_3 presumably goes through a thermal-stripping process with the removal of hydrogen and the formation of NH_2 and NH radicals in the NH_3 rich side of the diffusion flame. Subsequently, Fogarty and Wolfhard[2] studied the $NH_3 - NO$ flame and reported the presence of OH and NH radicals in the combustion species without reference to the presence of NH_2 radicals.

The NH_3 – RFNA and $NH_3 - NO_2$ diffusion flames were studied in an apparatus designed for gas-gas and liquid-gas diffusion flames mounted on a 1.5-meter grating-type visible and ultraviolet spectrograph. Gaseous diffusion flames were obtained by flowing the gases upward into the reaction zone through concentric tubes $\frac{1}{4}$- and $\frac{3}{4}$-inch i.d., and the liquid-gas flame was obtained by injecting a fine stream of the acid downward from a 0.01-inch-i.d. capillary tube into the NH_3 gas flowing downward from a $\frac{3}{4}$-inch i.d. tube. In all flames, a slight excess of NH_3 (<10 percent more

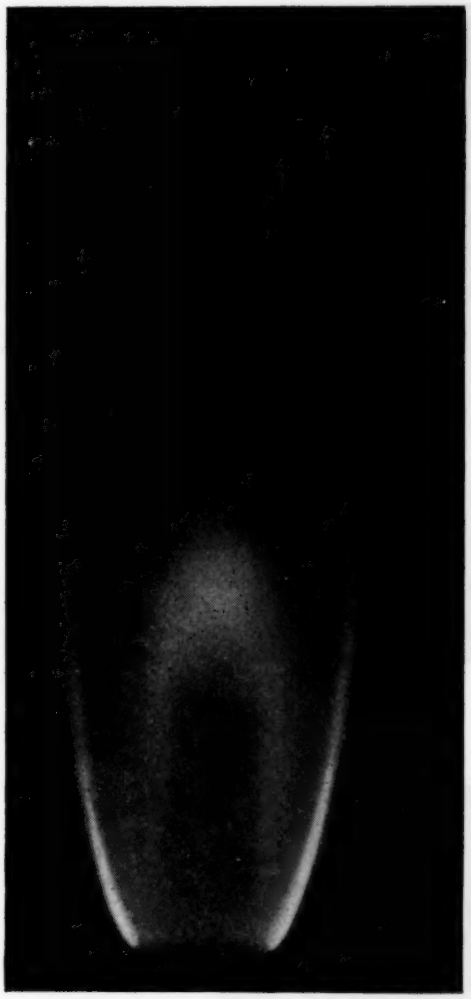

FIG. 1. $NH_3 - O_2$ diffusion flame; O_2 in the inner zone.

FIG. 2. $NH_3 - N_2O$ diffusion flame; N_2O in the inner zone.

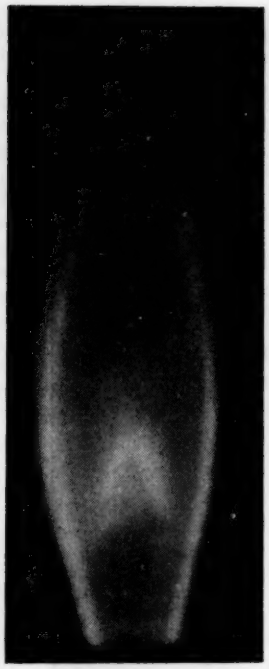

FIG. 3. NH_3-NO diffusion flame; NO in the inner zone.

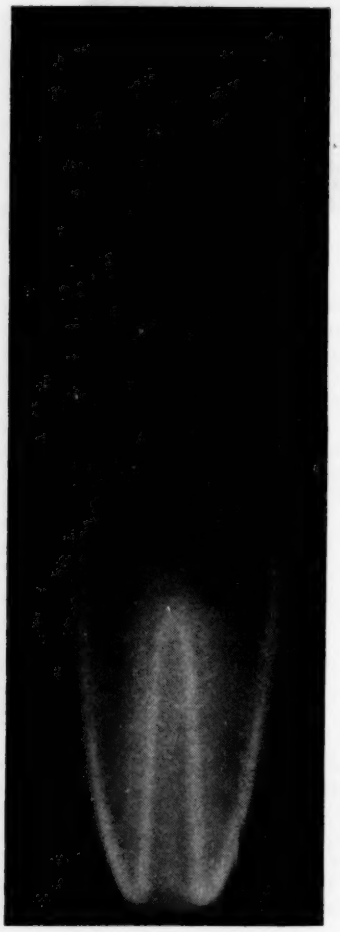

FIG. 4. NH_3-NO_2 diffusion flame; NO_2 in the inner zone.

than the stoichiometric amount) was introduced to facilitate the formation of a cone. The spectrographic slit was sighted on a portion of the central flame zone, and its width was adjusted in the range of 50 to 1000 microns depending on the emission intensity of the species being investigated. For the same reason film exposure time was varied from 2 to 8 hours. These variables were kept in mind in the interpretation of densitometer tracings showing relative emission intensities of significant spectrum lines from the ultraviolet and visible spectrograms.

Structures of the NH_3-O_2, NH_3-N_2O, NH_3-NO, NH_3-NO_2, and NH_3-RFNA diffusion flames were obtained with the apparatus described and are shown in Figs. 1 through 5. As can be seen from the photographs, the visible structure of the flame is different

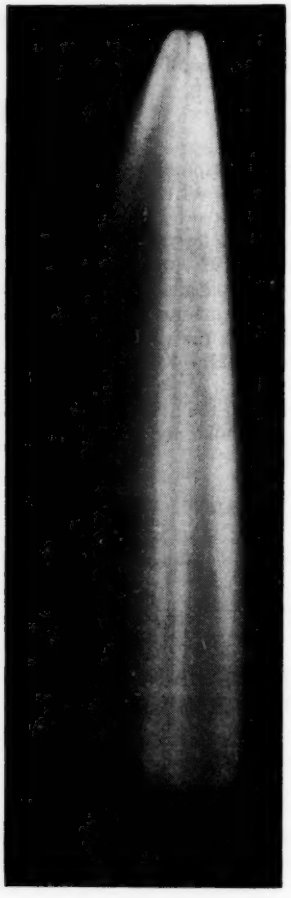

FIG. 5. NH_3-liquid RFNA flame; RFNA stream in the inner zone.

for each of the oxidants. Motion pictures of the NH_3-RFNA flame taken at 1000 frames/sec (Fig. 6) showed that the acid stream actually consisted of droplets approximately the diameter of the capillary tube.

Emission intensities of indentified-species spectrum lines from the NH_3-O_2 flame spectrogram (Fig. 7) are similar to those reported by Gaydon and Wolfhard.[1] The conventional OH band heads appear in the ultraviolet at 3063 and 3428A, and strong NH bonds are seen at 3660 and 3370A. NH_2 lines were found throughout the visible spectrum with strong lines appearing at 5700A. Figure 8 shows emission intensities from the same spectrum regions of the NH_3-NO_2 diffusion flame, and Fig. 9 depicts similar portions of the NH_3-RFNA flame spectrum.

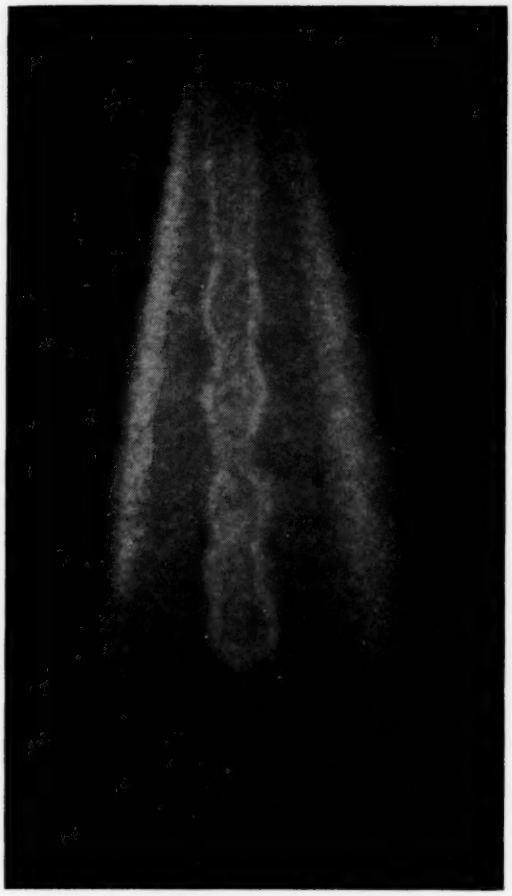

FIG. 6. NH_3-liquid RFNA flame taken at 1000 frames/sec; RFNA droplets in the inner zone.

A comparison of Figs. 7, 8, and 9 shows that, for comparable exposure times and slit widths, the intensity of the first and second OH band heads, the NH lines, and the NH_2 lines is similar for the NH_3-O_2 and NH_3-NO_2 diffusion flames with a slightly higher intensity for the NH_3-O_2 flame. The intensity of first OH

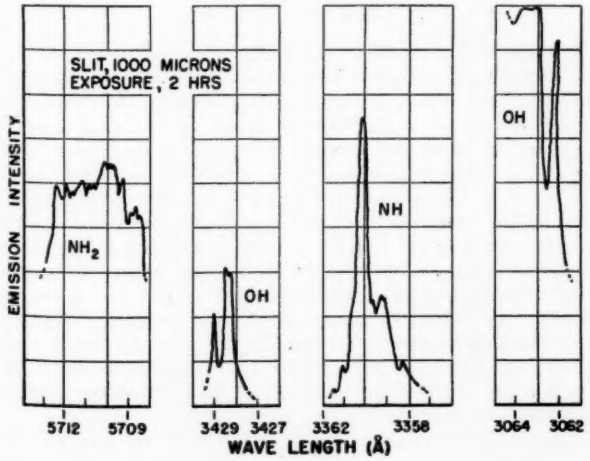

FIG. 7. Emission intensities of reactant species in NH_3-O_2 flame spectrum.

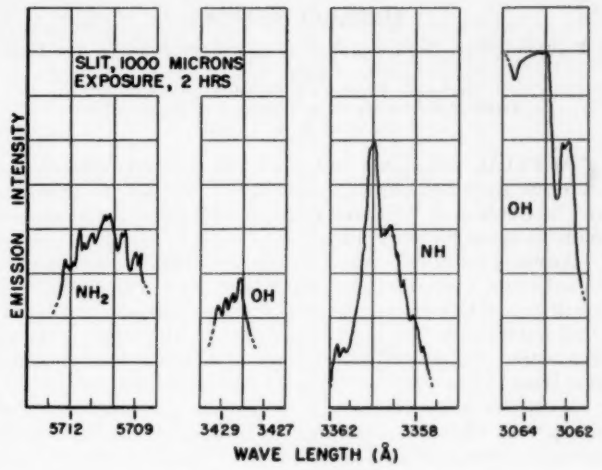

FIG. 8. Emission intensities of reactant species in NH_3-NO_2 flame spectrum.

and NH lines is slightly weaker in the NH_3-RFNA flame, whereas the second OH and NH_2 lines are very much weaker. The formation of NH_2 may result from thermal stripping of the NH_3, from reaction of NH with NH_3, or from reaction of NH_3

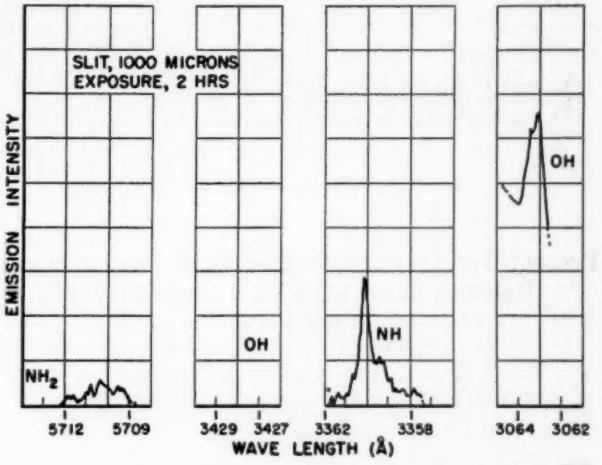

FIG. 9. Emission intensities of reactant species in NH_3-RFNA flame spectrum.

with oxygen derived from the decomposition of nitrogen oxides and RFNA. This latter assumption is supported by work of Fogarty and Wolfhard[2] and also by the present work at this Laboratory. The NH_2 lines are most intense in the NH_3-O_2 and NH_3-NO_2 flames, and least in the NH_3-RFNA flame. These observations may form a basis for the interpretation of the reaction mechanism since the quantity of oxygen obtainable from NO decomposition is very small and since the amount available from the RFNA flame is greater than that from NO but less than that from NO_2.

* This paper presents the results of one phase of research carried out at the Jet Propulsion Laboratory, California Institute of Technology, under contract No. DA-04-495-Ord 18, sponsored by the Department of the Army, Ordnance Corps.

[1] A. B. Gaydon and H. G. Wolfhard, Proc. Roy. Soc. (London) A194, 169 (1948).
[2] B. B. Fogarty and H. G. Wolfhard, Nature 168, 1112 (1951).

Hafnium Silicides

BENJAMIN POST, *Polytechnic Institute of Brooklyn, Brooklyn, New York*
AND
FRANK W. GLASER AND DAVID MOSKOWITZ,
American Electro Metal Corporation, Yonkers, New York
(Received April 27, 1954)

CRYSTAL structure[1,2] and phase diagram[3] investigations of the zirconium-silicon system have confirmed the existence of the compounds ZrSi and $ZrSi_2$. In this note, the analogous hafnium compounds are described.

Hafnium metal (97+ percent pure) and silicon powders were mixed in the desired proportions and hot pressed at 1200°C into small pellets. One group of pellets was then sealed into an evacuated quartz tube which had been flushed with argon prior to evacuation, and heated for 88 hours at 1125°C. Another group was heated for several minutes in a helium atmosphere at 1500°C.

X-ray diffraction diagrams of the powdered products revealed two phases which were identified as HfSi and $HfSi_2$, by analogy with the corresponding zirconium silicides. Both phases were present in all preparations.

TABLE I. Lattice constants of hafnium and zirconium silicides (in A).

	HfSi	ZrSi[3]	$HfSi_2$	$ZrSi_2$[2]
a	6.86	7.005	3.67	3.72
b			14.56	14.61
c	12.60	12.772	3.64	3.67
c/a	1.84	1.823		

HfSi is hexagonal; $HfSi_2$ is orthorhombic. The lattice constants of these silicides are listed in Table I, together with those of the isomorphous ZrSi and $ZrSi_2$.

[1] H. Seyfarth, Z. Krist. **67**, 295 (1928).
[2] S. v. Naray Szabo, Z. Krist. **A97**, 223 (1937).
[3] Lundin, McPherson, and Hansen, Am. Soc. Metals.

Errata: Temperature Independent Factor in the Relative Rates of Isotopic Three Center Reactions*

[J. Chem. Phys. **21**, 1972 (1953)]

JACOB BIGELEISEN AND MAX WOLFSBERG
Chemistry Department, Brookhaven National Laboratory, Upton, Long Island, New York
(Received May 7, 1954)

DR. N. B. Slater has kindly called our attention to an ambiguous definition of ν_L and an error in the sign in Eqs. (9) and (10), relating ν_L and m_B. The alternate definition of ν_L following Eq. (7) is not rigorously tenable. Equation (9) should read

$$\nu_L\alpha\{\alpha^2(m_B^{-1}+m_C^{-1})+\beta^2(m_B^{-1}+m_A^{-1})+2\alpha\beta m_B^{-1}\}^{\frac{1}{2}}$$

for the collinear model. A similar change should be made in Eq. (10).

Some of the curves published as Fig. 1 are, therefore, incorrect and the accompanying figure replaces it. The discussion of Eq. (10) and Fig. 1 is somewhat modified by the change in sign of the $p^{\frac{1}{2}}$ term. In the discussion of the decomposition of ammonium nitrate, the experimental fractionation factor of 1.023 now corresponds to p equal to 0.125, while the model, which gives 1.026 for the over-all fractionation factor, corresponds to p equal to 0.085. The agreement in this respect is, therefore, improved.

Application of the corrected equation for ν_L to the reactions of the isotopic hydrogen atoms and molecules, now serves to emphasize the inherent difference between the motion associated with ν_L and the conventional normal coordinates. A comparison between ν_L and the asymmetric stretching vibration of the linear

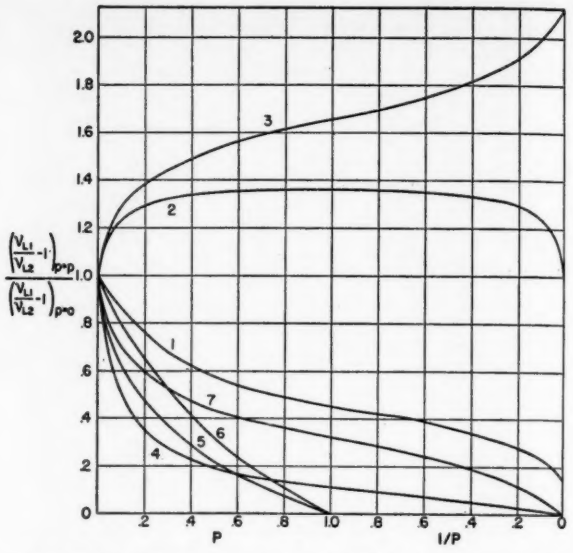

FIG. 1. Plot of the ratio $[(\nu_{L1}/\nu_{L2})-1]_{p=p}/[(\nu_{L1}/\nu_{L2})-1]_{p=0}$ as a function of p or $1/p$. The curves are for the following cases: (1) $m_B=m_C=12$, $m_A=1$, $m_{B'}=14$; (2) $m_A=m_B=m_C=12$, $m_{B'}=14$; (3) $m_B=m_C=12\ll m_A$, $m_{B'}=14$; (4) $m_B=m_C=12$, $m_A=1$, $m_{C'}=14$; (5) intramolecular isotope effect $m_A=13, 14$, $m_{A'}=12$, $m_B=12$, $m_C=12$, $m_{C'}=13, 14$; (6) intramolecular isotope effect $m_A=13,\ 14$, $m_{A'}=12$, $m_B=\infty$, $m_C=12$, $m_{C'}=13,\ 14$; (7) $m_A=m_B=m_C=12$, $m_{A'}=14$.

XYZ molecule is no longer fruitful. If one assumes that the zero point energy difference on isotopic substitution is correctly represented in both cases, then the product rule assures that calculated isotopic effects on the rate will be identical by both methods.

In passing it may be noted that Eq. (9) as corrected above leads, when p equals unity, to the asymmetric stretching vibration for the linear XY_2 molecule. If $\cos ABC$ is left explicitly in Eq. (9), the similar formula for the bent XY_2 molecule is obtained.

* Research carried out under the auspices of the U. S. Atomic Energy Commission.

A New Analysis of the Effect of Polar Solvents Upon ν(NH) of Pyrrole*

MARIE-LOUISE JOSIEN AND NELSON FUSON
Faculte des Sciences, Bordeaux, France, and Fisk University, Nashville, Tennessee
(Received May 3, 1954)

IN our recent study[1] of the effect of solvent upon the NH-stretching frequency of pyrrole and other compounds, we chose to present the data in the form of points on the graph of $(\nu_v-\nu_s)/\nu_v$ as ordinate *versus* $(D-1)/(2D+1)$ as abscissa, ν_v and ν_s being the pyrrole NH vapor and solution frequencies respectively, and D being the dielectric constant of the solvent in which the pyrrole is dissolved. The result is a grouping of nonpolar points through which a line drawn from the origin establishes what we have termed the Kirkwood-Bauer or KB line. The aromatic and most of the nonpolar points fall to the right of this line, only the few chlorinated solvent points lying to the left of the line. Jones and Badger, who obtained similar results for methanol,[2] suggested that the bonding of the methanol oxygen with, for example, the chloroform hydrogen was responsible for the increase in the frequency over that which would be expected from the effect of dielectric constant alone.

More recently an analysis of the effect of solvent upon $\nu(C=O)$ of acetone, acetophenone, and cyclohexanone[3] has shown that most of the solvent points plotted in the same way fall on the

TABLE I.

Solvent Name	Structure	$\frac{D-1}{2D+1}$ ×10³	$\frac{N^2-1}{2N^2+1}$ ×10³	$\frac{\nu_v-\nu_s}{\nu_v}$ ×10²
n-Hexane	C_6H_{14}	183	186	0.85
Cyclohexane	C_6H_{12}	205	205	0.91
Carbon tetrachloride	CCl_4	225	216	0.94
Benzene	C_6H_6	229	228	2.04
Mesitylene	$C_6H_3(CH_3)_3$	236	227	2.58
m-Xylene	$C_6H_4(CH_3)_2$	237	226	2.41
Toluene	$C_6H_5CH_3$	239	226	2.32
Carbon disulfide	CS_2	261	262	1.39
Chloroform	$CHCl_3$	360	210	1.25
1,2-Dichloroethane	$C_2H_4Cl_2$	428	210	1.84
Pyridine	C_5H_5N	443	230	8.0
Acetophenone	$C_6H_5COCH_3$	459	237	3.6
Acetone	CH_3COCH_3	466	180	4.0
Nitrobenzene	$C_6H_5NO_2$	478	242	2.30
Pyrrole (pure liquid)	C_4H_4NH	406	228	3.82

left side of the KB line, even though in some of these cases it is known that association between solute and solvent molecules is taking place. Whiffen's data on the ν(C−Cl) of chloroform[4] in different solvents when analyzed[3] in the same manner, also gives most of the points to the left of the KB line.

These additional results make clear that polar solvent points appear to the left of the KB line almost as frequently as to the right. The left-hand points are thus not limited to, nor are they characteristic of, halogenated solvents. At this stage[3] our attention was drawn to the remark of Bauer and Magat[5] that the dielectric constant D in the relationship $(\nu_v-\nu_s)/\nu_v=C(D-1)/(2D+1)$ should not be that which is measured at low frequencies but should be slightly greater than that which is calculated from index of refraction measurements,[5] i.e., slightly greater than the square of the index of refraction N.

When N^2 is used in place of D (see Table I), although the nonpolar solvent points on the $(\nu_v-\nu_s)/\nu_v$ *versus* $(N^2-1)/(2N^2+1)$ graph are essentially unchanged, the positions of the polar solvent points are markedly different from that previously given.[1] From Fig. 1 it can be seen that the chloroform, dichloroethane, and nitrobenzene points for ν(NH) of pyrrole have been lowered across to the right side of the KB line.[6]

While a more comprehensive analysis of this matter will be given elsewhere we should like to point out here that on the basis of solvent induced frequency shifts alone there is no clear-cut differentiation between polar solvents which enter into solvent-solute complexes with pyrrole and those which do not. However, the use of the mixed solvent technique in addition enables one to show[1] that at room temperature pyridine, acetophenone, acetone, toluene, and nitrobenzene form complexes while dichloroethane does not. From the position of the solvent points in the above figure it appears that at room temperature the division between polar or aromatic solvents forming complexes with pyrrole and polar solvents not forming such complexes occurs at a pyrrole NH-relative frequency shift of about 2 percent. At a higher temperature the complexes being less stable, the assumption is that this division would be displaced to the right, i.e., toward higher percentages.

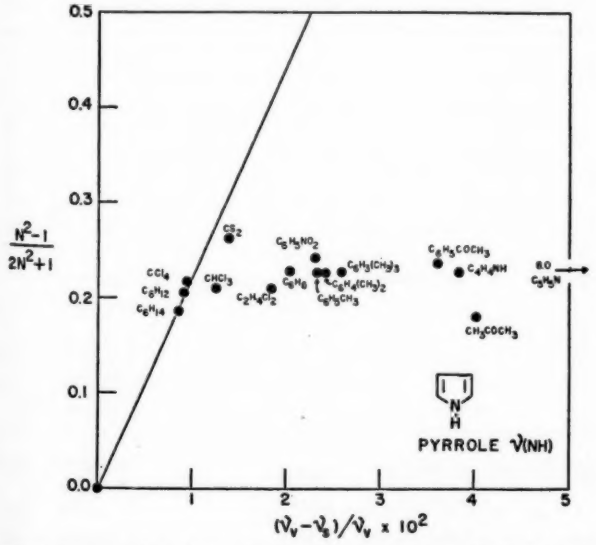

FIG. 1. A new analysis of the effect of polar solvents upon (NH) of pyrrole.

* This work has been supported jointly by research grant No. C-1520 from the National Cancer Institute of the National Institutes of Health, U. S. Public Health Service, and by a Frederick Gardner Cottrell grant from the Research Corporation.

[1] M. L. Josien and N. Fuson, J. Chem. Phys. **22**, 1264 (1954).
[2] L. H. Jones and R. M. Badger, J. Am. Chem. Soc. **73**, 3132 (1951).
[3] M. L. Josien *et al.*, Compt. rend. **236**, (to be published) (1954).
[4] D. H. Whiffen, Trans. Faraday Soc. **49**, 878 (1953).
[5] E. Bauer and M. Magat, J. phys. radium **9**, 319 (1938).
[6] This contrast can be seen most easily by comparing the figure given in this letter with Fig. 1 of reference 1 (to be found in this same issue).

The Critical Point and the Phase Rule

JOHAN VAN DRANEN
Laboratory for Analytical Chemistry, University of Amsterdam, Amsterdam, Netherlands
(Received April 12, 1954)

IF we apply the phase rule of Gibbs on a one-component system in the critical state, we have, according to Van der Waals, three phases.[1] The number of degrees of freedom of this system at the critical point is therefore equal to zero ($P=3$, $C=1$, and $F=C-P+2=0$).

It is better, in our opinion, to consider the critical state as representing one phase and thus having two degrees of freedom. To elucidate this point of view it is necessary to consider accurately the ordinary definition for the number of degrees of freedom of a system. This definition runs as follows: the number of degrees of freedom of a system is the number of variable factors, such as temperature, pressure or concentration, which need to be fixed in order that the condition of a system at equilibrium may be completely defined. An equivalent definition states that the number of degrees of freedom is the number of variable factors, which can be altered, without changing the number of phases.

If now we consider the fact that the critical point is the end point of the gas-liquid equilibrium curve, we see that it is possible to alter the pressure and the temperature, thus having two degrees of freedom and to remain in the homogeneous one-phase region. When we diminish the temperature or increase the pressure this homogeneous phase is called the liquid state; when we increase the temperature or diminish the pressure the system is in the gaseous state. The number of phases has therefore not been changed, but remains one; only the name of the phase changes.

In view of the first definition we can say that the difference between the critical point and for instance the triple point of a substance is, that when we consider this substance at its critical point we have already fixed pressure and temperature, whereas when we consider the triple point, we have chosen to have three phases in equilibrium. This problem is connected with the fact that by applying the theory of Van der Waals in this way, we mix up exact thermodynamics (the phase rule of Gibbs) with a semi-empirical formula.

Some time ago the author has enunciated the hypothesis that the critical point is the result of the fact that at the critical point the kinetic energy is equal to the potential energy.[2] The question has been raised whether this hypothesis is, from a physical point of view, unambiguous.[3] It has to be emphasized, however, that the critical point has no significance unless liquid and vapor are present. If we heat a liquid under a pressure higher than its vapor-

pressure or in a volume greater than the critical volume, we do not observe something particular at the critical temperature. According to our hypothesis the liquid state breaks down, going along the equilibrium curve if the kinetic energy becomes equal to the potential energy.

In other circumstances too a homogeneous state can have an energy equal to zero; the critical point has, however, the exceptional property that the total energy becomes equal to zero at the smallest pressure and the greatest volume. In Fig. 1 we have reproduced the general trend of the zero-energy curve.

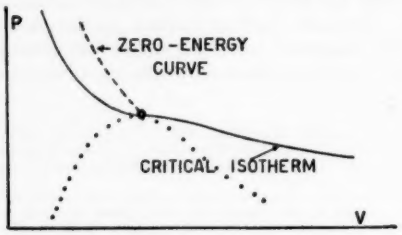

FIG. 1. The zero-energy curve.

It is perhaps interesting to mention that we have in astronomy a somewhat analogous situation. According to the theory of gravitational instability of Jeans stars are condensing from interstellar gas if in a certain part of the system the negative gravitational energy becomes greater than the kinetic energy.[4]

[1] J. D. van der Waals and P. Kohnstamm, *Lehrbuch der Thermostatik* (Verlag Barth, Leipzig, 1927), p. 140. We quote the following sentences of this book: ". . . when the liquid state and the gaseous state become identical, they belong to a region of labile states at the same time, which separates both coexisting states in ordinary circumstances. If we consider the number of phases of a certain system, we must therefore give the value three to a critical state."
[2] J. van Dranen, J. Chem. Phys. **20**, 1175 (1952), and J. Chem. Phys. **21**, 567, 1404, 2095 (1953).
[3] J. A. M. Cox, Ph.D. thesis (Leiden, 1954), sixth proposition.
[4] C. F. von Weizsäcker, Festschr. Akad. Wiss. Göttingen, **1**, 103, 114 (1951).

The Far Ultraviolet Absorption Spectra of Selected Isomeric Hexenes*

JULIA T. GARY AND LUCY W. PICKETT
Department of Chemistry, Mount Holyoke College, South Hadley, Massachusetts
(Received May 5, 1954)

A STUDY was made of the far ultraviolet absorption spectra of certain isomeric hexenes to test an observation[1] that there is a correlation between the direction of polarity of ethylenic hydrocarbon molecules and their point of maximum absorption in the Schumann region. Data on the butenes[1] and pentenes[2] show a shift in the absorption maximum of the broad intense band, designated $N \rightarrow V$, within a group of isomeric compounds. Similar results were obtained for the four hexenes studied, 1-hexene, *cis*-3-hexene, 2,3-dimethyl-1-butene, and 2,3-dimethyl-2-butene or tetramethylethylene.

The compounds, A.P.I. samples supplied by Standard Oil Development Company through the courtesy of Dr. R. F. Robey, had maximum impurity of 0.3 percent. The spectra are shown in Fig. 1 where logϵ, the molar extinction coefficient ($\epsilon = O.D./d$, $O.D.$ = optical density, c = concentration of absorbing material in moles/liter, and l = length of absorbing path in cm), is shown as a function of wave number. Measurements of flowing vapor were made with a Hilger fluorite prism vacuum spectrograph, using a hydrogen discharge as a light source.

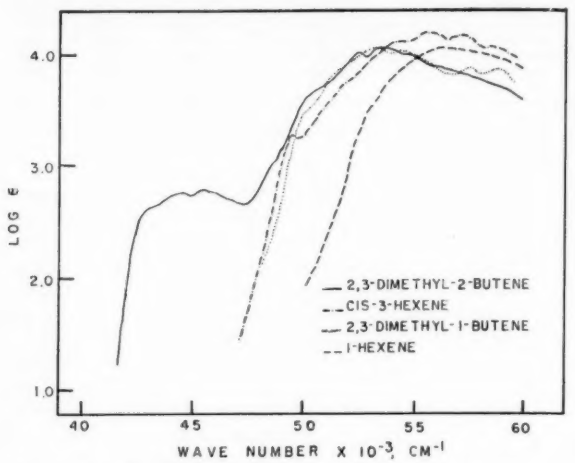

FIG. 1. Far ultraviolet absorption curves of four isomeric hexenes.

The hexenes exhibit, in general, the characteristic spectra of simple mono-olefins, where the beginning of absorption depends on the number of alkyl groups substituted on carbon atoms of the double bond.[3] The value of ϵ at the maximum of the broad absorption band is slightly above 10 000 and oscillator strengths are of the same order of magnitude as those obtained for other simple ethylenic derivatives.[1,2,4]

If 2,3-dimethyl-2-butene, where there is no dipole moment because of its D_{2h} or V_h symmetry, is taken as the norm, the other hexenes fall into a pattern on the basis of the relation of the dipole

TABLE I.

Type	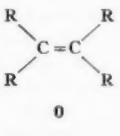	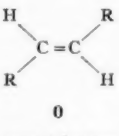	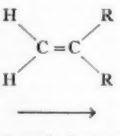	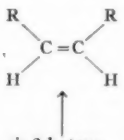	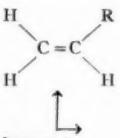	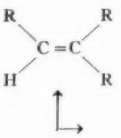
Vector	0	0	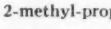			
Butenes		*trans*-2-butene	2-methyl-propene	*cis*-2-butene	butene-1	
Band maxima, cm^{-1}		56 270	53 100	57 000	57 100	
Pentenes		*trans*-2-pentene	2-methyl-1-butene	*cis*-2-pentene	pentene-1	2-methy-2-butene
Band maxima, cm^{-1}		55 500	53 200	56 600	56 600	56 575
					3-methyl-1-butene	
					56 800	
Hexenes	2,3-dimethyl-2-butene		2,3-dimethyl-1-butene	*cis*-3-hexene	hexene-1	
Band maxima, cm^{-1}	53 500		53 200	55 900	56 110	
f value	0.33		0.40	0.48	0.34	

vector of the molecule to the double bond and hence to the direction of charge displacement during the transition. The symmetrical molecule shows maximum absorption at 53 500 cm^{-1}. Both 1-hexene, whose largest component is perpendicular to the double bond, and *cis*-3-hexene with vertical vector, show maximum absorption at shorter wavelengths relative to the compound with no moment. Addition of the dipole vectors of 2,3-dimethyl-1-butene gives a resultant moment in the bond direction only, and here the band is displaced to slightly longer wavelengths.

Further measurements on the hexenes were discontinued when it was found that a study of their spectra in this region had already been made.[5] Results from this completed study, however, show a continued correlation between the direction of the dipole vector and the position of the $N \rightarrow V$ band.

Table I shows type formulas, direction of dipole vectors, and band maxima for the butenes,[1] pentenes,[2] and four hexenes studied. These results indicate that the direction of the dipole vector relative to the double bond is a contributory force in determining the energy required to excite an $N \rightarrow V$ transition, though not the only factor. Little or no relation is observed between the magnitude of the moments and that of the band shift.

* This work has been supported by grants from The National Science Foundation and Standard Oil Development Company.

[1] J. T. Gary and L. W. Pickett, J. Chem. Phys. **22**, 599 (1954).
[2] Semenow, Harrison, and Carr, J. Chem. Phys. **22**, 638 (1954).
[3] E. P. Carr and H. Stücklen, J. Chem. Phys. **4**, 760 (1936).
[4] Platt, Klevens, and Price, J. Chem. Phys. **17**, 466 (1949).
[5] L. C. Jones, Jr., and L. W. Taylor, Paper presented at Pittsburgh Conference on Analytical Chemistry and Applied Spectroscopy, March, 1954.

A Modified Atomic Orbital Method with its Application to Ethylene and Oxygen

KIMIO OHNO AND TAKASHI ITOH
Department of Physics, Faculty of Science, University of Tokyo, Tokyo, Japan
(Received April 12, 1954)

IT is well known that the usual ASMO LCAO method predicts energy intervals separating ionic and covalent states to be too large. Moffitt has investigated this difficulty in detail and devised "the method of atoms in molecules"[1] which works very well in the case of the π-energy levels of oxygen,[2] ethylene,[3] and benzene.[4] The recent semiempirical method of Pariser and Parr[5] also seems to be closely related to that method. Both of these methods are more or less semiempirical, and so we tried a nonempirical calculation which might be applicable to these problems.

The principal point of the new method is to use different atomic orbitals for covalent and ionic states of the molecules, that is to adopt different effective charges for the orbitals of neutral atoms and positive and negative ions. An intuitive basis of this procedure is as follows. The values of the effective charges suitable for atomic orbitals of neutral atoms are not appropriate for ionized states. In the negative ions, the wave functions of the electrons would be spread out by the interelectronic repulsion, and this means that the effective charges of the wave functions diminish, while in the positive ions the electron clouds would contract and the effective charges would increase.

In applying this method to the calculation of the π-energy levels of ethylene and oxygen, we first take all σ and π electrons into account and construct the wave function. We assume the electron pairing for the σ bonds, but neglect the effects of attached atoms except that we retain the carbon or oxygen atoms in their valence states. 1*s* electrons are shrunk into the nuclei. Moreover, we neglect all the overlap integrals between σ orbitals, to avoid the great complication of higher order permutations.

The energy matrix consists of three parts; (1) the π-electron part, (2) the σ-electron part and (3) the $\sigma-\pi$ electron part. In the σ-electron part, + and − terms always appear in pairs, and if we approximate them by the sum of neutral ones, this part becomes a common additive constant for all the π-electron states. So we can drop out the σ-electron part in the calculation of the π-electron levels. This corresponds to the usual π-electron approximation.

TABLE I. C_2H_4.[a]

	MAO I[b,c]	MAO II[b,d]	obs.[e]	ASMO[e]	Moffitt[f]
$V(^1B_{1u})$	7.7	8.6	7.6	11.4	7.3
$T(^3B_{1u})$	5.4	5.8	6.4	2.8	5.5
$N(^1A_{1g})$	0.0	0.0	0.0	0.0	0.0
$V-T$	2.3	2.8	1.2	8.6	1.8

[a] Equilibrium internuclear distance of 1.353A is used.
[b] The effective charges are chosen as $Z=3.25$, $Z^+=3.60$, $Z^-=2.90$.
[c] Modified atomic orbital method ($\sigma-\pi$ exchange neglected).
[d] Modified atomic orbital method ($\sigma-\pi$ exchange included).
[e] C. M. Moser, J. Chem. Phys. **21**, 2098 (1953).
[f] Reference 3.

In performing the numerical calculations we have used the Slater type atomic orbitals, and adopted the effective charges given in the footnotes of Tables I and II. The heteropolar integrals were evaluated by using the following approximations: 1. Coulomb-integrals: geometric mean approximation; 2. Hybrid-integrals and exchange-integrals: (Mulligan approximation[6]).

The results of the calculations are shown in Tables I and II.

TABLE II. O_2.[a]

	MAO I[b,c]	MAO II[b,d]	obs.[e]	ASMO[e]	Moffitt[e]
$^3\Sigma_g^-$	8.2	9.2	9.6	12.0	5.7
$^1\Delta_g$	6.9	7.0	8.2	2.5	4.8
$^1\Sigma_g^-$	0.0	0.0	0.0	0.0	0.0
$^3\Sigma_u^- - {}^3\Sigma_u^+$	1.3	2.2	1.4	9.5	0.9

[a] Equilibrium internuclear distance of 1.207A is used.
[b] The effective charges are chosen as $Z=4.55$, $Z^+=4.90$, $Z^-=4.20$.
[c] Modified atomic orbital method ($\sigma-\pi$ exchange neglected).
[d] Modified atomic orbital method ($\sigma-\pi$ exchange included).
[e] Reference 2.

The agreement with the experimental values is very satisfactory, although this agreement is rather fortuitous. It appears that the errors arising from the simplifying assumptions made above tend to cancel out. But it would be apparent that a great improvement upon the ASMO theory can be achieved by the present method.

The calculations of $^1\Delta_g$ and $^1\Sigma_g^+$ states of oxygen are now in progress. A full report will be published elsewhere.

We should like to express our hearty thanks to Professor Kotani for his valuable suggestions and deep interest in this work.

[1] W. Moffitt, Proc. Roy. Soc. (London) **A210**, 245 (1951); **218**, 486 (1953).
[2] W. Moffitt, Proc. Roy. Soc. (London) **A210**, 224 (1951).
[3] W. Moffitt and J. Scanlan, Proc. Roy. Soc. (London) **A218**, 464 (1953).
[4] W. Moffitt and J. Scanlan, Proc. Roy. Soc. (London) **A220**, 530 (1953).
[5] R. Pariser and R. G. Parr, J. Chem. Phys. **21**, 466 (1953); **21**, 767 (1953).
[6] J. F. Mulligan, J. Chem. Phys. **19**, 347 (1951).

The Structure of the Nitric Oxide Dimer

W. J. ORVILLE-THOMAS*
Department of Physics, Duke University, Durham, North Carolina
(Received March 29, 1954)

THE electronic structure of nitric oxide may be described in terms of molecular orbitals as

$$NO[KK(N{:}2s)^2(O{:}2s)^2(\sigma 2p_x)^2(\pi 2p_y)^2(\pi 2p_z)^2(\pi^* 2p_z)].$$

The group $(\pi 2p_z)^2(\pi^* 2p_z)$ is a three electron bond whose effective π-bond-order is about 0.5.

When the antibonding $\pi^* 2p_z$ electron is ionized or excited to a relatively nonbonding molecular orbital the NO^+ ion and the excited NO* molecule behave as if they possess triple bonds.

The existence of associated nitric oxide molecules was inferred on the basis of thermodynamic data[1,2] and it has now been shown that nitric oxide dimerises in the vapor, liquid, and solid states.[3–5]

A. L. Smith *et al.*[4] on the basis of the infrared and Raman spectra of liquid and solid nitric oxide have demonstrated the existence of $(NO)_2$ and suggested that the structure is

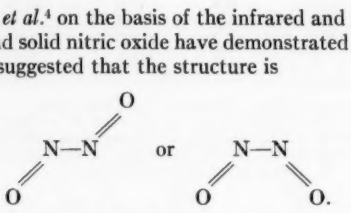

This suggested structure is not confirmed by x-ray diffraction work (Dulmage *et al.*[5]). They favor a rectangular structure

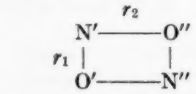

with $r_1=1.10$A and $r_2=2.38$A.

The possibility of a rectangular structure for the nitric oxide dimer had been pointed out previously by O. K. Rice.[6] The decrease in bond length of the shorter NO link indicates that the π^*2p_z electron originally present in the NO monomer has lost its antibonding character. The unusually large N′—O″ bond length indicated that this bond is not an ordinary covalent bond. This rectangular structure affords an explanation of why no vibrational frequency has been found which could be assigned to the stretching of the N—N bond in the proposed ONNO structure. There is no frequency in the infrared or Raman spectrum of $(NO)_2$ which can reasonably be assigned to ν(NN). This is almost conclusive evidence that no "normal" N—N (or N—O) bond joins the two units of the dimer. Taken in conjunction with the x-ray evidence the ONNO structure (*trans* or *cis*) containing a two-electron NN (or NO) bond is ruled out as a possibility.

Turning to the x-ray rectangular configuration it is clear that the bonds (N′—O″) and (O′—N″) must be equivalent. Their length of 2.38A indicates that they do not represent normal covalent bonds. The formation of this rectangular molecule can be pictured as follows (see Fig. 1). Let the plane of the dimer, $(NO)_2$ be the xz plane. σ and $2p\pi_y$ localized bonds are formed between the

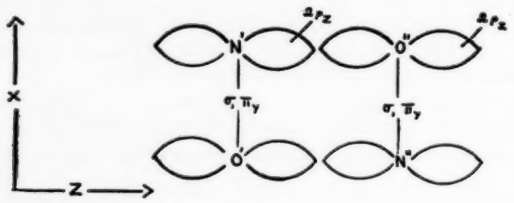

FIG. 1.

atom pairs, (N′O′) and (N″O″). We are left with six $2p_z$ electrons. These are to be fed into molecular orbitals (MO) formed from the O and N:$2p_z$ atomic orbitals (AO). The suggestion is made that MO's of two different types can be constructed by the overlapping of these similar AO's owing to the rectangular nature of the dimer.

(i) By the overlap of the (N′:$2p_z$) and (O′:$2p_z$) AO's and the N″ and (O″:$2p_z$) AO's localized $2p\pi_z$ MO's can be formed between the pairs of atoms. These MO's can accommodate four electrons. Together with the σ and π_y bonds these π_z bonds give the N′O′ and N″O″ links their typical "triple" bond properties.

(ii) σ-type MO's can be formed by the overlap of the N':$2p_z$ and (O″:$2p_z$) AO's and similarly for the atom pair O′ and N″.

For the filling of these two σ-type MO's there remain however only two electrons. It is suggested that one electron is fed into each of these σ-type MO's, the electrons having opposite spins thus accounting for the diamagnetism of $(NO)_2$. These one-electron σ bonds offer a partial explanation for the abnormally long bond lengths of these NO links. The mutual repulsion of nonpaired electrons would also operate in favor of a long N′O′ bond length.

Each oxygen and nitrogen atom has associated with it one σ bond, two localized π bonds, and a one-electron σ-type bond; i.e., the atoms have four bonding MO's associated with them; they are quadrivalent.

* Visiting Fulbright Scholar, 1953–1954. On sabbatical leave from The Edward Davies Chemical Laboratories, University College of Wales, Aberystwyth, Wales.

[1] A. Eucken and L. d'Or, Nachr. Ges. Wiss. Göttingen, Math.-physik. Kl. (1932), p. 107.
[2] H. L. Johnston and W. F. Giauque, J. Am. Chem. Soc. **51**, 3194 (1929).
[3] d'Or, de Lattre, Tarte, J. Chem. Phys. **19**, 1064 (1951).
[4] Smith, Keller, and Johnston, J. Chem. Phys. **19**, 189 (1951).
[5] Dulmage, Meyers, and Lipscomb, J. Chem. Phys. **19**, 1432 (1951)
[6] O. K. Rice, J. Chem. Phys. **4**, 367 (1936).

Heats of Combustion and Formation of Some Methoxy-polysilane and -polysiloxane: Si—O Bond Energy

TOSHIO TANAKA AND TAKEO WATASE
Department of Applied Chemistry, Faculty of Engineering, Osaka University, Osaka, Japan

(Received April 19, 1954)

PREVIOUSLY, we reported on the heats of combustion and formation of some organosilicon compounds containing alkyl or phenyl group, etc., and stated the technique used for burning them completely.[1] Organosilicon compounds containing only methoxy group are readily burnt completely by themselves without ampoule, by the ignition of the liquid pool in the crucible.

We measured the heats of combustion of four substances, i.e., methyl ortho-, di-, tri-silicate and hexamethoxydisilane, using Nenken type adiabatic bomb calorimeter. We have found the products of combustion to be carbon dioxide, water and silica by chemical analysis, without any soot. These samples used for the combustion measurements were prepared by alkolysis of its corresponding polychloro-polysilane and -polysiloxane. After completely dehydrochlorinated,[2] these products were rigorously distilled through a Stedman column of about 30 theoretical plates. Data on these materials are given in Table I.

TABLE I. Data on the substances used for combustion measurements.

Substance	Formula	b.p. °C/mm Hg	d_4^{20}	n_D^{20}	Si % Found	Si % Calc
Methyl orthosilicate	$Si(OCH_3)_4$	122/760	1.034	1.3688	18.48	18.45
Methyl disilicate	$Si_2O(OCH_3)_6$	118.5/30	1.122	1.3818	21.77	21.74
Methyl trisilicate	$Si_3O_2(OCH_3)_8$	95–6/2	...	...	23.17	23.12
Hexamethoxydisilane	$Si_2(OCH_3)_6$	98/20	1.095	1.4070	22.99	23.18

To determine the energy equivalent of the calorimeter at 20°C, we used the value 6319.0 cal/gram[3] for the heat of combustion of standard benzoic acid. The resulting molar heats of combustion, at 20°C and 1 atmos constant pressure, are given under $-\Delta H_c$ in Table II. Each value represents the average of four to seven combustion measurements and their mean deviations were not over ±0.1 percent. The corresponding values for the heat of formation from the elements have been computed by using −94.05 kcal,[4]

TABLE II. Heats of combustion and formation and Si—O bond energy (kcal/mole).

Formula	Mole wt	$-\Delta H_c$	$-\Delta H_f^0$	$-\Delta E$	$-E_{Si-O}$
$Si(OCH_3)_4$	152.23	694	300	1734	102
$Si_2O(OCH_3)_6$	258.38	1056	539	2796	101
$Si_3O_2(OCH_3)_8$	364.54	1399	798	3879	102
$Si_2(OCH_3)_6$	242.38	1150	445	2643	101

-68.32 kcal,[4] and -208.14 kcal[5] for the heats of formation of $CO_2(g)$, $H_2O(1)$ and SiO_2(amorph.) from standard elements, respectively, and are shown under $-\Delta Hf^0$. The heats of formation in the gaseous state from monoatomic gases, ΔE, were calculated using the values presented by Pauling[6] for the heats of atomization of the constituent elements (except silicon). The value 89.2 kcal/g-atom was used for that of silicon.[7] The latent heats of vaporization of these liquids were estimated from Trouton's rule. The value ΔE may be shown by the following expression:

$$\Delta E = aE_{\text{Si-O}} + bE_{\text{Si-Si}} + cE_{\text{C-O}} + dE_{\text{C-H}}.$$

In this expression E represents the energy value of bond corresponding to each suffix and the factors a, b, c, and d the number of bonds in the molecules in question. As the energy terms of C—O and C—H bonds are well known from many studies, we can evaluate the Si—O bond energy. In the case of hexamethoxydisilane Si—Si bond energy was considered as equal to the negative value of half of atomization heat of silicon. Si—O bond energy computed in this manner is shown in Table II, using the values proposed by Pauling[6] for C—O and C—H bond energies.

In the past several values have been reported for Si—O bond energy, and of these the value obtained by Thompson[5] is indicative of the considerable deviations in his results. We are not also satisfied with others.[6,8] The Si—O bond energy derived here from four substances is in good agreement.

[1] Tanaka, Takahashi, Ōkawara, and Watase, J. Chem. Phys. **19**, 1330 (1951).
[2] R. Ōkawara and T. Tanaka, Bull. Chem. Soc. Japan **27**, 120 (1954).
[3] Calculated from the result of Prosen and Rossini, J. Research Natl. Bur. Standards **33**, 439 (1944).
[4] Wagman, Kilpatrick, Taylor, Pitzer, and Rossini, J. Research Natl. Bur. Standards **34**, 143 (1945).
[5] R. Thompson, J. Chem. Soc. **1953**, 1908.
[6] L. Pauling, *The Nature of the Chemical Bond* (Cornell University Press, Ithaca, New York, 1940).
[7] L. H. Baughan, Quart. Rev. **7**, 103 (1953).
[8] K. S. Pitzer, J. Am. Chem. Soc. **70**, 2140 (1948); H. Gilman and G. E. Dunn, Chem. Revs. **52**, 77 (1953).

The Rule of Mutual Exclusion*

T. VENKATARAYUDU
The Harrison M. Randall Laboratory of Physics, University of Michigan, Ann Arbor, Michigan
(Received April 19, 1954)

IT is well known that in molecules possessing a center of inversion spectral lines corresponding to fundamental, overtone, and combination frequencies are mutually exclusive in Raman and infrared spectra, i.e., lines appearing in Raman effect are forbidden in infrared absorption and vice versa. The object of this note is to show that this rule is not universally true in crystals.

In molecules, the center of inversion is unique and it commutes with all other symmetry elements. The point group G of the molecule can be written as the direct product of two groups in the form $G=G_1\times G_2$ where G_2 is the group of order 2 consisting only of the elements E and i. Each irreducible representation of G can be designated g (gerade) or u (un-gerade) according as the trace of i in the representation is positive or negative. Further every eigenfunction can be described as symmetric or antisymmetric with respect to i. Modes of vibration which are symmetric with respect to i are permitted only in Raman effect and modes which are antisymmetric with respect to i are permitted only in infrared spectrum.

In the case of crystals, the center of inversion is not unique. Instead, we have an infinity of centers of inversion and they do not necessarily commute with the other symmetry elements. The modes of vibration can no longer be designated symmetric or antisymmetric with respect to the centers of inversion, nor even with respect to one center of inversion. However, all permitted fundamentals in crystals correspond to modes in which equivalent atoms in neighboring unit cells move in phase.[1] Such modes can be described symmetric or antisymmetric with respect to any one i (and therefore with all i) and the rule of mutual exclusion is still valid. However, the following example shows that the rule breaks down in general.

The finite space group O_h^7 obtained by taking twice the Bravais primitive translations as equivalent to the identity element is of order 48×8. This group has twenty irreducible representations, 4 one-dimensional, 2 two-dimensional, 4 three-dimensional, 4 six-dimensional, 4 four-dimensional, and 2 eight-dimensional. The one-, two-, and three-dimensional representations correspond to the irreducible representations of the isomorphic point group O_h. We give below the characters of the four three-dimensional and the four six-dimensional representations of our extended group. The first row refers to the order of the conjugate class. Typical symmetry elements in the first six conjugate classes are E, C_3, C_2, σ, S_4, and i. Modes coming under F_2 are Raman active (infrared in-active) while those coming under F_4 are infrared active (Raman in-active). Modes coming under all other representations are forbidden in both Raman and infrared absorption. The symmetry species of the combination modes of oscillations coming under H_1 and H_2 are given by the relation

	1	32	12	12	48	4	32	24	24	48	12	6	24	32	12	12	4	32	12	1
F_1	3	0	−1	−1	1	3	0	−1	−1	1	−1	3	−1	0	−1	−1	3	0	−1	3
F_2	3	0	−1	1	−1	3	0	−1	1	−1	1	3	1	0	1	−1	3	0	1	3
F_3	3	0	−1	−1	1	−3	0	1	1	−1	1	3	−1	0	−1	−1	−3	0	1	3
F_4	3	0	−1	1	−1	−3	0	1	−1	1	−1	3	1	0	1	−1	−3	0	−1	3
H_1	6	0	2	2	0	0	0	0	0	0	0	−2	−2	0	2	−2	0	0	0	6
H_2	6	0	−2	0	0	0	0	0	2	0	−2	−2	0	0	0	2	0	0	−2	6
H_3	6	0	2	−2	0	0	0	0	0	0	0	−2	2	0	−2	−2	0	0	0	6
H_4	6	0	−2	0	0	0	0	0	−2	0	2	−2	0	0	0	2	0	0	2	6

$$H_1\times H_2 = F_1+F_2+F_3+F_4+H_1+H_2+H_3+H_4.$$

This shows that the corresponding combination line is permitted in both spectra. Diamond is a specific case coming under the space group O_h^7. (See p. 157, *Theory of Groups and its Application to Physical Problems* by S. Bhagavantam and T. Venkatarayudu, 1951). Fuller details on the combination and overtone lines in this context will be published separately.

The author's thanks are due Professor D. M. Dennison and Professor G. B. B. M. Sutherland for their interest in this work.

* This work was sponsored by the U. S. Army Signal Corps under Contract DA-36-039 SC-5581.
[1] S. Bhagavantam and T. Venkatarayudu, Proc. Indian Acad. Sci. **9A**, 224 (1939).

Force Constants of the Hydrides of the Second and Third Periods

S. S. MITRA AND Y. P. VARSHNI
Department of Physics, Allahabad University, Allahabad, India
(Received April 19, 1954)

SYMBOLS: k_e—force constant; n—number of valence electrons of the element; Z—atomic number; A, B, a, α, β—constants.

Recently Mitra[1] has shown that $k_e^{\frac{1}{3}}$ is linear with n for the hydrides of the 2nd and 3rd periods.

It was shown by King[2] and Sheline[3] on semitheoretical grounds that $\log k_e$ should be linear with $\log Z$.

$$\log k_e = A\log Z + \log B \tag{1}$$

or

$$k_e = BZ^A.$$

Now for each period

$$Z = a+n$$

hence

$$k_e = B(a+n)^A$$

or

$$k_e^{1/A} = \alpha+\beta n \tag{2}$$

i.e., some power of k_e should be additive.

When Eq. (1) is tested for the 2nd group hydrides "A" comes out nearly 1.9, so the linearity of $k_e^{\frac{1}{3}}$ is justified in this case. But for the 3rd group hydrides, "A" is nearly 4. Hence $k_e^{\frac{1}{4}}$ should give

TABLE I.

n	Molecule	$k_e \times 10^{-4}$ (obs)	$k_e^{\frac{1}{2}}$ (obs)	$k_e^{\frac{1}{2}}$ (calc)
1	NaH	7.818	16.72	16.98
2	MgH	12.75	18.88	18.66
3	AlH	16.20	20.06	20.34
4	SiH	24.79	22.32	22.02
5	PH	32.57	23.89	23.70
6	SH	...	...	25.38
7	ClH	51.57	26.80	27.06

better linearity, which is tested in Table I. The equation is

$$k_e^{\frac{1}{2}} = 15.30 + 1.68n.$$

The value of the force constant of SH is predicted to be 41.5×10^4 dynes/cm.

The authors are thankful to Dr. K. Majumdar for his guidance. One of them (YPV) expresses his thanks to the Council of Scientific and Industrial Research (India) for the financial assistance.

[1] S. S. Mitra, J. Chem. Phys. (to be published 1954).
[2] G. W. King, J. Chem. Phys. **6**, 378 (1938).
[3] R. K. Sheline, J. Chem. Phys. **18**, 927 (1950).

Free Electron Network Model for Cyanines and Diphenyl Polyenes

SADHAN BASU
Indian Association for the Cultivation of Science, Calcutta 32, India
(Received April 12, 1954)

SOME valuable results have been obtained for the absorption spectra of conjugated organic dye molecules by Kuhn,[1] Bayliss,[2] and others by adopting a free electron gas model for these compounds. In addition to this assumption, further empirical assumptions were made while applying this theory to cyanines and diphenyl polyenes. For example, Kuhn[1] assumed that the phenyl group at the end of the conjugated chain of the cyanine molecule increases the path of the electron by 2/3 the length of the linear part, while Bayliss proposed that introduction of a phenyl group at the end of a polyene chain is equivalent to the introduction of another double bond in the chain. Although with these assumptions the agreement between the calculated and experimental frequencies of absorption was good, there is no theoretical justification for such assumptions. In recent years, the free electron model has been extended with encouraging results by various workers,[3,4] replacing the one-dimensional box approximation by a free electron network structure and applying continuity and conservation conditions at the junction of conjugated segments of the molecule under consideration. Especially interesting are the results obtained by Nakajima[5] using this model for styrene homologs, polyphenyls, nonalternate hydrocarbons, and pyridine. This model, when used for cyanines and diphenyl polyenes, also gave close agreement with experimental absorption values as reported in the present note.

For this purpose the cyanine molecule is divided into segments as shown in Fig. 1. The free electron wave function for the π electron in each segment is then expressed in the form

$$u(x) = a\cos\omega x + b\sin\omega x.$$

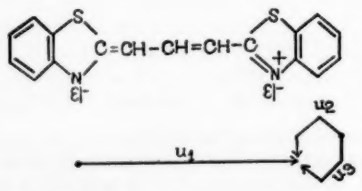

FIG. 1. Segments and wave function of cyanine molecule.

The origin of the coordinate of each wave function is taken at the point marked with a big dot and the coordinate x is expressed in units of C−C bond distance (1) taken as 1.39A. The energy states are given by

$$E = \frac{h^2\omega^2}{8\pi^2 ml^2}.$$

TABLE I. 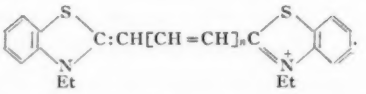

n	Transition from the state	λ(calculated)	λ(experimental)
1	7→8	5698	5550
2	8→9	6700	6500
3	9→10	7751	7600
4	10→11	8793	8700

At each junction point it is assumed that (i) the wave functions are continuous and (ii) the algebraic sum of the first derivative of the wave functions is zero. From these we get the two following relations,

$$\sin 3\omega = 0$$

and

$$\cos(n-3)\omega = 3\cos(n+3)\omega,$$

graphical solutions of which give the values of ω and hence E, the various energy states. (n in the above equation represents the number of bonds in the linear part starting from the terminal nitrogen atom to the junction point in the phenyl ring.) We then assume that each carbon atom in the conjugated system contributes one π electron each, while two nitrogen atoms together contribute 3. Electrons are distributed from the lowest energy state upwards, two on each state. Center of gravity of the absorption band corresponds to the transition from the highest filled level to the lowest vacant level. The results of such calculations are summarized in Table I. It is evident that the agreement is more than what can be expected and there is no need for making any empirical assumption as to the box dimension.

In the case of diphenyl polyenes the origin of the coordinate in the linear part is taken at the midpoint of the straight chain and relation obtained for ω are

$$\sin(3\omega) = 0$$

and

$$\cos(n/2-3)\omega = 3\cos(n/2+3)\omega.$$

Owing to symmetry of the molecule energy levels are doubly degenerate. The results are summarized in Table II. Since

TABLE II. 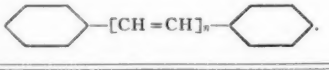

n	Transition from the state	λ(calculated)	λ(experimental)
3	9→10	3660	3770
4	10→11	4200	4040
5	11→12	4300	4240

graphical evaluation of ω was not very accurate it is expected that better agreement will be obtained by more accurate computation of ω (detailed calculations will be published elsewhere).

[1] H. Kuhn, J. Chem. Phys. **16**, 840 (1948).
[2] N. S. Bayliss, Quart. Revs. Chem. Soc. **6**, 319 (1952).
[3] K. Ruedenberg and C. W. Scherr, J. Chem. Phys. **21**, 1565 (1953).
[4] Y. Oshika, Busseiron Kenkyu **29**, 16 (1950).
[5] T. Nakajima, Sci. Repts. Research Insts. Tôhoku Univ. **5**, 98 (1953).

The Triple Point Temperature of Nitrogen Trifluoride (66.37°K) as a Possible Fixed Point*

LOUIS PIERCE AND E. L. PACE
Morley Chemical Laboratory, Western Reserve University, Cleveland, Ohio
(Received May 10, 1954)

A PRECISE study of the triple point temperature of two samples of nitrogen trifluoride has recently been made at this laboratory. In his survey of possible fixed points below 90°K, Hoge[1] has listed the melting point of nitrogen trifluoride as being unsuitable for a calibration point. His basis for this classification was the work of Ruff and Menzel,[2] this being the only previous study of the triple point temperature of nitrogen trifluoride. Our data suggest that it might serve very adequately as a fixed point. The compound melts very sharply (0.001–0.003° melting range). The difference in the triple point temperatures determined for the two samples was only 0.012 degree. The experimental results are summarized in Tables I and II.

The transition temperature (56.62°K) of nitrogen trifluoride was also investigated. However, this transformation occurred over a range of 0.05°, and will not be discussed here.

The gas was prepared by electrolysis of molten ammonium bifluoride, using essentially the same method that Ruff[3] has described. The most important difference was that a nickel anode was used in place of graphite to prevent contamination of the sample with carbon tetrafluoride. The anode gases were passed through a concentrated solution of potassium iodide and then distilled isothermally from a trap immersed in a frozen slush of isopentane to a trap immersed in liquid nitrogen. Finally, the liquid thus obtained was fractionally distilled at one atmosphere pressure in a low-temperature distilling column.

The triple point temperatures of two separate samples of nitrogen trifluoride, prepared in the above manner, were determined in an adiabatic calorimeter similar to that described by Yost *et al.*[4] Temperatures were measured with a platinum resistance thermometer calibrated against a standard thermometer by the Bureau of Standards in the range 11 to 90°K. In both determinations the nitrogen trifluoride was first cooled below the transition temperature and then warmed into the melting point. Six measurements were then taken at different proportions of solid melted over a period of three hours for run number 1, and seven hours for run number 2. The maximum temperature variation was 0.001 degree for run number 1, and 0.003 degree for run number 2. The triple point temperature determined by run number 1 was 66.361°K, while the second run gave the value 66.373°K.

TABLE I. The melting point of nitrogen trifluoride—run number 1. 5.675 grams. 0°C = 273.16°K.

Temperature °K	Percent melted
66.360	16.7
66.361	31.2
66.361	45.6
66.361	60.0
66.361	74.4
66.361	88.8
66.361	100 (extrapolated)

TABLE II. The melting point of nitrogen trifluoride—run number 2. 46.139 grams. 0°C = 273.16°K.

Temperature °K	Percent melted
66.370	3.2
66.372	14.9
66.372	38.5
66.372	50.3
66.372	67.9
66.373	85.6
66.373	100 (extrapolated)

We wish to thank Mr. W. T. Berg for his assistance in the experimental work, and Professor C. A. Brown for his many helpful suggestions on the preparation and purification of nitrogen trifluoride.

* This work was supported in part by a grant from the National Science Foundation.

[1] *Temperature—Its Measurement and Control in Science and Industry* (Reinhold Publishing Corporation, New York, 1941), p. 153.
[2] O. Ruff and W. Menzel, Z. anorg. allgem. Chem. **217**, 93 (1934).
[3] Ruff, Fischer, and Luft, Z. anorg. allgem. Chem. **172**, 417 (1934).
[4] Yost, Gerner, Osborne, Rubin, and Russel, Jr., J. Am. Chem. Soc. **63**, 3488 (1941).

The Calculation of Equilibrium Constants for Several Exchange Reactions of Nitrogen-15 between Oxy Compounds of Nitrogen*

W. SPINDEL
Chemistry Department, New York State College for Teachers, Albany, New York
(Received May 17, 1954)

UREY[1,2] and others[3] have outlined methods for calculating equilibrium constants for isotope exchange reactions, and Urey[2] has calculated constants for a large number of exchange reactions involving isotopes of the light elements. Very few calculations are available however for exchange reactions possible between the various oxides and oxy-ions of nitrogen.

TABLE I. Fundamental frequencies of isotopic molecules.

Molecule	ν_1	ν_2	ν_3	ν_4	α[a]	Force constants ($\times 10^5$ dynes/cm)		Reference
$N^{14}O^{16}$	1906.54							Urey[c] p. 567
$N^{15}O^{16}$	1872.34							
$N^{14}O_2^{16}$	1320	648	1621		60°	k_1	k_{δ/l^2}	Herzberg[d,e] pp. 161, 170
$N^{15}O_2^{16}$	1296.4	644.3	1587			9.13	1.52	
$N^{14}O_2^{16}$	1320	648	1621		60°	a_{11}	a_{33}	Herzberg[d,f] p. 160
$N^{15}O_2^{16}$	1313	636	1587			9.13	4.34	Spindel[g]
$N^{14}O_2^{16-}$	1050	831	1390(2)	720(2)				Herzberg[d,e] p. 178
$N^{15}O_2^{16-}$	1050	809.3	1351.9(2)	720(2)[b]				
$N^{14}O_2^{16-}$	1320	750	1220		43°	a_{11}	a_{33}	Williams[h,f]
$N^{15}O_2^{16-}$	1304.51	741.16	1198.93			6.87	4.31	

[a] α is half the angle at the apex of the triangle.
[b] The calculation actually gave a value of 721.0 cm^{-1} for ν_4. Since in theory substitution of a heavier isotope should lower the frequency, ν_4 was assumed to remain unchanged by isotopic substitution. This introduces an error of less than 2 parts in a thousand in the calculated equilibrium constant.
[c] See reference 2, p. 567.
[d] See reference 4, pp. 160, 161, 170, 178.
[e] Calculated using valence forces.
[f] Calculated using central forces.
[g] See reference 6.
[h] See reference 7.

Although calculations of equilibrium constants from spectroscopic frequencies are quite unambiguous, calculations of spectroscopic frequencies for the rarer isotopic molecules from fundamental frequencies of the abundant molecules yield only approximate results in the case of polyatomic molecules. In particluar, a choice of formulas is available, depending upon whether central forces or valence forces are assumed for the molecule.[2] In order to evaluate equilibrium constants for isotopic exchange, we have calculated the vibrational frequencies of rarer isotopic species for several molecules. The results of these calculations are tabulated in Table I, together with notations as to type of force field used and sources for the fundamental frequencies of the abundant molecules.

Equations used in calculating frequencies of isotopic molecules are derived directly from equations in Herzberg,[4] which relate vibrational frequencies to atomic masses and force constants. Illustrating this for the plane symmetrical NO_3^- ion we derive the following set of relationships by substituting an isotopic species X^i for the central X atom only:

$$\nu_1^i=\nu_1, \quad \frac{(\nu_2^i)^2}{(\nu_2)^2}=\frac{1+3m_y/m_x^i}{1+3m_y/m_x},$$

$$\frac{(\nu_3^i)^2+(\nu_4^i)^2}{(\nu_3)^2+(\nu_4)^2}=\frac{1+\frac{3}{2}m_y/m_x^i}{1+\frac{3}{2}m_y/m_x}, \quad \frac{(\nu_3^i\nu_4^i)^2}{(\nu_3\nu_4)^2}=\frac{1+3m_y/m_x^i}{1+3m_y/m_x}.$$

The frequencies for $N^{15}O_2$ are somewhat disturbing since the fundamental frequency ν_1 for the abundant molecule is still in doubt.[4] Calculations for this molecule have been made previously[5,6] but the frequencies used by Leifer[5] appear questionable enough to warrant recalculation. Earlier calculations by the author[7] were made using central forces.

Frequencies for the $N^{15}O_2^-$ ion were calculated using an assumption of central forces, since studies by Williams[7] indicated that the central force field approximation yielded more satisfactory results for NO_2^-.

Equilibrium constants for the various exchange reactions are calculated by well-known methods,[2,3] once frequencies for isotopic species are available. For the reactions listed, where the symmetry of the molecules remains unchanged, the equilibrium constant for an exchange reaction simply reduces to the ratio of partition functions of the product over the reactant species.

In Table II are recorded the ratio of partition functions and equilibrium constants for several exchange reactions involving isotopes of nitrogen. This table is essentially similar to the very extensive and convenient tables of such equilibria listed by Urey.[2]

TABLE II. Equilibrium constants for nitrogen exchange at 25°C.

	$N^{15}O_3^-$ / $N^{14}O_3^-$	$N^{15}O_2$[a] / $N^{14}O_2$	$N^{15}O_2$[b] / $N^{14}O_2$	$N^{15}O_2^-$ / $N^{14}O_2^-$	$N^{15}O$ / $N^{14}O$
Q_2/Q_1	1.16_9	1.08_9	1.10_9	1.07_2	1.06_6
$N^{15}O_3/N^{14}O_3^-$	(1.00)	1.07_3	1.05_3	1.09_0	1.09_6
$N^{15}O_2/N^{14}O_2$[a]		(1.00)		1.01_5	1.02_1
$N^{15}O_2/N^{14}O_2$[b]			(1.00)	1.03_4	1.04_0
$N^{15}O_2^-/N^{14}O_2^-$				(1.00)	1.00_6
$N^{15}O/N^{14}O$					(1.00)

[a] Central force field.
[b] Valence force field.

At the top under the chemical formula for the substances are listed the ratio Q_2/Q_1 at 25°C. The values in the body of the table are equilibrium constants for the reactions. In all cases the equilibrium constants are arranged so that the heavier isotope concentrates preferentially in the compound listed at the left. Calculations have been made using both central force and valence force field approximations for the NO_2 molecule. The differences are surprisingly large and may presumably be due to the large difference in the frequency ν_1. It seems reasonable to place more reliance on the valence force calculations for the NO_2 molecule since Herzberg[8] indicates that the valence force approximation is generally much superior for XY_2 molecules. The central force calculations are included for completeness.

Of the equilibria calculated, the constant for exchange between NO_3^- and NO is of most encouraging magnitude.

The author wishes to thank Miss A. Christodulu for her assistance with many of the calculations.

* The work reported here was supported by the U. S. Atomic Energy Commission under Contract No. AT(30–3)–91.

[1] H. C. Urey and L. G. Greiff, J. Am. Chem. Soc. **57**, 321 (1935).
[2] H. C. Urey, J. Chem. Soc. 562 (1947).
[3] J. Bigeleisen and M. G. Mayer, J. Chem. Phys. **15**, 261 (1947).
[4] G. Herzberg, *Infrared and Raman Spectra of Polyatomic Molecules* (D. Van Nostrand Company, Inc., New York, 1945) p. 302, p. 178.
[5] E. Leifer, J. Chem. Phys. **8**, 301 (1940).
[6] W. Spindel, Ph.D. thesis, Columbia University (1950).
[7] D. Williams, J. Am. Chem. Soc. **61**, 2987 (1939).
[8] G. Herzberg, *Infrared and Raman Spectra of Polyatomic Molecules* (D. Van Nostrand Company, Inc., New York, 1945), p. 171.

Homogeneous Activation of Molecular Hydrogen by Cupric Acetate

J. HALPERN AND R. G. DAKERS
Department of Mining and Metallurgy, University of British Columbia, Vancouver, Canada
(Received May 17, 1954)

WITH few exceptions the known catalysts for hydrogenation reactions are solids such as metals or metallic oxides. Although widely studied, the detailed mechanism by which they function is still not fully understood. In general it appears that the reactants become activated through adsorption on the catalyst surface, and that the catalyzed reaction occurs heterogeneously. Most theories of hydrogenation catalysis are concerned with this adsorption process and thus relate primarily to heterogeneous catalysts.

Only two instances involving homogeneous catalysis of hydrogenation reactions in solution appear to have been reported. Cuprous acetate, dissolved in quinoline, was found by Calvin[1] to catalyze the hydrogenation of compounds such as quinone, the hydrogen apparently becoming activated through formation of a complex with a dimer of cuprous acetate.[2] Similar catalytic activity in a variety of hydrogenation reactions, has been attributed to dicobalt octacarbonyl.[3]

We have found recently that under certain conditions molecular hydrogen can also be activated homogeneously by solutions of cupric acetate. This effect is reflected in the following reaction between cupric acetate and hydrogen which takes place homogeneously in aqueous solution:

$$2\,CuAc_2+H_2+H_2O\rightarrow Cu_2O+4HAc. \qquad (1)$$

When hydrogen is present in excess, the reaction goes essentially to completion, all the copper being precipitated as Cu_2O.

The kinetics of this reaction were investigated over the range 80° to 140°C and 6.8 to 34 atmospheres of H_2 and the rate was shown to be represented by the following expression:

$$\frac{-d[H_2]}{dt}=\frac{-d[CuAc_2]}{2dt}=k_2[H_2][CuAc_2]. \qquad (2)$$

The second-order rate constant k_2 was found to be independent of $[H_2]$ and $[CuAc_2]$ and of the pH of the solution. The solutions contained an excess of acetate ion so that most of the cupric acetate was in the form of the undissociated $CuAc_2$ molecule.[4] It was conclusively established that the reaction is homogeneous, the rate being independent of the surface of the stainless steel reaction vessel and of the cuprous oxide product. The activation energy of the reaction is 24.2 kcal per mole and the frequency factor, 8×10^{11} 1 mole^{-1} sec^{-1}, corresponding to an entropy of activation at 100°C of −6.5 eu.

The kinetic results suggest that the rate-determining step of the reaction is a homogeneous bimolecular process involving the formation of a complex between a molecule of hydrogen and a molecule of cupric acetate. The hydrogen apparently becomes activated in this step, so that subsequent hydrogenation of the cupric acetate and formation of cuprous oxide are rapid. The following sequence of steps would appear to be involved:

$$H_2+CuAc_2 \xrightarrow[\text{slow}]{k_2} CuAc_2\cdot H_2 \qquad (3)$$

$$CuAc_2\cdot H_2+CuAc_2+H_2O \xrightarrow[\text{fast}]{} Cu_2O+4HAc. \qquad (4)$$

The measured rate constant k_2 thus refers to reaction (3) which determines the rate of the over-all process.

It is evident from these considerations that cupric acetate should also be able to function as a catalyst for the homogeneous hydrogenation of other compounds. Peters and Halpern[5] have confirmed this in a recent study in this laboratory and have shown that when a reducible substrate such as $Cr_2O_7^{--}$ is present in the solution along with the cupric acetate, it is preferentially hydrogenated in accordance with the following scheme:

$$3H_2+3CuAc_2 \xrightarrow[\text{slow}]{k_2} 3CuAc_2\cdot H_2 \qquad (5)$$

followed by

$$3CuAc_2 \cdot H_2 + Cr_2O_7^{--} + 8H^+ \xrightarrow[\text{fast}]{} 2Cr^{+++} + 7H_2O + 3CuAc_2. \quad (6)$$

Under these conditions the $CuAc_2$ is regenerated and functions as a true homogeneous catalyst. No reduction of $CuAc_2$ was observed until all the $Cr_2O_7^{--}$ had reacted. This reaction is kinetically similar to that between $CuAc_2$ and H_2. For both reactions the rate at which hydrogen is consumed is represented by Eq. (2). This is to be expected since the rate controlling step is the same in each case.

Support of this work through a grant from the National Research Council of Canada is gratefully acknowledged.

[1] M. Calvin, Trans. Faraday Soc. **34**, 1181 (1938), J. Am. Chem. Soc. **61**, 2230 (1939).
[2] S. Weller and G. A. Mills, J. Am. Chem. Soc. **75**, 769 (1953).
[3] M. Orchin, *Advances in Catalysis* (Academic Press Inc., New York, 1953), Vol. **5**, pp. 385–415.
[4] K. J. Pedersen, Kgl. Danske Videnskab. Selskab. Mat.-fys. Medd. **22**, No. 12 (1945).
[5] E. Peters and J. Halpern (unpublished results).

A Fine Structure in Absorption Spectrum of Tricesium Cobaltous Pentachloride in Crystalline State

SHOICHIRO YAMADA AND RYUTARO TSUCHIDA
Department of Chemistry, Faculty of Science, Osaka University, Nakanoshima, Osaka, Japan
(Received March 24, 1954)

RECENTLY Katzin *et al.*[1] reported the reflection spectrum of dipyridinium cobaltous tetrachloride and dicesium cobaltous tetrachloride in the visible region. Their measurements, however, were made with powdered solid, and, therefore, their results, limited to the visible region, were only qualitative. In the course of study on nonplanar quadricoordinated complexes, we have obtained with a single crystal of Cs_3CoCl_5, which contains $CoCl_4^{=}$ ions, a quantitative absorption spectrum involving a regular series of sharp peaks in the visible and ultraviolet region, and succeeded in correlating those bands with electronic-vibrational transitions and in expressing wave numbers of those band maxima by a simple equation. Such a regular structure in the visible and ultraviolet has hardly been recorded before with crystals of inorganic coordination compounds.

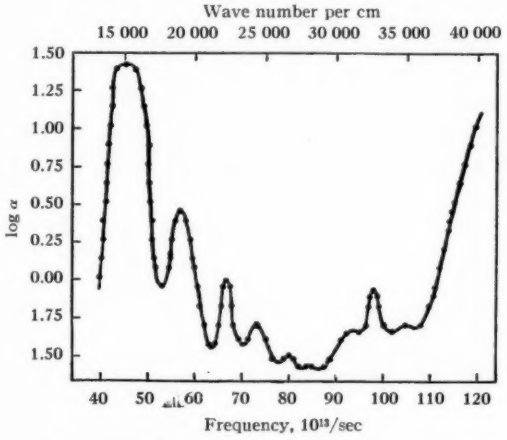

FIG. 1. Absorption spectrum of Cs_3CoCl_5 in crystalline state at room temperature.

Blue, tetragonal crystals of Cs_3CoCl_5 were prepared from an aqueous solution of cobaltous chloride and excess of cesium chloride. Quantitative absorption spectra were determined at room temperature by Tsuchida-Kobayashi's microscopic method[2] using a microcrystal in the region from 2400 to 7500A with polarized light having its electric vector along and perpendicular to the c-plane.[3] The absorption bands in the region of the measurement (Fig. 1) are evidently due to the $CoCl_4^{=}$ ions under influence of cesium and chlorine ions. Between the spectra corresponding to the two directions there could be observed only a very slight difference. The slight dichroism, which is supposed to be caused by dissymmetrical crystalline field, confirms the tetrahedral configuration of $CoCl_4^{=}$ ions in this crystal.[3] Positions of absorption peaks almost correspond with those reported in the visible region,[1] and displaced slightly toward shorter wavelength compared with the data in solution.[4] It is readily noticed that absorption peaks in the region covering ν 40 to 85×10^{13}/sec form a series. It has been found that the set of absorption peaks, considered to be due mainly to coordination linkages in the complex, can be expressed satisfactorily by the equation:

TABLE I. A series of absorption bands of Cs_3CoCl_5 in crystalline state.

m in Eq. (1)	0($\tilde{\nu}_0$)	1	2	3	4	5
$(\tilde{\nu})_{cal}$ 10^3/cm	15.0	18.8	22.0	24.6	26.6	28.1
$(\tilde{\nu})_{obs}$ 10^3/cm	15.0	18.9	22.2	24.4	26.6	28.1
logα[a]	1.43	0.47	1.99	1.71	1.50	1.43

[a] α represents absorption coefficient per mm of the crystal.

$$\tilde{\nu} = \tilde{\nu}_0 + am - bm(m+1) \quad (1)$$

where $\tilde{\nu}$ denotes wave number of a band maximum, $\tilde{\nu}_0$ that of the band head, a and b constants, and m positive integer including zero (Table I). For a and b, the following values have been obtained: $a=4.37\times10^3$/cm and $b=2.92\times10^2$/cm. The above expression might be derived approximately on the assumption that the mentioned peaks correspond to transitions from the ground electronic state with vibrational quantum number zero to the excited electronic states with m as vibrational quantum number, and that the vibrational frequency is changed very little in the transition. The intensity relation may also be understood qualitatively on this basis.[5] Assuming the above mechanism of the transition, the dissociation energy of the complex ion can be estimated,[6] in the rough approximation, as 40.2 kcal/mole. The above approximate value seems reasonable, favoring the above assumption.

[1] L. I. Katzin and E. Gebert, J. Am. Chem. Soc. **75**, 2830 (1953).
[2] (a) R. Tsuchida and M. Kobayashi, *The Colours and the Structures of Metallic Compounds*, (Zoshindo, Osaka, Japan, 1944), p. 180. (b) See, for example, S. Yamada, J. Am. Chem. Soc. **73**, 1182 (1951).
[3] About the crystal structure, see H. M. Powell and A. F. Wells, J. Chem. Soc. **1935**, 359.
[4] A. von Kiss and M. Gerendas, Z. physik. Chem. **A180**, 117 (1937).
[5] See, for example, G. Herzberg, *Spectra of Diatomic Molecules* (D. Van Nostrand Company, Inc., New York, 1950), p. 193.
[6] See, for example, K. S. Pitzer, *Quantum Chemistry* (Prentice-Hall Inc., New York, 1953), p. 255.

Correlation Between Infrared Intensities, Dissociation Energies, and Equilibrium Internuclear Distances for Diatomic Molecules*

HENRY AROESTE
Guggenheim Jet Propulsion Center, California Institute of Technology, Pasadena, California
(Received April 19, 1954)

ONE may expand the dipole moment as a function of internuclear distance as follows:

$$\mu = \mu_0 + \left(\frac{\partial\mu}{\partial r}\right)_{r=r_0}(r-r_0) + \cdots. \quad (1)$$

The derivative $(\partial\mu/\partial r)_{r=r_0}$ may be obtained from infrared intensity measurements. Using the best available data of $(\partial\mu/\partial r)_{r=r_0}$ for NO, CO, HCl, and HBr,[1] and the most generally accepted values for the dissociation energies and equilibrium internuclear distances of these diatomic molecules,[2] $(\partial\mu/\partial r)_{r=r_0}$ is found to be proportional to the dissociation energy divided by the square of the equilibrium internuclear distance. A graph of $(\partial\mu/\partial r)_{r=r_0}$ as

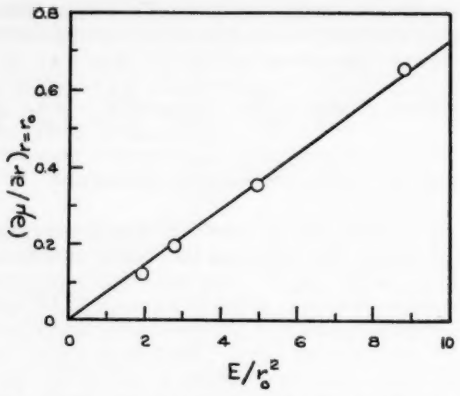

FIG. 1. Graph of $(\partial\mu/\partial r)r=r_0$ in e (electronic charge units) as a function of $E/r_0^2(ev/A^2)$.

a function of E/r_0^2 s given in Fig. 1. The values used for E, r_0, and $(\partial\mu/\partial r)_{r=r_0}$ are given in Table I. It is pleasant to observe that the data may be correlated so that a straight line goes through the origin, which, in a sense, constitutes a fifth plotted point.

The higher values of CO and NO, which are perhaps more widely accepted, were used here. It is interesting that the value of $(\partial\mu/\partial r)_{r=r_0}$ reported by Penner and Weber for NO, which differs

TABLE I. Molecular parameters.

	$\left(\frac{\partial\mu}{\partial r}\right)_{r=r_0}$	r_0(A)	E(ev)
HBr	0.121e	1.414	3.75
HCl	0.198e	1.275	4.43
NO	0.352e	1.151	6.48
CO	0.655e	1.128	11.11

appreciably from previously reported values, correlates with these results. It is further interesting to note that the constant of proportionality has a value of approximately one electronic charge per cubic angstrom.

A fair correlation for overtone intensities on HBr, HCl, and CO has also been noted by plotting one of the possible values of $(\partial^2\mu/\partial r^2)_{r=r_0}$ against E/r_0^2.[3] These relations should be useful for estimating infrared intensities of molecules such as HF and OH, where measurement is difficult.

* Supported by the U. S. Office of Naval Research, Contract Nonr-220(03), NR 015 210.

[1] S. S. Penner and D. Weber, J. Chem. Phys. **21**, 649 (1953); **19**, 1351 (1951).

[2] G. Herzberg, *Spectra of Diatomic Molecules* (D. Van Nostrand Company, Inc., New York, 1950); A. Gaydon, *Dissociation Energies and Spectra of Diatomic Molecules* (John Wiley and Sons, Inc., New York, 1947).

[3] In the paper of S. S. Penner and D. Weber, J. Chem. Phys. 21, 649 (1953), the coefficients of ξ^2 in Eq. (4) for NO should be changed to 8.77×10^{-18} or -3.06×10^{-18}; in Eq. (5) for HCl to 2.96×10^{-18} or -0.140×10^{-18}. The indicated corrections are the result of recalculation of appropriate coefficients using (a) the intensity data given in the original paper and (b), other required spectroscopic constants listed by Herzberg, reference 2.

Navier-Stokes' Equations for Non-Newtonian Liquids

ALI A. K. IBRAHIM
Physics Department Faculty of Science, The University of Alexandria, Alexandria, Egypt

(Received April 23, 1954)

IN Navier-Stokes' equation[1,2] we have neglected the elastic forces. Let us introduce them.

Let V_x, V_y, and V_z be the components of the velocity V; S_x, S_y, and S_z be the components of the displacement S; and S_x and S_x+dS_x be the displacements in the x direction at two planes dy apart (see Fig. 1). If A and C be such laminas, while B is a plane between them, A exerts a force per unit area on $B=-N(\partial S_x/\partial y)$, where N is the modulus of rigidity of the liquid in dyne/cm². Also, C exerts a force per unit area on

$$B=\left[N\frac{\partial S_x}{\partial y}+\frac{\partial^2 S_x}{\partial y^2}dy\right].$$

Therefore, the net force on B per unit mass $=(N/\rho)(\partial^2 S_x/\partial y^2)$, where ρ is the density of the liquid in g/cm³. In the general case, the total elastic force per unit mass due to the component of displacement S_x is

$$\frac{N}{\rho}\left[\frac{\partial^2 S_x}{\partial x^2}+\frac{\partial^2 S_x}{\partial y^2}+\frac{\partial^2 S_x}{\partial z^2}\right],$$

or, briefly

$$\frac{N}{\rho}\nabla^2 S_x.$$

Also, that due to S_y is $(N/\rho)\nabla^2 S_y$, and that due to S_z is $(N/\rho)\nabla^2 S_z$.

This force must be added to those on the right-hand side of Navier-Stokes' equation, and the general equations of flow become

$$\left.\begin{aligned}\frac{dV_x}{dt}&=X-\frac{1}{\rho}\frac{\partial P}{\partial x}+\nu\nabla^2 V_x+\frac{N}{\rho}\nabla^2 S_x\\ \frac{dV_y}{dt}&=Y-\frac{1}{\rho}\frac{\partial P}{\partial y}+\nu\nabla^2 V_y+\frac{N}{\rho}\nabla^2 S_y\\ \frac{dV_z}{dt}&=Z-\frac{1}{\rho}\frac{\partial P}{\partial z}+\nu\nabla^2 V_z+\frac{N}{\rho}\nabla^2 S_z\end{aligned}\right\},\qquad(1)$$

where X, Y, and Z are the external forces, P is the instantaneous pressure, and ν is the kinematic viscosity.

The first two terms on the right-hand side of each of the Eqs. (1) express the rate of variation of the component of velocity in consequence of the external forces and of the instantaneous distribution of pressure (this is the case of a frictionless liquid). The terms $\nu\nabla^2 V_x$, $\nu\nabla^2 V_y$, and $\nu\nabla^2 V_z$, due to viscosity, give an additional

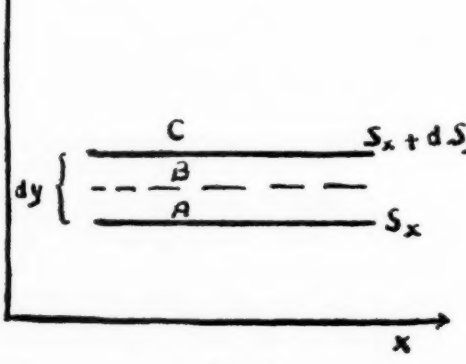

FIG. 1.

variation (this is the case of Newtonian liquid), and the remaining terms $(N/\rho)\nabla^2 S_x$, $(N/\rho)\nabla^2 S_y$, and $(N/\rho)\nabla^2 S_z$, due to elasticity, give another additional variation (this is the case of a non-Newtonian liquid).

[1] Navier-Stokes, Mém. Acad. Sci. **VI**, 389 (1822).

[2] Navier-Stokes, Compt. rend. **17**, 1240 (1843).

The Pure Quadrupole Spectrum of 1,2,4-Trichlorobenzene

ANDRÉ MONFILS AND JULES DUCHESNE
Institut d'Astrophysique, University of Liège, Cointe-Sclessin, Belgium
(Received April 23, 1954)

THE aim of this paper is to study to what extent the quadrupole spectrum of 1,2,4-trichlorobenzene fits the theory recently put forward by the authors[1] governing the behavior of the frequencies of the chlorine derivatives of benzene. A frequency modulated super-regenerative oscillator has been used and the spectra have been automatically recorded after phase sensitive detection of the signals. The measured frequency values corresponding to Cl^{35}, expressed in Mc/sec units, are given, for different temperatures, in Table I. The mean error for these measurements

TABLE I.

	77°K	164°K	178°K
I	35.189	35.085	35.053
	35.617	35.450	35.409
II	36.173	36.045	36.014
	36.380	36.196	36.155
	36.400	36.209	36.167
	36.623	36.468	36.429

is approximately ±2 kc/sec. The results fall into two groups which correspond to two chemically distinct chlorines, in 4-position for the lower frequency group and in 1- and 2-position for the higher frequency group. The basis for this statement rests on the fact that each chlorine atom in the molecule gives rise to two lines and that the group of the four closest lines is obviously due to the two similar atoms, whereas the two other lines have therefore to be identified with the remaining one. From these data, it is easy to deduce by interpolation the frequency values to be expected at 173°K, the temperature chosen in our previous work.[1] We thus find 35.065 and 35.424 Mc/sec for group I and 36.025, 36.170, 36.182, and 36.444 Mc/sec for group II, the average values corresponding to each group being 35.244 and 36.205 Mc/sec, respectively. Now, the average quadrupole coupling constants are 70.488 and 72.410 Mc/sec. The graph in Fig. 1, which has already

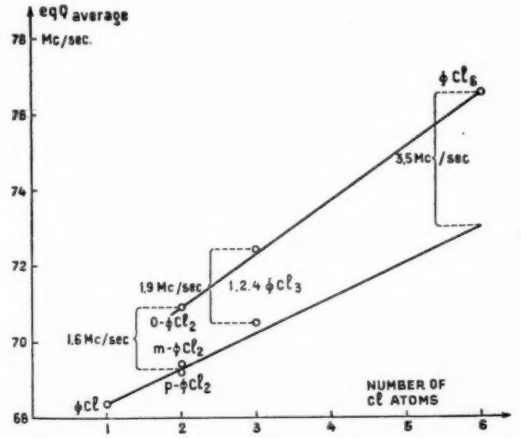

FIG. 1. Cl^{35} average quadrupole couplings in terms of the number of Cl atoms in chlorobenzenes at 173°K.

been given previously,[1] represents these constants for chlorobenzenes in terms of the number of substituted atoms. It is seen that the values obtained agree satisfactorily with those given by the theoretical curves, within the range of the incertitude due to out method of removing the difficulty resulting from the multiplicity of lines. The difference in eQq is 1.9 for 1,2,4-trichlorobenzene, whereas it amounts to 1.6 for dichlorobenzenes and to 3.5 Mc/sec for hexachlorobenzene. However, no change would have been expected on going from the first to the second compound, as the steric hindrance between the closest chlorines would appear to be identical in both cases. If the discrepancy is real, this would indicate that the out-of-plane bending of the CCl bonds in 1,2,4-trichlorobenzene depends upon the chlorine atom in 4-position. According to the method given before[1] a value of 20° is obtained as compared with 18° adopted for *o*-dichlorobenzene.

It is perhaps worth while noticing that the six lines of 1,2,4-trichlorobenzene have almost the same intensity and are very weak with respect to *p*-dichlorobenzene even when the spreading due to the multiplicity of lines is taken into account. This fact might perhaps result from the presence of syncrystallizing impurities in 1,2,4-trichlorobenzene, which, as has been recently demonstrated by the authors,[2] might considerably decrease the intensity of the lines even for very low concentrations.

We wish to express our thanks to Professor G. Duyckaerts of the Department of Analytical Chemistry for the loan of a sample of 1,2,4-trichlorobenzene.

[1] J. Duchesne and A. Monfils, J. Chem. Phys. **22**, 562 (1954).
[2] J. Duchesne and A. Monfils, Compt. rend **238**, 1801 (1954).

Quantum Yield of Para-Diazo N−N, Dimethylaniline Zinc Chloride Dihydrate at 3660A

ALBERT BARIL, JR.
Biophysics Laboratory, Tulane University, New Orleans, Louisiana
(Received April 23, 1954)

ACCORDING to Andresen[1] diazonium salts irradiated in aqueous solution are decomposed into a phenol and nitrogen. In the case of para-diazo N−N, dimethylaniline zinc chloride dihydrate, the photochemical decomposition is

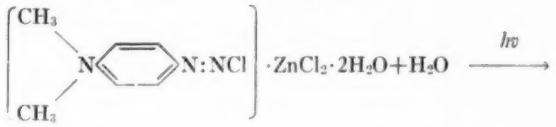

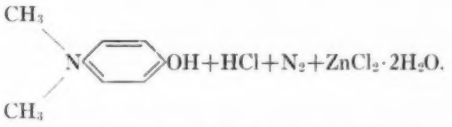

Since this reaction is unimolecular the quantum yield can be readily obtained by a measure of the appearance of nitrogen upon irradiation by the proper wavelength.

Prior to the determination of the quantum yield, the ultraviolet and visible absorption spectrum of para-diazo N−N, dimethylaniline zinc chloride dihydrate was investigated. A Beckman Model DU Quartz Spectrophotometer was used to measure the absorption spectrum of the diazonium compound at room temperature (about 25°C) from 2200A to 6000A. The aqueous solution of the diazonium salt was introduced into silica cells having plane parallel windows which were in the parallel light beam from the Beckman hydrogen discharge or from the incandescent source of the spectrophotometer. A cell length of 1 cm and solution concentration of 0.00006 *M* were used. The plot of the absorption spectrum was used to calculate the molecular extinction coefficients from the equation

$$\epsilon = 1/Cl \log_{10} I_0/I$$

where C is expressed in moles/liter and l in cm. These coefficients are plotted as a function of wave number in Fig. 1.

The absorption spectra of para-diazo N−N, dimethylaniline zinc chloride dihydrate consist of a visible region of weak absorption followed by an ultraviolet region of rapidly increasing absorp-

tion. In the near ultraviolet region there is strong absorption in the band between 4200A and 3200A, and weaker absorption in the band starting at 2800A and continuing into the ultraviolet.

Considering the absorption spectrum, the wavelength selected for the determination of the quantum yield was the mercury line of 3660A. This wavelength falls within a well-defined band and is totally absorbed by the diazonium salt. The light source employed was a General Electric AH-6 mercury arc. The 3600A line was isolated by the combination of Corning Filter Violet ultra No. 7–37, and H.R. clear chemical glass No. 0–53. As determined by the Beckman Spectrophotometer, this filter combination had a transmission of 18 percent at 3660A and was opaque at wavelengths below 3500A and above 3850A. For quantum yield measurements, the light incident on the reaction system was determined by a Hilger thermopile coupled to a sensitive galvanometer. The

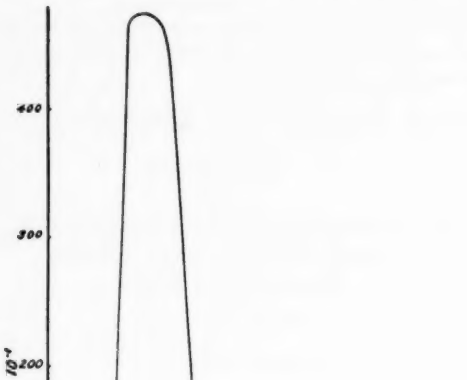

FIG. 1. Absorption spectra of para-diazo N−N, dimethylaniline zinc chloride dihydrate.

thermopile had been calibrated with Radiation Standard C-551 supplied by the National Bureau of Standards. A value of 4.34×10^{14} quanta/sec/cm^2 was obtained.

The number of molecules of para-diazo N−N, dimethylaniline zinc chloride dihydrate decomposed upon irradiation was determined by measuring the amount of nitrogen released. This was accomplished by using a constant volume manometer technique capable of detecting $\frac{1}{2}$ microliter of nitrogen. The apparatus consisted of a photolytic cell, modified to accommodate magnetic stirring, connected to a Warburg type manometer. The system was calibrated according to the method of Umbreit, Burris, and Stauffer[2] so that the amount of evolved gas was given by the product of the alteration in the manometric fluid level and a flask constant. The flask constant is given by the relation

$$k=\frac{V_g 273/T+\alpha V_f}{P_0},$$

where V_g is the volume of gas phase of the system, V_f is the volume of the diazonium solution in the reaction cell, α is the solubility of nitrogen in water, and P_0 is standard pressure expressed in terms of the manometric fluid (Brodie solution).

Table I is a tabulation of experimental runs conducted at a temperature of 23°C with irradiation periods of 600 sec. The

TABLE I.

Trial	Nitrogen evolved (molecules)	Quantum efficiency
A	1.238×10^{18}	0.969
B	1.214×10^{18}	0.950
C	1.262×10^{18}	0.988
D	1.238×10^{18}	0.969

(Number of quanta $=1.276\times10^{18}$)

values obtained for the quantum yield approach unity as was expected from the theoretical consideration of the photochemical decomposition of the diazonium compound. These values are in close agreement with those determined by Gavlin[3] conducting similar experiments.

The author would like to thank the Ringwood Chemical Corporation for supplying the para-diazo N−N, dimethylaniline zinc chloride dihydrate used in this investigation.

[1] Andresen, *Photographische Correspondenz* (Leipzig) Vol. 31 (1895).
[2] Umbreit, Burris, and Stauffer, *Manometric Technique and Tissue Metabolism* (Burgess Publishing Company, Minneapolis, Minnesota, 1949).
[3] G. Gavlin, Armour Project Report 90–595C, Armour Research Foundation.

The Energy Difference of the Two Rotational Isomers of 1,2-Dichloroethane in Various Solutions

AKIYOSHI WADA AND YONEZO MORINO
Department of Chemistry, Faculty of Science, Tokyo University, Bunkyo-ku, Tokyo, Japan
(Received May 11, 1954)

THE influence of the solvent upon the energy difference, ΔE, of the rotational isomers was calculated theoretically in the previous article[1] by considering the reaction field on the assumption that the medium around a molecule is a continuous dielectric. In order to confirm this effect the energy difference between the rotational isomers of 1,2-dichloroethane is measured at various mixing ratios with several solvents which have considerably different dielectric constants. Now the isomeric ratio is given by the energy difference between the two isomers, ΔE[2]:

$$n_g/n_t=w\exp(-\Delta E/kT), \tag{1}$$

where n_g and n_t are the numbers of molecules belonging to the two isomeric forms, the *gauche-* and *trans*-forms, respectively, w a constant specific to the compound: 1.93 for 1,2-dichloroethane at room temperature, k Boltzmann constant, and T the absolute temperature. The ratio of the intensities of the Raman lines corresponding to the isomers is proportional to the isomeric ratio

$$I_g/I_t=C(n_g/n_t), \tag{2}$$

where C is a constant. From Eqs. (1) and (2), the energy difference

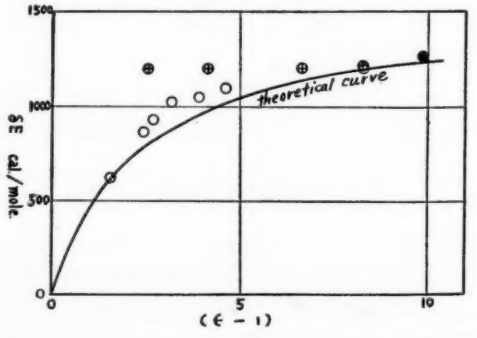

FIG. 1. The stabilization energy of 1,2-dichloroethane in nonpolar solutions. ○—n-heptane solution; ⊕—benzene solution; ●—pure liquid.

between the two rotational isomers is related to the intensity ratio as follows:

$$\Delta E = kT[\log Cw - \log(I_g/I_t)]. \tag{3}$$

The unknown constant Cw is decided by the experimental fact that the energy difference is zero in the case of the pure liquid of 1,2-dichloroethane.[3]

The intensity ratio of the Raman lines 754 cm^{-1} and 654 cm^{-1} of 1,2-dichloroethane, which are assigned to the *trans*- and *gauche*-forms, respectively, is measured by an automatic pen-recording Raman spectrometer which has recently been constructed by us[4] by use of a multiplier phototube RCA 1P21. The observed energy differences ΔE_{soln} in *n*-heptane and benzene solutions are plotted in Fig. 1 in terms of the stabilization energy $\delta E = \Delta E_{gas} - \Delta E_{soln}$ *versus* dielectric constant of the solutions,* and in Fig. 2 those in

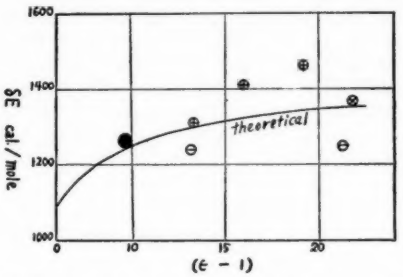

FIG. 2. The stabilization energy of 1,2-dichloroethane in polar solutions. ⊕—acetone solution; ⊖—methyl alcohol solution; ⊗—nitrobenzene solution; ●—pure liquid.

acetone, methyl alcohol, and nitrobenzene solutions. Acetone has a strong Raman line at 768 cm^{-1} and this is so close to the line 754 cm^{-1} of 1,2-dichloroethane that the influence of the bottom of the former line is estimated by taking into account the intensity distribution in the Raman spectrum of pure acetone liquid.

The stabilization energies δE in solutions are in good agreement with the values calculated by the theory reported previously.[1] It is, however, easily seen in Figs. 1 and 2 that for the solutions in benzene and in acetone the stabilization energy could not be explained by such a simple electrostatic model. This gives a strong evidence to support the former conclusion[1,5] that a kind of short-range force must be considered in these cases.

[1] A. Wada, J. Chem. Phys. **22**, 198 (1954).
[2] S. Mizushima, *Internal Rotation* (Academic Press, Inc., New York, 1954).
[3] K. Kuratani, Rept. Inst. Sci. and Technol. Univ. Tokyo **6**, 221 (1953); **7**, 11 (1953). H. Garding and P. C. Meermann, Rec. trav. chim. **61**, 523 (1942). Rank, Kagarise, and Axford, J. Chem. Phys. **17**, 1354 (1949).
[4] Y. Morino *et al.*, (to be published soon elsewhere).
* The macroscopic dielectric constant is used here, although, rigorously speaking, the constant to be used in the theory should be modified somewhat from the average one.
[5] Mizushima, Morino, and Higashi, Sci. Papers Inst. Phys. Chem. Research Tokyo **25**, 159 (1934).

On the Phase Transition

SHIGETOSHI KATSURA
Department of Applied Science, Faculty of Technology, Tôhoku University, Sendai, Japan
(Received May 6, 1954)

LET us consider phase transition by the example of lattice gas. We denote grand partition function by $\Xi(T,N,z)$ (N is the total number of sites), configurational partition function by $Q_n(T,N)$, fugacity by z, and cluster integral by $b_l(T,N)$. Then

$$\Xi(T,N,z) = \sum_{n=0}^{N} Q_n(T,N) z^n = \exp \sum_{l=1}^{\infty} b_l(T,N) z^l. \tag{1}$$

We consider Bragg-Williams approximation of lattice gas, whose configurational partition function is

$$Q_n(T,N) = \binom{N}{n} \beta^{[4n(N-n)]/N}, \quad (\beta = e^{-J/kT}). \tag{2}$$

This system has the following properties.

(i) Q_n has two maxima as functions of n in low temperature and these two maxima merge into one above the critical temperature.
(ii) Consequently, the specific volume

$$\frac{1}{v} = \frac{1}{N} z \frac{\partial}{\partial z} \log \Xi = \frac{\sum_{n=0}^{N} n Q_n(T,N) z^n}{N \sum_{n=0}^{N} Q_n(T,N) z^n} \tag{3}$$

jumps at $z = z_{COND} = 1$ in low temperature.[1,2] The isotherm obtained from grand canonical ensemble has horizontal part. z_{COND} is the point where gaseous phase and condensed phase reach equilibrium in the grand canonical ensemble. When $N \to \infty$, z_{COND} becomes nonanalytic singularity z^* of the limit function

$$\lim_{N\to\infty} \left(\sum_{n=0}^{N} Q_n(T,N) z^n \right)^{1/N}. \tag{4}$$

(iii) The pressure obtained from the canonical partition function

$$\frac{p}{kT} = \frac{\partial \log Q_n(T,N)}{\partial N} \tag{5}$$

gives Van der Waals type isotherm according to (i).
(iv) The expansion by cluster integrals

$$\frac{p}{kT} = \lim_{N\to\infty} \sum_{l=1}^{\infty} b_l(T,N) z^l, \quad \frac{1}{v} = \lim_{N\to\infty} \sum_{l=1}^{\infty} l b_l(T,N) z^l \tag{6}$$

agrees with the one obtained from (4). On the other hand

$$\frac{p}{kT} = \sum_{l=1}^{\infty} \lim_{N\to\infty} b_l(T,N) z^l, \quad \frac{1}{v} = \sum_{l=1}^{\infty} \lim_{N\to\infty} l b_l(T,N) z^l \tag{7}$$

agrees with the one given from (5), and the analytical singular point of (7) on the positive real axis z_s is the end point of supersaturation, as supposed in the previous paper.[3] Where

$$b_l^0 = \lim_{N\to\infty} b_l(T,N) = (-)^{l-1} \frac{\beta^{4l}}{l} \sum_{i=0}^{l-1} \frac{1}{(i+1)!} \binom{l-1}{i} (8^l \log\beta)^i. \tag{8}$$

(v) $b_l^0(T)$ for fixed l becomes always positive if we make T sufficiently small, but for given fixed T, no matter how small, there exist negative b_l^0 if we make l sufficiently large. This system does not satisfy the condition of Ikeda's theorem.[4]

(vi) The zero points of (1) lie on the unit circle of z plane. Yang-Lee's theorem[5] holds not only for the exact solution but also for some kind of approximate solution of the lattice gas. $g(\theta)$, the distribution function of zero points, is given by

$$g(\theta) = \frac{1}{2\pi}(1 + r\cos\varphi), \tag{9}$$

where r and φ are related to θ by

$$\theta = -\frac{4J}{kT} r \sin\varphi - \varphi - \pi + \tan^{-1} \frac{r\sin\varphi}{2 + r\cos\varphi},$$
$$r = \left\{ \frac{4 \exp\left[-\frac{8J}{kT}(1 + r\cos\varphi) \right] (1 + r\cos\varphi)}{1 - \exp\left[-\frac{8J}{kT}(1 + r\cos\varphi) \right]} \right\}^{\frac{1}{4}} \quad (T < T_c). \tag{10}$$

The zero of smallest argument tends to $z_{YANG} = 1$ as $N \to \infty$ where $T < T_c$.

(vii) However $z_{YANG} (= z^*)$ is not the analytic singularity of limit function (4). Mayer's conclusion cannot be justified from Yang-Lee theory.

These properties (i)–(vii) have been proved for Bragg-Williams approximation of lattice gas (the detailed calculations will be published at another opportunity). The author conjectures that these properties are realized in general.

Particularly, (iii) is inconsistent with usually accepted opinion[6] that the complete evaluation of canonical partition function can never lead to isotherms with loops corresponding to metastable

FIG. 1.

states. *In order that* p given by (v) has horizontal part, Q_n must be such one as seen in Fig. 1b. The fact that Q_n has two maxima below the critical temperature, (Fig. 1a), however, is shown in Van Vleck's method[7] of Heisenberg model of ferromagnetism besides Bragg-Williams approximation. Moreover, it is the same with complete evaluation of finite system for the Ising model, and the sharpness of the maxima becomes more remarkable as the number of sites increases.[8] These facts have led the author to the doubt about the usually accepted opinion. Is that opinion really firmly founded? There seems to be room for discussions, whether the adiabatic condition is satisfied or not, and whether the canonical ensemble can be led by neglecting the interaction energy between the system and heat reservoir (between partial systems[9]) at the point of phase transition. It may be also necessary to discuss the external variable to be extensive variable or intensive variable.

[1] See S. Katsura and H. Fujita, Progr. Theoret. Phys. (Japan) **5**, 997 (1950), Sec. 4.
[2] K. Husimi has given another proof for his multidimensional model (Lecture at the meeting of Physical Society of Japan, May, 1953).
[3] S. Katsura and H. Fujita, J. Chem. Phys. **19**, 795 (1951); Progr. Theoret. Phys. (Japan) **6**, 498 (1951).
[4] K. Ikeda, Busseiron Kenkyu, No. 65 (1953); Lecture at the International Conference on Theoretical Physics (Kyoto, 1953, September).
[5] C. N. Yang and T. D. Lee, Phys. Rev. **87**, 404 (1952); T. D. Lee and C. N. Yang, Phys. Rev. **87**, 410 (1952).
[6] For example, Mayer and Mayer, *Statistical Mechanics* (John Wiley and Sons, Inc., New York, 1940), p. 274; S. Katsura and H. Fujita, reference 1, Sec. 6.
[7] J. H. Van Vleck, *The Theory of Electric and Magnetic Susceptibilities*, (Clarendon Press, Oxford), p. 328.
[8] S. Katsura, Lecture at the International Conference on Theoretical Physics, S. Katsura and C. Katsura, Busseiron Kenkyu, No. 70 (1954).
[9] The neglect of the interaction energy between cells plays a dominant role in S. Katsura and H. Fujita, reference 1 and Van Hove, Physica **15**, 951 (1949).

The Free-Electron Theory and the Virial Theorem

WILLIAM LICHTEN*
Laboratory of Molecular Structure and Spectra, Department of Physics, The University of Chicago, Chicago 37, Illinois
(Received May 4, 1954)

IN the free-electron (FE) model for molecules,[1] the electrons are confined in a square well, usually with potential energy zero inside, infinity outside (Fig. 1a).[2] The total energy of the molecule is set equal to a constant plus the energy E of the free electrons, which equals their kinetic energy T.

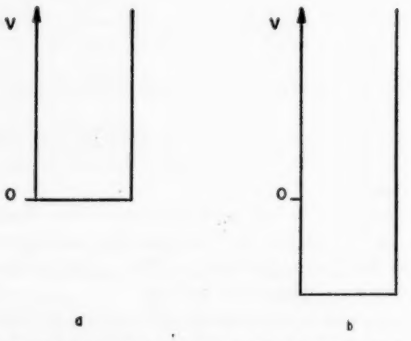

FIG. 1. Potential energy wells for the FE model. (a) Usual well. (b) Present well, with $V \neq 0$.

Since free electrons exert only an outward pressure on the walls of the "box," this scheme neglects their bonding properties. In fact, it violates the virial theorem, which states that the total energy of a molecule in equilibrium is the *negative* of its kinetic energy.[3]

A simple model of the molecule will show how a change in the energy zero can meet these objections. Let all the electrons of a molecule move freely in the box, but with $V \neq 0$ inside. This changes only the zero of the total energy, and leaves the kinetic energy unchanged (Fig. 1b).

Denote the coordinates of the N nuclei by $(x_1, x_2, \cdots x_{3N})$. It is convenient to define another set of variables $(y_1, y_2, \cdots y_{3N})$, where $y_1 = x_1$, $y_2 = x_2/x_1$, $y_3 = x_3/x_1 \cdots y_2 \cdots y_{3N}$ are dimensionless variables and determine only the shape of the nuclear framework, while y_1 fixes its scale.[4] Assume that the y's fix the dimensions of the potential well likewise, and that they alone determine its depth. Now hold $y_2 \cdots y_{3N}$ constant. Each linear dimension of the molecule will be proportional to y_1. Then, for a given state S, this must hold for the wavelength λ_i of the ith electron, and therefore for the arguments of its FE eigenfunction. The corresponding kinetic energy $T = \Sigma_i T_i = (h^2/2m)\ \Sigma_i\ 1/(\lambda_i^2) = B/(y_1^2)$, where B will be a function of $y_2 \cdots y_{3N}$ only (Fig. 2a).

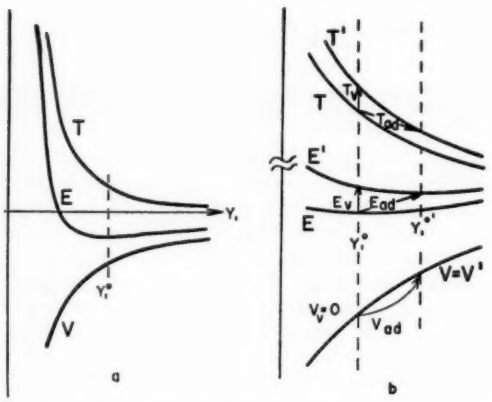

FIG. 2. Energy curves: (a) For state S; (b) For states S and S', showing details of the energies involved in transition.

The potential energy of the entire system $V = \Sigma_{i,j}(e_i e_j)/r_{ij}$, where e's represent all electronic or nuclear charges. Since both the nuclear framework and electronic eigenfunctions are assumed to expand linearly in y_1, every r_{ij} is proportional to y_1, and $V = [A(y_2 \cdots y_{3N})]/y_1$ (Fig. 2a). For a state S, $E = T + V = A/y_1 + B/(y_1^2)$. If $A < 0$, E has a minimum value, a case of stable binding. Since E is stationary at equilibrium, $(\partial E/\partial y_i) = 0$, for all i. In particular $0 = (\partial E/\partial y_1) = -A/(y_1^0)^2 - 2B/(y_1^0)^3$, where $y_i^0 = y_i$ at equilibrium. This gives $E^0 = -T^0 = \frac{1}{2}V^0$, satisfying the virial theorem.

Consider a new state S' of the same system. It will have a new equilibrium position $(y_1^{0'} \cdots y_{3N}^{0'})$ and, following the above reasoning, equilibrium energies $E^{0'} = -T^{0'} = \frac{1}{2}V^{0'}$. The adiabatic transition energy, $E_{ad} = E^{0'} - E^0 = -(T^{0'} - T^0)$, which is opposite in sign to the usual FE prediction.

This apparent paradox can be resolved by decomposing the adiabatic transition into two parts. First, make a vertical transition from $S(y_1^0 \cdots y_{3N}^0)$ to $S'(y_1^0 \cdots y_{3N}^0)$. Since (by assumption) the well depth, and therefore V, is unchanged, the vertical transition energy $E_v = T' - T = T_v$, the FE value. Second, change the molecular coordinates to the new equilibrium point $S'(y_1^{0'} \cdots y_{3N}^{0'})$. During this process T' and V' redistribute themselves, and the virial theorem is satisfied at equilibrium.

This is illustrated most simply if the old equilibrium point is near the new one (Fig. 2b). Since E' is stationary near its minimum, it is hardly changed during the second part. Then $E_{ad} \approx E_v$, despite the fact that $T_{ad} \approx -T_v$, because of the change in V during

TABLE I. Energies involved in transition.

Transition	T	V	E
(1) Vertical	E_v	0	E_v
(2) Adiabatic	$-E_v$	$2E_v$	E_v
(3) (2)–(1) Coordinate shift	$-2E_v$	$2E_v$	0

this shift (Table I). The apparent paradox in FE theory is dispelled.

If the molecule should retain its shape in the new equilibrium position, the energy would be an explicit function of x_1. It can be shown that

$$y_1^{0\prime}/y_1^0 = 1-(E_v/E^0); \quad E_{ad} = E_v/[1-(E_v/E^0)].$$

The following conclusions can be seen to hold, even if the above simplified model does not describe the specific molecule correctly: (1) if a vertical transition is to a state with substantially unchanged potential energy $E_v \approx T_v$; (2) if the new equilibrium lies close to the old equilibrium position $E_{ad} \approx E_v$; (3) if both conditions are true $E_{ad} \approx T_v$.

G. W. Wheland first pointed out the apparent contradiction between the virial theorem and the FE model. I am indebted to Dr. Wheland and Dr. J. R. Platt for helpful discussions, and to Dr. Platt for criticism of this note.

* National Science Foundation Pre-doctoral Fellow, 1953–1954.

[1] The formalism of the FE model is given in Ruedenberg and Scherr, J. Chem. Phys. **21**, 1565 (1953).

[2] Bayliss modified the well depth to make FE theory fit ionization potentials in Australian J. Sci. Research Ser. **A3**, 109 (1950).

[3] J. C. Slater, J. Chem. Phys. **1**, 687 (1933). A similar treatment is in Eyring, Walter, and Kimball, *Quantum Chemistry* (John Wiley and Sons, Inc., 1944), p. 355.

[4] y_1 is the reciprocal of a scale factor s, previously used to make variational calculations satisfy the virial theorem, J. O. Hirschfelder and J. F. Kincaid, Phys. Rev. **52**, 658 (1937).

Mass Spectrometric Analysis of Ions from the Field Microscope*

MARK G. INGHRAM AND ROBERT GOMER
University of Chicago, Chicago, Illinois, and Argonne National Laboratory, Lemont, Illinois

(Received May 11, 1954)

THE desorption of positive ions from surfaces by high electrostatic fields was first noted by E. W. Müller, who utilized the phenomenon in the ion microscope.[1] Our work was undertaken to determine the nature of the ions and the mechanism of their production.

A field emission microscope was modified by introducing a small hole in the screen, through which a beam passed into a mass spectrometer with an electron multiplier as detector. In most experiments an area of 900 A² at the edge of the 110 plane of a tungsten tip was "seen" by the detector. The peak width of monoenergetic 10 000-volt ions was 20 volts, permitting resolution of ions formed within 3A of each other.

Results are summarized in Table I. Figure 1 shows a current-voltage curve for hydrogen. Details vary with tip condition and pressure. No sizable mass effect was detected when D_2 replaced H_2. The peak widths in Fig. 1 show that ions are formed farther from the tip as the field is increased. This probably accounts for

TABLE I. Ion yields for various parent gases from a tungsten tip (probably oxygen contaminated) at indicated field strengths. Numbers in parentheses after ions indicate relative amounts.

Parent gas	Field	Ions observed
H_2	5.6 v/A	$H^+(0.5)H_3^+(0.5)$
D_2	5.6 v/A	$D^+(0.5)D_3^+(0.5)HD^+(0.025)$
O_2	5.6 v/A	$O_3^+(1.0)O^+(0.000?)$
C_2H_6	3.6 v/A	$C_2H_6^+(0.7)C_2H_5^+(0.03)C_2H_4(0.06)$ $C_2H_3^+(0.04)CH_3(\text{or } C_2H_6^{++})(0.15)$ Traces of various other fragments

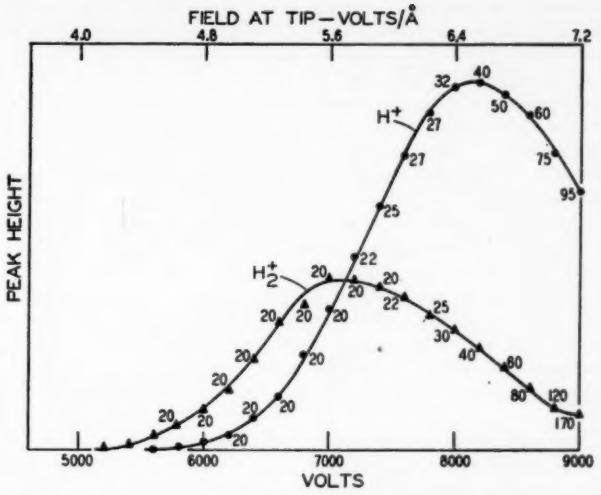

FIG. 1. Peak height *versus* applied voltage and field for hydrogen; $p = 3.10^{-4}$ mm Hg. Peak half-widths in volts are indicated by the numbers adjacent to experimental points. Field values somewhat uncertain because of oxygen contamination and time-dependent local field enhancement.

the decrease in peak heights when $F > 6$ v/A. It is significant that Müller[1] observed loss of sharpness above $F \sim 3.10^8$ v/cm. Temperature had an effect on peak heights which became more pronounced with decreasing field, where ionization near the tip predominates.

These facts suggest:

(1) At $F \gtrsim 6$ v/A autoionization (Fig. 2b) at 3–100A from the tip predominates (decrease in height and increase in width of current-voltage profiles).

(2) Since all peaks are broadened at high fields, autoionization produces fragmentation as well as ionization.

(3) At lower fields ionization occurs within 5A of the tip (sharp peaks, Müller's high resolution[1]). Fragmentation and ionization occur. It is not clear whether chemisorption or physical adsorption alone are involved. We hope to elucidate this point by pulsed desorption or increased energy resolution.

These conclusions suggest that field ionization occurs by electron tunneling (Fig. 2a). Appreciable ionization will occur at fields which reduce the barrier sufficiently to give molecules a lifetime short compared to the time spent near the surface. Although shown for an H atom, the mechanism probably is responsible for the ionization of impinging and physically adsorbed

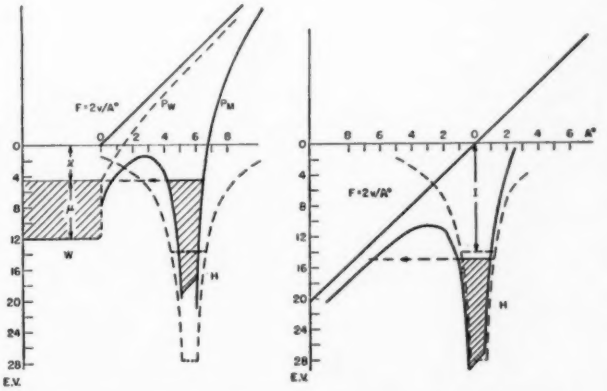

FIG. 2. Diagrams showing proposed mechanism for field ionization. (a) Ionization of physically adsorbed hydrogen atom. (b) Pure autoionization. F, applied field; W, tungsten metal; H, hydrogen atom; P_w, image potential, distorted by field; P_m, proton electron potential distorted by field; I, ionization potential of H atom; x, work function; μ, Fermi level; dotted lines represent H potential in absence of metal and field.

molecules. As the field is increased, the effect of the image potential (Fig. 2a) on the barrier becomes less important, so that ionization occurs farther from the surface, eventually going over into pure autoionization (Fig. 2b).

The above probably accounts for the second step in the ionization of chemisorbed atoms or molecules, held on the surface by a two-electron bond. The first electron can be removed only when $F \geqslant H/a$, where H is the heat of binding and a the mean bond-electron to surface distance. This places a sharp limit on F since the required potential difference must occur within ~1A. If $F \cdot a$ raises the bonding electrons above the Fermi level of the metal, one electron will tunnel; vibrational excitation of the atom will then move the latter to a distance where the situation of Fig. 2b applies. The loss of either electron could be rate-controlling. It is probable that the failure to detect O^+ ions from O_2 is due to the high heat of binding of atomic oxygen on tungsten. At fields where O^+ would be produced, O_2 is ionized before reaching the surface.

We hope to develop this technique as a tool for studying fragmentation processes occurring on catalyst surfaces. The combination of ion microscopy and mass spectrometry promises other applications: detection of molecular beams; measurement of decay times; sticking coefficients on surfaces; photoionization; etc.

* This work was supported in part by a grant from the National Science Foundation and by the U. S. Air Force under Contract No. AF33(616)-2090.

[1] E. W. Müller, Feldemission, Ergeb. exakt. Naturw. **27**, 290 (1953).

s-Triazine. V. The Raman Spectrum

ROBERT F. STAMM AND JOHN E. LANCASTER
Stamford Research Laboratories, American Cyanamid Company, Stamford, Connecticut

(Received May 15, 1954)

A PREVIOUS note[1] discussed some of the frequency assignments of the bands observed in the infrared. Since then, the Raman spectrum of the molten material (~85°C) has been studied both photographically and photoelectrically using natural and polarized incident radiation (Hg λ4358A). The frequency shifts (cm^{-1} in vacuum), photoelectric peak intensities, qualitative depolarization ratings, and symmetry classifications are as follows: 341 (11, *D*, *E''*), 676 (22, *D*, *E'*), 991 (78, *P*, A_1'), 1132 (100, *P*, A_1'), 1176 (6, *D*, *E'*), 1410 (6, *D*, *E'*), 1555 (10, *D*, *E'*), and 3042 (72, *P*, A_1', diffuse). Additional lines observed are 733 (v.w.), 1460 (v.w.), 2212 (*P*), 2943 (7, *P*), and 3107 (18, *P*). The lines 341, 676, 991, and 1132 also appeared as anti-Stokes shifts. A weak satellite having an intensity 4.8 percent of that of 1132 was resolved and measured as 1117 cm^{-1}; presumably, this could arise from isotopic species involving ^{13}C and/or ^{15}N.

The three strong, polarized lines at 3042, 1132, and 991 cm^{-1} can be assigned at once to ν_1, ν_2, and ν_3. (The ρ value for 3042 is increased considerably inasmuch as this line nearly coincides with ν_6, 3056 cm^{-1}.) The ring bending mode ν_{14} must be the line at 341 cm^{-1}. A weak infrared band at 1175 cm^{-1} is now confirmed as ν_9, since a depolarized line is observed here.

The appearance of a strong depolarized line at 676 cm^{-1} shows us that the infrared band observed at the same frequency must be ν_{10}, and not ν_{12}, as previously proposed. There is a weak infrared band at 837 cm^{-1}, which had been thought to be $2\nu_{14}$. It is difficult to explain as an overtone or combination of the lower frequencies now that ν_{14} is known to be at 340 cm^{-1}. Hence, it appears that the bands at 837 and 735 cm^{-1} are ν_{11} and ν_{12}, respectively.

All of the fundamentals have now been assigned except ν_{13}, which has not been located in the Raman spectrum as yet.*

[1] J. E. Lancaster and N. B. Colthup, J. Chem. Phys. (to be published).

* *Note added in proof.*—Since the date of submission of this note, Dr. C. Grundmann has sent us a copy of a manuscript by Goubeau, Jahn, Kreutzberger, and Grundmann which they have submitted to J. Phys. Chem. and which discusses their assignments of the infrared and Raman bands observed by them in solutions of *s* triazine. We wish to acknowledge their priority in this infrared and Raman work on *s* triazine, and to thank them for their courtesy in cooperating in a mutual exchange of data subsequent to the submission of the several papers for publication. However, our more extensive work on all phases (solid, liquid, and vapor) in the infrared[1] and our data on the Raman spectrum of the molten material have led us to frequency assignments which differ in several cases from those proposed by the above authors. Complete details will be submitted later.